The Thesis committee for David Benjamin Garber
Certifies that this is the approved version of the following thesis:

Shear Cracking in Inverted-T Straddle Bents

APPROVED BY
SUPERVISING COMMITTEE:

Oguzhan Bayrak, Supervisor

Wassim Ghannoum

Shear Cracking in Inverted-T Straddle Bents

by

David Benjamin Garber, B.S.C.E.

Thesis

Presented to the Faculty of the Graduate School of

The University of Texas at Austin

in Partial Fulfillment

of the Requirements

for the Degree of

Master of Science in Engineering

The University of Texas at Austin

August, 2011

Dedication

To my mom and dad for all their encouragement and support.

Acknowledgements

I would first and foremost like to thank God for the opportunity and gifts He has blessed me with; I would be nothing without Him. I would like to thank all of my family for their support during my time at the University of Texas. Thank you specifically to my parents; you have both always been there for me. I could not have accomplished anything without the backing and motivation you both provided.

I greatly appreciate the financial support from the Texas Department of Transportation that made this project possible. In particular, I would like to thank TxDOT bridge engineer Jamie Farris, the project director, for her continued participation in the research.

I would also like to thank my advising professors, Dr. Oguzhan Bayrak and Dr. Wassim Ghannoum. I have learned so much from both of you and greatly appreciate all the support and guidance you have provided.

I am so thankful for the opportunity to work with my project team and all the other brilliant students at Ferguson Structural Engineering Laboratory. I would specifically like to thank Eulalio Fernandez, Nancy Larson, and Michelle Wilkinson for their help in and out of the lab, building beams and making sense of test results. I would also like to thank Laura Chimelski, Daniel Bejarano, and Allison Lehman for their stout and adept hands helping to build an impressive number of full scale beams.

Lastly, I would like to thank all of the staff at FSEL. I am very much appreciative of Andrew Valentine, Blake Stasney, Mike Watson, Eric Schell and Dennis Fillip for all of their assistance on the lab floor and Jessica Hanton and Barbara Howard for all the help behind the scenes.

August 12, 2011

Shear Cracking in Inverted-T Straddle Bents

David Benjamin Garber, M.S.E

The University of Texas at Austin, 2011

Supervisor: Oguzhan Bayrak

Significant diagonal cracking in reinforced concrete inverted-T (IT) straddle bent caps has been reported throughout the State of Texas. Many of the distressed structures were recently constructed and have generally been in service for less than two decades. The unique nature of the problem prompted a closer look into the design and behavior of such structural components. A preliminary investigation highlighted outdated design requirements and a scarcity of experimental investigations pertaining to inverted-T bent caps. This research project (TxDOT Project 0-6416, *Shear Cracking in Inverted-T Straddle Bents*) aims to improve current understanding of the behavior of inverted-T caps, while providing updated design provisions.

In order to develop strength and serviceability guidelines for inverted-T beams, an extensive experimental program was developed. This series of large-scale tests was used to evaluate the strength and serviceability of IT deep beams in relation to the following parameters – shear span-to-depth (a/d) ratio, web reinforcement ratio, ledge height, ledge length, number of point loads, and member depth. This report focuses mainly on results from a first series of tests conducted within this experimental program.

Table of Contents

List of Tables

List of Figures

CHAPTER 1
Introduction

1.1 INTRODUCTION

Significant diagonal cracking in reinforced concrete inverted-T (IT) straddle bent caps has been reported throughout the State of Texas (e.g., Figure 1-1). Many of the distressed structures were recently constructed and have generally been in service for less than two decades. The unique nature of the problem prompted a closer look into the design and behavior of such structural components. A preliminary investigation highlighted outdated design requirements and a scarcity of experimental investigations pertaining to inverted-T bent caps. This research project (TxDOT Project 0-6416, *Shear Cracking in Inverted-T Straddle Bents*) aims to improve current understanding of the behavior of inverted-T caps, while providing updated design provisions.

The following sections provide a brief explanation of project scope and tasks. An outline for the remainder of this thesis is also provided.

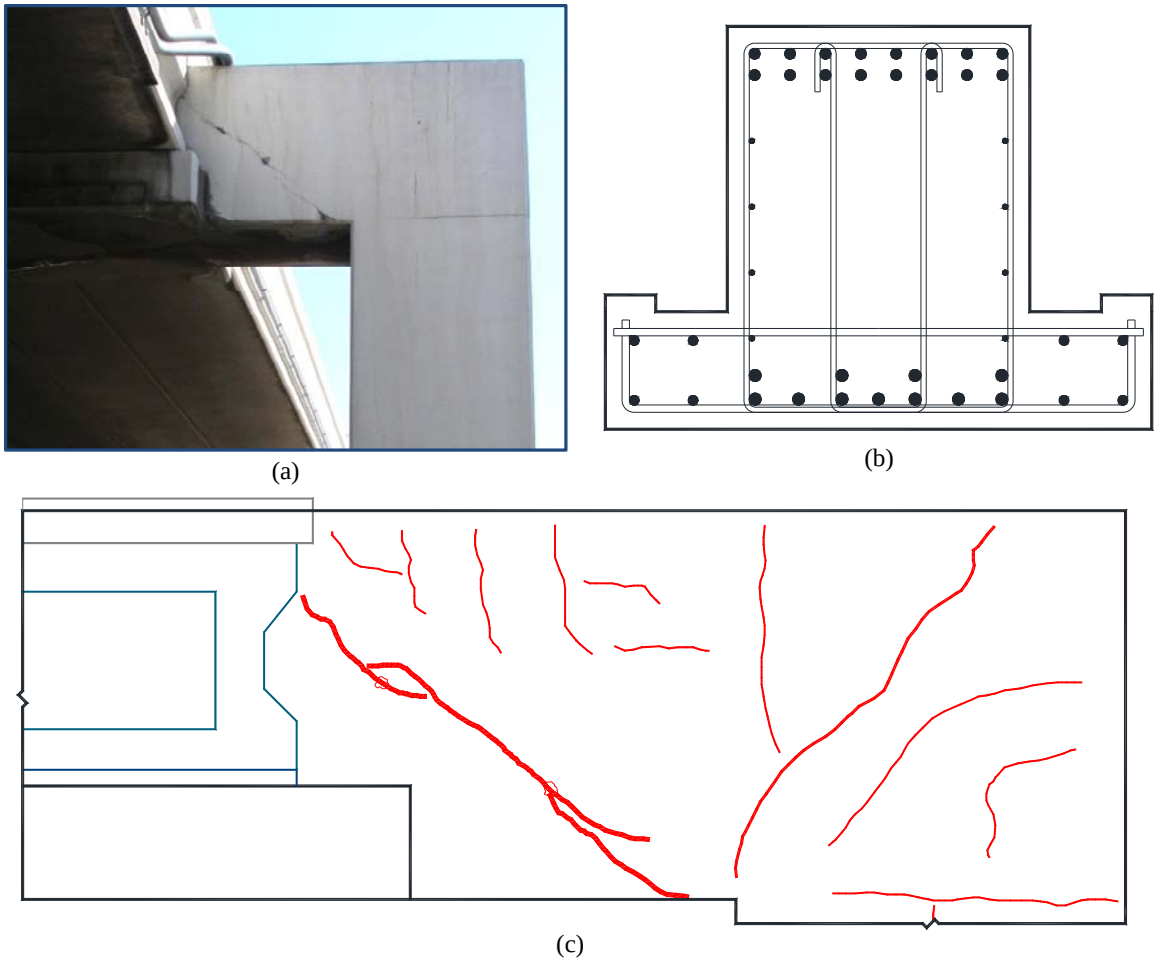

Figure 1-1: Cracked inverted-T beam in El Paso, TX; (a) inspection photograph, (b) typical reinforcement details, and (c) mapped cracks

1.2 PROJECT BACKGROUND AND OBJECTIVES

Most, if not all, IT beams qualify as "deep" members for shear design (i.e. possess a relatively low shear span-to-depth ratio). Geometric and loading-related discontinuities further render IT beams as *D*-regions (i.e. regions that contain *D*isturbed stress fields). Historically, design procedures for deep members (or *D*-regions) were based on empirically derived expressions and rules of thumb. Strut-and-tie modeling (STM) provisions were introduced as an alternate, more general design method for deep

members in the AASHTO LRFD Bridge Design Specifications and ACI Building Code in 1994 and 2002, respectively. STM is a design method that reduces complex stress flows within a member into a simplified truss model comprised of steel tension ties and concrete compression struts.

Recently, University of Texas at Austin researchers produced improved strut-and-tie modeling (STM) for the design of deep beam members. That work was performed as part of TxDOT Project 0-5253, *Strength and Serviceability Design of Reinforced Concrete Deep Beams*. In contrast to previous code implementations, the STM recommendations of TxDOT Project 0-5253 represent a substantial improvement in the safe and consistent application of strut-and-tie modeling to a variety of structures. The recommendations of TxDOT Project 0-5253 were based upon a large database of experimental results from 179 deep beam tests. The database included 37 large-scale tests conducted at the Ferguson Structural Engineering Laboratory. The members studied in Project 0-5253 were loaded on the top (or compression) chord of the beam, where the load could be directly transferred from the load point to the support, as shown in Figure 1-2 (a). In contrast, IT beams are loaded on the bottom chord of the beam through a ledge (Figure 1-2 (b)). When the bottom chord is loaded, the load does not have a direct path from the point of application to the support and must be "hung" up to the top chord.

This indirect load path changes the behavior of the beam and creates a tension field that is not present in the compression-chord-loaded member. Due to the unique load transfer mechanisms perceived in deep members loaded through the bottom chord, it is unclear whether the STM recommendations of TxDOT Project 0-5253 will be directly applicable to inverted-T straddle bents.

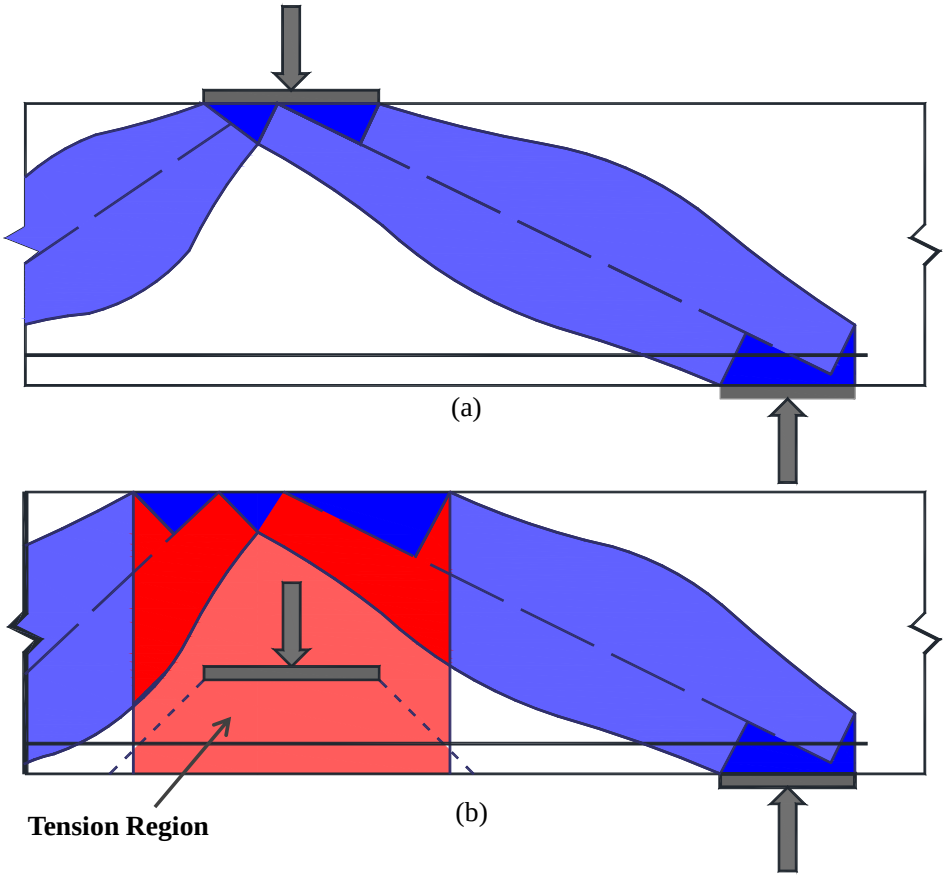

Figure 1-2 – (a) Direct load path does not contain the tension region present in an (b) indirect load path

The project scope outlined in the following section is focused on investigating the influence of various geometric and reinforcement parameters on the shear behavior of IT beams. As detailed in later chapters, specimens tested within the current research program reproduce many of the details used within the top-chord-loaded beams of TxDOT Research Project 0-5253. This approach enables clear comparisons to be made between the results of both Projects 0-5253 and 0-6416.

1.3 SCOPE AND ORGANIZATION OF THESIS

In order to develop strength and serviceability guidelines for inverted-T beams, an extensive experimental program was developed. This series of large-scale tests was used

to evaluate the strength and serviceability of IT deep beams in relation to the following parameters – shear span-to-depth (a/d) ratio, web reinforcement ratio, ledge height, ledge length, number of point loads, and member depth. This thesis focuses mainly on results from a first series of tests conducted within this experimental program. The thesis also contains details from field investigations of multiple inverted-T straddle bent caps throughout the state of Texas, which are presented in Appendix A. This thesis is divided into five chapters which provide a brief overview of the analytical and experimental methods, as well as a preliminary analysis of test results.

Chapter 2 provides a more detailed introduction to strut-and-tie modeling and an examination of the effects of bottom-chord loading. *Chapters 3* and *4* discuss the experimental program and results, respectively. Details of all specimens, including those tested to date and discussed in this thesis and those to be tested in the future as part of the broader experimental program to TxDOT project 0-6416, are presented in these chapters. Particular emphasis is placed on providing a clear explanation for the selection of parameters examined within the testing program. Following the discussion on specimen strength and serviceability results, implications of these results are examined.

Chapter 5 is designed to further analyze the results from the tests completed to date. The IT beams subjected to bottom-chord loading are compared with the equivalent members from TxDOT Project 0-5253 (subjected to top-chord loading). These comparisons, in turn, provide a basis for the applicability of the TxDOT Project 0-5253 provisions to be analyzed. *Chapter 6* includes a summary of the thesis and observations.

CHAPTER 2
Background of Strut-and-Tie Modeling of IT Deep Beams

2.1 INTRODUCTION

IT deep beams are under a complex state of stresses, where the interaction of flexure, shear, and tension-chord loading can govern the behavior. Strut-and-tie modeling (STM) idealizes this complex state of stress as a truss of axially loaded elements. In this chapter a brief review of the theoretical background of strut-and-tie modeling is presented and the application of STM to inverted-T beams is examined.

2.2 BACKGROUND ON STRUT-AND-TIE MODELING

A strut-and-tie model (STM) idealizes a complex flow of stresses in reinforced concrete members as a collection of compression elements (struts), tension elements (ties), and the intersections of such elements (nodes). While the use of STM is applicable to all design scenarios, this method is more widely used in deep beams and disturbed regions where the Bernoulli hypothesis that plane sections remain plane in flexure does not apply.

2.2.1 B and D- Regions

Typical sectional behavior is based on the Bernoulli hypothesis that axial strains vary linearly across the depth of the member (i.e. plane sections remain plane). Regions that exhibit this behavior are considered to be B-regions and are designed using sectional design methods.

A region is considered to be a D-region when the strains vary nonlinearly across the depth. In these D-regions the Bernoulli hypothesis and sectional design no longer apply. Typically, these D-regions are considered to extend a member depth to either side of a discontinuity, as shown in Figure 2-1. A discontinuity is considered to be a location

in the member where there is a change in geometry, a load is applied, or a support point exists. In Figure 2-1, the location of the point load and the supports are the discontinuities present in the member.

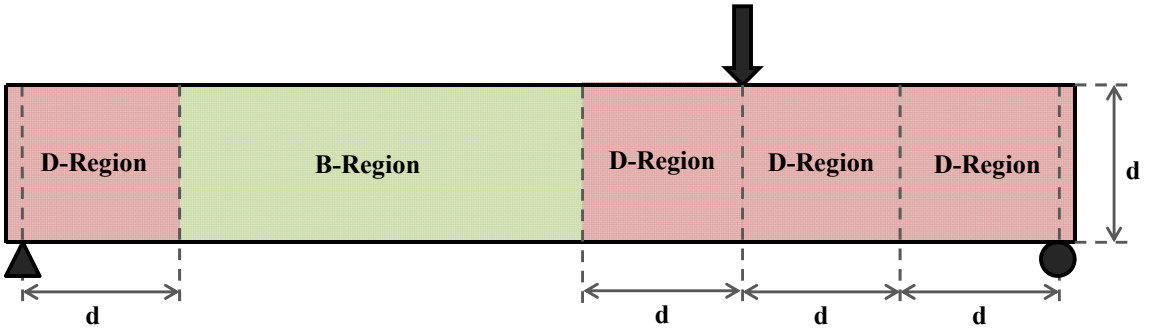

Figure 2-1: Location of D- and B-regions

In D-regions sectional design assumptions are not valid and a different shear design procedure must be used. Various design codes provide empirical relations for designing specific element types with D-regions. Such empirical relations are limited in use to the specific structural systems they were developed for and often lack behavioral transparency. Strut-and-tie modeling provides an alternative method that gives the engineer a flexible and conservative method for the design of D-regions.

2.2.2 Struts, Ties, and Nodal Zones

A strut-and-tie model is designed to simply model the flow of stresses through a structure using a series of compression elements (struts) and tension elements (ties) connected by nodes. The STM must be in equilibrium and will be more efficient if it closely follows the true stress paths. A simple strut-and-tie model for a rectangular section under compression is given as an example in Figure 2-2. The load is only applied across a portion of the width at the ends of the section, but the stresses spread to the entire width of the section by mid-depth, as shown in Figure 2-2 (a). A simple strut-and-tie model can be created to represent this stress flow, as shown in Figure 2-2 (b). The struts (dashed lines) are placed to follow the flow of compression forces and the ties (solid lines) are required to ensure equilibrium of the truss. More detailed models, as

shown in Figure 2-2 (c), can be selected to follow the stress field more closely for improved accuracy.

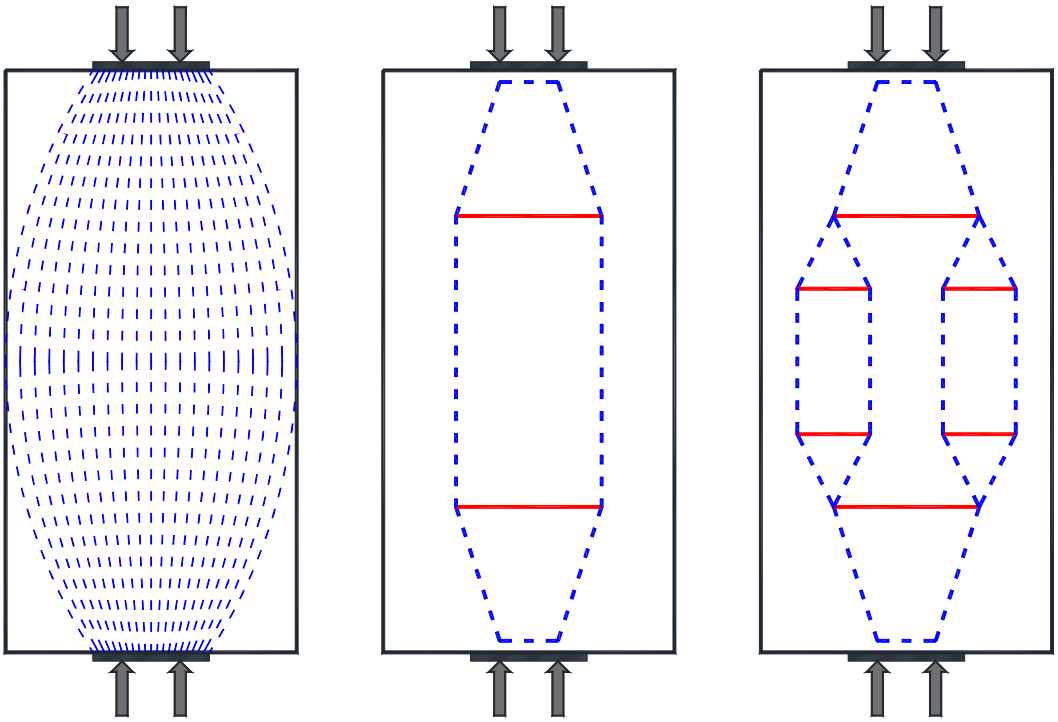

Figure 2-2: Typical flow of forces through rectangular section

2.2.3 Struts

Struts are the compression elements in the strut-and-tie model. Struts often idealize a compression stress field as a single line and are often illustrated as dashed lines (Figure 2-2). Actual behavior of a strut can be represented by two different strut types, prismatic and bottle-shaped, as shown in Figure 2-3 (a,c) and (b,d), respectively. A bottle-shaped strut represents the spreading of load to utilize more of the available cross section. The spreading of the forces results in a tension tie that is not present in the prismatic strut, as shown in Figure 2-3 (d).

A prismatic strut is a compressive strut with a uniform width along the entire cross section, due to either geometric limitations or tension region boundaries. An

example of a prismatic strut bound by a tension region is found in a beam under flexure loads, as shown in Figure 2-4. The compression strut formed by flexure has a uniform width and is assumed to be bound by the tensile stresses in the lower section of the beam. Prismatic struts behave more favorably than bottle-shaped struts because they transmit stresses strictly in compression; no tension stresses are developed by load spreading. This behavioral advantage is taken into account in the ACI 318-08 (2008) design specification, but not the AASHTO (2009) design specification.

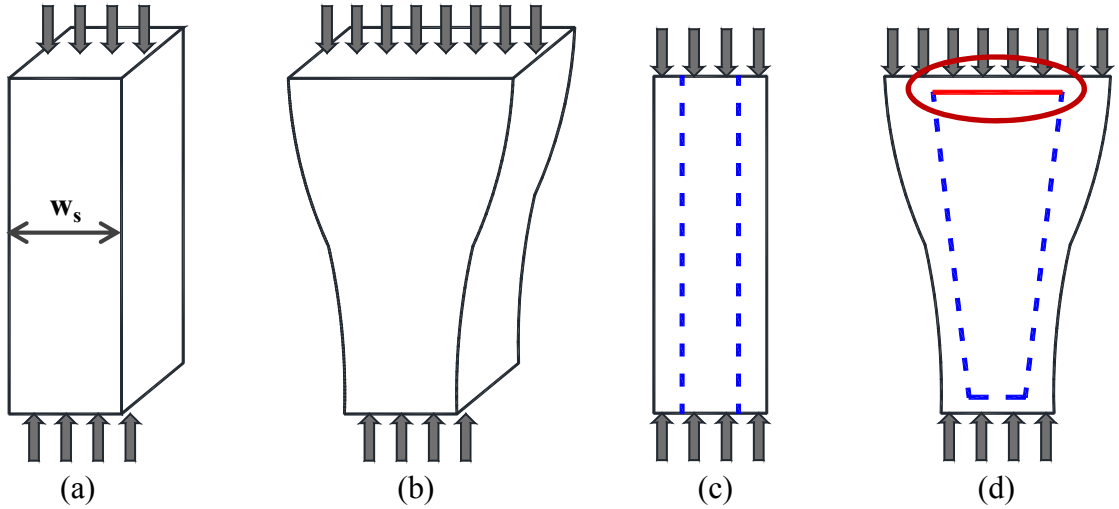

Figure 2-3: Two main types of struts; (a,c) prismatic and (b,d) bottle-shaped

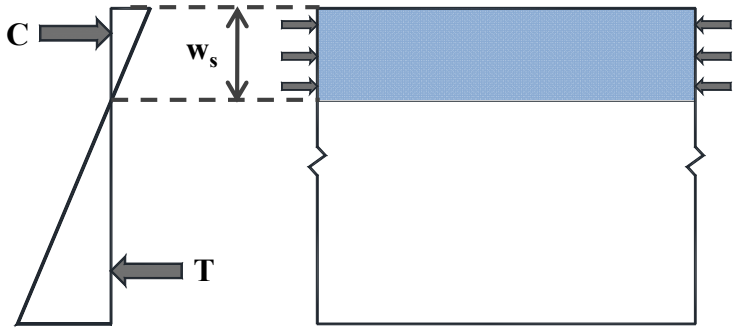

Figure 2-4: Prismatic strut bounded by tension stresses

2.2.4 Ties

Ties are tension elements in the strut-and-tie model and are illustrated in Figure 2-2 as solid lines. Tension ties coincide with the location of tension reinforcement, as shown in Figure 2-5. Enough reinforcement must be provided to carry the tensile demand of the tie, with the centerline of the reinforcement coinciding with the centerline of the tie. The reinforcement must be properly developed in order to reach yield strength upon leaving the nodal zone.

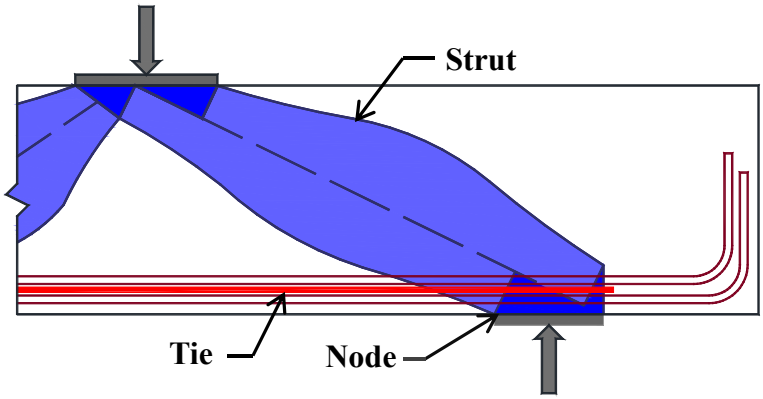

Figure 2-5: Strut, node, and tie locations

2.2.5 Nodal Zones

Nodes are named based on the elements that intersect at the node location, where a C is assigned for compressive stresses applied by struts and external loads and a T for tension created by tie reinforcement. For example, a node at the support point with a tension tie and a compression strut is considered to be a CCT node, as shown in Figure 2-6. More than three elements framing into one node should be resolved to three elements, as the CCC and CTT nodes in Figure 2-6. The type of node governs its behavior and thus also its design.

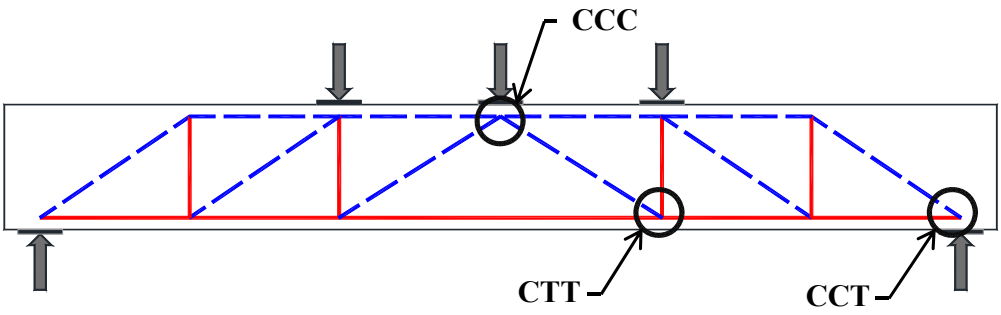

Figure 2-6: Node designation

Nodes can either be detailed based on equal pressure on all of the faces of the node, hydrostatic nodes, or by geometries where the sides are allowed to have unequal pressures, non-hydrostatic nodes. Non-hydrostatic nodes are subject to internal shear stresses, whereas hydrostatic nodes are not. These two node types and their independent advantages are discussed in detail in the technical report for TxDOT Project 0-5253 (Birrcher, et al., 2008).

The design specifications provided by Project 0-5253 use non-hydrostatic nodes in the strut-and-tie model. Two of the types of nodes that need to be designed in a strut-and-tie model are CCC and CCT nodes, as shown in Figure 2-7 (a). The geometry of these nodes is based on the bearing area and the overall geometry of the strut-and-tie model. Other node types are typically smeared nodes and therefore do not control design.

The geometry of a CCC node under the top load point is presented in Figure 2-7 (b). The bearing pad is divided into two distances based on the proportion, α, of the load that travels to the near support. The length, αl_b, defines the top dimension of the node. The back face of the node is the height, a, determined by a stress block analysis. Using the angle of the strut and the lengths of defined node faces, the total length of the strut-to-node interface is obtained using trigonometry.

The geometry of a CCT Node above the support is presented in Figure 2-7 (c). The length of the bottom face of the node is the entire length of the bearing support, l_s. The height of the back face is generally accepted to be twice the distance from the bottom of the beam to the centerline of the tension steel, h_a. Using these two lengths and the

angle of the strut, the total length of the strut-to-node interface is again obtained using trigonometry.

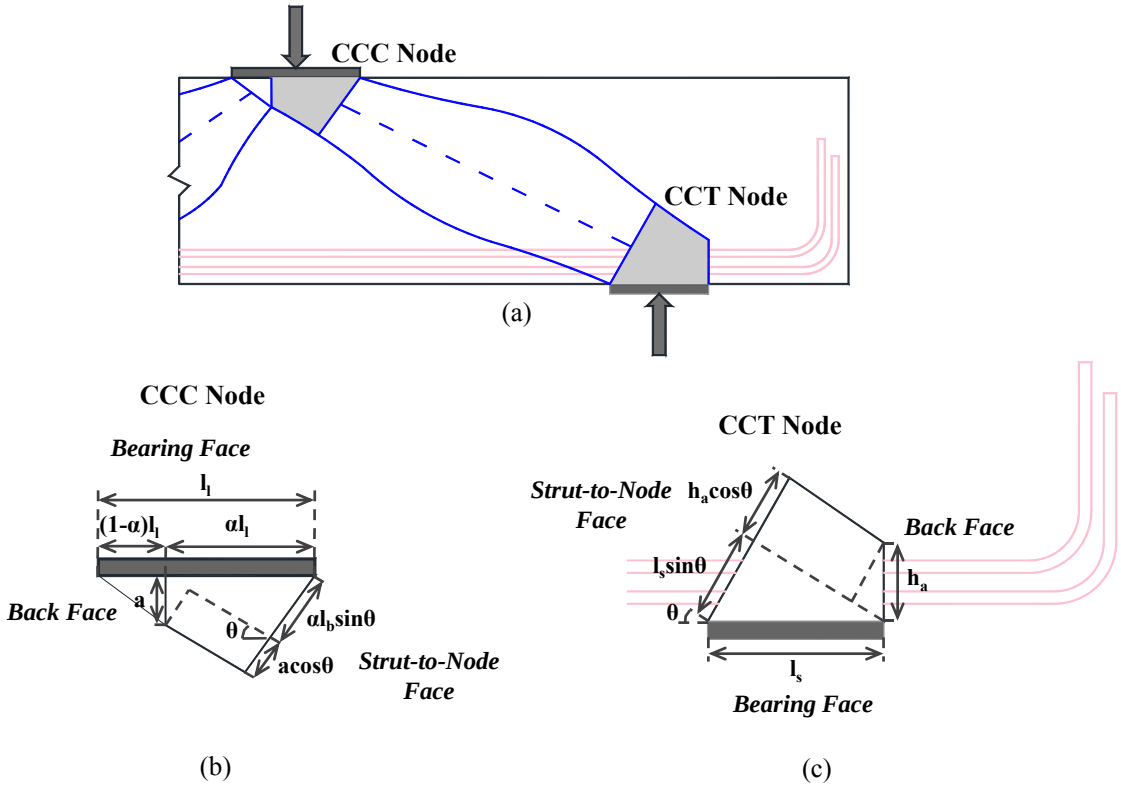

Figure 2-7: Typical node types and size requirements from Project 0-5253

2.3 NOMENCLATURE FOR INVERTED-T BEAMS

In order to facilitate later discussions, most of the terms and details relevant to inverted-T construction and behavior must be introduced. Typical reinforcement details will be introduced and terminology will be explained for the different components.

A typical inverted-T beam has two different cross sections along its length (Figure 2-8). A longitudinal view of a typical reinforcing cage is shown in Figure 2-8 (a). In Figure 2-8 (b) a typical cross section without ledges is illustrated. The size of the web, b_w wide by h tall, remains constant along the entire length of the specimen. In Figure 2-8 (c) a typical cross section with ledges is illustrated. The ledge depth, shown in Figure 2-8 (c), is taken from the bottom of the beam to the top of the ledge. In most inverted-T

beams in Texas, the ledge does not extend the entire length of the beam, as shown in Figure 2-8 (a).

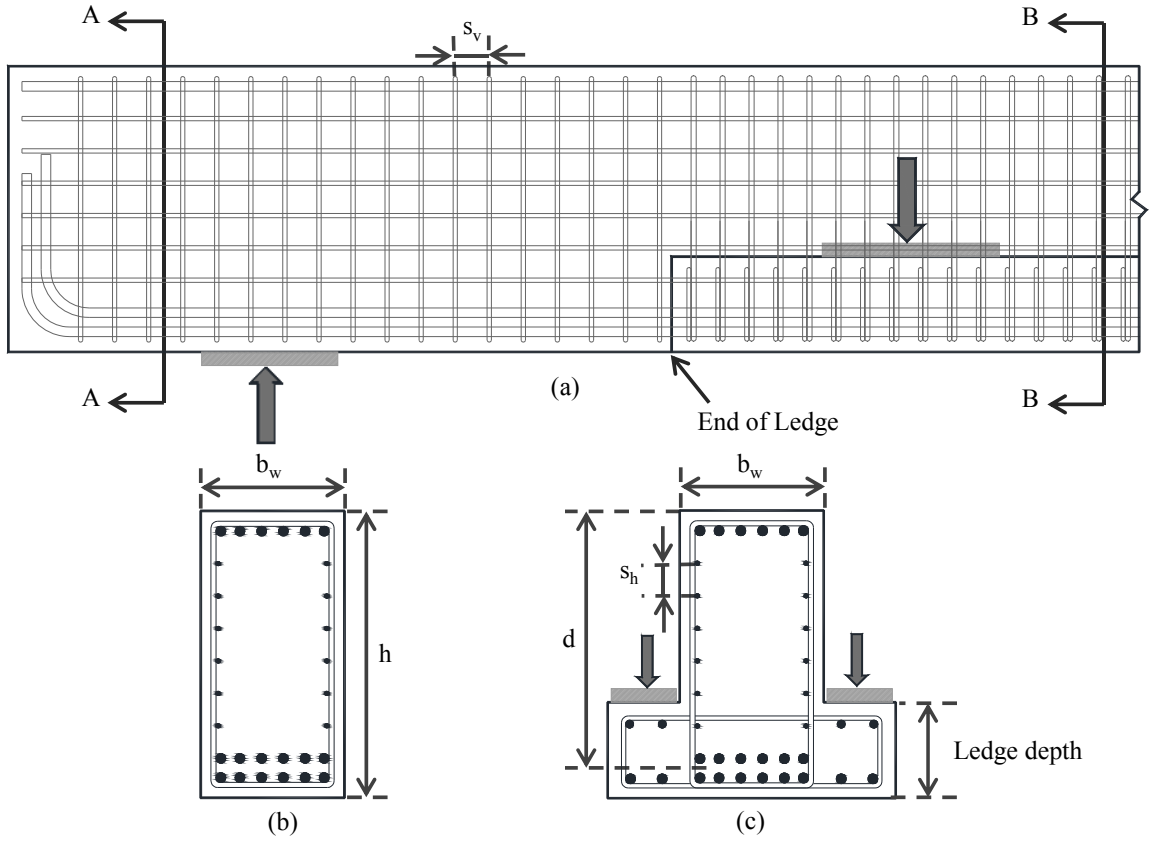

Figure 2-8 - Typical reinforcement detail for specimens; (a) longitudinal, (b) Section A-A, and (c) Section B-B

The spacing of the vertical and horizontal web reinforcement, s_v and s_h, respectively, are shown in Figure 2-8 (a) and (c). The spacing of this reinforcement was chosen to obtain certain reinforcement ratios. The reinforcement ratios are determined by dividing reinforcement areas, shown in Figure 2-9, by the area of concrete that the steel effects.

A_s = total area of longitudinal tension reinforcement provided

A_s' = total area of longitudinal compression reinforcement provided

A_h = area of a pair of horizontal web reinforcement bars

A_v = area of one set of vertical web reinforcement bars provided

The reinforcement ratios are then:

ρ_l = ratio of longitudinal tensile reinforcement to effective web area ($A_s / b_w d$)

ρ_l' = ratio of longitudinal compression reinforcement to effective web area ($A_s' / b_w d$)

ρ_h = ratio of horizontal web reinforcement to effective area ($A_h / b_w s_h$)

ρ_v = ratio of vertical web reinforcement to effective area ($A_v / b_w s_v$)

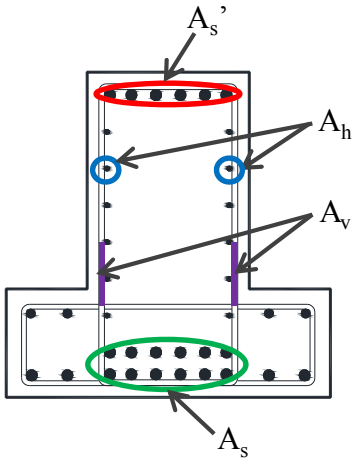

Figure 2-9 - Areas used in reinforcement ratio calculations

Load is applied on the ledge of an inverted-T beam, as shown in Figure 2-8 (c). Ledge reinforcement, highlighted in Figure 2-10 (a), is necessary to transfer the load to the web of the beam. Hanger reinforcement, highlighted in Figure 2-10 (b), serves to hang the load from the ledge to the compression block in the web. In this study, ledge and hanger reinforcements were sized and spaced to attempt to make the specimens fail in shear before failure of the ledge occurred.

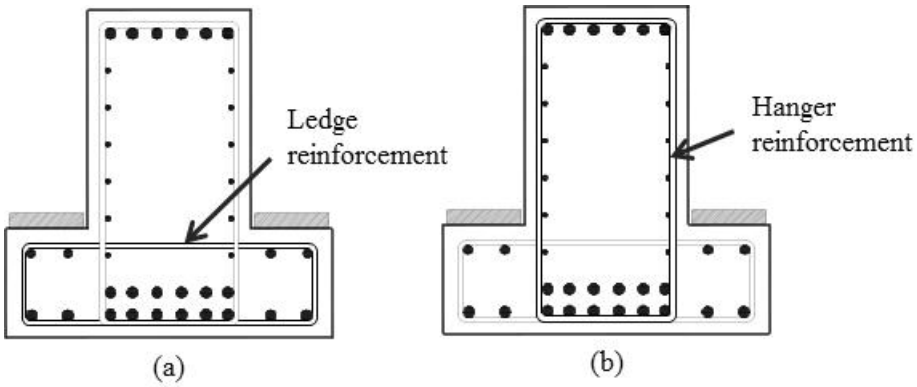

Figure 2-10 - (a) Ledge and (b) hanger reinforcement highlighted

Hanger reinforcement is defined as the vertical reinforcement within a "transfer" distance of the load point; illustrated in Figure 2-11 (a). The transfer distance is typically taken to be the length of the bearing pad plus a distance encompassed by 45 degree projection lines, extending from the edge of the bearing pad to the bottom of the hanger reinforcement. Vertical reinforcement outside of this range is defined as vertical web reinforcement; highlighted in Figure 2-11 (b). Horizontal web reinforcement is highlighted in Figure 2-11 (c).

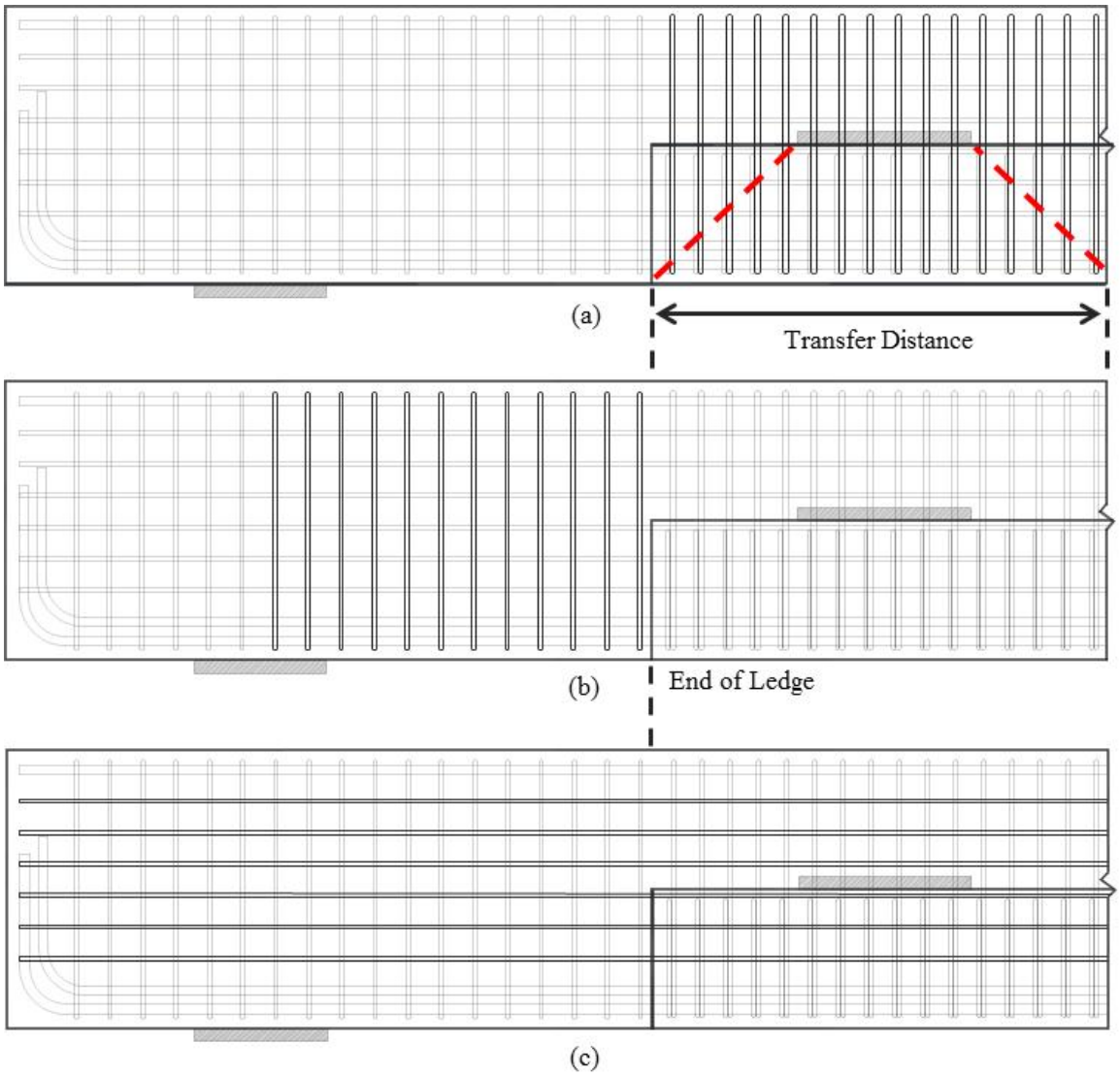

Figure 2-11 - Location of (a) hanger reinforcement, (b) vertical web reinforcement and (c) horizontal web reinforcement

2.4 APPLICATION OF STM TO INVERTED-T BEAMS

In the design of inverted-T beams, load must be transferred in multiple dimensions (across the width, height and length of the beam) and across multiple discontinuities. Strut-and-tie models (both two- and three-dimensional) can greatly simplify design in such a scenario.

2.4.1 Behavior of Top- vs. Bottom-Chord Loaded Beams

In order to help facilitate the discussion of the behavior of a member directly loaded on its top chord vs. one indirectly loaded on its bottom chord, simple two-dimensional STMs for top- and bottom-chord loaded beams are presented in Figure 2-12. A member is considered to be top-chord loaded when the load is applied directly to the top or compression side of the member (Figure 2-12 (a)). IT beams are considered to be bottom-chord loaded members because the load is applied on the tension chord of the specimen (Figure 2-12 (b)).

Differences between the strut-and-tie models for top-chord and bottom-chord-loaded beams are highlighted in Figure 2-12. In the bottom-chord-loaded beam, the load must be "hung" on the compression chord. This requires the addition of a center tie (relative to the top-chord-loaded model) and results in increased forces within the immediately adjacent ties. As an aside, it should be noted that the additional reinforcement necessary in bottom-chord-loaded beams is typically referred to as 'hanger' reinforcement. Forces within the outer shear span (between the outermost load and support) are nonetheless similar in both models. This would suggest that the outer shear span in each beam could exhibit similar behavior and therefore be designed in the same manner. In truth, the behavior of the outer shear span in bottom-chord-loaded beams may be quite different due to the tension field introduced by the indirect load path. As discussed in Chapter 1, the primary objective of this project is to discern the effects of the tension field on the strength and serviceability of bottom-chord-loaded members.

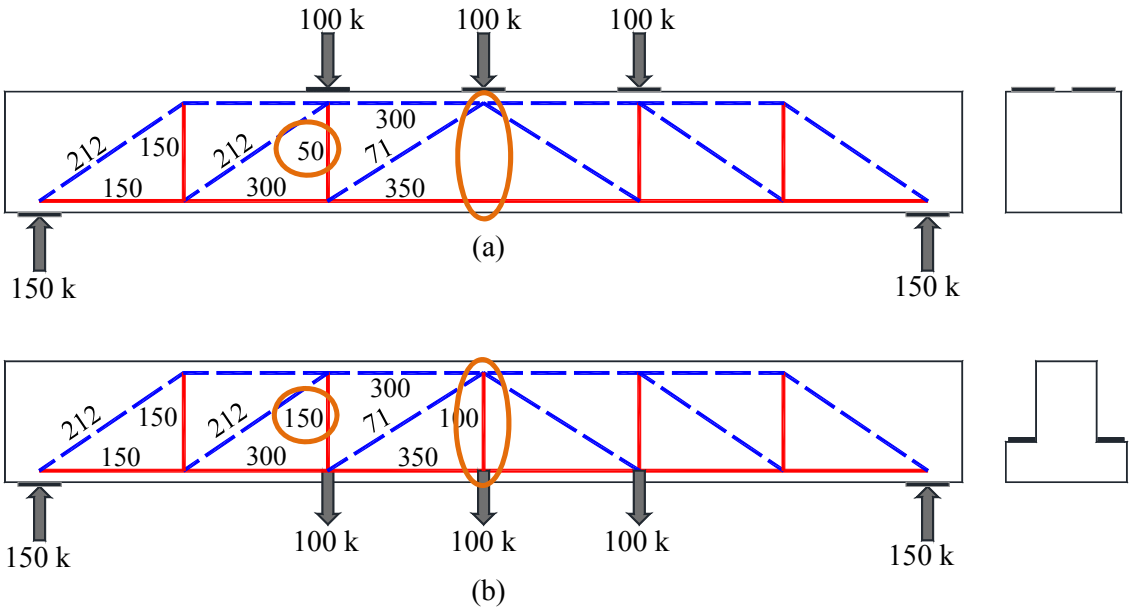

Figure 2-12: STM for (a) top-chord loaded and (b) bottom-chord loaded specimens

2.4.2 One- vs. Two-Panel Failure Modes

In deep beams, the load is assumed to be directly transferred from the load point to the support through a compression stress field. This compression stress field is typically modeled as a bottle-shaped strut as shown in Figure 2-13 (a), (Schlaich, et al., 1987). As the shear span-to-depth (a/d) ratio increases, the load carried through the compression field is gradually picked up by the vertical reinforcement. This behavior changes the load path from a direct load path, or one-panel mechanism shown in Figure 2-13 (a), to an indirect load path, or two-panel mechanism shown in Figure 2-13 (b). When the minimum amount of web reinforcement is provided, the shear strength of the one-panel model is controlled by the compressive strength of the concrete and the geometry of the nodal regions. The strength of the two-panel model, on the other hand, is usually dependent on the size and strength of the vertical tie.

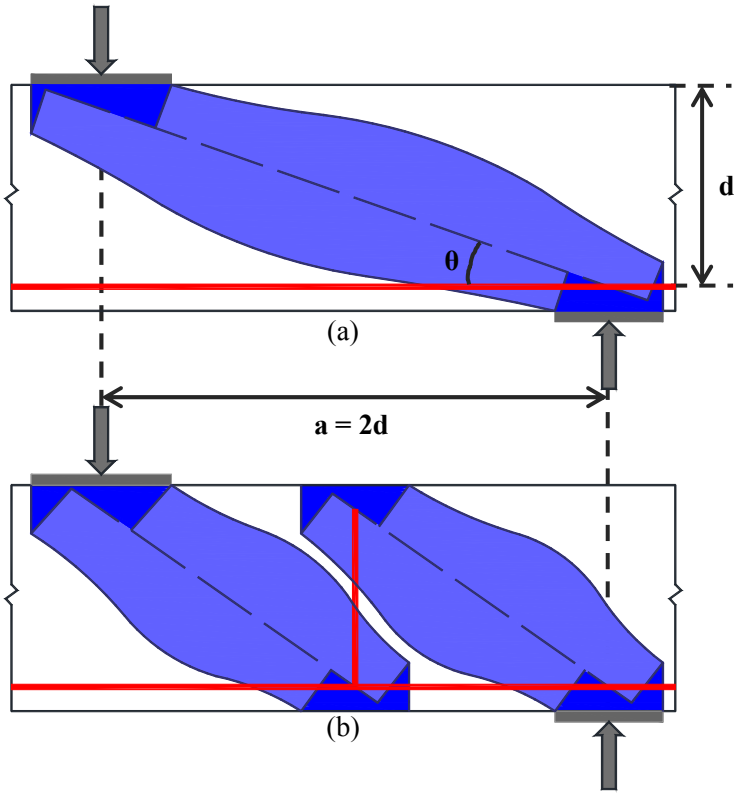

Figure 2-13: Load transfer mechanisms; (a) one and (b) two-panel

Although the transition from a one-panel to a two-panel mechanism is gradual from a behavioral standpoint (occurring between beam shear span to effective depth (a/d) ratios of 2.0 and 2.5), an a/d ratio of 2.5 is generally accepted as the transition point for design purposes (Kani, et al., 1979). This transition point is generally reflected in the strut angle limitations presented in current design codes and accepted research. For example, ACI (2008) places a limit on the minimum angle that is permissible between a strut and tie. This angle is shown as θ in Figure 2-13 (a) and is limited to 25 degrees. The 25-degree limit corresponds to an a/d ratio of 2.14 in a one-panel STM.

2.4.3 Cross-Sectional STM for Inverted-T Beams

The struts, nodes, and ties (hanger and ledge reinforcement) within a typical IT beam cross-section are presented in Figure 2-14. Loads applied to the bearing pads travel from the CCT nodes to the smeared nodes within the web of the cross-section via direct

struts. Loads are then hung on the compression chord by hanger reinforcement. The load transfer after this is shown using the longitudinal STM provided in Figure 2-15 (b), where the load is transferred to the supports through either a one- or two-panel mechanism discussed in Section 2.4.2. In Section 2.2.5, the geometry of each node was constrained by a bearing pad at a minimum. Examination of the cross-sectional strut-and-tie model in Figure 2-14, reveals that the bottom pair of nodes are not constrained in such a manner. Nodes without clearly defined geometries were labeled as smeared nodes in TxDOT Project 0-5253 and were not subject to independent stress checks. The same approach was taken in the current study. The CCT nodes within the cross-sectional model were proportioned using the procedure described in Section 2.2.5.

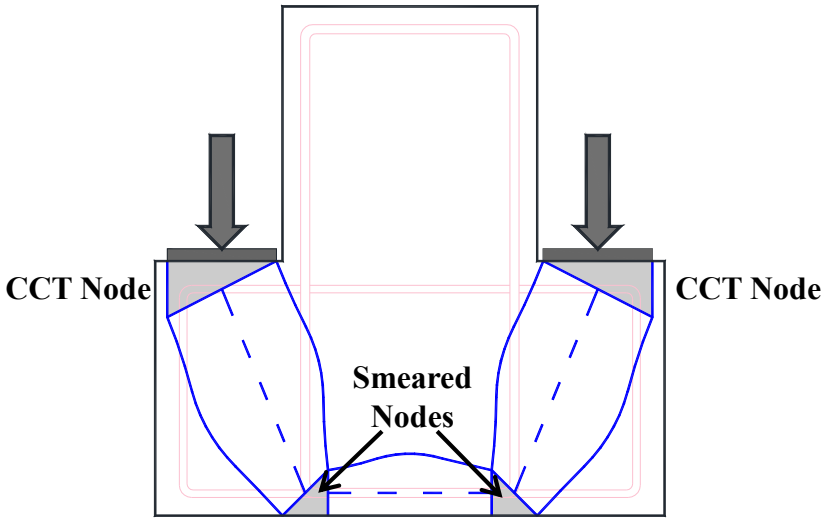

Figure 2-14: Typical cross-sectional STM for IT specimen

2.4.4 Three-Dimensional STM for Inverted-T Beams

In IT beams, the multi-directional load transfers require a three dimensional STM to fully capture load paths from loading points to supports. The three-dimensional problem (Figure 2-15(a)) can however be simplified into two interdependent two-dimensional strut-and-tie models, as shown in Figure 2-15 (b) and (c).

To design the IT beam specimens for this study (TxDOT Research Project 0-6416), the external loads were first applied to the longitudinal STM (Figure 2-15 (b)). Vertical tie forces obtained from analysis of the longitudinal model were then applied to the cross-sectional STM. Each of the vertical tie forces in the longitudinal model were evenly distributed among the two stirrup legs (ties) of the cross-sectional model. The cross-sectional STM (Figure 2-15 (c)) was then used to design the horizontal ledge tie and perform stress checks on the CCT nodes underneath the load points.

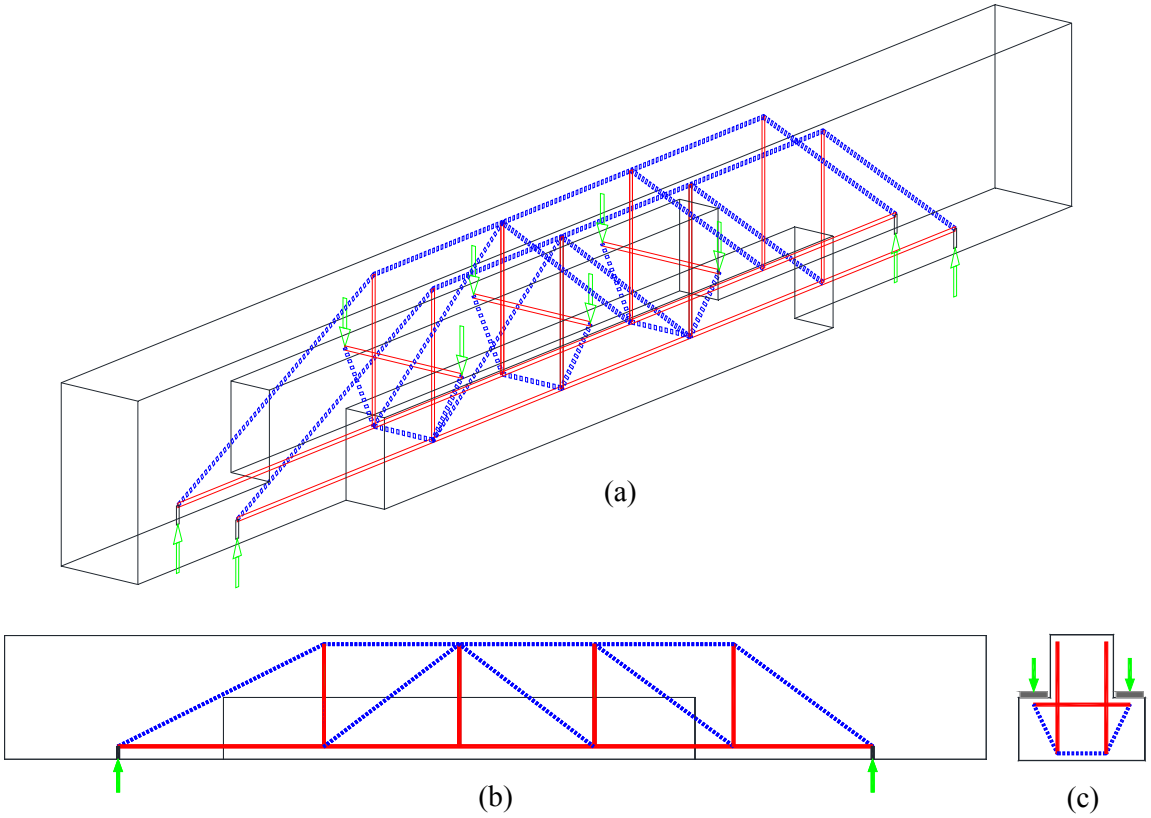

Figure 2-15: STMs used for IT design; (a) three-dimensional, (b) longitudinal, and (c) cross-sectional

2.5 SUMMARY

Background information about strut-and-tie modeling is given in this chapter. STM is used in design to simplify the flow of forces in D-regions, where strains vary

nonlinearly across the depth of a section. A STM is comprised of compression elements (struts), tension elements (ties) and the intersection of such elements (nodes). When using STM for design, enough reinforcement must be provided to resist forces in all ties, while section geometry must be selected to ensure stresses at nodal faces do not cause concrete crushing.

When a deep beam is loaded at the bottom chord, as is the case in inverted-T deep beams vertical ties at the load points need to "hang" the load to the top compression chord and are therefore stressed higher than those in top-chord loaded beams. The additional tension created around loading points in inverted-T beams can affect the behavior significantly. Inverted-T deep beams also require more elaborate STMs to account for both cross sectional and longitudinal behaviors; which can be achieved with either a three dimensional model or two two-dimensional models.

An introduction and explanation of the experimental program is discussed in detail in Chapter 3. The specimens designed in the experimental program are all designed using the STM procedure as discussed in this chapter.

CHAPTER 3
Experimental Program

3.1 INTRODUCTION

The experimental program is discussed in this chapter. The experimental program was carefully designed to investigate the effects of differing shear span-to-depth ratios, web reinforcement ratios, ledge lengths, ledge depths and web depths. To date, 11 specimens have been constructed and 22 tests have been performed on nine of the constructed specimens. The focus of the program to date has been on the effects that different web reinforcement ratios and ledge lengths have on strength and serviceability performance. Following the discussion on the testing program, the materials used, test set-up, and the construction and testing of the members are described.

3.2 TESTING PROGRAM

An ongoing literature search has yet to reveal experimental data which addresses the objectives of the current study. While a significant number of inverted-T tests (over 50 specimens; refer to Figure 3-1) have been reported within the literature, few of the specimens have been of relevant size and achieved the appropriate failure mode: shear. Furthermore, very few of the studies include information on diagonal cracking under service loads; a detail which is essential to the study of serviceability in the current project. Distressed inverted-T bent caps found within the field are included in Figure 3-1 to highlight the small nature of the specimens reported within the literature.

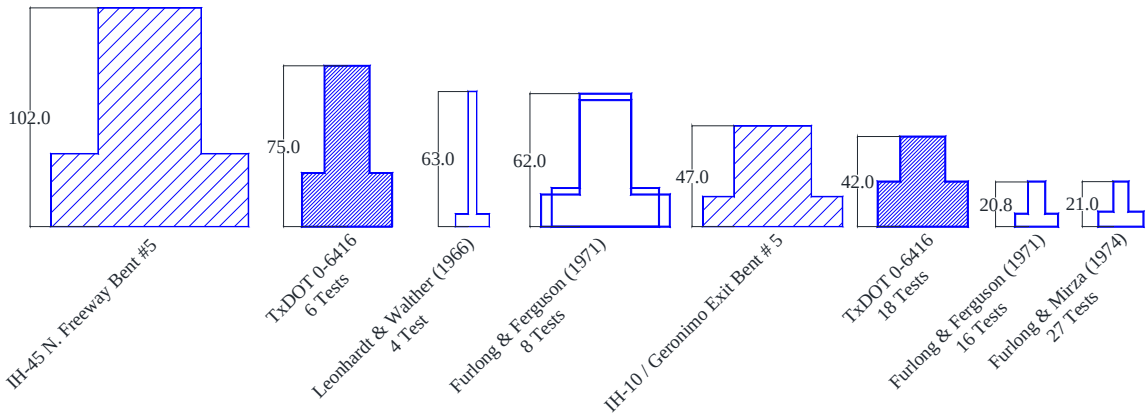

Figure 3-1: Scaled comparison between actual bent caps and beams included in past research programs.

Due to the lack of relevant information within the literature, a comprehensive testing program was developed to study the strength and serviceability of inverted-T beams. As shown in Figure 3-2, the experimental program is designed to consider the variables that are most relevant to the shear behavior of IT beams.

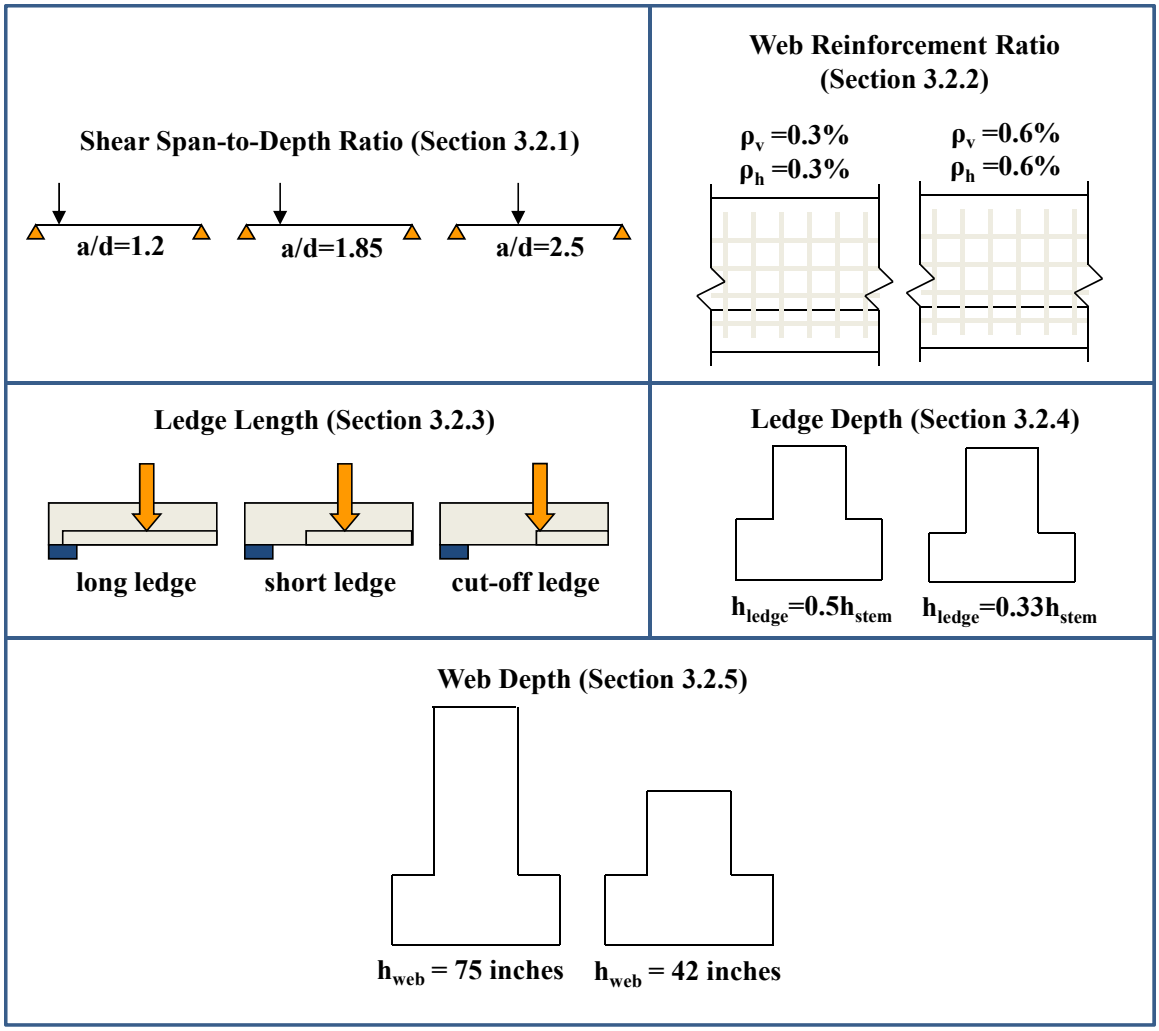

Figure 3-2 - Summary of experimental variables

In order to independently investigate each variable (with one exception: shear span-to-depth ratio), the IT beam tests were divided into five different series. The shear span-to-depth ratio was varied within each series to examine its interaction with each of the five other variables. Each of the five series of tests are outlined below and detailed within Table 3-1 through Table 3-4.

- Series I: Web Reinforcement Ratio
- Series II: Ledge Length
- Series III: Ledge Depth
- Series IV: Web Depth

A general description of each test series and the details of the specimens used in each series are provided in Sections 3.2.2 through 3.2.5. Due to the relevance of shear span-to-depth ratio to each test series, the following section (3.2.1) provides a definition and general discussion of shear span-to-depth ratio within the context of this project.

3.2.1 Shear Span-to-Depth Ratio

Although the shear span is defined in many ways within the literature, it is typically taken as the distance between the point of maximum and minimum (i.e. zero) shear in a member. For a beam subjected to a single point load, the shear span is simply the distance between the point load and the closest support. This loading scenario is depicted in Figure 3-3. The shortest shear span is denoted as *a*.

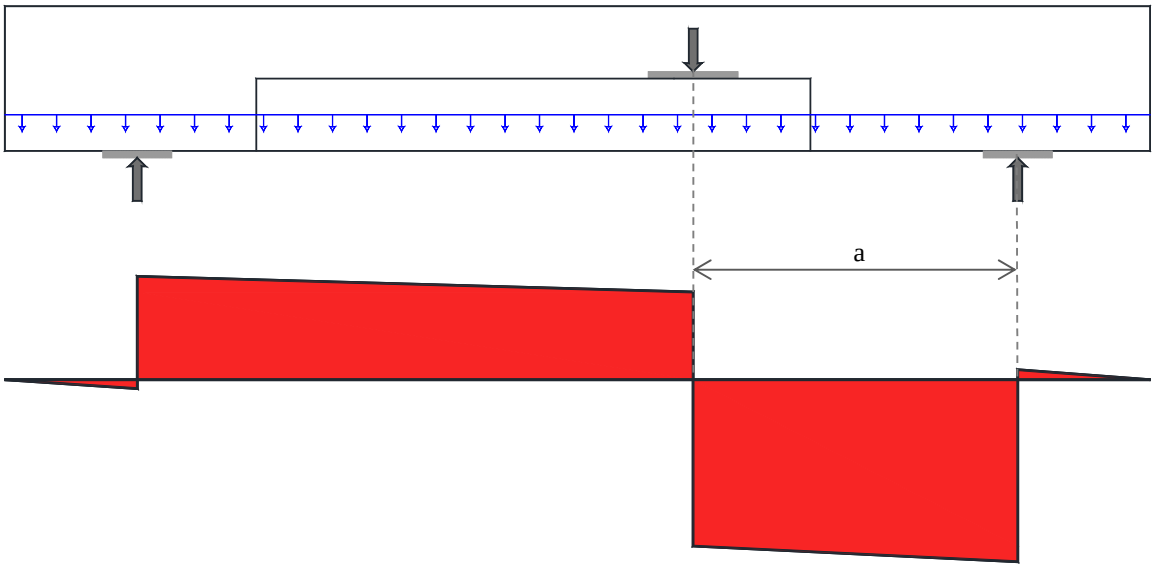

Figure 3-3: Free-body and shear force diagrams for a member subjected to a single point load

The effective depth, *d*, of the member is typically taken as the distance between the extreme compression fiber and the centroid of the flexural tension reinforcement, as shown in Figure 3-4. The resulting ratio of the shear span to the effective depth (*a/d*) is generally indicative of the member behavior under load: (*a/d* < 2.0) deep beam behavior,

or (a/d > 2.5) sectional shear behavior. Members with a shear span-to-depth ratio between 2.0 and 2.5 typically display mixed (transitional) behavior.

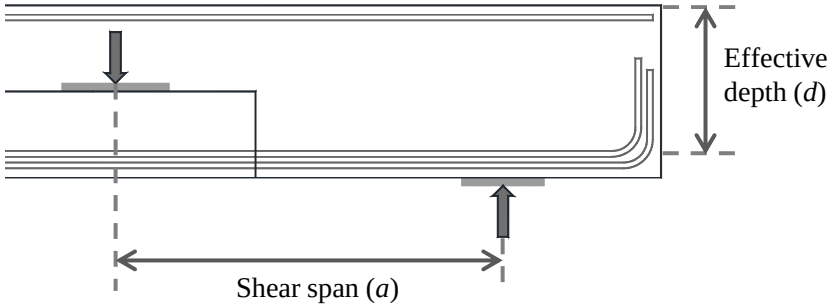

Figure 3-4: Shear span and effective depth definitions for a member subjected to a single point load

Determination of the shear span in a beam loaded at several points, or subject to continuous loads, is not as straightforward as the case above. In a member subjected to three point loads, as shown in Figure 3-5, the shear span should (per earlier definition) be the distance from the center point load to the near support; again denoted a. The a/d ratio derived according to this rationale, however, may not adequately represent the controlling behavior. A more useful value for computation of the shear span-to-depth ratio may be the distance from the fascia load, or outermost load point, to the support. This value is denoted as a_f in Figure 3-5. All further reference to the shear span-to-depth ratio in this thesis, denoted as a/d in Table 3-1 through Table 3-4, will be based upon the latter definition.

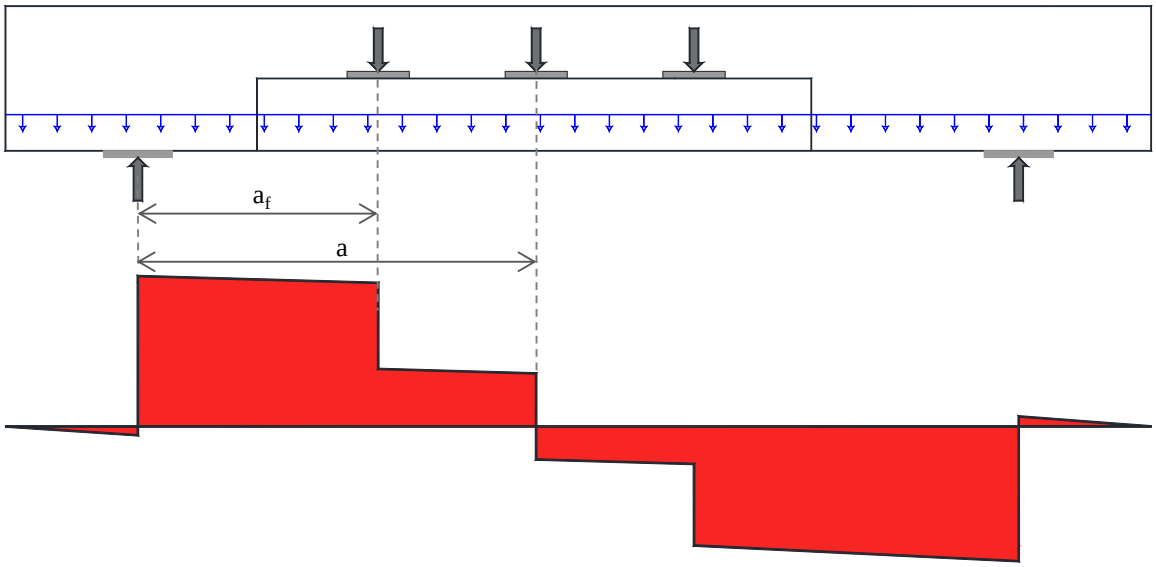

Figure 3-5: Free-body and shear force diagrams for a member subjected to three point loads

Shear span-to-depth ratios of 1.85 and 2.50 were selected for the purposes of the test program; see Figure 3-6. Two critical factors guided the selection of these shear span-to-depth ratios:

1. *Shear span-to-depth ratios of 1.85 and 2.50 were representative of the harshest loading conditions experienced by cracked inverted-T straddle bents in the field.* Referencing the IT straddle cracking database (Bayrak 2009), the inverted-T shear spans subject to cracking in the field ranged from an a/d ratio of 0.8 to an a/d ratio of 2.5. The a/d ratio of 1.85 was selected to capture the "deep" beam behavior of IT beams, while the a/d ratio 2.5 was selected to capture behavior at the transition to sectional behavior.

2. *Use of shear span-to-depth ratios of 1.85 and 2.50 would facilitate comparisons between the indirectly loaded IT specimens and the directly loaded specimens of TxDOT Project 0-5253.* Detailed justification for the use of shear span-to-depth ratios of 1.85 and 2.50 can be found within the final report of TxDOT Project 0-5253 (Birrcher, et al. 2008).

In short, the shear span-to-depth ratios represented the controlling load configurations for both deep beam and sectional behavior.

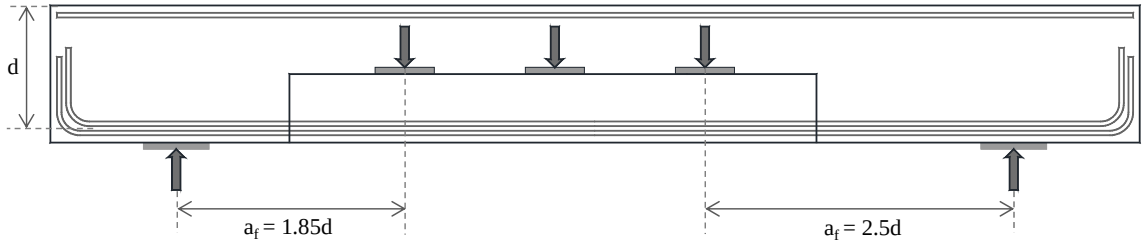

Figure 3-6: Typical specimen for TxDOT Project 0-6416

Members were constructed to include shear spans of 1.85d and 2.5d at alternate ends; shown in Figure 3-6. Two tests could therefore be performed on one beam specimen. As a deep beam region generally has greater load-carrying capacity than a sectional region, the sectional shear span was tested first and then repaired to allow failure of the alternate (deep beam) shear span.

3.2.2 Series I: Web Reinforcement Ratio

The first series of tests was designed to examine the effect of the web reinforcement ratio on the strength and serviceability of both deep beam and sectional shear spans. Web reinforcement is described in detail in Chapter 2.

Two reinforcement ratios, 0.3% and 0.6%, were chosen for the experimental program. The relative distribution of reinforcement for both ratios is illustrated in Figure 3-7. Selection of the web reinforcement ratios was based upon current TxDOT design requirements (TxDOT 2009), the findings of TxDOT Project 0-5253 and typical reinforcement details found in the field:

1. *TxDOT currently requires a minimum of 0.3% crack control reinforcement in both the horizontal and vertical directions of inverted-T beams.* The TxDOT design requirements for IT beams are based on the AASHTO LRFD Bridge Design Specifications (2009), summarized below. It should be noted that AASHTO LRFD permits designers to

utilize crack control reinforcement to satisfy the requirements of tie (shear) and hanger reinforcement.

$$\frac{A_v}{b_w s_v} \geq 0.003 \qquad (5.6.3.5\text{-}1)$$

$$\frac{A_h}{b_w s_h} \geq 0.003 \qquad (5.6.3.5\text{-}2)$$

2. *The minimum amount of web reinforcement (0.3%) specified in the AASHTO LRFD Bridge Design was reaffirmed by the results of TxDOT Project 0-5253.* The maximum web reinforcement ratio tested over the course of TxDOT Project 0-5253 corresponds to the minimum crack control requirements of the current AASHTO LRFD (i.e. 0.3%). TxDOT Project 0-5253 researchers found that additional web reinforcement generally decreased crack widths, and in the case of sectional shear spans, increased capacity. With respect to the current study, the use of 0.3% and 0.6% web reinforcement will help to establish whether or not the same benefits apply to indirectly loaded specimens.

3. *The minimum and maximum web reinforcement ratios selected for this study correspond to the reinforcement details typically found in cracked inverted-T beams found within the field.* For inverted-T beams listed within the straddle cracking database (Bayrak 2009), the lowest web reinforcement ratio was about 0.3%, while the highest web reinforcement ratio was about 0.6%.

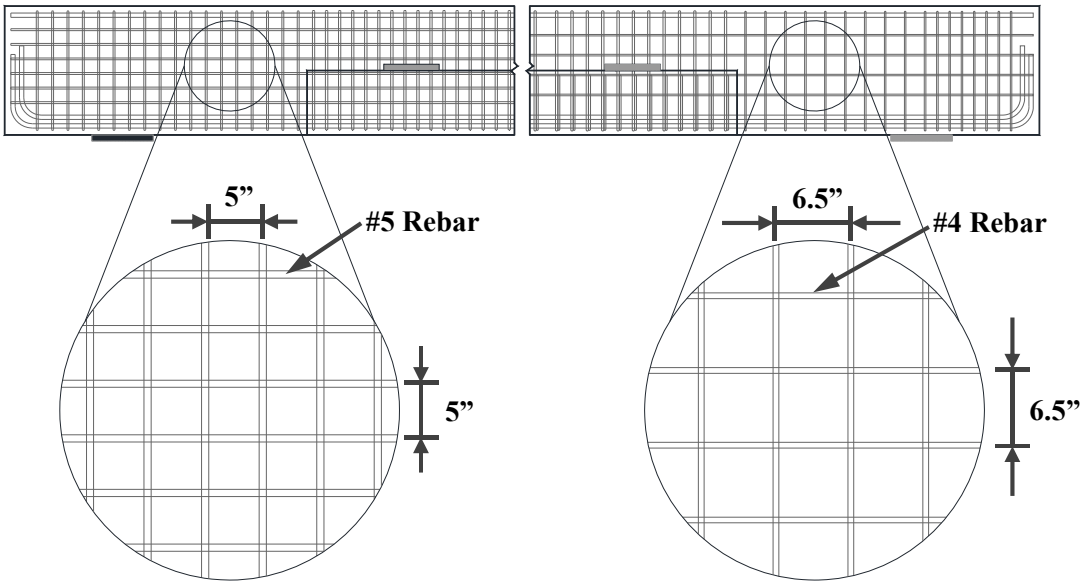

Figure 3-7: Typical web reinforcement ratios; (a) 0.6% and (b) 0.3%

As shown in Table 3-1, Series I includes the necessary specimens to investigate the strength and serviceability effects of 0.3% and 0.6% web reinforcement relative to each of the other variables. It should be noted that both shear spans within each specimen are generally reinforced to the same degree; either 0.3% on both ends or 0.6% on both ends.

Table 3-1: Series I: Web Reinforcement

Series	b_w in.	d in.	No. of Point Loads	Ledge Depth	Ledge Length	a/d ratio	ρ_v	ρ_h
Series I: Web Reinforcement Effect	21	38.5	1	0.5h	Short	1.85	0.003	0.003
							0.006	0.006
						2.5	0.003	0.003
							0.006	0.006
					Long	1.85	0.003	0.003
							0.006	0.006
						2.5	0.003	0.003
							0.006	0.006
			3		Short	1.85	0.003	0.003
							0.006	0.006
						2.5	0.003	0.003
							0.006	0.006
				0.33h		1.85	0.003	0.003
							0.006	0.006
						2.5	0.003	0.003
							0.006	0.006
					Long		0.003	0.003
							0.006	0.006
	21	68.9	1		Short	1.2	0.003	0.003
							0.006	0.006
						1.85	0.003	0.003
							0.006	0.006
						2.5	0.003	0.003
							0.006	0.006

3.2.3 Series II: Ledge Length

The length of the ledges utilized within the cracked inverted-T beams was noted to vary greatly during compilation of the straddle cracking database. At the extremes, the ledge either extended all the way to the support, or stopped at the very outer edge of the fascia bearing pad. Series II testing was therefore designed to investigate the effect of

ledge length on the strength and serviceability of both deep beam and sectional shear spans. The selected ledge configurations are illustrated in Figure 3-8. They effectively represent the extreme and intermediate ledge configurations found in the field.

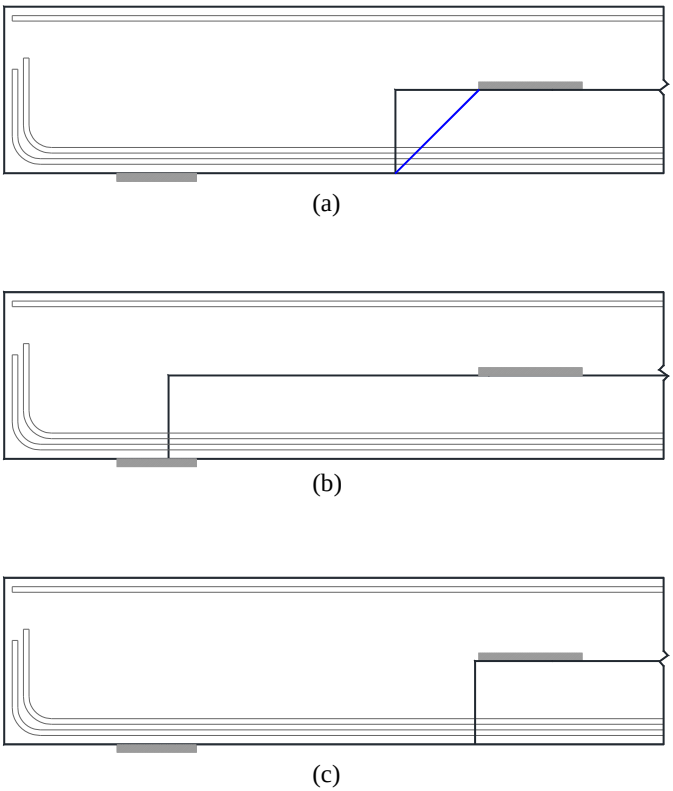

Figure 3-8: Typical ledge configurations; (a) short ledge, (b) long ledge and (c) cut-off ledge

More specifically, the various ledge configurations were introduced to investigate their effects on the transfer of ledge loads to the hanger reinforcement. AASHTO LRFD (2009) currently recommends distributing the hanger reinforcement over an assumed influence length. This influence length is defined by extending a 45-degree line from each edge of the bearing pad to the bottom face of the inverted-T, as shown in Figure 3-9. However, the validity of this assumption comes into question when the ledge is potentially too short to engage all of the hanger reinforcement within the web. This is the case in the "cut-off" ledge shown in Figure 3-9. Examination of all three ledge configurations will establish: (1) the degree to which the ledge loading 'spreads' to the

hanger reinforcement and (2) the effect of ledge configuration on the transfer of ledge loads to the hanger reinforcement.

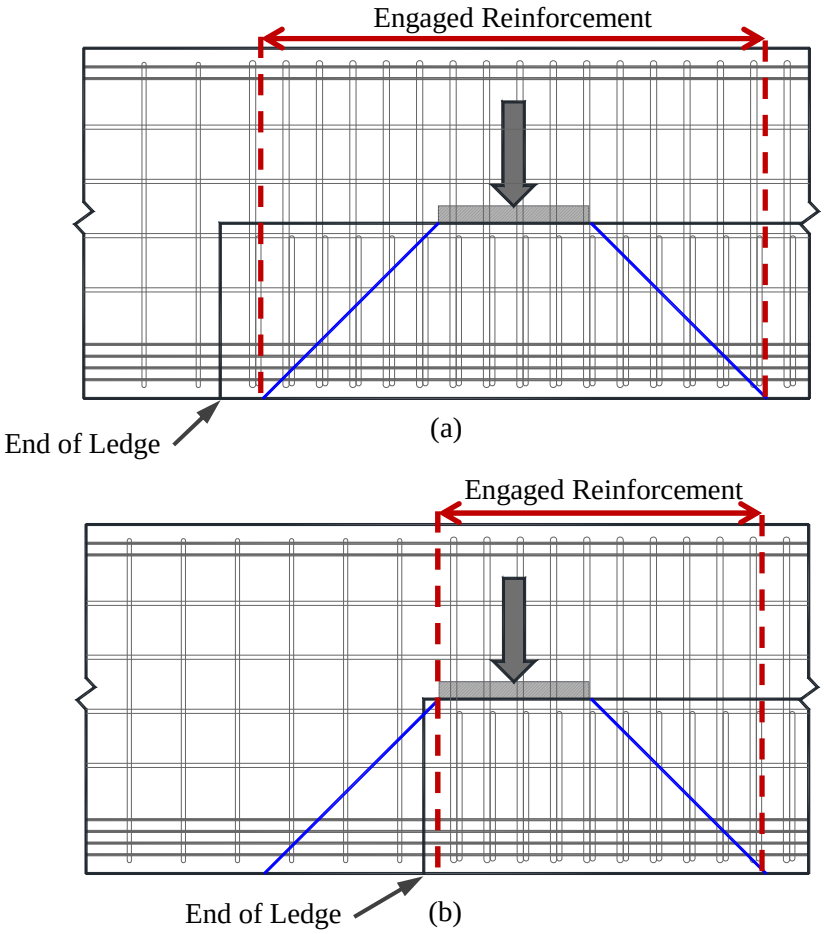

Figure 3-9: 45-degree load spread shown on (a) short ledge length and (b) cut-off ledge length

The test matrix for the second series was designed to isolate the effect of varying ledge length in different specimen configurations (see Table 3-2). In general, each long or cut-off ledge specimen can be directly compared to a short ledge specimen, with all other variables kept constant.

Table 3-2: Series II: Ledge Length Effects

Beam I.D.	b_w in.	d in.	No. of Point Loads	Ledge Depth	Ledge Length	a/d ratio	ρ_v	ρ_h
Series II: Ledge Length Effects	21	38.5	1	0.5h	Short	1.85	0.003	0.003
					Long			
					Short		0.006	0.006
					Long			
					Short	2.5	0.003	0.003
					Long			
					Short		0.006	0.006
					Long			
			3	0.33h	Short	2.5	0.003	0.003
					Long			
					Short	1.85	0.006	0.006
					Cut-off			
					Long			
					Short	2.5	0.006	0.006
					Cut-off			
					Long			

3.2.4 Series III: Ledge Depth

Series III testing was designed to investigate the effect of ledge depth on the strength and serviceability of inverted-T beams. Varying the ledge depth was important for two reasons. Multiple ledge depths were required in order to encompass various ledge depths found in the field and to study the transition between top chord and bottom chord loading.

1. *The minimum and maximum ledge depths selected for this study correspond to the ledge depths typically found in cracked inverted-T beams found within the field.* For inverted-T beams listed within the straddle cracking database (Bayrak 2009), the ledge depth-to-web height ratio generally ranged from 0.3 to 0.45. Minimum and maximum ledge depths of 0.33h and 0.5h (Figure 3-10) were therefore selected to

encompass most, if not all, field configurations within the limitations of the laboratory.

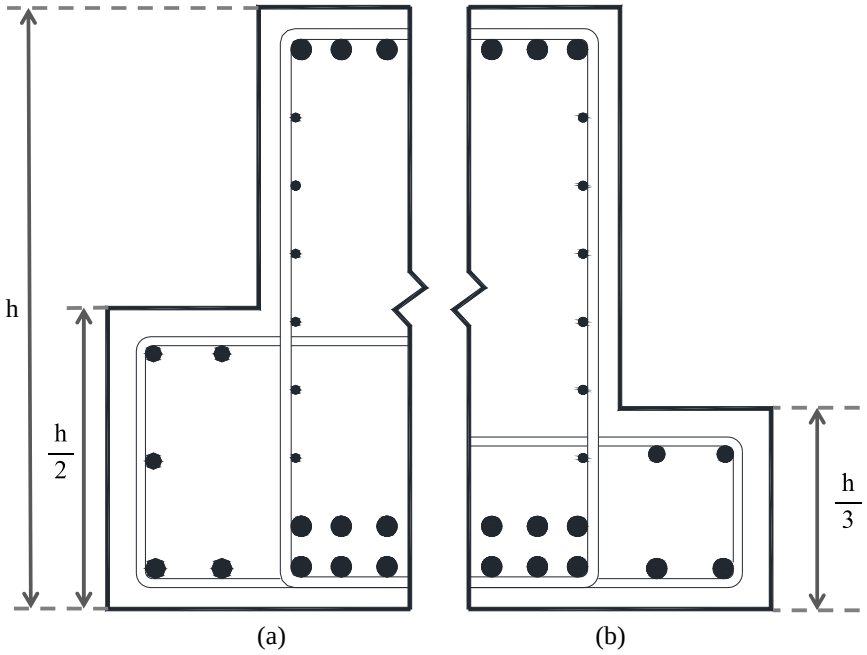

Figure 3-10: Typical ledge depths; (a) half web height and (b) third web height

2. *The shallower the ledge, the larger the distance the load must travel to be hung on to the compression chord.* Assuming a 45 degree load spread, the beam with a shallower ledge will perform closer to an ideal bottom chord loaded specimen. Figure 3-11 shows the increased distance the load must travel when a shallower ledge is introduced.

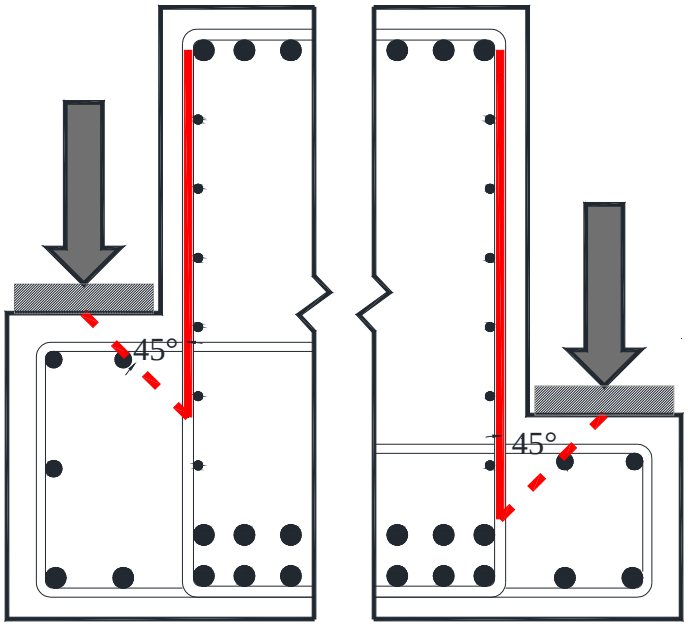

Figure 3-11 - Effect of (a) deep and (b) shallow ledge depth on hanger reinforcement engagement

Members were constructed to have either a ledge depth of 0.33h or 0.5h along the length of the entire ledge. The ledge was designed not to control the design. The ledge depths selected for investigation are shown in Figure 3-10; Series III is outlined in Table 3-3.

Table 3-3: Series III: Ledge Depth Effects

Beam I.D.	b_w in.	d in.	No. of Point Loads	Ledge Depth	Ledge Length	a/d ratio	ρ_v	ρ_h
Series III: Ledge Depth Effects	21	38.5	3	0.5h	Short	1.85	0.003	0.003
				0.33h				
				0.5h			0.006	0.006
				0.33h				
				0.5h		2.5	0.003	0.003
				0.33h				
				0.5h			0.006	0.006
				0.33h				

3.2.5 Series IV: Web Depth

The purpose of Series IV was to investigate the effect of member depth on the strength and serviceability performance of inverted-T beams. It has been demonstrated by numerous past research that beam depth can have a significant effect on shear behavior (Kani 1967). It is therefore important to test specimens with heights that adequately represent members in the straddle bent database (Figure 3-1).

1. *Project 0-5253 suggested that using a strut-and-tie analysis for deep beam design (a/d < 2) nearly eliminates size effect (reduction in shear strength due to an increase in beam depth) (Birrcher, et al. 2008).* This conclusion was made analyzing results only from compression-chord loaded specimens. The applicability of size effect on tension-chord loaded specimens is unknown and will be studied in this series.
2. *Testing larger specimens will allow us to validate the data taken from our smaller specimens to larger beams found in the field.* As shown in Figure 3-1, although the smaller 42 inch specimens tested more closely resemble beams in the field than past research, beams in the field are still much larger. This series will allow the results of the smaller specimens to be applied in the design and analysis of the larger members.
3. *Results from Project 0-5253 suggest that an increase in beam depth from 42 inches to 75 inches does not affect either the diagonal cracking strength or the widths of the diagonal cracks in compression chord loaded members.* This conclusion was made based on the results from compression chord loaded specimens found in four different studies: Birrcher, et al. 2008, Tan and Lu 1999, Walraven and Lehwalter 1994, and Zhang and Tan 2007. These results must now be verified for tension chord loaded specimen in order to verify serviceability applications.

Two member depths were selected for this project, h=42” and h=75”, shown in Figure 3-12. These depths cover a good range of IT depths found in the field and match depths used in Project 0-5253; thus allowing for direct comparison between top and bottom-chord loaded specimen. The specimens to be constructed and tested in the experimental program are summarized in Table 3-4.

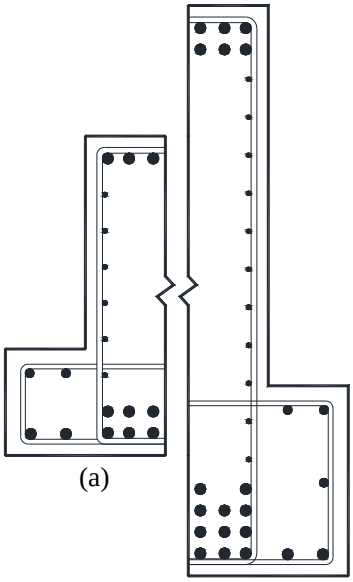

Figure 3-12: Web heights; (a) 42 inches and (b) 75 inches

Table 3-4: Series IV: Depth Effect

Beam I.D.	b_w in.	d in.	No. of Point Loads	Ledge Depth	Ledge Length	a/d ratio	ρ_v	ρ_h
Series IV: Depth Effect	21	38.5	3	0.33h	Short	1.85	0.003	0.003
		68.9	1					
		38.5	3				0.006	0.006
		68.9	1					
		38.5	3			2.5	0.003	0.003
		68.9	1					
		38.5	3				0.006	0.006

3.2.6 Progress to Date

The specimens constructed to date are presented in Table 3-5. To date, 11 specimens have been constructed and nine specimen tests have been completed. This thesis includes results and analysis of the first five specimens. The testing of the other specimens has occurred since the completion of this thesis. In order to reference the different test specimens, a general nomenclature was developed. This nomenclature is presented in Figure 3-13.

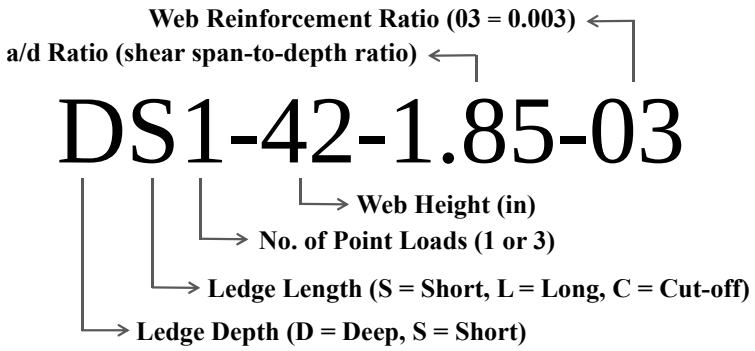

Figure 3-13: Nomenclature used for testing program

With the exception of the bearing plate dimensions, definitions for all of the variables included in

Table 3-5 can be found in Chapter 2. Dimensions of the load and support plates are measured in the longitudinal and transverse direction (i.e. l x w) of each inverted-T specimen. The variables used in

Table 3-5 are also introduced and discussed in Chapter 2.

Table 3-5: Details for specimen constructed to date

Beam I.D.	Series	b_w in.	h in.	d in.	Ledge Depth	Ledge Length	ρ_l	ρ_l'	ρ_v	Size and Spacing (s_v)	ρ_h	Size and Spacing (s_h)	Support Plate in.	Load Plate in.	a/d ratio
DS1-42-1.85-03	I, II	21	42	38.5	0.5h	Short	0.0231	0.0115	0.0029	#4 @ 6.5”	0.0029	#4 @ 6.5”	20x21	26x9	1.96
DS1-42-2.5-03	I, II	21	42	38.5	0.5h	Short	0.0231	0.0115	0.0029	#4 @ 6.5”	0.0029	#4 @ 6.5”	20x21	26x9	2.65
DS1-42-1.85-06	I, II	21	42	38.5	0.5h	Short	0.0231	0.0115	0.0059	#5 @ 5”	0.0062	#5 @ 4.75”	20x21	26x9	1.85
DS1-42-2.5-06	I, II	21	42	38.5	0.5h	Short	0.0231	0.0115	0.0059	#5 @ 5”	0.0062	#5 @ 4.75”	20x21	26x9	2.5
DL1-42-1.85-06	I, II	21	42	38.5	0.5h	Long	0.0231	0.0115	0.0059	#5 @ 5”	0.0062	#5 @ 4.75”	20x21	26x9	1.85
DL1-42-2.5-06	I, II	21	42	38.5	0.5h	Long	0.0231	0.0115	0.0059	#5 @ 5”	0.0062	#5 @ 4.75”	20x21	26x9	2.5
SS3-42-1.85-03	I, II, III, IV	21	42	38.5	0.33h	Short	0.0231	0.0115	0.0029	#4 @ 6.5”	0.0029	#4 @ 6.5”	20x21	18x9	1.85
SS3-42-2.5-03	I, II, III, IV	21	42	38.5	0.33h	Short	0.0231	0.0115	0.0029	#4 @ 6.5”	0.0029	#4 @ 6.5”	20x21	18x9	2.5
SS3-42-1.85-06	I, III, IV	21	42	38.5	0.33h	Short	0.0231	0.0115	0.0059	#5 @ 5”	0.0062	#5 @ 4.75”	20x21	18x9	1.85
SS3-42-2.5-06	I, III, IV	21	42	38.5	0.33h	Short	0.0231	0.0115	0.0059	#5 @ 5”	0.0062	#5 @ 4.75”	20x21	18x9	2.5
SC3-42-1.85-03	II	21	42	38.5	0.33h	Cut-Off	0.0231	0.0115	0.0029	#4 @ 6.5”	0.0029	#4 @ 6.5”	20x21	18x9	1.85
SC3-42-2.5-03	II	21	42	38.5	0.33h	Cut-Off	0.0231	0.0115	0.0029	#4 @ 6.5”	0.0029	#4 @ 6.5”	20x21	18x9	2.5
SS1-75-1.85-03	I, IV	21	75	67.8	0.33h	Short	0.0237	0.0129	0.0029	#4 @ 6.5”	0.0029	#4 @ 6.5”	20x21	30x9	1.85
SS1-75-1.85-06	I, IV	21	75	67.8	0.33h	Short	0.0237	0.0129	0.0059	#5 @ 5”	0.0059	#5 @ 5”	20x21	30x9	1.85
SS1-75-1.2-06	I, IV	21	75	67.8	0.33h	Short	0.0237	0.0129	0.0059	#5 @ 5”	0.0059	#5 @ 5”	20x21	30x9	1.2
SS1-75-2.5-06	I, IV	21	75	67.8	0.33h	Short	0.0237	0.0129	0.0059	#5 @ 5”	0.0059	#5 @ 5”	20x21	30x9	2.5

3.3 TEST SETUP

The large-scale beam test facility, shown in Figure 3-14 and Figure 3-15, was initially designed and constructed for TxDOT Project 0-5253. The facility was utilized as originally configured with one exception. A specialized loading fixture had to be fabricated in order to load the beam through the ledges (tension chord), as opposed to the compression chord (bottom face as illustrated). The major components of the testing frame, design and construction of the loading fixture, and the different loading schemes are discussed in this section.

3.3.1 Test Frame

The test frame is primarily composed of a 96,000-pound steel strong floor that accepts six 3-inch diameter steel rods and a 7,000-pound transfer girder on each end. The test frame was configured for an upside-down simply-supported beam test. The load is typically applied to each specimen via a 5 million pound capacity hydraulic ram or three 2 million pound capacity hydraulic rams. Specialized fixtures, placed atop each hydraulic ram, allow the load to the transferred around the compression chord to the ledges of each inverted-T specimen. The 3-inch diameter steel rods resisted the applied loads at each support. The major components of the testing frame are shown in Figure 3-14. The current configuration of the testing frame can support an applied load of approximately 3 million pounds at midspan.

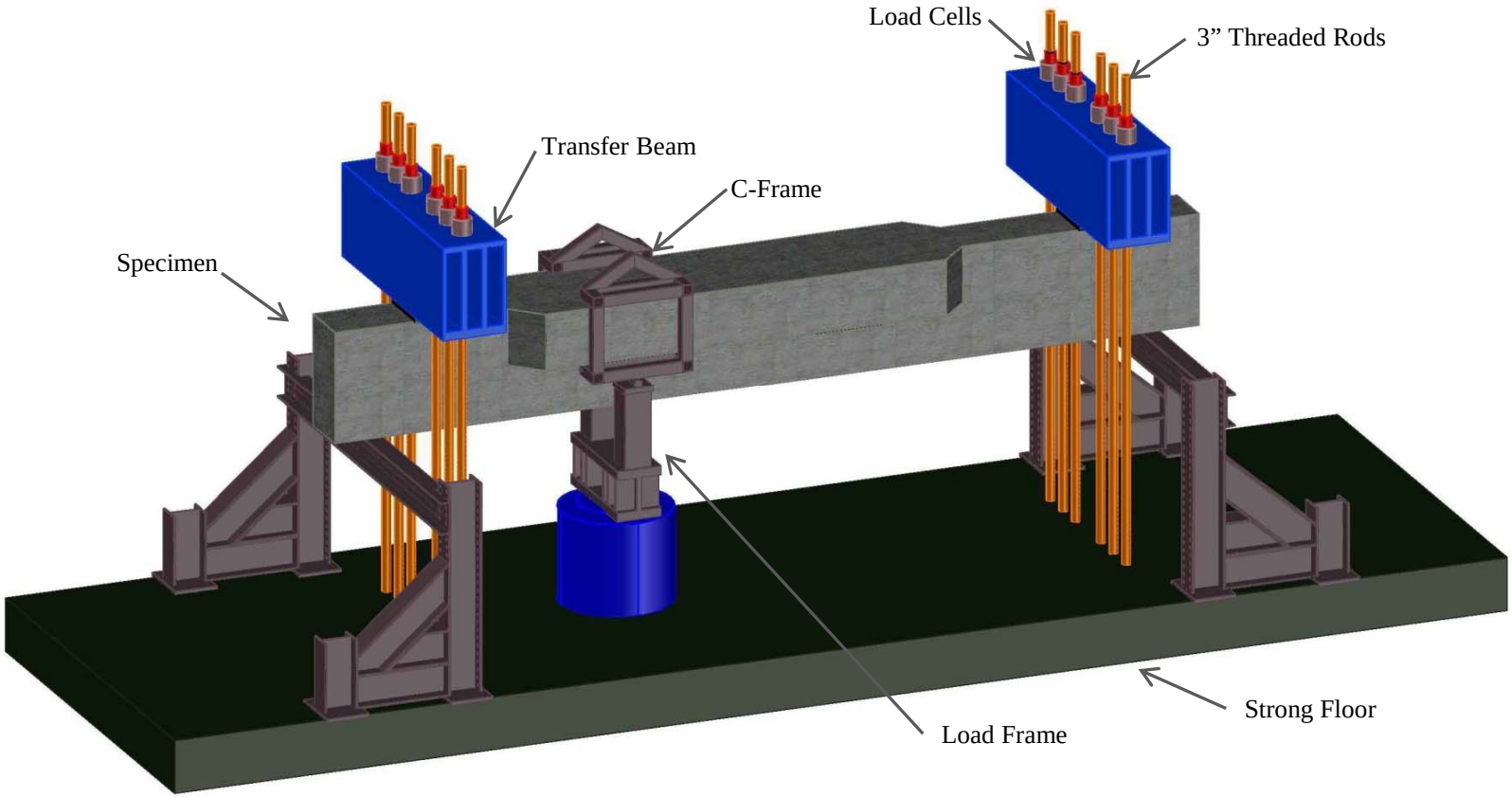

Figure 3-14: Sketch of typical beam in test frame

Figure 3-15: Inverted-T specimen subjected to single point load in test frame

3.3.2 Loading Fixture

A specialized fixture had to be constructed to load the inverted-T beams on the ledges. The fixture, shown in Figure 3-16, was designed to support a load of 3 million pounds with minimal deflection. The load fixture consists of a stiffened, 19-inch deep steel wide flange member with 3-inch thick flanges. This member transfers the load from the center point of the hydraulic ram to vertical structural tubes (2 at 10" x 10" x 5/8") at either end. Each structural tube carries the load to a 2-inch thick steel plate topped with a 2-inch diameter steel roller. 7-inch thick steel plates topped with ¼-inch thick reinforced neoprene bearing pads then distribute the load evenly among the bearing areas on opposite ledges.

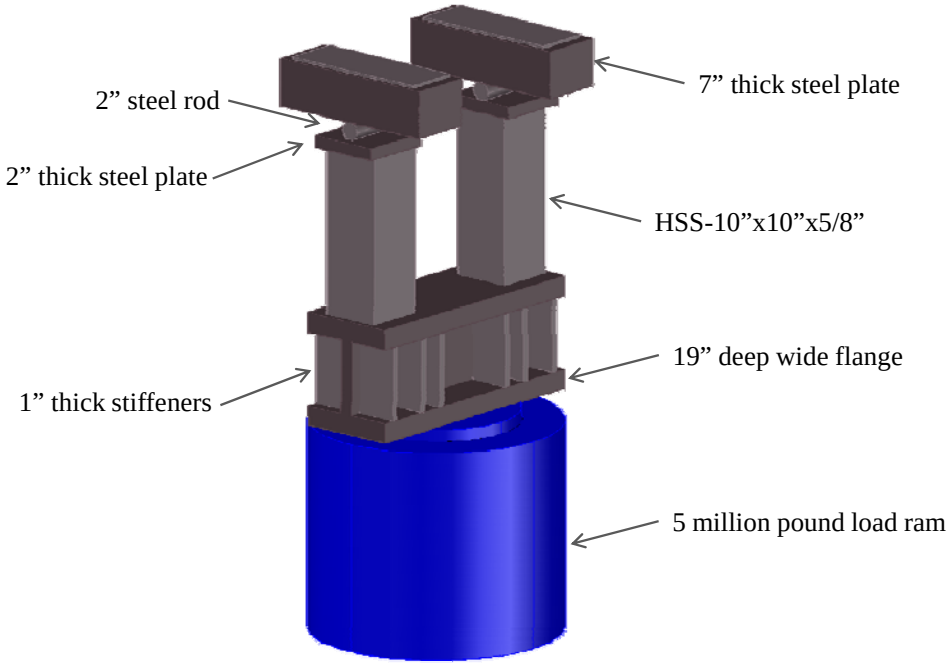

Figure 3-16: Sketch of typical loading fixture

3.3.3 Loading Schemes

Through the use of multiple hydraulic rams and loading fixtures, a number of loading schemes could be achieved. A total of three loading fixtures were constructed to

apply up to three point loads on a test specimen (Figure 3-18). If multiple point loads were to be applied, the hydraulic rams were connected in parallel to ensure equal pressure and load distribution along the ledges. In general, only one- and three-point loading schemes have been utilized to date, shown in Figure 3-17 and Figure 3-18.

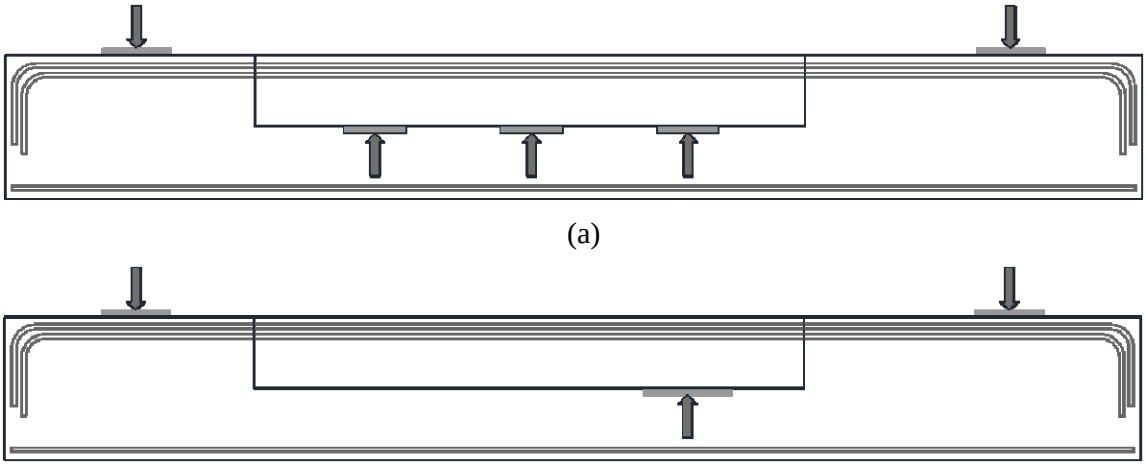

(a)

(b)

Figure 3-17: Typical loading schemes; (a) three point loads and (b) single point load

Figure 3-18: Beam specimen in test set-up with three point loads

It should be noted that utilization of different loading schemes was required to achieve the desired failure mechanism in particular beam configurations (e.g. a 42" deep beam with a third-height ledge). This in no way impaired the ability to compare the results of a one- and three-point loaded specimen. The distance between the outermost load and nearest support was maintained as a constant in both cases. The resulting shear span-to-depth ratio remained unchanged, and the loading scheme therefore had no impact on the behavior of the test regions (i.e. shear span).

3.4 FABRICATION OF SPECIMENS

Specimens were constructed using conventional materials and methods. Pre-existing formwork was customized for the current project to ensure dimensional accuracy and to expedite the construction process. The following sections document the general construction process from reinforcement cage assembly to curing measures.

3.4.1 Steel Reinforcement

All steel reinforcement was domestic Grade 60 deformed bars meeting the requirements of ASTM A615. Each shipment of the reinforcement bar was accompanied by four coupons of each bar type. These coupons were tested to find the actual yield strength and behavior of each of the reinforcement bars used in each specimen. Actual yield strengths of reinforcement bars are summarized with the experimental results in *Chapter 4*.

3.4.2 Concrete Mixture Design

TxDOT engineers typically specify Class C concrete (f'_c = 3600 psi) for IT straddle bents, but design compressive strengths of up to 5000 psi are also commonly used. In the experimental program, a design compressive strength of 4000 psi was selected to guarantee representative results. To date, measured 28-day compressive strengths of specimen concrete have ranged from 4780 psi to 6250 psi. Concrete compressive strengths were obtained from concrete cylinders conforming to ASTM C31

and tested in accordance with ASTM C39. A typical concrete mixture is presented in Table 3-6.

Table 3-6: Concrete mixture proportions

Material	Quantity
Type I Portland Cement	387 lb/cy
Fly Ash	94 lb/cy
CA: ¾" River Rock	1657 lb/cy
FA: Sand	1537 lb/cy
Water	22 gallons/cy
HRWR Admixture	19 oz/cy
Set Retardant Admixture	7 oz/cy
Water/Cement Ratio	0.48
Slump	7 inches

3.4.3 Construction of Specimen

The typical construction process of an inverted-T specimen is illustrated in Figure 3-19. Construction began with the assembly of the reinforcing cage, shown in Figure 3-19 (a). The cage was assembled in an inverted fashion to accommodate the inverted testing configuration. The longitudinal tension steel was placed and tied, using wood spacers to ensure proper spacing, and the vertical stirrups and ledge reinforcement were placed and tied. The compression longitudinal steel, horizontal web reinforcement and longitudinal ledge reinforcement were then placed and tied. After the cage was completed, internal strain gauges were installed, as discussed in 3.5.1.

Following assembly of the formwork, the fully instrumented reinforcement cage was dropped inside (Figure 3-19 (b) and (c)). Top and bottom cross-ties were used to prevent spreading of the formwork sidewalls during concrete placement.

Figure 3-19: Fabrication of a typical specimen; (a) Construction and instrumentation of cage, (b) fully instrumented reinforcement cage being dropped in formwork, (c) reinforcement cage in the fully assembled formwork, (d) concrete bucket used in concrete placement, (e) internal vibration used to ensure proper consolidation, (f) screeding to obtain a proper concrete level, (g) troughs were used to finish the top of the specimen

The concrete used to fabricate each specimen was provided by a local ready-mix supplier. Concrete was placed into the formwork using a one cubic yard bucket attached to an overhead crane, shown in Figure 3-19 (d). After the concrete was placed within the formwork, both internal "stinger" vibrators and external vibrators attached to the formwork were used to ensure proper consolidation. Proper consolidation was of utmost importance due to the extremely tight bar spacing, shown in Figure 3-20. The external vibrators were attached to the sideforms on tracks that allowed the vibrators to be moved along the length of the beam. After concrete placement and initial set of the concrete, screeding and finishing operations were performed, shown in Figure 3-19 (f) and (g), respectively. The finished specimen was then covered in plastic to cure for seven days followed by at least 21 additional days before testing of the specimen, to allow the concrete to reach at least a 28 day compressive strength.

(a) (b)

Figure 3-20: Congested reinforcement cages

3.5 INSTRUMENTATION

The response of each shear span was captured with several different instruments during the shear tests. The instruments included electrical strain gages, linear potentiometers, load cells, a pressure transducer, and crack comparator cards. Details regarding these instruments and their use are outlined in the following sections.

3.5.1 Strain Measurements: Reinforcing Bars

Internal strain gages were utilized to accomplish two objectives: (1) examine the effectiveness of 0.3% and 0.6% crack control reinforcement in the compressive strut regions, and (2) identify the nature of the load transfer mechanisms between the ledge and hanger reinforcement. With reference to the first objective, internal strain gages were placed on the crack control (web) reinforcement (and aligned with the strut axes) to provide a clear indication of the strut performance (Figure 3-22 and Figure 3-23). As for the second objective, additional gages were placed on the ledge and hanger reinforcement to establish which bars were engaged in the transfer of load (Figure 3-24) for various ledge configurations. A typical arrangement of all steel gauges for an IT specimen is shown in Figure 3-21.

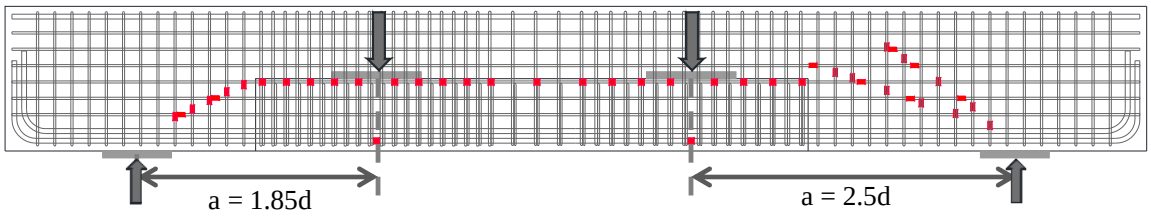

Figure 3-21: Typical layout of strain gages

Depending on the shear span-to-depth ratio, the strain gages were placed on the crack control reinforcement in different locations. The gages for a shear span of 1.85*d* were positioned along the centerline of the direct strut spanning from the support to the compression chord above the load point, as shown in Figure 3-22. The internal strain gages were placed along the centerline of the direct strut to capture the splitting behavior expected to occur in that region.

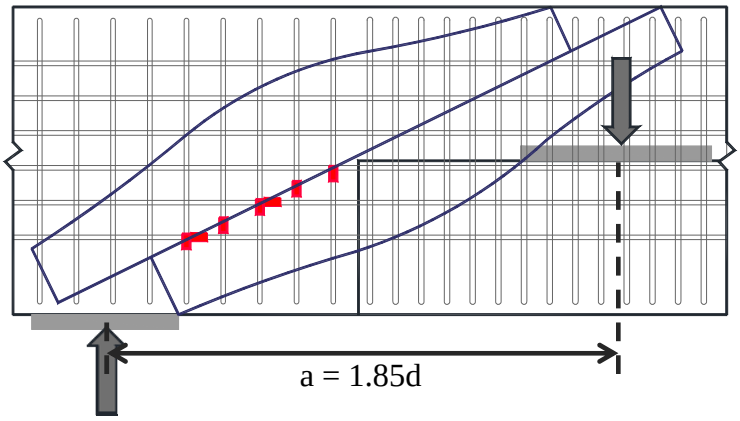

Figure 3-22: Typical gage location in a/d = 1.85 span

For a shear span of 2.5*d*, a transitional failure mechanism, between one- and two-panel failure modes, was expected to occur. The strain gages in these spans were strategically placed along: (1) the centerline of the strut closest to the support in a two-panel mechanism, and (2) the centerline of a direct strut between the support and compression chord. The gage configurations for the two-panel and one-panel mechanisms are shown in Figure 3-23 (a) and (b) respectively.

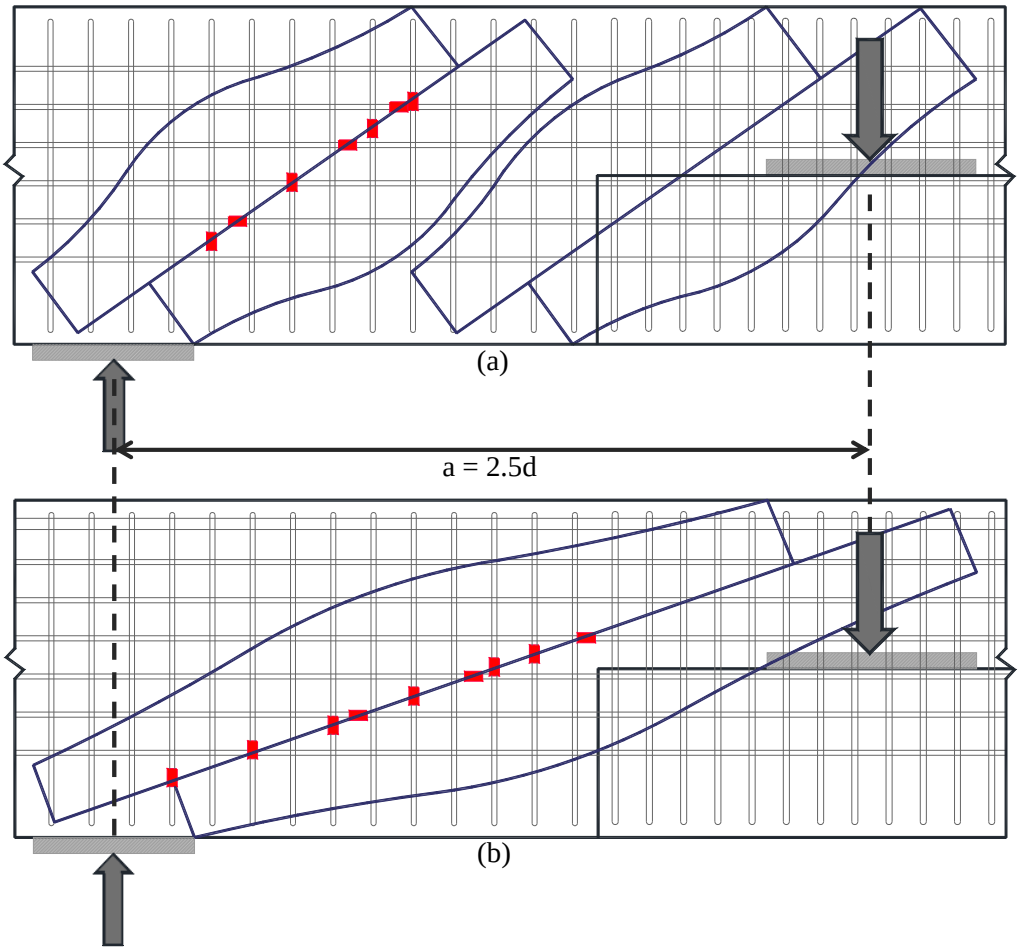

Figure 3-23: Typical gage location in a/d = 2.5 span

Strain gages placed on the ledge and hanger reinforcement were intended to measure the effectiveness of the reinforcing bars in the vicinity of each load point. The typical gage layout for the hanger and ledge reinforcement is shown in Figure 3-24. Figure 3-24 (a) illustrates the typical longitudinal locations of the gauges with respect to the load points, and Figure 3-24 (b) shows the location of the gauges on each pair of hanger and ledge reinforcement.

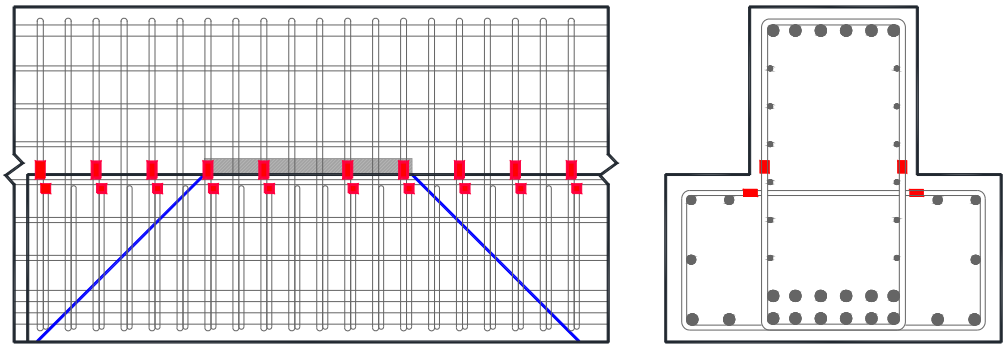

Figure 3-24: Typical ledge and hanger gage locations; (a) longitudinal and (b) cross-sectional views

The internal strain gages were FLA-3-11-10LT manufactured by Tokyo Sokki Kenkyujo Co. and intended for general purpose mild steel applications. The reinforcing bar strain gage installation process is depicted in Figure 3-25. The first step was to prepare the surface of the bar by grinding off the deformations (a), and cleaning away residue with acetone (b). The gauge was then attached to the reinforcing bar with specialized adhesive (c & d). Water and impact protection was applied via a white putty tape (e), followed by foil tape (f), and electrical tape (g). The possibility of damage to the gage from the wire pulling was minimized by providing slack in the wire (h).

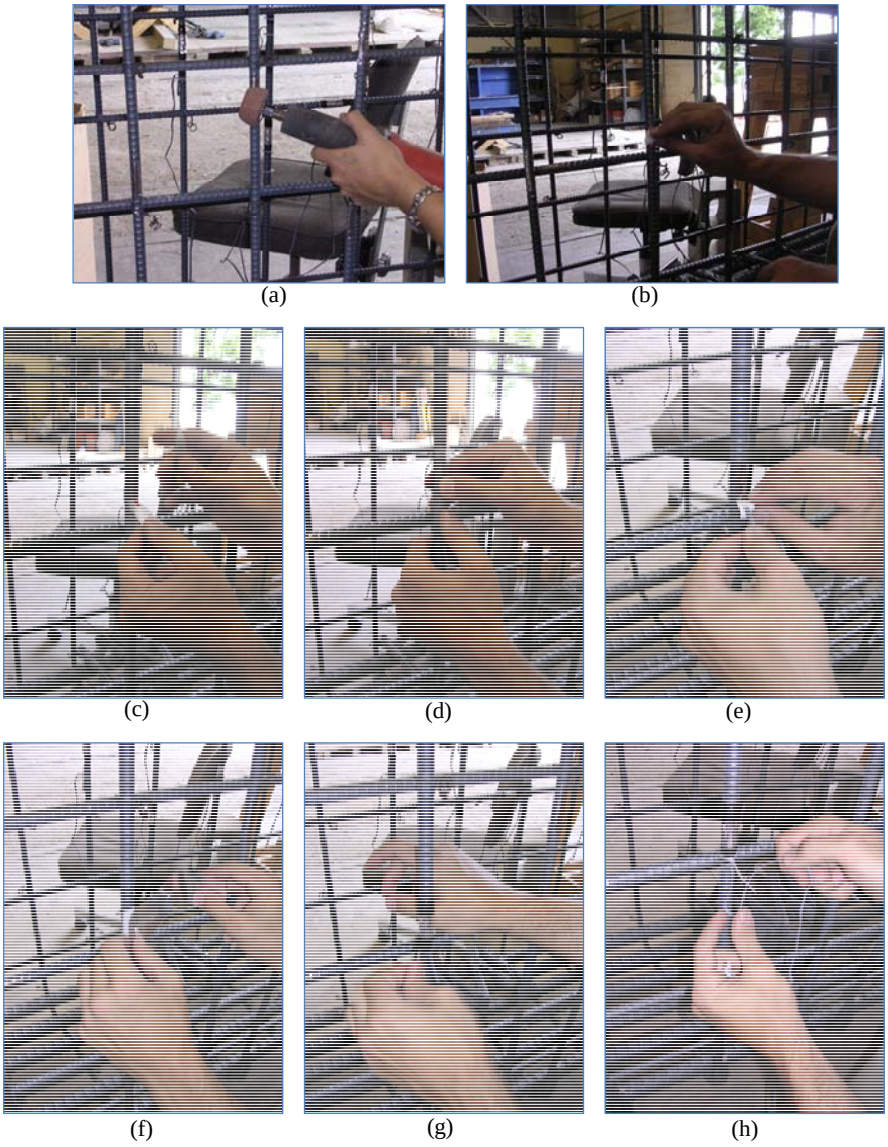

Figure 3-25: Installation of internal strain gages; (a) Deformations on reinforcement bar grinded off using a die grinder, (b) smooth surface cleaned using acetone, (c) adhesive used in attachment of gage, (d) pressure applied to the gage to ensure proper setting of adhesive, (e) putty tape applied between the entering wires and the reinforcement bar, (f) foil tape placed over the puttied gage, (g) electrical tape used to seal the ends, (h) slack provided in the wire

3.5.2 Load and Displacement Measurements

During each of the tests, the total applied load was measured via 12 load cells and a pressure gage. At the end of each of the twelve steel rods, a 500-kip load cell was sandwiched between the transfer girder and a reaction nut (Figure 3-26). Each of the load cells provided the magnitude of the load being carried by its paired rod. Uniform distribution of the support reaction over the six rods (corresponding to zero specimen torsion), was accomplished through simultaneous review of the load cell data and adjustment of the reaction nuts. A pressure gauge was attached to the hydraulic pump to record the pressure and confirm readings from the load cells.

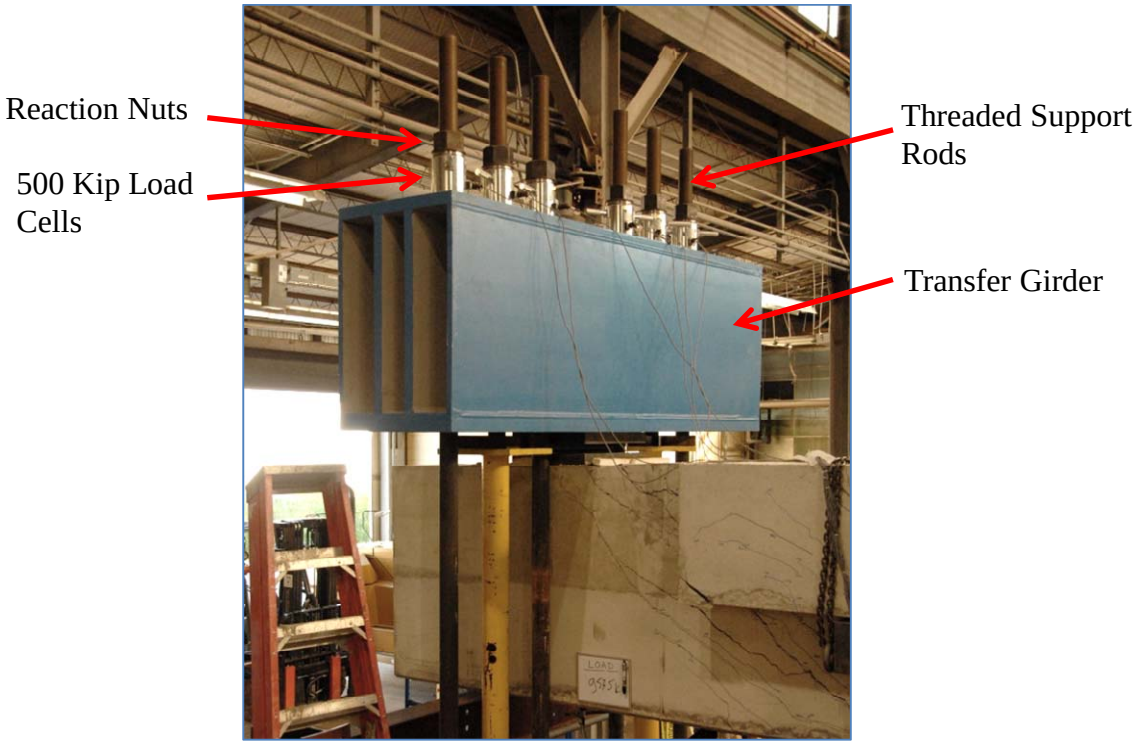

Figure 3-26: Typical support configuration

Displacements were measured by linear potentiometers placed at various locations along the member length. For specimens loaded at a single point, displacements were typically measured at the bottom (compression) side of the specimen at the support points, load point, and midspan. The location of the linear potentiometers

is shown in Figure 3-27 and Figure 3-28. Two linear potentiometers were used at the load point to check for symmetric loading and deformation of the specimen (i.e. no torsion). For specimens loaded at three points, linear potentiometers within the main span were placed at the center load point and the load point closest to the test region.

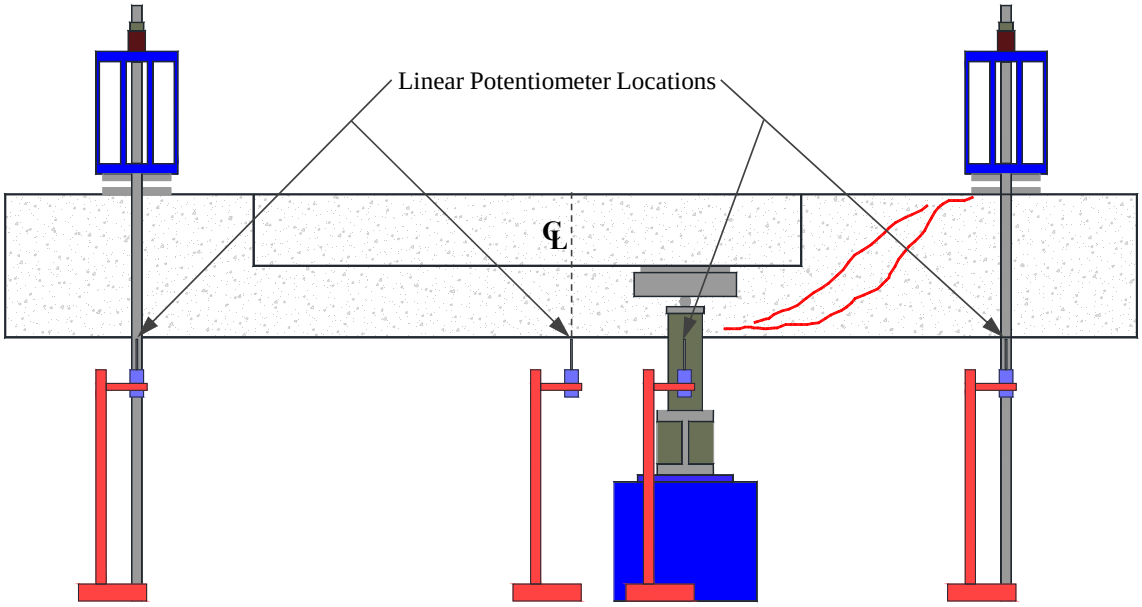

Figure 3-27 - Typical linear potentiometer locations

Figure 3-28: Typical placement of linear potentiometers at midspan and beneath the load point

3.5.3 Crack Width Measurements

In TxDOT Project 0-5253, detailed crack width measurements enabled the researchers to create a table correlating the maximum diagonal crack width to the load acting on a member (as a percentage of the ultimate capacity). Due to the utility of the resource for directly loaded beams, a similar effort was undertaken for indirectly loaded inverted-T beams.

During the testing of each specimen, crack widths were measured and recorded at 50 to 100 kip load increments. Visual measurements were made by multiple members of the research team, and averaged to reduce the effect of human error on the readings. Toward the beginning of each test, different crack locations of interest were flagged with a circle and numbered as shown in Figure 3-29. This technique enabled the research team to monitor the crack widths at specific locations throughout the course of a test. It should be noted that the exact location of the widest crack was rarely captured with one of the flagged cracks. Along with the measurement of crack widths at flagged locations, the maximum shear crack on both the north and south face was found, measured, and recorded.

Figure 3-29: Visual crack width measurement

3.6 TEST PROCEDURE

Inclusion of test regions at both ends (one shear span at 1.85*d* and one shear span at 2.5*d*) of each inverted-T beam allowed two tests to be performed sequentially per specimen; one for each region. For single-point load cases, the specimen was first tested to failure at the 1.85*d* shear span. The shear span of 1.85*d* was tested first because the initial cracking load of this span was more pertinent to the objectives of the current project. Most IT straddle bent caps in the field can be considered "deep" beams. The far shear span of 2.5*d* was typically clamped in more lightly reinforced specimens (0.3% web reinforcement) to ensure that it did not fail before the span of interest (Figure 3-30 (a)). After failing the member during the first test, each specimen was unloaded. The hydraulic ram and load fixture were then moved to the load point on the opposite end of the beam. To repair the failed region of the beam, external post-tensioning clamps were installed as shown in Figure 3-30 (b).

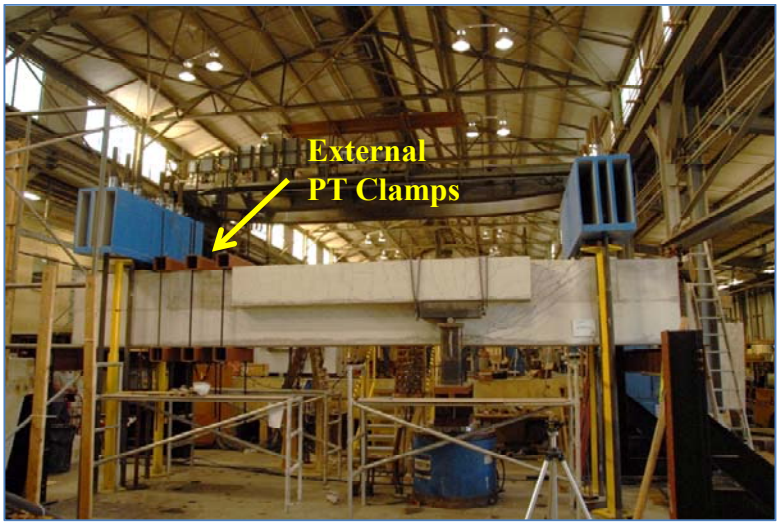

(a)

(b)

Figure 3-30: Typical single point load testing procedure for one specimen; (a) Test 1 and (b) Test 2

A similar procedure was utilized for the three-point loaded specimen, with one exception. Both test regions of a specimen loaded at three points were tested simultaneously. Thus no external post-tensioning clamps were initially installed on the specimen, as shown in Figure 3-31**Error! Reference source not found.** (a). After failure of the weaker side of the specimen, it was unloaded and external post-tensioning

clamps were installed on the failed span, shown in Figure 3-31 (b). The beam was then reloaded until failure of the alternate span.

(a)

(b)

Figure 3-31:Typical three point load testing procedure for one specimen; (a) Test 1 and (b) Test 2

To begin each test, the load was applied at a slow rate to allow for accurate documentation of the diagonal cracking load. The total applied load was typically increased in 50 kip increments. After the appearance of the first diagonal crack, the load

was increased incrementally by 100 kips. In between each of the load steps, propagation of the cracking was recorded through surface marking, still and video photography, as well as individual crack width measurements. Values recorded via the instrumentation were also checked at this time to ensure that the behavior was not deviating wildly from the original test expectations. The typical progression of cracking for a shear span of 2.5*d* is shown Figure 3-32.

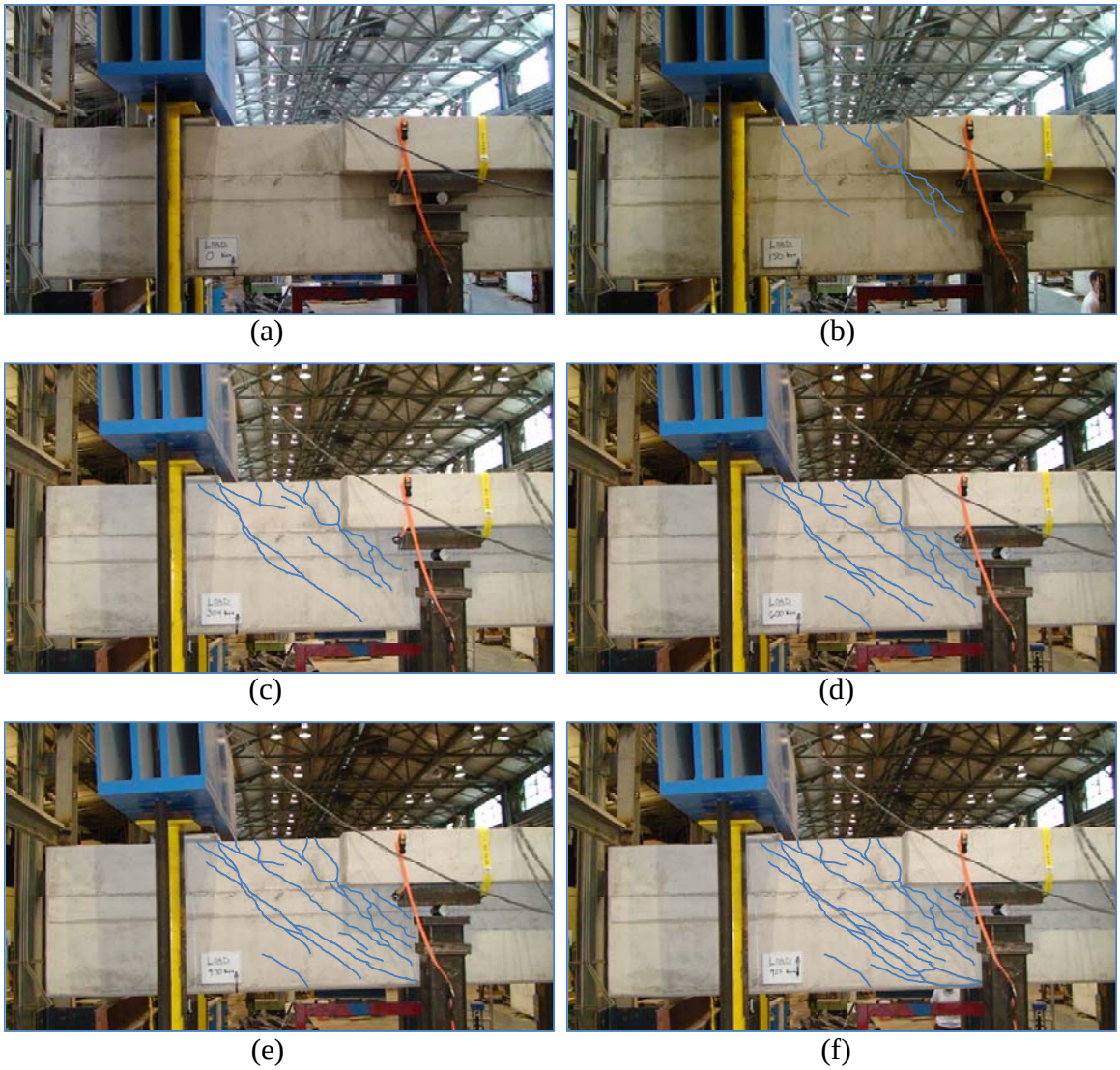

(a) (b) (c) (d) (e) (f)

Figure 3-32: Typical load step progression; at (a) 0%, (b) 16%, (c) 33%, (d) 65%, (e) 98%, and (f) 100% of the ultimate capacity of the specimen

3.7 SUMMARY

In this chapter, the experimental program was reviewed. An explanation of the different design variables was presented. The test specimen were designed to specifically address the effect of (1) web reinforcement; (2) ledge length; (3) ledge depth; and (4) beam depth on strength and serviceability performance. The number and relatively small size of experimental specimens found in literature led to the construction of specimens in the experimental program of comparable size to those found in the field. Twenty-seven tests were conducted or plan to be conducted with varying cross-sectional sizes and varying ledge depths and lengths.

The details of the testing set-up, loading apparatus, and testing procedure were provided in this chapter. The testing set-up from Project 0-5253 was slightly modified in order to enable loading on the ledges. The testing procedure was designed to obtain two tests from each specimen with the aid of external post-tensioning clamps. During testing, various instruments were monitored, crack sizes were measured, and photographs were taken.

Test results for the experimental program are presented in Chapter 4. Results corresponding to the strength and serviceability performance of each individual series will be discussed. An analysis of the information gathered from the experimental program and possible implications the findings will have on IT design are presented in Chapter 5.

CHAPTER 4
Experimental Results

4.1 INTRODUCTION

The strength and serviceability performance of the specimens tested to date will be presented and discussed within this chapter. The data from 10 tests has been analyzed and is presented and summarized in this paper, eight tests within Series I and four tests within Series II (more than the total number of tests performed because some tests fall into more than one of the test series).

4.2 SUMMARY OF EXPERIMENTAL RESULTS

This paper covers the results and preliminary analyses from 10 load tests. The completed tests were generally geared toward evaluating the effects of web reinforcement and ledge length on the strength and serviceability of inverted-T beams (as outlined in Series I and II Chapter 3). The preliminary results presented within this chapter will therefore be limited to data and observations relating directly to the aforementioned variables. In order to facilitate the study of each variable, the results from the first ten tests are grouped by series (and may be repeated) in Table 4-1. Variables in Table 4-1 not already defined will be defined in Section 4.2.1 and 4.2.2.

Table 4-1: Summary of experimental strength and serviceability results

	Beam I.D.	b_w in.	d in.	f'_c psi	f_{yl} ksi	f_{yv} ksi	f_{yh} ksi	a/d ratio	V_{crack} kip	$\frac{V_{crack}}{\sqrt{f'_c}b_w d}$	$\frac{V_{crack}}{V_{test}}$	V_{test} kip	$\frac{V_{test}}{f'_c b_w d}$	$\frac{V_{test}}{\sqrt{f'_c}b_w d}$
Series I	DS1-42-1.85-03	21	38.5	5258	70	63	63	1.96	172	2.9	0.24	712	0.17	12.1
	DS1-42-1.85-06	21	38.5	5024	64	61	61	1.85	188	3.3	0.30	621	0.15	10.8
	DS1-42-2.5-03	21	38.5	5389	70	63	63	2.65	-	-	-	406	0.09	6.8
	DS1-42-2.5-06	21	38.5	5088	64	61	61	2.5	-	-	-	504	0.12	8.7
	SS3-42-1.85-03	21	38.5	5891	69	67	67	1.85	126	2.0	0.23	523	0.11	8.4
	SS3-42-1.85-06	21	38.5	6250	70	61	61	1.85	151	2.4	0.25	617	0.12	9.7
	SS3-42-2.5-03	21	38.5	5891	69	67	67	2.5	140	2.2	0.31	447	0.09	7.1
	SS3-42-2.5-06	21	38.5	6250	70	61	61	2.5	115	1.8	0.23	496	0.10	7.8
Series II	DS1-42-1.85-06	21	38.5	5024	64	61	61	1.85	188	3.3	0.30	621	0.15	10.8
	DL1-42-1.85-06	21	38.5	4830	68	63	63	1.85	168	3.0	0.23	741	0.19	13.2
	DS1-42-2.5-06	21	38.5	5088	64	61	61	2.5	-	-	-	504	0.12	8.7
	DL1-42-2.5-06	21	38.5	4986	68	63	63	2.5	-	-	-	622	0.16	10.9

Note: Results presented in table are repeated for the reader's convenience

4.2.1 Evaluation of Strength Data

Load cells and a pressure gage were used to measure the beam reactions and total load during each test (detailed in Chapter 3). Due to the inverted nature of the test setup, presented in Figure 4-1, the reactions recorded by the load cells did not represent all of the loads applied to the beam. Specifically, the load cell measurements did not include the effects of the beam self-weight or the weight of the transfer girders. Post-processing of the test data was therefore used to obtain the shear at the critical section of the test region, denoted V_{test} in Figure 4-1. The critical section for the beam was taken at the midpoint of the shear span, a distance of a/2 from the center of the support. The calculation of V_{test} is presented in Figure 4-1. P_D is the weight of the beam. R_A and R_B are the beam reactions measured by the load cells on each side of the beam. P_L is the sum of R_A and R_B. The pressure gage was only used to verify the forces recorded by the load cells and obtained via post-processing. The pressure gage measurement included all the components of beam loading: the sum of the reactions (P_L), the weight of the beam (P_D), the weight of the loading fixture and weight of both transfer girders ($2P_{TR}$). The weight of the loading fixture was factored out when verifying the load.

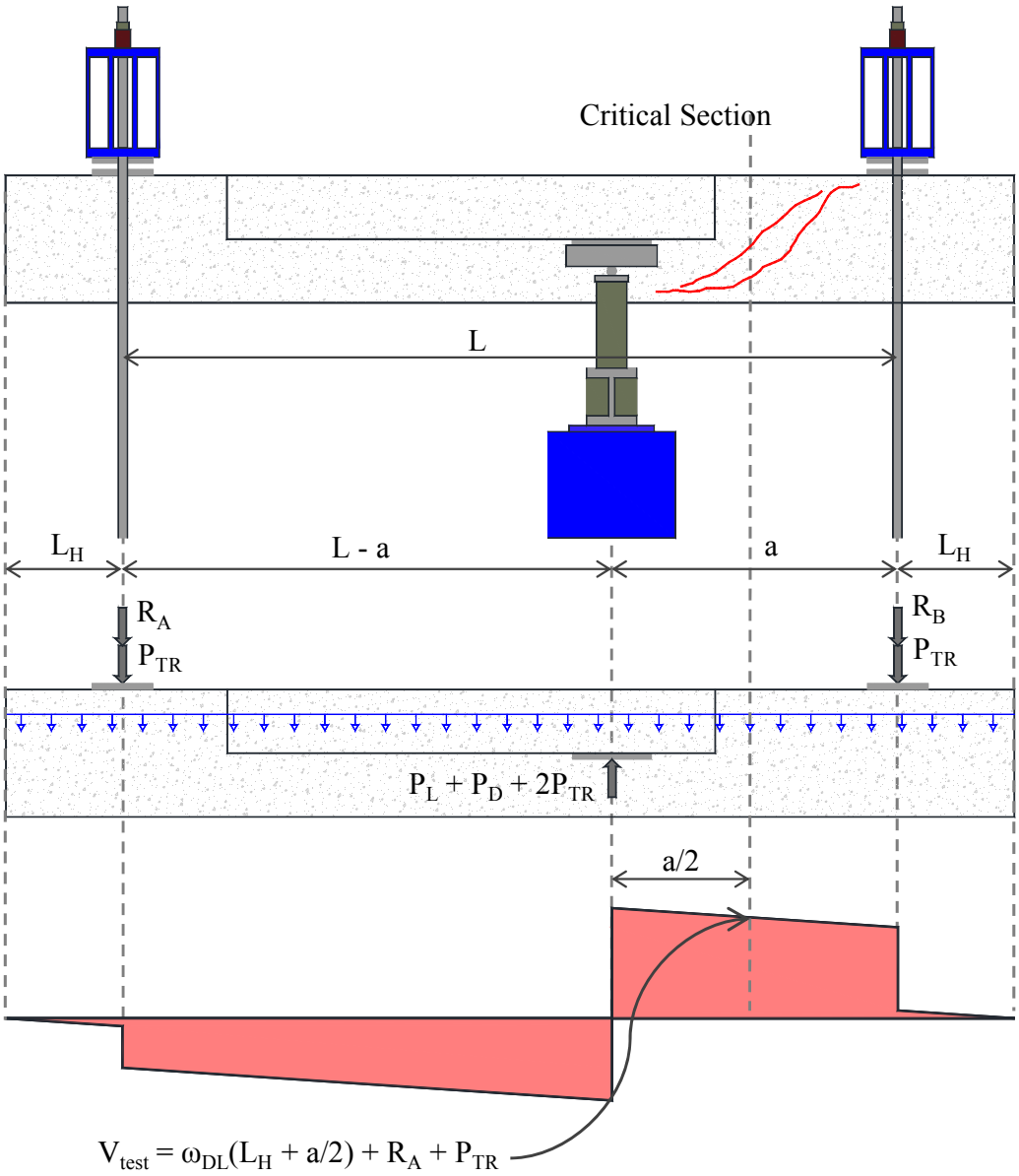

Where: $P_L = R_A + R_B$ $L = 255.25$” $\omega_{DS} = 0.094$ kip/ft
$P_{TR} = 7.8$ kip $L_H = 38.375$” $\omega_{DL} = 0.106$ kip/ft
$P_D = \omega_{DL}(2L_H + L)$ $\omega_{SS} = 0.088$ kip/ft

Figure 4-1: Calculation of V_{test} from load cell data

The test setup and inverted loading procedure were presented in their true orientation within Chapter 3. In order to examine the experimental results in a more conventional manner, the beam is assumed to be simply supported throughout the

remainder of this thesis. Photos and figures illustrating results have therefore been rotated 180 degrees to reflect the conventional orientation, as shown in Figure 4-2.

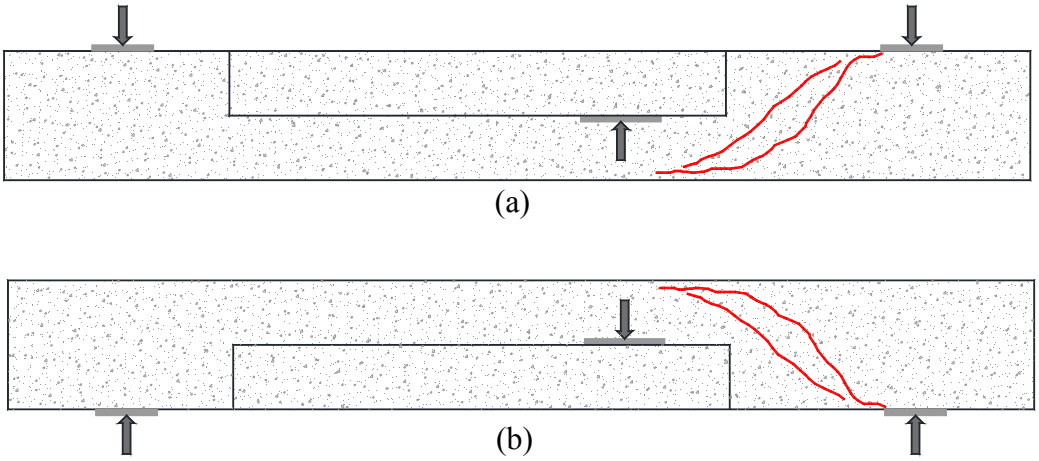

Figure 4-2: (a) Inverted orientation for testing and (b) conventional orientation for presentation of results

Since the concrete strength and cross-sectional dimensions varied among the specimens, it was inappropriate to simply compare the maximum applied shear force for each member. Therefore, the maximum applied shear force was normalized by $f'_c b_w d$ and $\sqrt{f'_c} b_w d$ for each of the two different failure modes: deep beam and sectional, respectively. In sectional shear spans, the behavior is closely associated with the tensile strength of concrete, and it is most appropriate to normalize the shear force by $\sqrt{f'_c}$ (Birrcher, et al. 2008). Conversely, the concrete compressive strength governs direct strut failure in a deep beam, and the shear force is thereby normalized by f'_c.

4.2.2 Evaluation of Serviceability Data

The two major points of interest for evaluation of serviceability were: (1) the shear at which the first diagonal crack occurred in the test region, V_{crack}, and (2) the relationship between the width of the diagonal crack and the percent of the maximum applied load.

To obtain an initial estimate of the load at diagonal cracking, the maximum load for the increment in which diagonal cracking occurred was noted during each test. This visual method established the diagonal cracking load within a 50 kip range corresponding to the initial loading increment. A more precise estimate of the diagonal cracking load was later obtained through analysis of the reinforcement strain gage data. For each test, the strains measured by the reinforcement gages were plotted against the applied shear force, as shown in Figure 4-3. The point at which cracking first occurred can be identified as the location where the shear reinforcement was first engaged. Initial deformation of the reinforcement commonly appears as a jump in the strain gage record. For the example shown in Figure 4-3, the strain measured by gage "SSV5" increases suddenly at 173 kips of applied shear; a value which was verified to fall within the range established by visual observations. For a specimen subject to a single point load, the diagonal cracking load was only identified for the first test performed on each specimen, as discussed in Chapter 3. For a specimen subject to three point loads, the diagonal cracking load was determined for both test regions as they were being tested simultaneously.

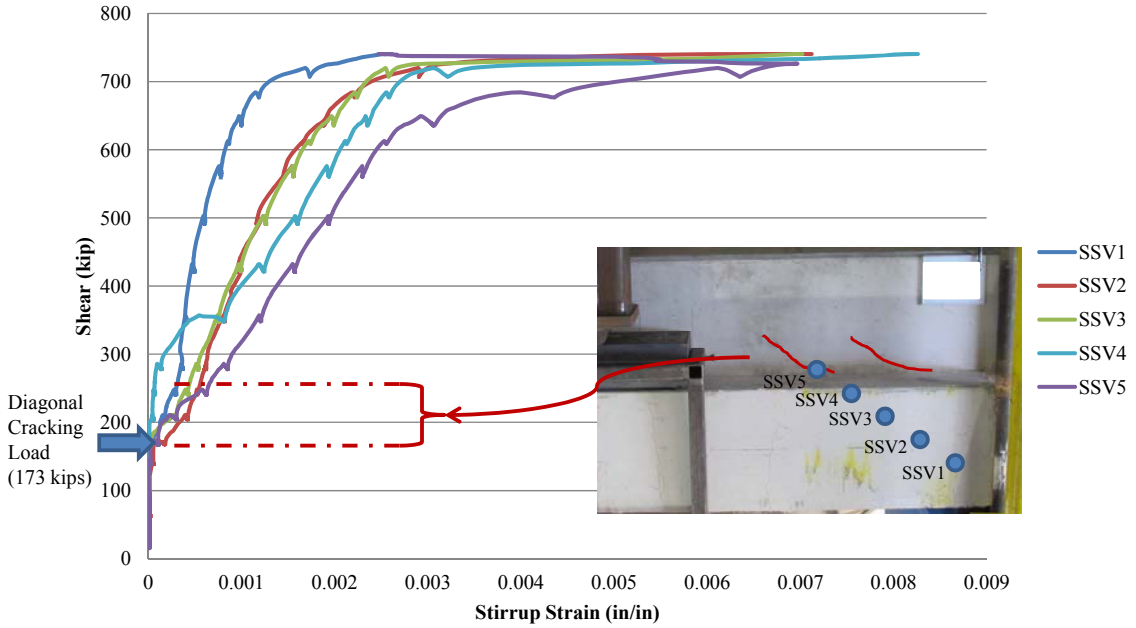

Figure 4-3: Method for determination of shear force at first diagonal cracking

Analogous to the efforts of TxDOT Project 0-5253, one of the primary project goals was to establish the relationship between the diagonal crack width and the percent of the maximum applied load. Serving as the basis for field evaluations, the relationship could allow an engineer to measure field cracks and estimate the demands on a structure in terms of the ultimate capacity. A sample plot of the percent of ultimate capacity versus the maximum diagonal shear crack width is presented in Figure 4-4. A benchmark crack width of 0.016 inches was used for data comparison. This value was chosen as an approximate boundary between acceptable and unacceptable performance based on ACI 224R-01 provisions. The approximate service load was assumed to be 33% of ultimate capacity, as based on a study by Grob and Thurlimann (1976) and discussed in the *Strength and Serviceability of Reinforced Concrete Deep Beams* (Birrcher, et al. 2008). Serviceability performance is therefore categorized as acceptable when crack widths do not exceed 0.016 inches at service level loads (i.e. up to 33% of ultimate capacity).

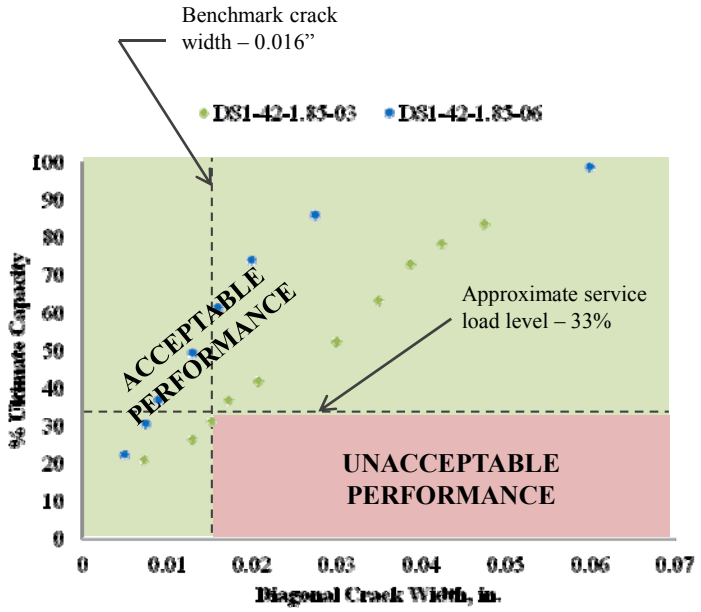

Figure 4-4: Typical plot of diagonal crack width versus percent of ultimate capacity

4.3 WEB REINFORCEMENT RATIO

The general scope of the first series of testing was to evaluate the effect of web reinforcement on the behavior of inverted-T beams. The results of Series I testing will ultimately form the basis for recommendations regarding the minimum web reinforcement necessary to achieve adequate strength and serviceability. The findings discussed below are based upon a large fraction of the tests completed to date (8 out of 10 specimens). Following a brief review of the minimum web reinforcement requirements in current code provisions, the strength and serviceability results from the tests will be presented and synthesized.

4.3.1 Background

ACI 318 (2008) and AASHTO LRFD (2009) take much different approaches regarding the use of web reinforcement. The minimum web reinforcement specifications for both are briefly outlined below. It should be noted that the minimum web reinforcement specifications are analogous to those recommended by TxDOT Project 0-5253.

4.3.1.1 ACI 318-08

The ACI 318-08 expression for the minimum allowable web reinforcement in a compression strut is based on the angle at which the reinforcement crosses the axis of the strut. The goal of the web reinforcement is to counteract the tensile forces that are caused along the strut centerline. The ACI expression is chosen "so that a tensile force in the bar causes a compressive force in the concrete perpendicular to the crack" (ACI 208 2008). The web reinforcement must satisfy:

$$\sum \frac{A_{si}}{bs_i} \sin \gamma_i \geq 0.003$$

where A_{si} is the total area of reinforcement at a spacing s_i in a layer of bars at an angle γ_i to the axis of the strut. If the reinforcement provided does not meet the minimum requirements, ACI 318-08 requires a reduction of the strut efficiency (β_s) from 0.75 to 0.60 for normal weight concrete.

4.3.1.2 AASHTO LRFD 2010

AASHTO LRFD (2010) requires that the web reinforcement ratio, defined as the ratio of the total reinforcement to gross concrete area, meet or exceed 0.003 (0.3%) in both the horizontal and vertical directions. This means that web reinforcement must satisfy:

$$\frac{A_{sv}}{bs_v} \geq 0.003$$

and

$$\frac{A_{sh}}{bs_h} \geq 0.003$$

where b is the web width, A_{sv} and A_{sh} are the web reinforcement areas in the vertical and horizontal direction, respectively, and s_v and s_h are the vertical and horizontal bar spacing. The maximum bar spacing allowed is 12.0 inches.

4.3.2 Strength Results

Eight of the twenty-four tests currently planned for the web reinforcement series have been performed to date. The strength results from the tests are presented in Table

4-2. The eight tests were conducted on two deep-short ledge specimens and two shallow-short ledge specimens with varying amounts of web reinforcement. Table 4-2 is organized by groups of directly comparable tests, where each partitioned section contain two identically configured beams with different web reinforcement ratios (0.3% versus 0.6%).

Table 4-2: Summary of strength results for specimens in web reinforcement series

Beam I.D.	b_w in.	d in.	ρ_h	Bar size	s_h in	ρ_v	Bar size	s_v in	a/d ratio	Ledge info	V_{test} kip	$\frac{V_{test}}{f'_c b_w d}$	$\frac{V_{test}}{\sqrt{f'_c} b_w d}$
DS1-42-1.85-03	21	38.5	0.0029	#4	6.5	0.0029	#4	6.5	1.85	DS	712	0.17	12.1
DS1-42-1.85-06	21	38.5	0.0062	#5	4.75	0.0059	#5	5	1.85	DS	621	0.15	10.8
DS1-42-2.5-03	21	38.5	0.0029	#4	6.5	0.0029	#4	6.5	2.5	DS	406	0.09	6.8
DS1-42-2.5-06	21	38.5	0.0062	#5	4.75	0.0059	#5	5	2.5	DS	504	0.12	8.7
SS3-42-1.85-03	21	38.5	0.0029	#4	6.5	0.0029	#4	6.5	1.85	SS	523	0.11	8.4
SS3-42-1.85-06	21	38.5	0.0062	#5	4.75	0.0059	#5	5	1.85	SS	617	0.12	9.7
SS3-42-2.5-03	21	38.5	0.0029	#4	6.5	0.0029	#4	6.5	2.5	SS	447	0.09	7.1
SS3-42-2.5-06	21	38.5	0.0062	#5	4.75	0.0059	#5	5	2.5	SS	496	0.10	7.8

4.3.2.1 Shear Span-to-Depth Ratio of 1.85

A total of four tests were conducted on specimens with a shear span-to-depth ratio of 1.85: two on shallow-short (SS) ledge and two on deep-short (DS) ledge specimens. The expected failure mechanism for each of the short shear spans (a/d < 2.0) was crushing of the strut between the compression chord and support. Failure of a direct strut is primarily controlled by the compressive strength of the concrete. As reaffirmed by the researchers of TxDOT Project 0-5253, the transverse reinforcement equilibrates tension across the strut, but does not contribute to the shear strength in any significant manner. With respect to the current test program, any web reinforcement provided beyond the minimum necessary to equilibrate strut splitting, should not affect the ultimate strength of the specimens. The normalized ultimate shear capacity of the two pairs of specimens is presented in Figure 4-5.

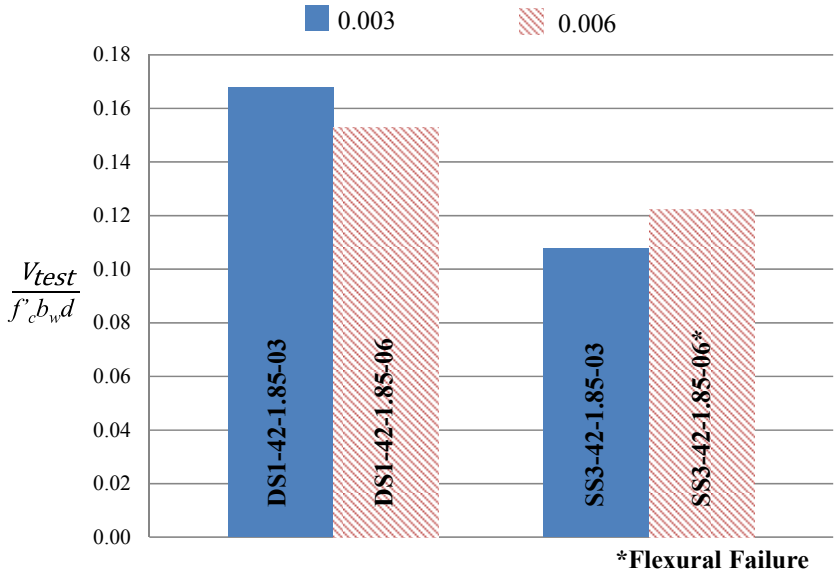

Figure 4-5: Normalized ultimate shear capacity of specimens with a/d = 1.85

Prior to drawing conclusions regarding the effects of the web reinforcement ratio, a comment regarding the variability of shear strength should be made. Two deep beam specimens featuring nearly identical geometry and reinforcement within TxDOT Project 0-5253 yielded normalized strength results which differed by as much as $0.02f'_c b_w d$. With this in mind, a review of the results presented in Figure 4-5 suggests that there is no appreciable change in strength as a result of increased web reinforcement (0.3% to 0.6%). The observed difference in strength from one companion specimen to the next is insignificant and can be attributed to the variability of shear behavior. These preliminary results support the conclusion drawn by the researchers of TxDOT Project 0-5253: "any reinforcement greater than that which is required to maintain equilibrium in the bottle-shaped strut is unnecessary for strength."

Photographs of the deep-short and shallow-short ledge specimens at ultimate capacity are presented in Figure 4-6 and Figure 4-7. The ultimate capacities for these specimens are presented alongside the failure photographs. The similarities between the crack patterns of the companion specimens further illustrate the ineffectual presence of the additional reinforcement.

DS1-42-1.85-03

V_{test} = 712 kips

$12.1\sqrt{f'_c}b_wd$

$0.17f'_cb_wd$

(a)

DS1-42-1.85-06

V_{test} = 621 kips

$10.8\sqrt{f'_c}b_wd$

$0.15f'_cb_wd$

(b)

Figure 4-6: Ultimate shear capacities and cracking at ultimate load for deep-short ledge specimens with (a) 0.003 and (b) 0.006 web reinforcement

SS3-42-1.85-03

V_{test} = 523 kips

$8.4\sqrt{f'_c}b_w d$

$0.11f'_c b_w d$

(a)

SS3-42-1.85-06

V_{test} = 617 kips*

$9.7\sqrt{f'_c}b_w d$*

$0.12f'_c b_w d$*

*Flexure Failure

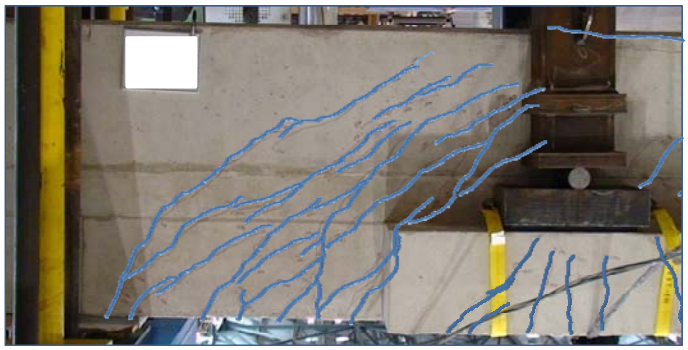

(b)

Figure 4-7: Ultimate shear capacities and cracking at ultimate load for shallow-short ledge specimens with (a) 0.003 and (b) 0.006 web reinforcement

All strut-and-tie modeling was completed using the provisions recommended by TxDOT Project 0-5253. The proposed provisions are significantly simpler than the current ACI 318 (2008) and AASHTO LRFD (2010) STM Provisions. They were largely based on the STM recommendations of *fib* (1999) while maintaining consistency with other aspects of the AASHTO LRFD Bridge Specifications (2008). Use of the Project 0-5253 STM provisions within the current test program is aimed at evaluating the applicability of the recommendations to deep beams loaded at the bottom chord (as opposed to the top chord as in TxDOT Project 0-5253). In Figure 4-8, the measured shear capacities are presented alongside the strut-and-tie modeling results. For a shear span-to-depth ratio of 1.85, the expected capacity is primarily controlled by the concrete strength. This is reflected by the similarity between the STM calculated shear capacities

of the four specimens. As shown in Figure 4-8, the provisions of Project 0-5253 were generally conservative with respect to the experimental results.

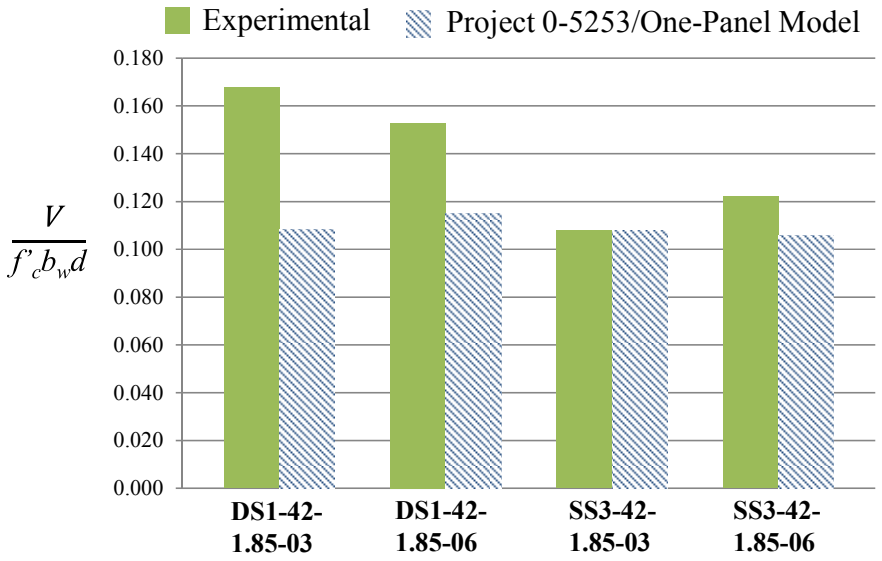

Figure 4-8: Experimental and calculated ultimate shear capacities

The ratio of the experimental to calculated capacity for each test region is presented in Figure 4-9. The values calculated for the deep-short ledge specimens were consistent with the experimental results of Project 0-5253. Database evaluation of the Project 0-5253 provisions yielded a mean experimental-to-calculated ratio of 1.54. The lower values calculated for the shallow-short ledge specimens, equal to 1.0 for SS3-42-1.85-03, indicate a lower level of conservatism, but are still within the experimental variability for shear. Future testing will provide more information regarding the effects of shallow ledges and the resulting indirect tension fields. In general, the initial results suggest that increased web reinforcement does not affect the strength of deep beams shear spans (a/d = 1.85) loaded at the bottom chord.

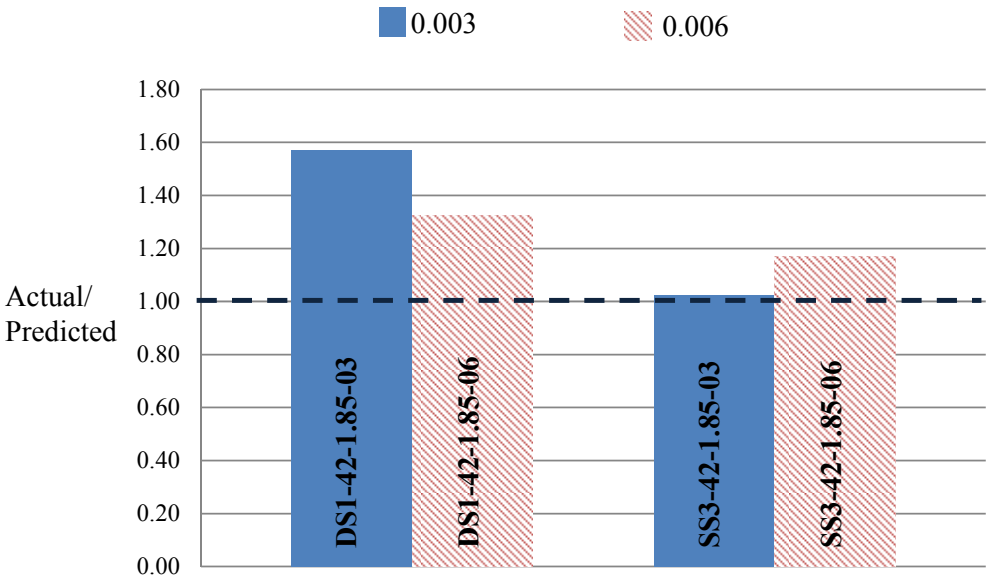

Figure 4-9: Actual capacity to predicted capacity ratio

4.3.2.2 Shear Span-to-Depth Ratio of 2.5

In the web reinforcement series, four tests were conducted on specimens with a shear span-to-depth ratio of 2.5: two with a deep-short ledge and two with a shallow-short ledge. The shear span-to-depth ratio of 2.5 falls within the upper end of the transition zone ($2.0 < a/d < 2.5$) from a deep beam (one-panel) to a sectional (two-panel) shear mechanism. An increased amount of web reinforcement, specifically in the vertical direction, should strengthen the vertical tie of the two-panel mechanism, as shown in Figure 4-10. Moreover, since the vertical tie generally controls the capacity of a two panel mechanism, an increased amount of web reinforcement should increase the capacity of the more slender test regions.

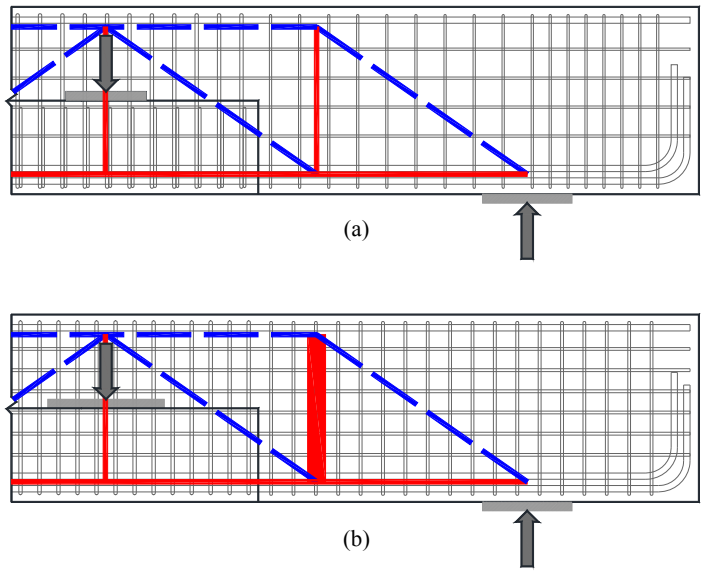

Figure 4-10: Effect of increasing web reinforcement on tie area; (a) 0.003 and (b) 0.006

Preliminary results indicate that a consistent increase in shear strength occurred as a result of increased web reinforcement. The experimental capacities of the members with a shear span-to-depth ratio of 2.5 are presented in Figure 4-11. Increasing the web reinforcement ratio from 0.003 to 0.006 increased the shear capacity of the deep and shallow ledge specimens by 28% and 10%, respectively. The smaller strength gain exhibited by the shallow ledge specimen (SS3-42-2.5-06) is not representative of the potential effects of increased web reinforcement due to a premature flexural failure. The vertical tie was not the controlling STM element and the full benefits of the additional web reinforcement were therefore not utilized.

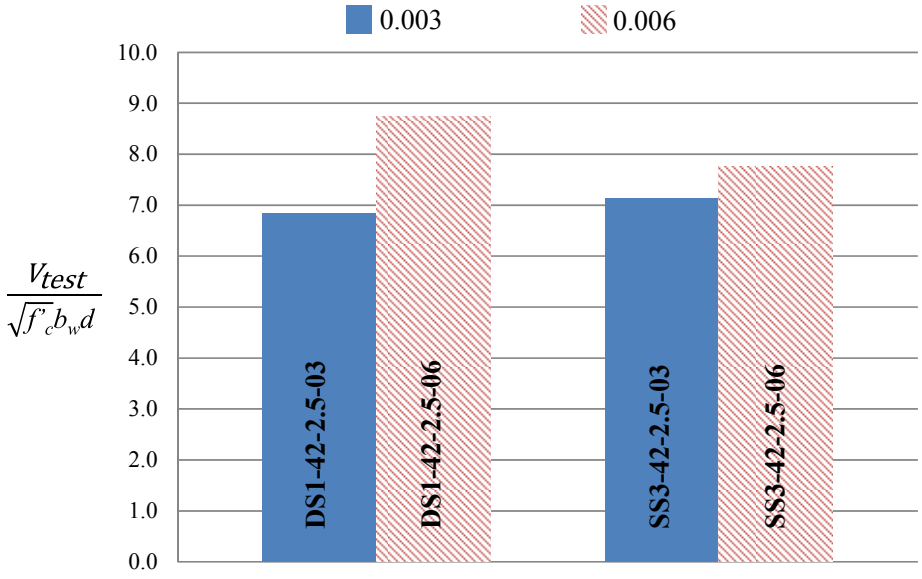

Figure 4-11: Ultimate shear capacity of specimens with a/d = 2.5

Photographs of the deep-short and shallow-short ledge specimens at ultimate capacity are presented in Figure 4-12 and Figure 4-13. The measured capacity of each specimen is presented alongside the relevant failure photograph. The impact of the web reinforcement is clearly illustrated by the increased distribution of cracks within the more heavily reinforced test regions.

DS1-42-2.5-03

V_{test} = 406 kips

$6.8\sqrt{f'_c}b_w d$

$0.09f'_c b_w d$

(a)

DS1-42-2.5-06

V_{test} = 504 kips

$8.7\sqrt{f'_c}b_w d$

$0.12f'_c b_w d$

(b)

Figure 4-12: Ultimate shear capacities and cracking at ultimate load for deep-short ledge specimens with (a) 0.003 and (b) 0.006 web reinforcement

SS3-42-2.5-03

V_{test} = 447 kips

$7.1\sqrt{f'_c}b_wd$

$0.09f'_cb_wd$

(a)

SS3-42-2.5-06

V_{test} = 496 kips*

$7.8\sqrt{f'_c}b_wd$*

$0.1f'_cb_wd$*

*Flexure Failure

(b)

Figure 4-13: Ultimate shear capacities and cracking at ultimate load for shallow-short ledge specimens with (a) 0.003 and (b) 0.006 web reinforcement

The STM recommendations of TxDOT Project 0-5253 were utilized to estimate the one-panel (deep beam) and two-panel (sectional) STM capacities of each specimen. The experimental capacity is presented alongside the one-panel and two-panel STM estimates in Figure 4-14. As expected, the one-panel mechanism did not accurately represent the effect of the increased web reinforcement; strength estimates for all four specimens were virtually equivalent. The increase in the two-panel capacity, on the other hand, illustrates the effect of the increased web (i.e. vertical tie) reinforcement.

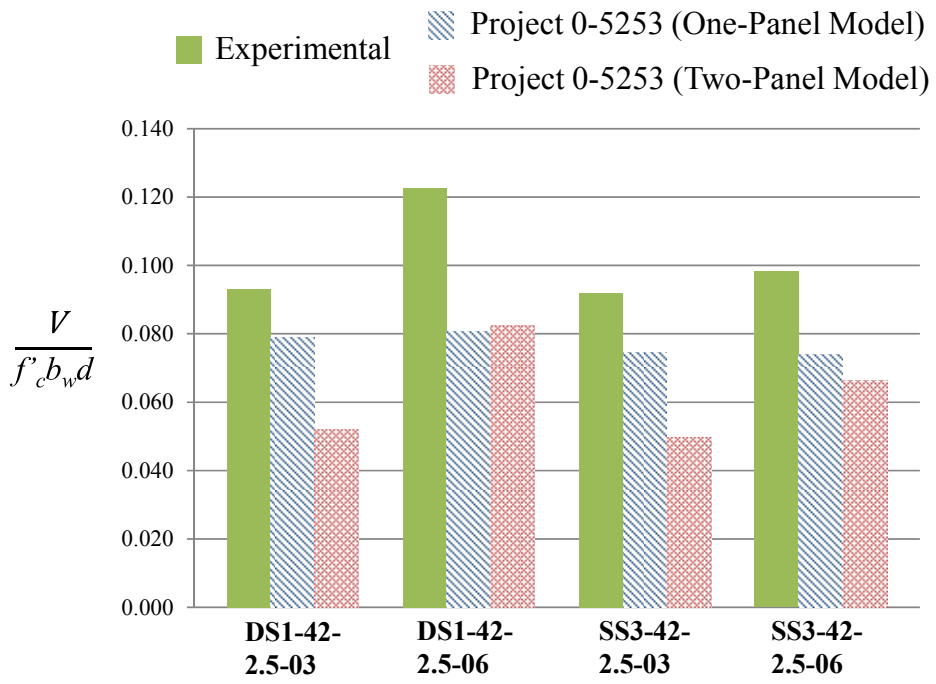

Figure 4-14: Experimental and calculated ultimate shear capacities

In Figure 4-15, the ratio of the experimental capacity to calculated capacity for each specimen is presented in terms of both the one-panel and two-panel mechanisms. The STM provisions of TxDOT Project 0-5253 resulted in conservations estimations of the shear capacity, regardless of the web reinforcement ratio and ledge depth. The ratio of the experimental capacity to calculated capacity, using a two-panel model, varied from 1.2 to 2.2; well within the evaluation database scatter observed during TxDOT Project 0-5253.

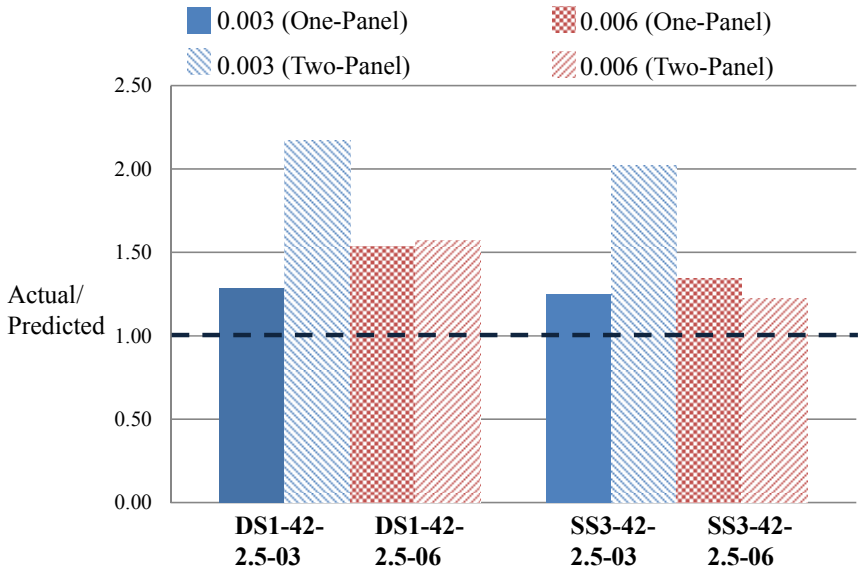

Figure 4-15: Actual capacity to predicted capacity ratio for both one- and two-panel failures

4.3.3 Serviceability Results

The serviceability results for Series I testing are summarized in Table 4-3, which includes the diagonal cracking load (V_{crack}) as well as the ratio of the diagonal cracking load to the experimental capacity (V_{crack}/V_{test}). All of the diagonal cracking loads were normalized by $\sqrt{f'_c}$ (the most relevant indicator of tensile strength and hence cracking), irrespective of the shear span-to-depth ratio of the specimen.

Table 4-3: Summary of serviceability results for web reinforcement series

Beam I.D.	b_w in.	d in.	ρ_v	Bar size	s_v in	ρ_v	Bar size	s_v in	a/d ratio	Ledge info	V_{test} kip	V_{crack} kip	$\frac{V_{crack}}{\sqrt{f'_c} b_w d}$	$\frac{V_{crack}}{V_{test}}$
DS1-42-1.85-03	21	38.5	0.0029	#4	6.5	0.0029	#4	6.5	1.85	DS	712	172	2.9	0.24
DS1-42-1.85-06	21	38.5	0.0062	#5	4.75	0.0059	#5	5	1.85	DS	621	188	3.3	0.30
DS1-42-2.5-03	21	38.5	0.0029	#4	6.5	0.0029	#4	6.5	2.5	DS	406	-	-	-
DS1-42-2.5-06	21	38.5	0.0062	#5	4.75	0.0059	#5	5	2.5	DS	504	-	-	-
SS3-42-1.85-03	21	38.5	0.0029	#4	6.5	0.0029	#4	6.5	1.85	SS	523	122	2.0	0.23
SS3-42-1.85-06	21	38.5	0.0062	#5	4.75	0.0059	#5	5	1.85	SS	617*	151*	2.4	0.25
SS3-42-2.5-03	21	38.5	0.0029	#4	6.5	0.0029	#4	6.5	2.5	SS	447	140	2.2	0.31
SS3-42-2.5-06	21	38.5	0.0062	#5	4.75	0.0059	#5	5	2.5	SS	496*	115*	1.8	0.23

In general, an increased amount of web reinforcement should improve the serviceability performance of members under both deep beam and sectional loading scenarios. Following initial formation of a crack, the web reinforcement restrains the crack growth. An increased amount of web reinforcement should therefore provide greater restraint and hence smaller crack widths. Initial formation of diagonal cracks within a member is dependent on the principal stresses within the concrete alone and should not be affected by increased web reinforcement. The validity of the former statements to the serviceability results of the Series I (web reinforcement) specimens, including shear span-to-depth ratios of 1.85 and 2.5, is examined in the following sections.

4.3.3.1 Shear Span-to-Depth Ratio of 1.85

The serviceability data for the deep-short ledge specimen and shallow-short ledge specimen are presented in Figure 4-16 and Figure 4-17. The growth of the cracks (as a function of the applied load) and the crack pattern at failure are included for each ledge type.

In the deep-short ledge specimens, the web reinforcement was not perceived to have any significant effect on the failure crack patterns. However, the effect of the increased web reinforcement is clearer when the diagonal crack growth is examined through each of the loading histories (Figure 4-16). Increased web reinforcement reduced the maximum width of the primary diagonal crack at first cracking and throughout the loading history. Maximum crack widths at equivalent load steps were reduced by nearly a factor of 2 on average. Furthermore, increased web reinforcement resulted in more acceptable serviceability behavior. The deep-short ledge specimen with 0.3% web reinforcement exhibited poor serviceability within the initial loading stages.

Contrary to the deep-short ledge results, increased web reinforcement did not appear to impact the growth of the cracks within the shallow-short ledge specimens. While the crack widths within the more heavily reinforced specimen were slightly smaller at failure, differences between the failure crack patterns are negligible (Figure

4-17). Further investigation into the effects of both the web reinforcement and ledge height is needed before any meaningful conclusions can be drawn.

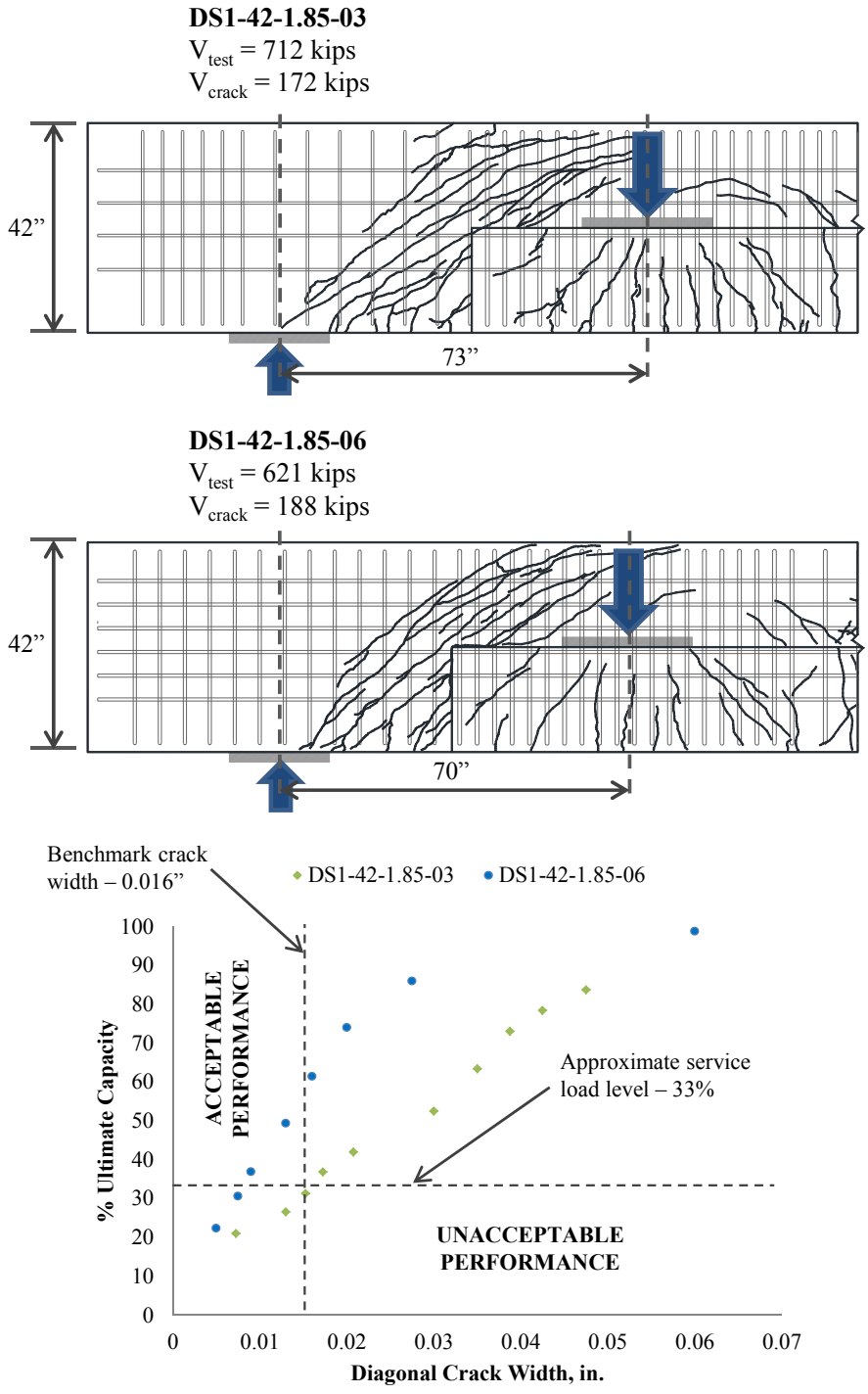

Figure 4-16: Serviceability data for deep-short ledge with a/d = 1.85: Crack patterns (at ultimate capacity) and crack widths

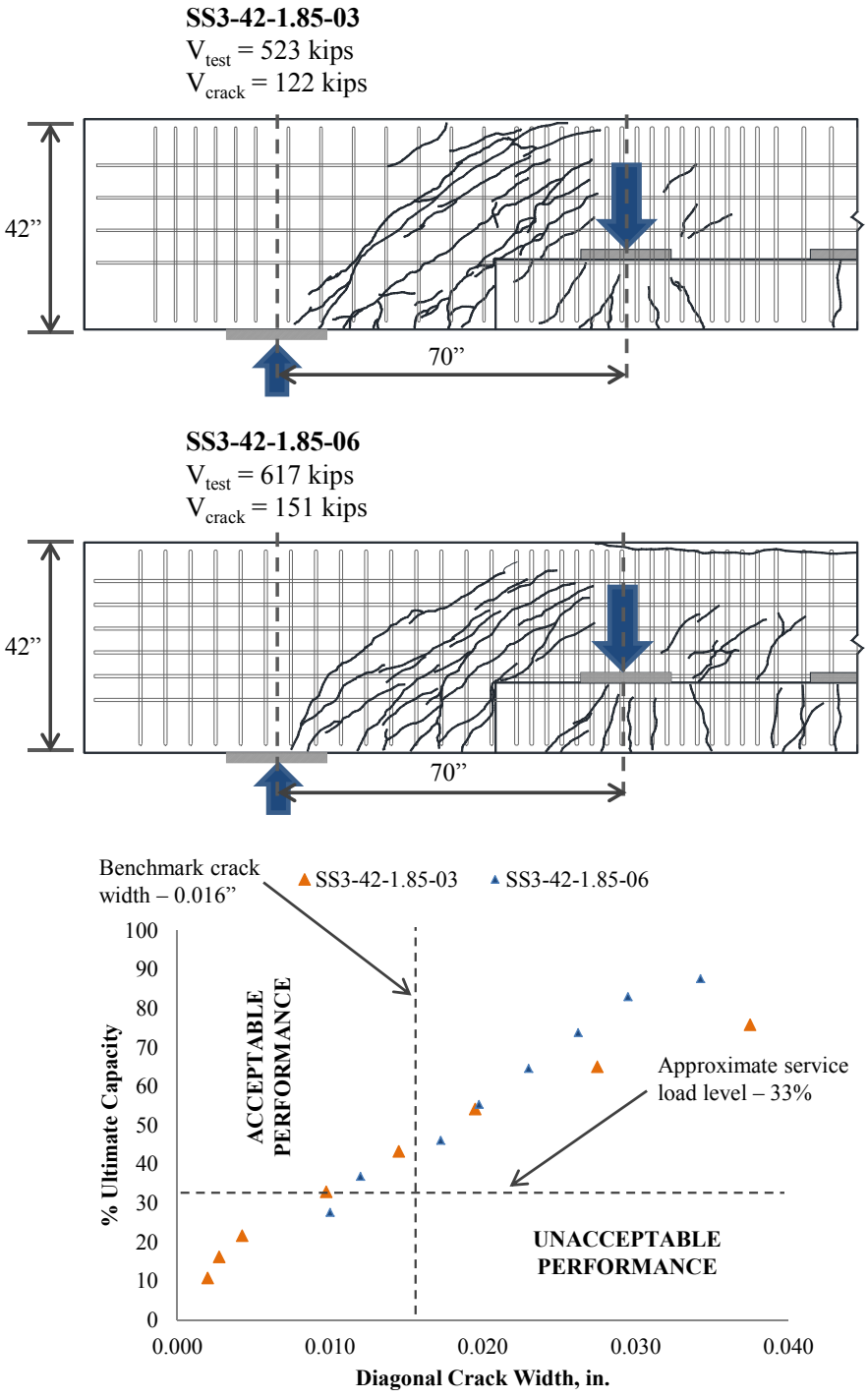

Figure 4-17: Serviceability data for shallow-short ledge with a/d = 1.85: Crack patterns (at ultimate capacity) and crack widths

4.3.3.2 Shear Span-to-Depth Ratio of 2.5

The serviceability behavior of the deep-short ledge specimen and shallow-short ledge specimen is presented in Figure 4-18 and Figure 4-19. The growth of the cracks (as a function of the applied load) and the crack pattern at failure are included for each ledge type.

In the deep-short ledge specimens, crack growth and the failure crack patterns were greatly influenced by the web reinforcement ratio. As illustrated in Figure 4-18, use of additional web reinforcement in DS1-42-2.5-06 resulted in a greater distribution of the cracking between the compression chord and support. Furthermore, the growth of the cracks was noticeably restrained throughout the loading history. Doubling of the web reinforcement (0.3% to 0.6%) was not as effective as previously witnessed (Section 4.3.3.1), but did markedly improve the serviceability behavior of the shear span. The specimen with minimum web reinforcement provided satisfactory performance nonetheless.

The short-shallow ledge specimen serviceability data is presented in Figure 4-19. The effect of the additional web reinforcement on the crack pattern was similar to that observed in the deep-short ledge specimens; use of additional web reinforcement in SS3-42-2.5-06 resulted in a greater distribution of the cracking between the compression chord and support. Increased web reinforcement had a negligible effect on the growth of the maximum diagonal crack under service loads (less than 33% of the maximum applied shear). Restraint of the crack widths within the more heavily reinforced specimen was only marginally improved at higher loads. With that said, the serviceability performance resulting from both 0.3% and 0.6% web reinforcement was satisfactory.

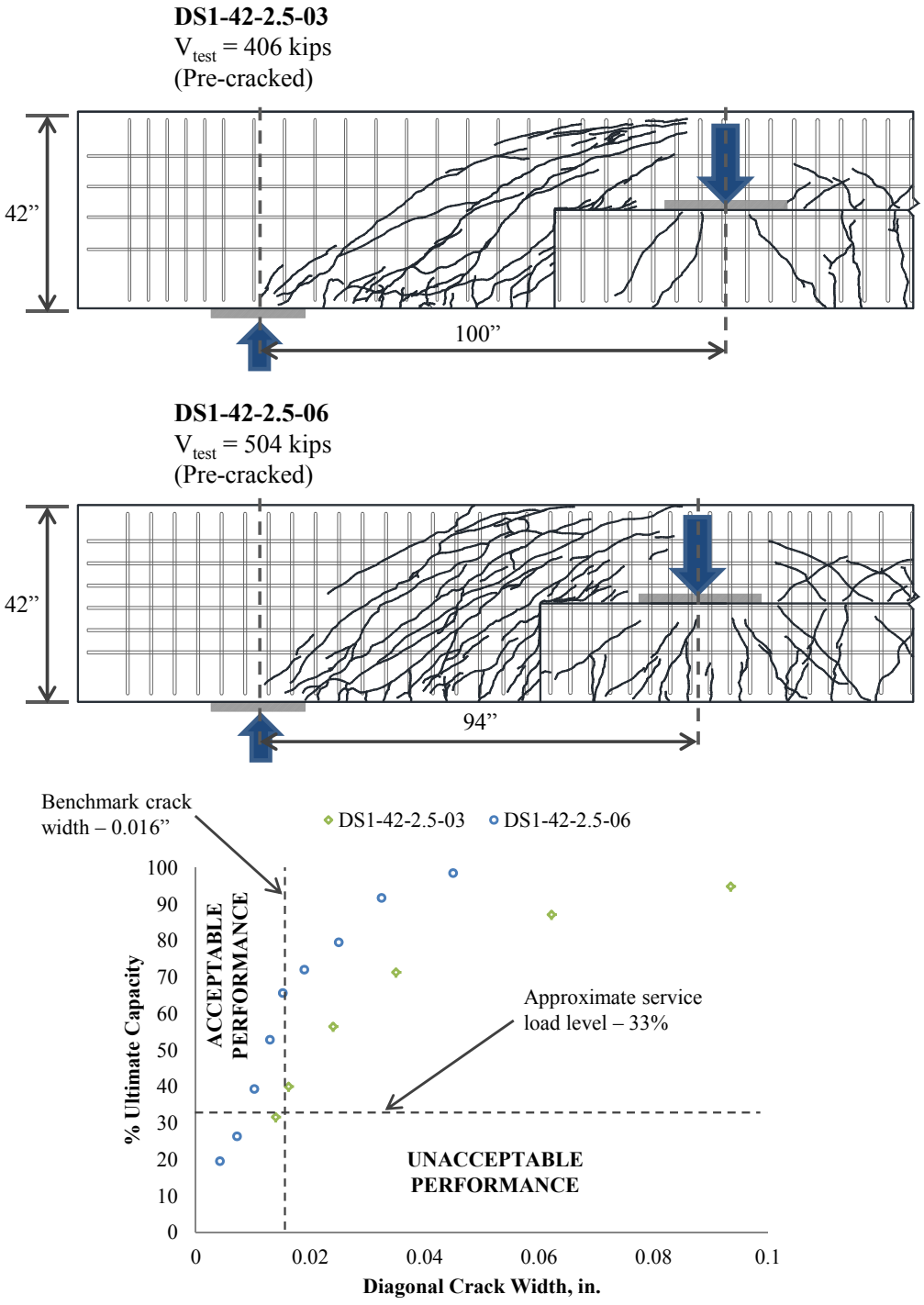

Figure 4-18: Serviceability data for deep-short ledge with a/d = 2.5: Crack patterns (at ultimate capacity) and crack widths

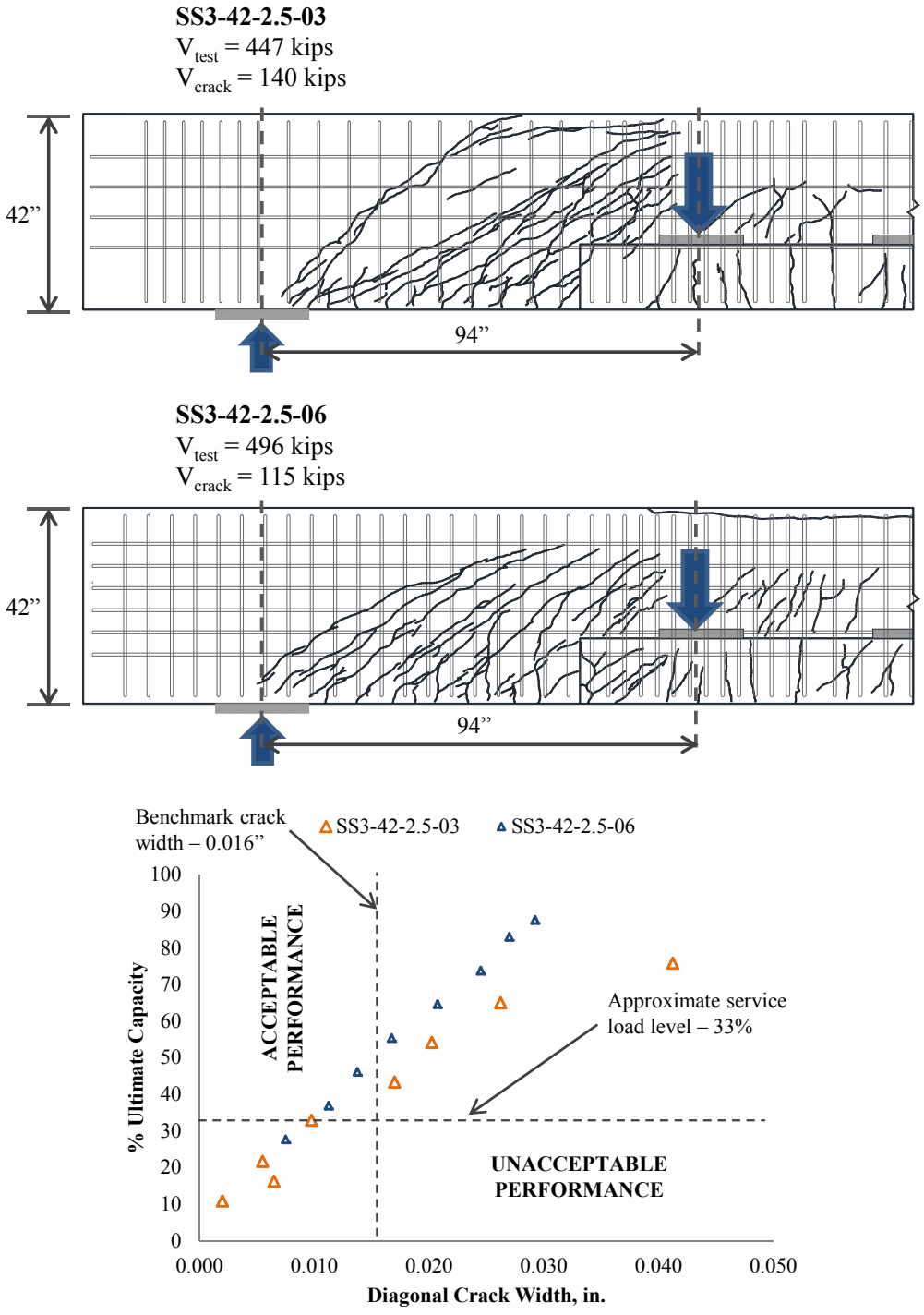

Figure 4-19: Serviceability data for shallow-short ledge with a/d = 2.5: Crack patterns (at ultimate capacity) and crack widths

4.3.4 Summary

Eight tests have been performed to study the impact of varying the web reinforcement ratio between 0.003 (0.3%) and 0.006 (0.6%). These tests were performed on specimens with two different shear span-to-depth ratios, 1.85 and 2.5, and two different ledge geometries, deep-short (DS) and shallow-short (SS).

Strength results indicate that increased web reinforcement has no appreciable effect on the shear capacity of deep beam shear spans (a/d = 1.85), but appears to increase the shear capacity of sectional shear spans (a/d = 2.5). These results are in agreement with the results of TxDOT Project 0-5253 (study of top-chord loaded beams) and common wisdom regarding shear behavior (refer to Sections 4.3.2.1 and 4.3.2.2). The applicability of the strut-and-tie modeling provisions recommended by TxDOT Project 0-5253 was evaluated through a comparison of the STM-generated strength estimates and the experimental capacities. Application of the TxDOT Project 0-5253 provisions generally yielded conservative strength estimates. However, more data is needed to comment on the overall accuracy of the method as applied to inverted-T (top-chord loaded) members.

Serviceability test results suggest that, in general, increasing the amount of web reinforcement decreases the crack widths measured throughout the loading history. This observation applies to both deep beam (a/d = 1.85) and sectional (a/d = 2.5) shear spans; though the magnitude of the crack width reduction appears (i.e., more testing is needed) to be dependent on the ledge depth. Increased web reinforcement also influenced the failure crack pattern in the test regions with a shear span-to-depth ratio of 2.5. Use of additional web reinforcement in resulted in a greater distribution of the cracking between the compression chord and support.

4.4 LEDGE LENGTH

The second series of testing (outlined within Chapter 3) was designed to study the effect of ledge length on the shear behavior of inverted-T beams. The results of Series II testing will form the basis for recommendations regarding the optimal ledge length for

adequate strength and serviceability. Four of the sixteen tests planned within Series II have been completed and underlie the preliminary findings presented below. Following a brief review of the potential strength and serviceability implications of cut-off, short and long ledges, experimental results from the four tests will be discussed and analyzed.

4.4.1 Background

Three ledge lengths are commonly found in inverted-T straddle bents within the field: (1) 'long' – the ledge typically extends to the support, (2) 'cut-off' – the ledge is terminated at outside face of the fascia girder, and (3) 'short' – a ledge of intermediate length. These three ledge lengths are all represented within the final test matrix, but only 'short' and 'long' ledges have been evaluated to date. In general, the ledge of an inverted-T beam is designed to support the weight of incoming girders and the loads superimposed on the girders.

The effects of an exceedingly short ledge were previously discussed in Chapter 3. An exceedingly short ledge will impact the amount of hanger reinforcement available for transfer of the ledge loads to the hanger reinforcement. Ending the ledge immediately outside of the fascia girder limits the size of the vertical tie at the load point. This will decreases the area of the tension region that is present in bottom chord loaded specimens as discussed in Chapter 1.

At the opposite extreme, a ledge extended to the support may influence the inverted-T strength and serviceability in other manners. When the ledge is extended to the supports, an additional 50% of cross-sectional area is provided in the shear span. Although this is not accounted for in the STM or in classic sectional shear analysis, this additional area may affect the shear behavior and needs to be investigated.

4.4.2 Strength Results

Four tests have been performed to evaluate the effect of ledge length. A summary of the strength results from these four tests is presented in Table 4-4. The specimens are grouped into pairs according to their shear span-to-depth ratio. The only difference between paired specimens is their ledge length. Experimental results can therefore be

directly compared to one another in order to discern the effects of short and long ledge lengths. The maximum applied shear for each specimen within Table 4-4 has been normalized according to the scheme discussed in Section 4.2.1.

Table 4-4: Summary of strength results for specimens in ledge length task

Beam I.D.	**b_w in.**	**d in.**	**ρ_v**	**Bar size**	**s_v** in	**ρ_v**	**Bar size**	**s_v** in	**a/d ratio**	**Ledge info**	**V_{test} kip**	**$\frac{V_{test}}{f'_c b_w d}$**	**$\frac{V_{test}}{\sqrt{f'_c} b_w d}$**
DS1-42-1.85-06	21	38.5	0.0062	#5	4.75	0.0059	#5	5	1.85	DS	621	0.15	10.8
DL1-42-1.85-06	21	38.5	0.0062	#5	4.75	0.0059	#5	5	1.85	DL	741	0.19	13.2
DS1-42-2.5-06	21	38.5	0.0062	#5	4.75	0.0059	#5	5	2.5	DS	504	0.12	8.7
DL1-42-2.5-06	21	38.5	0.006	#5	4.75	0.0059	#5	5	2.5	DL	622	0.16	10.9

Prior to review of the results, a note regarding the preliminary nature of the findings should be repeated. The following observations and conclusions are based upon four tests for which comparisons may only be drawn between two pairs. This data is insufficient to confidently define the variability inherent to these shear tests. An additional twelve tests are planned and sufficient confidence in the results will be apparent in the final report. The observations and conclusions drawn during the course of the four tests are only reported here if there is a notable trend among both pairs of specimens.

In both deep beam (a/d = 1.85) and sectional (a/d = 2.5) shear spans, the long ledge appears to have a beneficial effect on the load carrying capacity. The results of the deep beam and sectional shear tests are summarized in Figure 4-20 and Figure 4-21, respectively. The experimental capacity of each shear span type was approximately 25% greater when the ledge was extended to the support, rather than terminated a short distance from the load point.

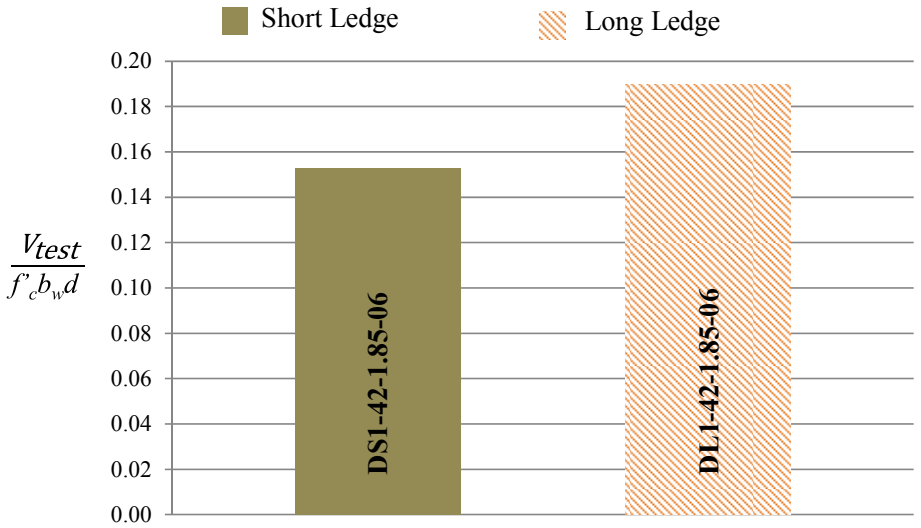

Figure 4-20: Ultimate shear capacity of specimens with a/d = 1.85

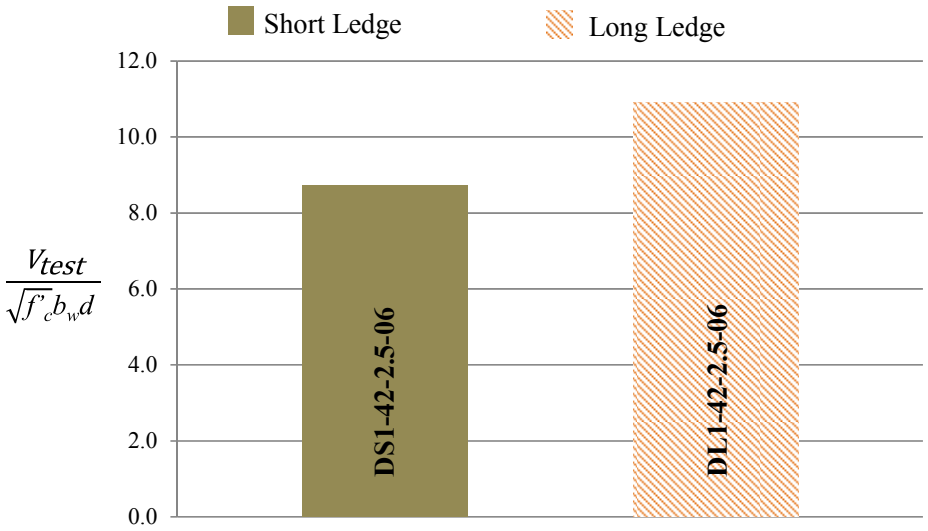

Figure 4-21: Ultimate shear capacity of specimens with a/d = 2.5

This increase in strength is likely due to two different behavioral changes that the longer ledge creates in the specimens. In both shear spans, running the ledge to the supports creates a larger cross-sectional area in the shear span, shown in Figure 4-22 (a) compared to (b). In the short ledge specimen the cross sectional area was smaller in the shear span. The extra area is not accounted for in the STM or in classical sectional shear

resistance, where only the web area is considered in the concrete contribution of shear strength.

In the shorter shear span, a/d = 1.85, running the ledge the entire way to the supports created more area for the spreading of the compression strut. These larger areas would result in lower compressive stresses developing in the long ledge specimen, compared to those in the smaller area of the short ledge specimen. Because this additional area does not entirely surround the support, confinement of the concrete beneath the support is not accounted for in the calculated capacity.

In the longer shear span, a/d = 2.5, the increased concrete area classically would not directly increase the area contributing to the sectional shear resistance in the member, consequently increasing capacity. In a sectional model, the areas of the ledge may want to be considered within the concrete contribution. Due to the vertical tension tie controlling the behavior of the two-panel STM, the additional area was not accounted for when calculating the capacity of the specimens.

Because the ledge runs the entire way to the support and the load is applied on the ledge, the inverted-T beam may behave more like three separate beams. If this is the case, a more complicated STM, including a longitudinal model in the ledges, may represent the behavior of the shorter shear span more accurately. Also, this would provide reasoning to include the additional area in sectional shear calculations. More research needs to be conducted and more analysis must be performed to investigate this theory.

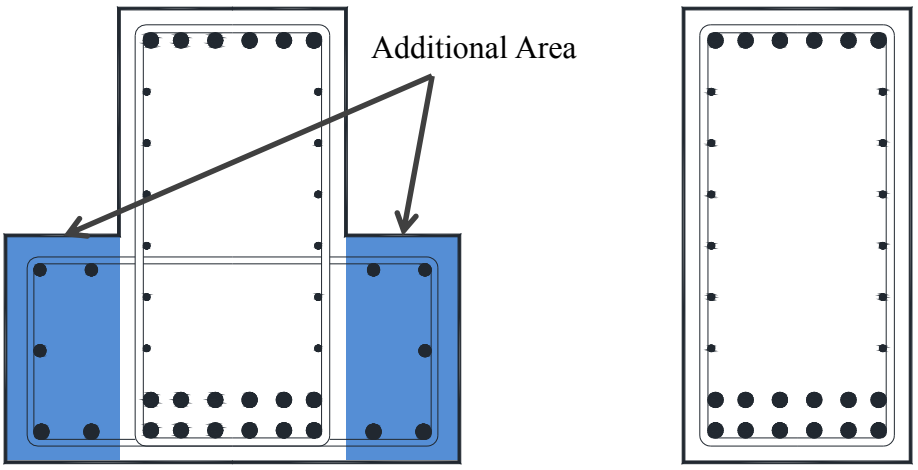

Figure 4-22: Difference between cross-section in the shear span for (a) long ledge and (b) short ledge specimen

As previously discussed, the specimens were designed and analyzed using proposed design specifications presented by Project 0-5253. The normalized experimental and calculated shear capacities are shown in Figure 4-23, for a/d = 1.85, and Figure 4-24, for a/d = 2.5. The first observation made from the plots is that the normalized predicted capacities of the specimens are similar for both the short and long ledge, and both shear span, cases. This is due to the fact that the ledge length did not affect the controlling element of the models for either shear span.

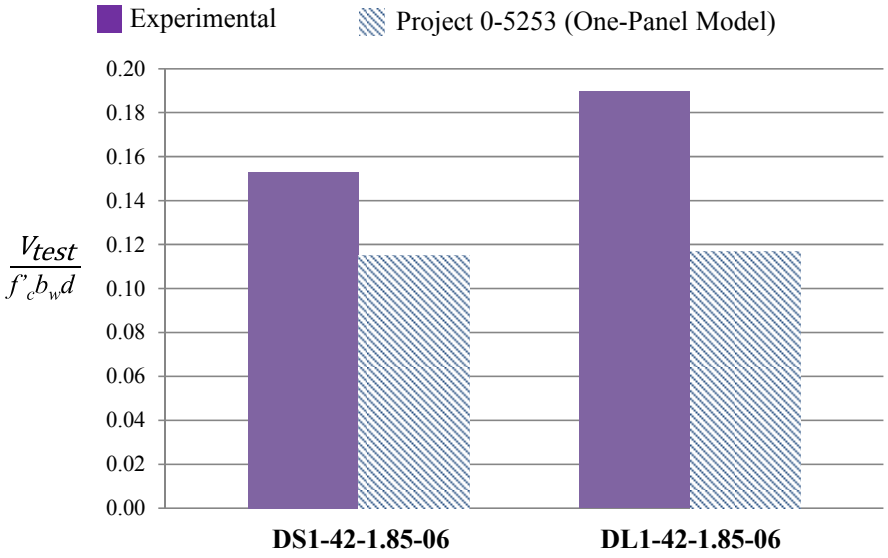

Figure 4-23: Experimental and calculated ultimate shear capacities for a/d = 1.85

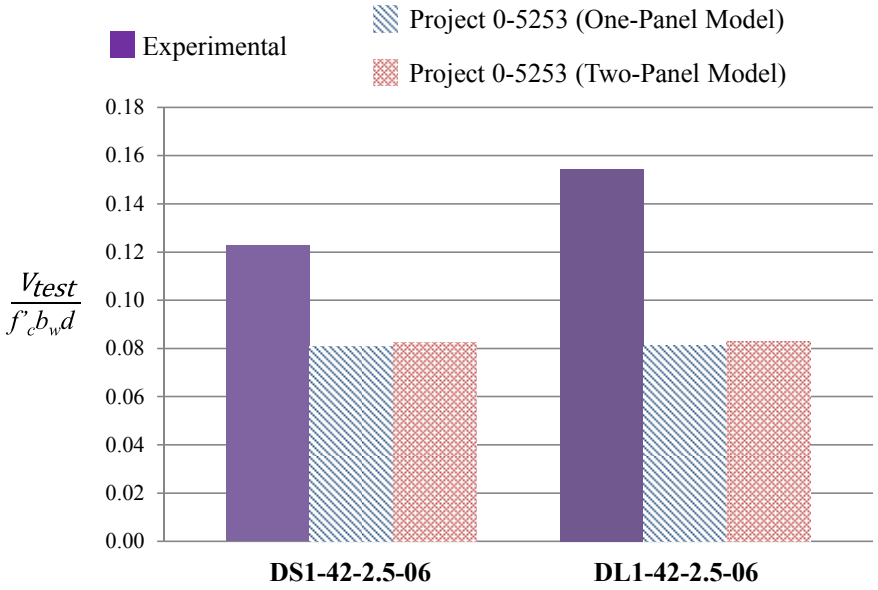

Figure 4-24: Experimental and calculated ultimate shear capacities for a/d = 2.5

The fact that the ledge length did not affect the controlling element is reflected in the conservativeness of the different models. The actual failure capacity to predicted failure capacity ratios are presented in Figure 4-25 and Figure 4-26, for a/d = 1.85 and 2.5, respectively. The first observation is the general conservativeness of the models for

all the specimens, with actual to predicted ratios between 1.33 and 1.9. The conservativeness experienced in these tests was similar to that of Project 0-5253.

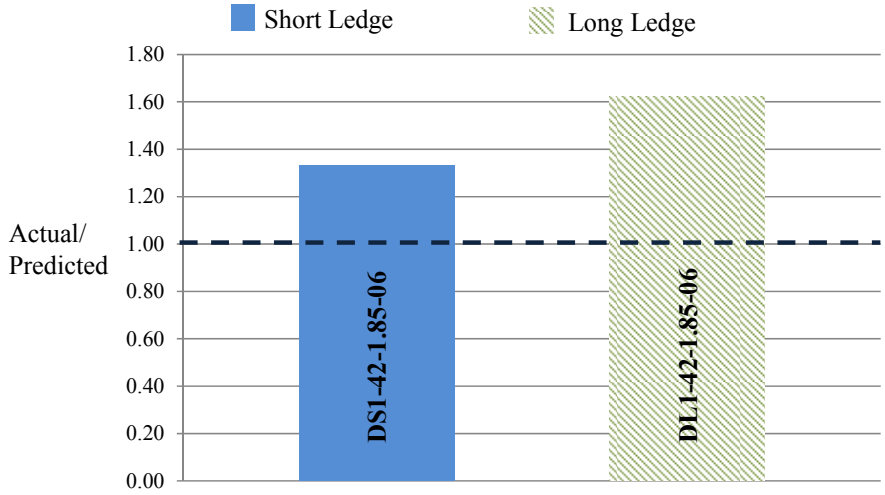

Figure 4-25: Actual capacity to predicted capacity ratio for one-panel failure (a/d = 1.85)

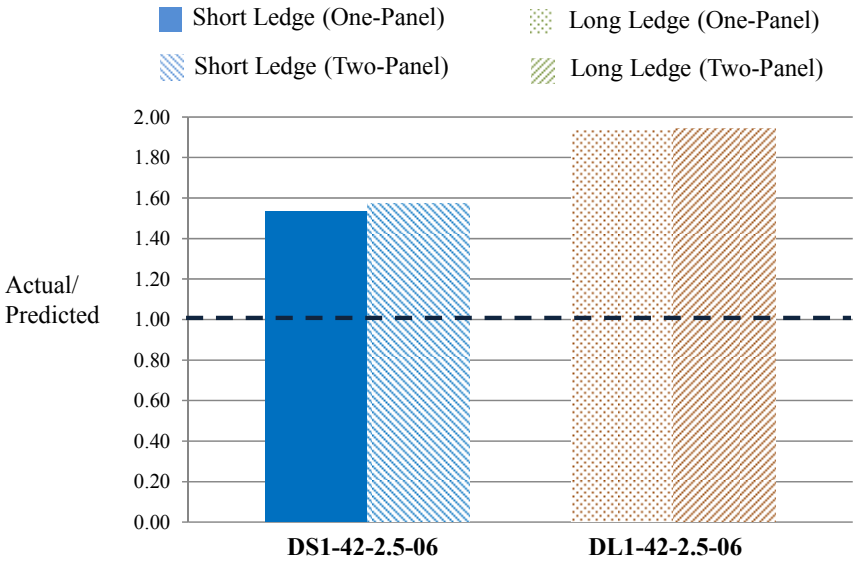

Figure 4-26: Actual capacity to predicted capacity ratio for both one- and two-panel failures (a/d = 2.5)

The next observation is the fact that the longer ledge model was more conservative than the short ledge specimen. This is a reflection of the model not being

influenced by the increased ledge length. Typical strut-and-tie models used for analysis and design of the specimen are shown in Figure 4-27. In the two-panel strut-and-tie model used for a/d = 2.5, shown in Figure 4-27 (a), the controlling element was the highlighted vertical tie. By increasing the length of the ledge, the advantages of the extra concrete area is not passed to the controlling tie, which increases the conservativeness of the model's ultimate capacity prediction. In the one-panel strut-and-tie model for a/d = 1.85, shown in Figure 4-27 (b), the controlling element was the highlighted node directly above the support. When the ledge is lengthened, the area of the node-strut interfaces is increased and therefore the ultimate capacity should also increase. Because it was unclear the exact amount the additional ledge area would increase the strut-node interface, the extra area was not included in the model to error on the conservative side.

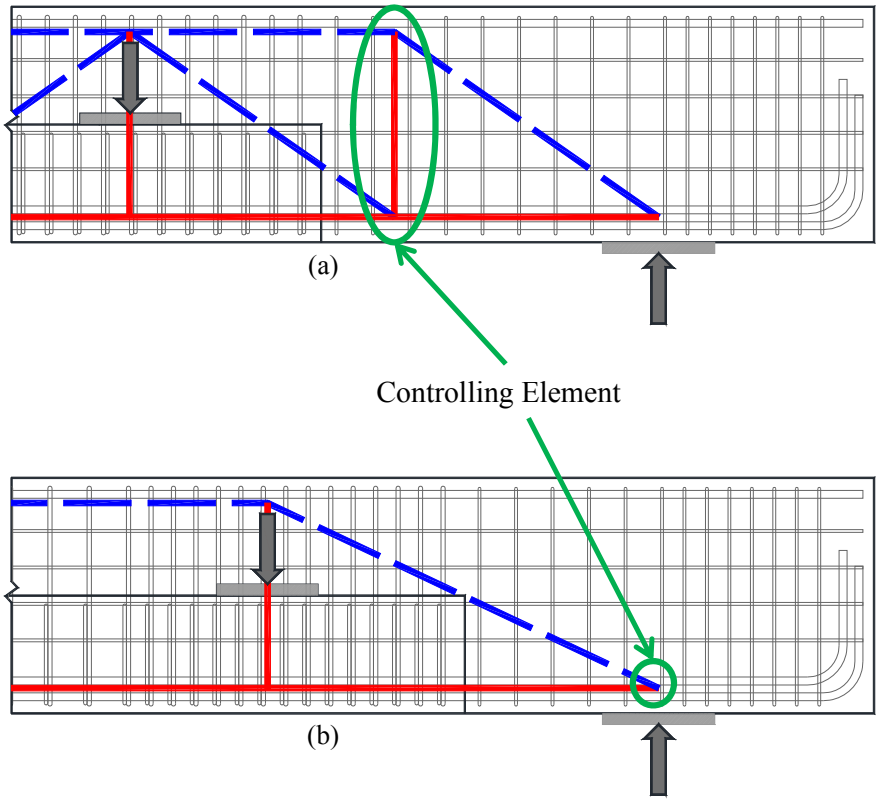

Figure 4-27: Typical STM used for design and analysis showing the controlling element; for (a) a/d = 1.85 and (b) a/d = 2.5

The photographs from after the failure of the short ledge and long ledge specimen in this series are presented in Figure 4-28 and Figure 4-29. The ultimate capacities for these specimens are presented alongside the failure photographs.

DS1-42-1.85-06

V_{test} = 621 kips

$10.8\sqrt{f'_c}b_w d$

$0.15f'_c b_w d$

(a)

DL1-42-1.85-06

V_{test} = 741 kips

$13.2\sqrt{f'_c}b_w d$

$0.19f'_c b_w d$

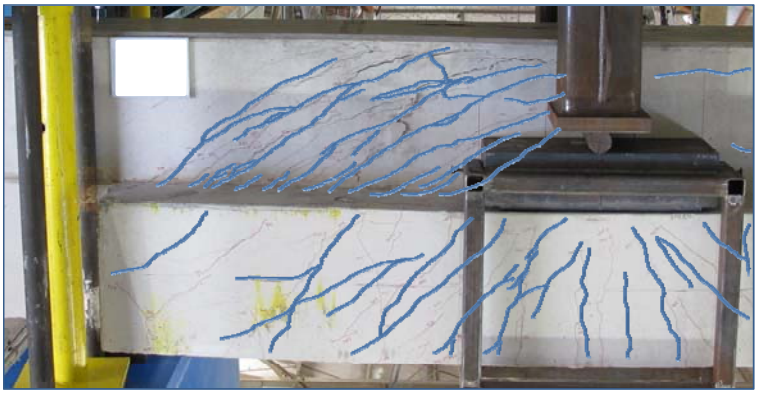

(b)

Figure 4-28: Ultimate shear capacities and cracking at ultimate load for specimen with a/d = 1.85 and (a) 0.003 and (b) 0.006 web reinforcement

DS1-42-2.5-06

V_{test} = 504 kips

$8.7\sqrt{f'_c}b_w d$

$0.12f'_c b_w d$

(a)

DL1-42-2.5-06

V_{test} = 622 kips

$10.9\sqrt{f'_c}b_w d$

$0.16f'_c b_w d$

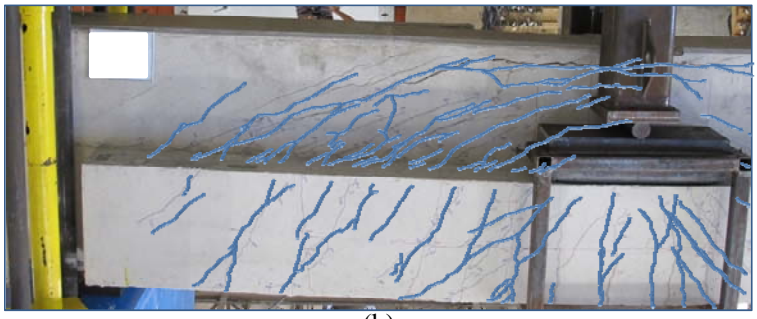

(b)

Figure 4-29: Ultimate shear capacities and cracking at ultimate load for specimen with a/d = 2.5 and (a) 0.003 and (b) 0.006 web reinforcement

4.4.3 Serviceability Results

The serviceability effects of the ledge length are examined with respect to deep beam and sectional shear spans in Figure 4-30 and Figure 4-31, respectively. The growth of the cracks (as a function of the applied load) and the crack pattern at failure are included for each shear span-to-depth ratio.

Regarding the serviceability of the two deep beam shear spans, the crack pattern developed within the deep-short (DS) ledge specimen was representative of a classic direct-strut failure mechanism. Strut splitting cracks extended from the compression chord directly to the support. The stem, or web, portion of the deep-long (DL) ledge specimen exhibited cracking similar to that found in the upper portion of the deep-short ledge specimen. However, the diagonal cracking did not extend to the vertical faces of the ledge in any significant manner. Cracks within the stem instead appeared to turn and run along the length of the ledge at the intersection of the stem and ledges. Despite

drastically different cracking patterns, the maximum diagonal crack width was not impacted by the presence or absence of a long ledge at any point in the loading history, as shown in Figure 4-30.

The serviceability behavior of the deep-short and deep-long ledge specimens with a shear span-to-depth ratio of 2.5 was very similar to that described above. Diagonal cracking within the short ledge specimen was representative of a typical sectional shear span. Initial cracks formed within the panel zones and extended to the compression chord and support. Distribution of the cracks along the span continued as load was applied. When the longer ledge specimen was tested, analogous cracking appeared within the stem, but again tended to terminate into the top of the ledge. The ledge length had no significant impact on the maximum diagonal crack widths within the sectional shear span.

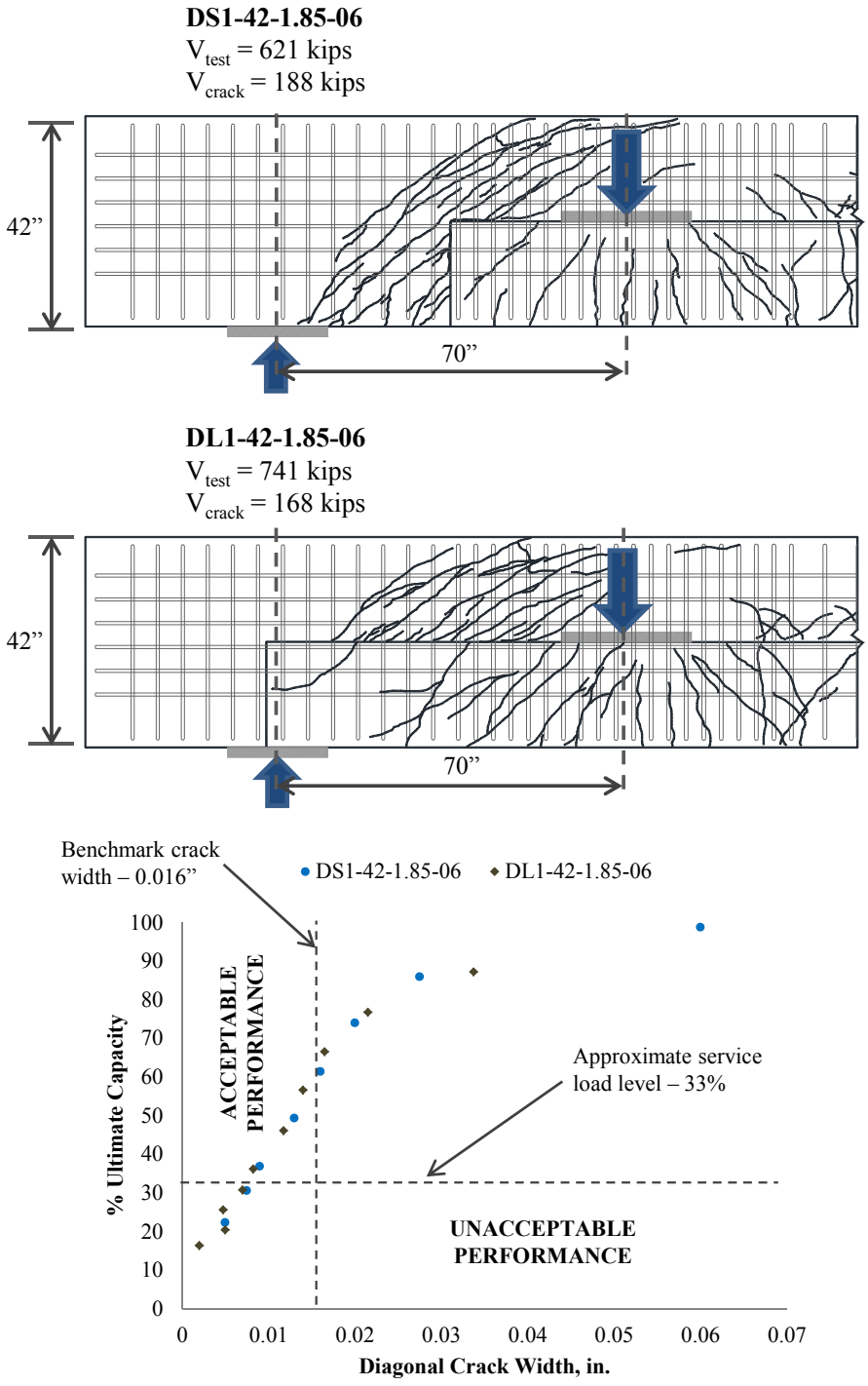

Figure 4-30: Serviceability data for deep-short and deep-long ledges with a/d = 1.85: Crack patterns (at ultimate capacity) and crack widths

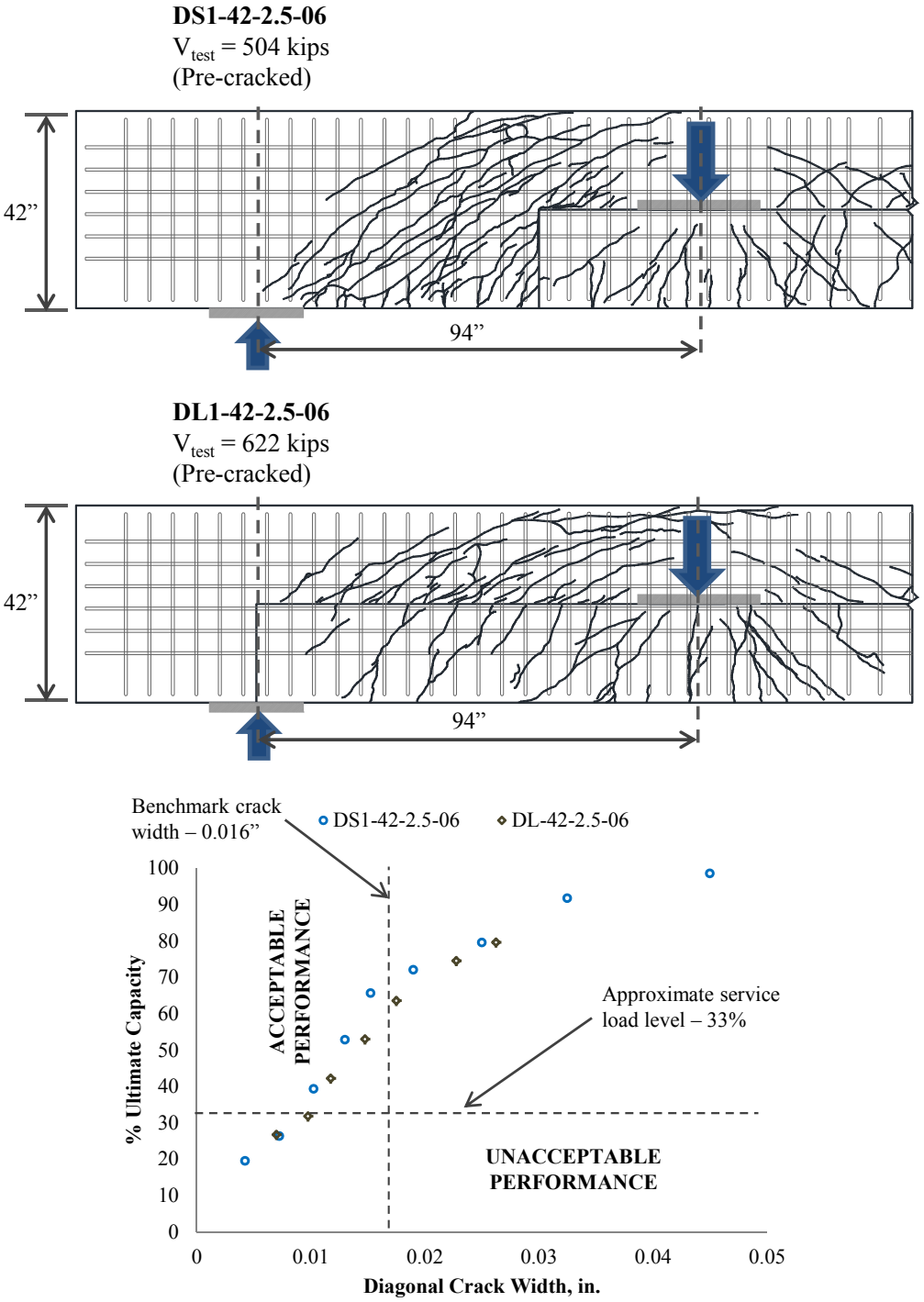

Figure 4-31: Serviceability data for deep-short and deep-long ledges with a/d = 2.5: Crack patterns (at ultimate capacity) and crack widths

4.4.4 Summary

Four tests, out of 16 planned, have been performed to provide initial insights into the behavioral impacts of long, short, and cut-off ledges. The specimens tested to date were designed to specifically address the effects of a longer ledge on the strength and serviceability performance of beams with shear span-to-depth ratios of both 1.85 and 2.5.

Initial strength results suggest that the longer ledge length increases the capacity of the specimen with both shear span-to-depth ratio of 1.85 and 2.5. Because the strut-and-tie model capacity is not influenced by the increased ledge length, the conservativeness of the design specifications was greater for the longer ledge specimen. All tests were generally similarly conservative to the tests performed in Project 0-5253. More testing is required to verify that the increased strengths are not simply due to the variability of shear tests.

Initial serviceability results indicate that the long ledge has no effect on the maximum diagonal crack width, but does appear to obscure/redirect cracking outside of the stem region.

4.5 SUMMARY

In this chapter the experimental results were presented and discussed. The ultimate shear capacities were presented and compared with the predicted capacities. Cracking patterns were shown for the various tests alongside crack size versus percent ultimate capacity comparisons. Only results from Series I and Series II tests were examined in this thesis.

Within Series I, eight initial tests (of twenty-four planned) have been performed to study the impact of varying the web reinforcement ratio between 0.003 (0.3%) and 0.006 (0.6%). These tests were performed on specimens with two different shear span-to-depth ratios, 1.85 and 2.5, and two different ledge geometries, deep-short (DS) and shallow-short (SS).

Initial strength results indicate that increased web reinforcement has no appreciable effect on the shear capacity of deep beam shear spans (a/d = 1.85), but

appears to increase the shear capacity of sectional shear spans (a/d = 2.5). These results are in agreement with the results of TxDOT Project 0-5253 and common wisdom regarding shear behavior.

Initial serviceability test results suggest that, in general, increasing the amount of web reinforcement decreases the crack widths measured throughout the loading history. This observation applies to both deep beam (a/d = 1.85) and sectional (a/d = 2.5) shear spans; though the magnitude of the crack width reduction appears (i.e., more testing is needed) to be dependent on the ledge depth. Increased web reinforcement also influenced the failure crack pattern in the test regions with a shear span-to-depth ratio of 2.5. Use of additional web reinforcement in resulted in a greater distribution of the cracking between the compression chord and support.

Within Series II, four tests, out of 16 planned, have been performed to provide initial insights into the behavioral impacts of long, short, and cut-off ledges. The specimens tested to date were designed to specifically address the effects of a longer ledge on the strength and serviceability performance of beams with shear span-to-depth ratios of both 1.85 and 2.5.

Initial strength results suggest that the longer ledge length increases the capacity of the specimen with both shear span-to-depth ratio of 1.85 and 2.5. More testing is required to verify that the increased strengths are not simply due to the variability of shear tests. Initial serviceability results indicate that the long ledge has no effect on the maximum diagonal crack width, but does appear to obscure/redirect cracking outside of the stem region.

In both series, the applicability of the strut-and-tie modeling provisions recommended by TxDOT Project 0-5253 was evaluated through a comparison of the STM-generated strength estimates and the experimental capacities. Application of the TxDOT Project 0-5253 provisions generally yielded conservative strength estimates. However, more data is needed to comment on the overall accuracy of the method as applied to inverted-T (top-chord loaded) members.

The data gathered from the experimental results will be further analyzed in Chapter 5. The experimental results will be compared to results from top chord loaded specimens.

CHAPTER 5
Analysis of Results

5.1 INTRODUCTION

A more detailed analysis of the preliminary experimental results is provided within this chapter. Specifically, results from the 10 inverted-T specimens tested to date are examined with respect to the strut-and-tie modeling provisions of TxDOT Project 0-5253 and the experimental results which underlie those provisions. This exercise goes beyond the Chapter 4 evaluation of the STM conservatism as applied to each specimen. Behavioral differences between the top-chord loaded specimens of TxDOT Project 0-5253 and the bottom-chord loaded specimens of the current project are examined (Section 5.2). The results of this study are utilized to identify necessary modifications to the recommended design specifications. The development of rational design expressions for ledge and hanger reinforcement in inverted-T beams is one of the foremost concerns within the current project (Section 5.3).

5.2 TOP- VS. BOTTOM-CHORD LOADED SPECIMENS

A detailed discussion regarding the differences between, and potential implications of, top- and bottom-chord loading was included within Chapter 2. A brief overview is included here for the sake of convenience. A member subject to 'top-chord' loading is directly loaded through the top side (which also corresponds to the compression chord in a simply-supported beam) as shown in Figure 5-1 (b). A member subject to 'bottom-chord' loading is indirectly loaded through the bottom side (which corresponds to the tension chord in a simply-supported beam) as shown in Figure 5-1 (a). Bottom-chord loading is typically accomplished with ledges or some other structural attachment. When an inverted-T is loaded through the bottom-chord, a tension tie is required to carry the load from the ledge to the compression chord; this tie is not explicitly required in top-chord loaded members.

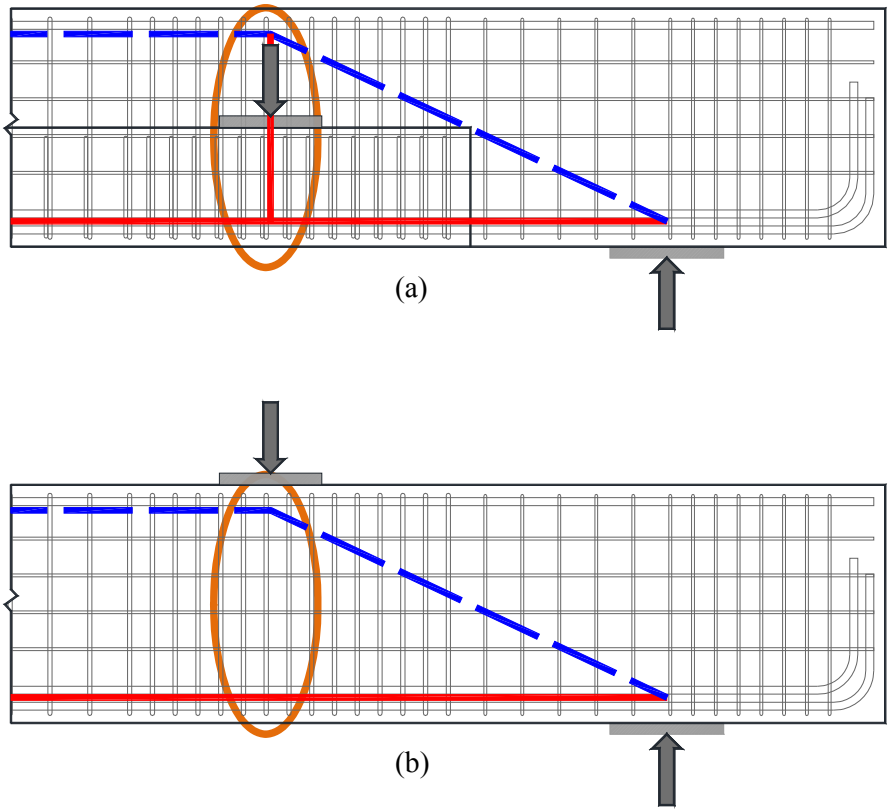

Figure 5-1: Strut-and-tie models for (a) bottom-chord loading and (b) top-chord loading

The resulting tension region within a bottom-chord loaded beam may have negative strength and serviceability implications as illustrated in Figure 5-2. In particular, the nodal regions at the compression chord will be subjected to the tension and will likely exhibit a lower efficiency as a result of it. Reduced capacity of the strut-to-node interface directly above the load point is a distinct possibility of the conditions depicted in Figure 5-2 (a). The strut-to-node interface is not affected by the presence of tension in a top-chord loaded specimen, as shown in Figure 5-2 (b). In truth, the region of tension within a bottom-chord loaded beam may not have any behavioral implications relative to the top-chord loaded beam; the nodal region at the compression chord does not typically control the strength of the strut-and-tie model for either loading condition. Irrespective of what the modeling may suggest, the primary purpose of the current

experimental program is to establish the strength and serviceability effects of the indirect (bottom-chord) loading condition.

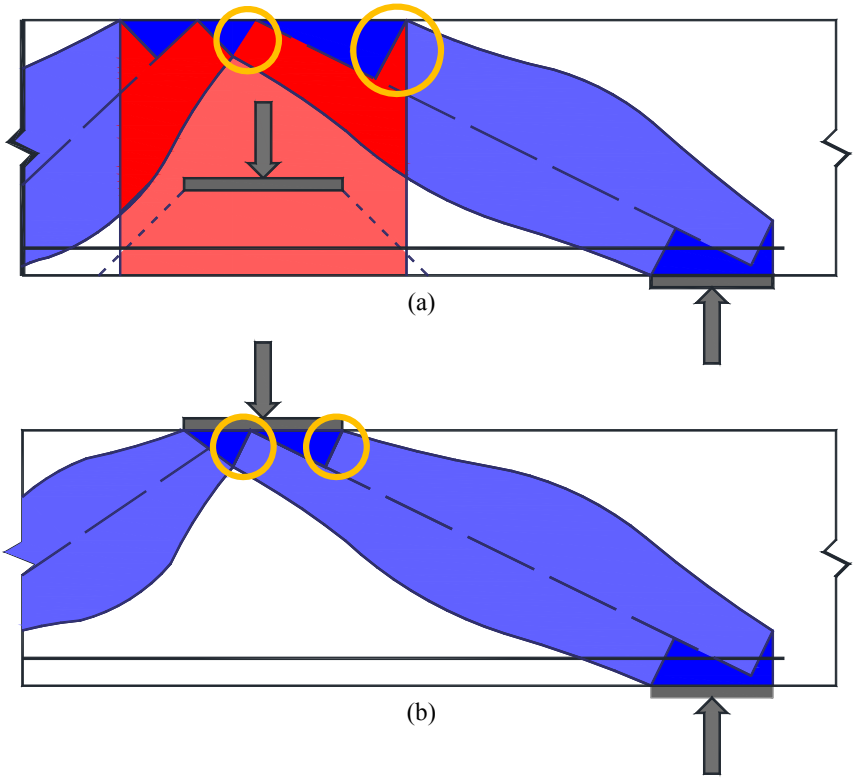

Figure 5-2: Strut-node interface (a) above load point in bottom-chord loaded and (b) below load point in top-chord loaded specimens

In regards to top-chord loaded members, the researchers of TxDOT Project 0-5253 investigated the strength and serviceability effects of several variables including: distribution of stirrup legs across the beam width, triaxially confined nodal regions, minimum web reinforcement, and beam depth. At the conclusion of the project, the results of 37 large-scale tests were analyzed in conjunction with 179 specimens from the literature to support the development of new strut-and-tie modeling provisions (Birrcher, et al. 2008). All of the data contributing to the development of these design specifications was collected from top-chord loaded specimens. The experimental program was designed to allow: (1) direct comparison with the top-chord loaded specimens (Section 5.2.1), and (2) verification of the TxDOT Project 0-5253 provisions for use on bottom-chord loaded members (Section 5.2.2).

5.2.1 Top- versus Bottom-Chord Loaded Comparison of Experimental Results

Two tests were performed that can be directly compared with specimens from TxDOT Project 0-5253. A summary of the experimental results from these tests, with regards to both strength and serviceability, is presented in Table 5-1 and Table 5-2. In Table 5-1, the measured shear capacities of the bottom- and top-chord loaded tests are grouped by shear span-to-depth ratio. The diagonal cracking loads are summarized in a similar manner within Table 5-2.

All of the specimens presented in Table 5-1 and Table 5-2 have a web reinforcement ratio of 0.003 (0.3%), both horizontally and vertically. All of the specimens also share the same web dimensions, 42 inches by 21 inches. The first four specimen presented have an a/d ratio of 1.85, the first being a bottom-chord loaded specimen with the other three being top-chord loaded specimens from TxDOT Project 0-5253. The last two have an a/d ratio of 2.5, the first being a bottom-chord loaded specimen and the other being a top-chord loaded specimen.

Table 5-1: Summary of strength performance for top- and bottom-chord loaded specimens

Beam I.D.	b_w in.	d in.	ρ_h	Bar size	s_h in	ρ_v	Bar size	s_v in	a/d ratio	Ledge info	V_{test} kip	$\frac{V_{test}}{f'_c b_w d}$	$\frac{V_{test}}{\sqrt{f'_c} b_w d}$
DS1-42-1.85-03	21	38.5	0.0029	#4	6.5	0.0029	#4	6.5	1.85	DS	712	0.17	12.1
I-03-2	21	38.5	0.0033	#4	5.75	0.0029	#4	6.5	1.84	-	569	0.13	9.7
III-1.85-03	21	38.6	0.0029	#5	10.1	0.0029	#5	10	1.84	-	412	0.10	7.2
III-1.85-03	21	38.6	0.0029	#5	10.1	0.0032	#4	6	1.84	-	471	0.18	10.1
DS1-42-2.5-03	21	38.5	0.0029	#4	6.5	0.0029	#4	6.5	2.5	DS	406	0.09	6.8
III-2.5-03	21	38.6	0.0029	#5	10.1	0.0032	#5	9.5	2.49	-	516	0.13	9.0

Table 5-2: Summary of serviceability performance for top- and bottom-chord loaded specimens

Beam I.D.	b_w in.	d in.	ρ_h	Bar size	s_h in	ρ_v	Bar size	s_v in	a/d ratio	Ledge info	V_{test} kip	V_{crack} kip	$\frac{V_{crack}}{\sqrt{f'_c} b_w d}$	$\frac{V_{crack}}{V_{test}}$
DS1-42-1.85-03	21	38.5	0.0029	#4	6.5	0.0029	#4	6.5	1.85	DS	712	172	2.9	0.24
I-03-2	21	38.5	0.0033	#4	5.75	0.0029	#4	6.5	1.84	-	569	144	2.5	0.25
III-1.85-03	21	38.6	0.0029	#5	10.1	0.0029	#5	10	1.84	-	412	137	2.4	0.33
III-1.85-03	21	38.6	0.0029	#5	10.1	0.0032	#4	6	1.84	-	471	114	2.4	0.24
DS1-42-2.5-03	21	38.5	0.0029	#4	6.5	0.0029	#4	6.5	2.5	DS	406	-	-	-
III-2.5-03	21	38.6	0.0029	#5	10.1	0.0032	#5	9.5	2.49	-	516	-	-	-

5.2.1.1 Strength Results

The strength results from the top- and bottom-chord loaded specimens are compared in order to identify the effects of ledge-induced tension on the strength performance. As previously discussed, the ledge-induced tension may affect the capacity of the strut-to-node interface in the compression chord. The results from these specimens may be directly compared since the nature of the loading is the only difference between the specimens. In order to determine the differences in strength between top- and bottom-chord loaded specimens, the ultimate shear capacities are presented for specimens with shear span-to-depth ratios of 1.85 and 2.5.

The results of four tests (one from Project 0-6416 and three from Project 0-5253) conducted at a shear span-to-depth ratio of 1.85 are included in Figure 5-3. The strength of the bottom-chord loaded specimen (DS1-42-1.85-03) fell within the range of capacities measured during tests of similar specimens in TxDOT Project 0-5253. The wide range of capacities measured during the top-chord tests ($0.10f'_c b_w d$ to $0.18\ f'_c b_w d$) clearly illustrates the variable nature of shear behavior, and helps to establish reasonable expectations for the review of test data. While there is not sufficient data to support firm conclusions, similarity of the results can most likely be attributed to the fact that the tension introduced by bottom-chord loading does not interfere with the controlling strut-to-node interface at the support.

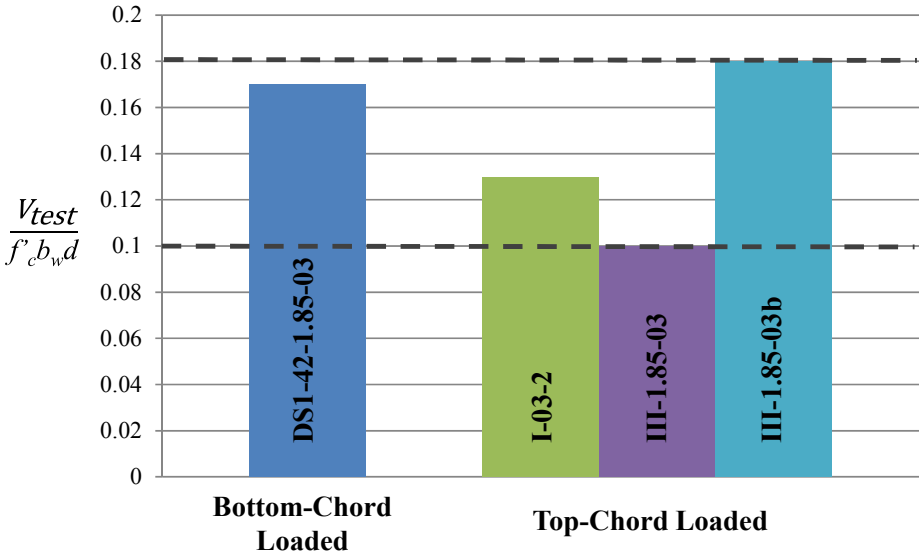

Figure 5-3: Ultimate shear capacities for bottom- and top-chord loaded specimens with a/d = 1.85

The results of two tests (one from Project 0-6416 and one from Project 0-5253) conducted at a shear span-to-depth ratio of 2.5 are included in Figure 5-4. Only one comparable specimen with a web reinforcement ratio of 0.003 was tested within the duration of Project 0-5253. The bottom-chord loaded specimen had a significantly lower capacity, 31 percent less than the top-chord loaded specimen, as shown in Figure 5-4. Prior to drawing any conclusions regarding the effects of bottom-chord loading in section shear spans, additional tests must be conducted to establish the variability related to this testing configuration. Future testing will reveal whether or not the tension resulting from bottom-chord loading is detrimental to the capacity of a longer (sectional) shear span. Theoretical implications of the ledge-induced tension were previously explored in Section 1.2.

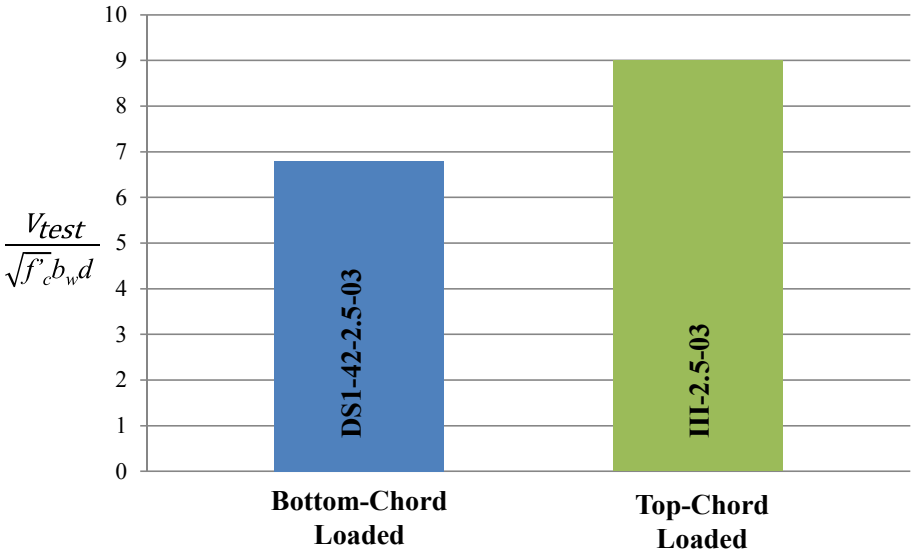

Figure 5-4: Ultimate shear capacities for bottom- and top-chord loaded specimens with a/d = 2.5

5.2.1.2 Serviceability Results

The serviceability results from the top- and bottom-chord loaded specimen are compared in order to identify the effects of ledge-induced tension on the service level performance. The first diagonal cracking load is first reviewed. Crack width history is then reviewed to identify other behavioral effects of ledge-induced tension. This review of the crack width history may provide insights into the failure mode and failure strength of the specimens. Comparing the serviceability results from the top- and bottom-chord loaded specimens will also reveal the applicability of crack width to ultimate capacity relationships developed by TxDOT Project 0-5253.

The normalized shear force measured at first diagonal cracking is summarized in Table 5-2 for each of the specimens. From the initial results, it would appear that loading the bottom chord, rather than the top chord, does not adversely influence the shear force required to cause first diagonal cracking. It is important to reemphasize that the current discussion is limited to specimens with a shear span-to-depth ratio of 1.85; pre-cracking of the longer shear span (a/d = 2.5) during the deep beam test eliminated the opportunity to record the first diagonal cracking load. The results are summarized in Figure 5-5.

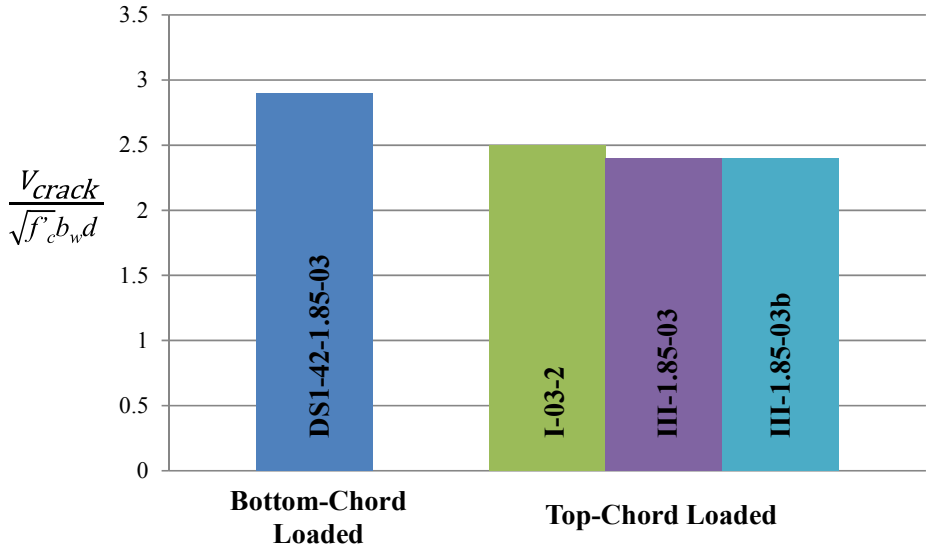

Figure 5-5: First cracking shear force for bottom- and top-chord loaded specimens with a/d = 1.85

The ratio of the shear force measured at first cracking to the ultimate shear capacity of each specimen is presented in Figure 5-6. Each of the specimens cracked and failed at similar shear force magnitudes, resulting in relatively similar diagonal cracking ratios (V_{crack}/V_{test}). Regardless of the loading configuration (top- vs. bottom-chord), all of the specimens cracked at or below the service load level of shear (33% of the ultimate capacity).

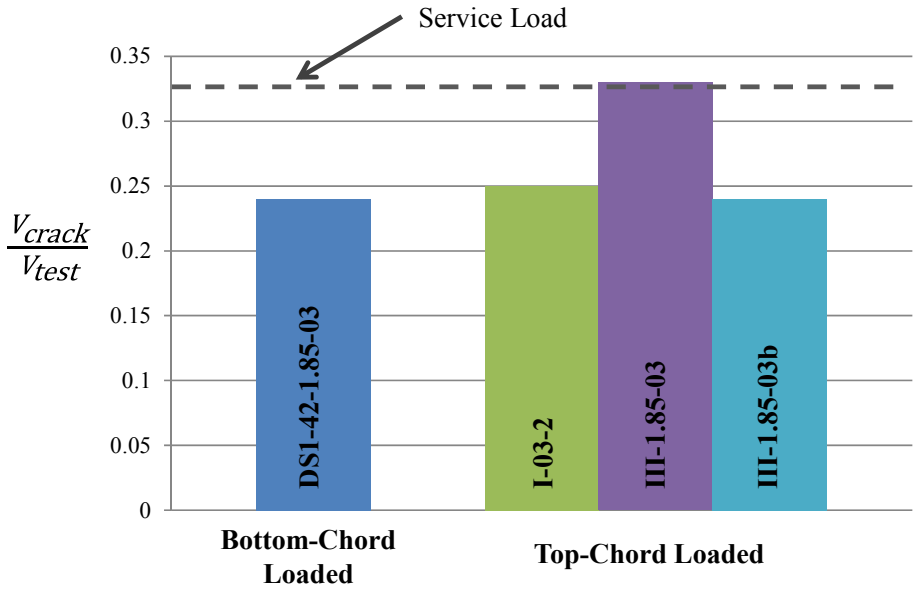

Figure 5-6: Ratio of first cracking shear force to ultimate shear capacity for bottom- and top-chord loaded specimens with a/d = 1.85

The percentage of the maximum applied shear force in both top- and bottom-chord loaded specimens is presented as a function of the maximum diagonal crack width in Figure 5-7 (for an a/d ratio of 1.85) and Figure 5-9 (for an a/d ratio of 2.5). The web reinforcement ratio in all of the specimens was 0.003.

The bottom-chord loaded specimens with an a/d ratio of 1.85 exhibited cracking that was very similar to that experienced by the top-chord loaded specimen, as shown in Figure 5-7. These initial results suggest that the TxDOT Project 0-5253 table (reproduced in Figure 5-8) relating crack width to percent ultimate capacity may be applicable to inverted-T beams. Further test results are nonetheless needed to verify these results.

The crack widths measured during the bottom-chord load tests (at an a/d ratio of 2.5) were notably smaller than those measured during the top-chord load tests (please see Figure 5-9). In fact, the TxDOT Project 0-5253 specimen loaded at the top-chord performed unacceptably at service loads, while the two bottom-chord loaded specimens did not.

The smaller crack width is contrary to what was thought would logically occur: the introduction of tensile forces at the load point would increase the crack widths in the bottom-chord loaded specimens. As shown in Figure 5-10, the crack patterns for the top and bottom-chord loaded specimen were very similar, while the shear capacity of the bottom-chord loaded specimen was significantly less than that of the top-chord loaded specimen. If the shear capacity of the bottom-chord loaded specimen was higher (closer to that of the top-chord loaded specimen), then the crack widths in relation to the ultimate capacity would have been similar. This tells us that at similar loads, the two specimens had similar crack sizes (Figure 5-11) and the difference in the plot simply reflects the fact that the bottom-chord loaded specimen failed at a lower shear force, which may have simply been due to variability present in shear tests. More testing needs to be completed before any conclusions can be made.

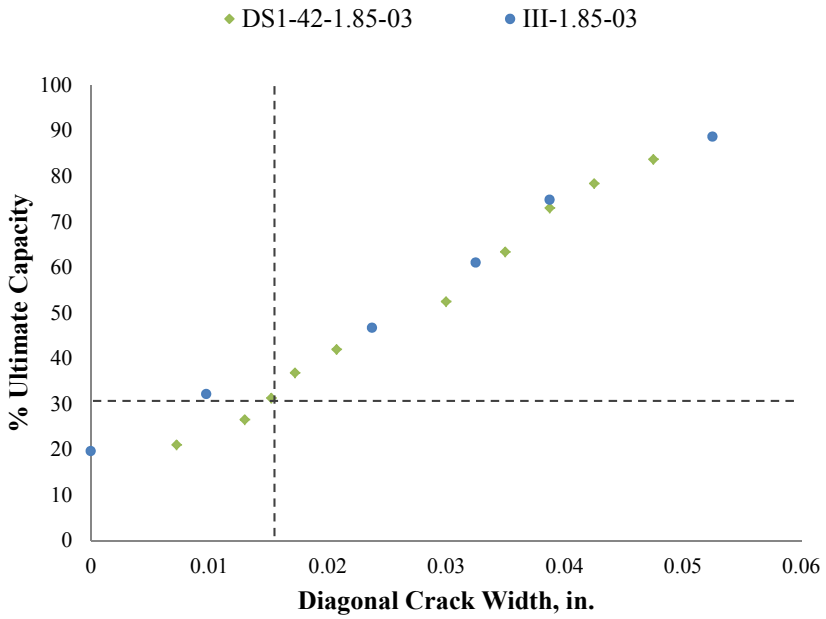

Figure 5-7: Diagonal crack widths versus percent ultimate capacity for bottom- and top- chord loaded specimens with a/d = 1.85 and reinforcement ratio of 0.003

Load on the Member, Quantified as a Percent of Ultimate Capacity on Average (± scatter)						
Reinforcement \ w_{max} (in.)	**0.01**	**0.02**	**0.03**	**0.04**	**0.05**	**0.06**
ρ_v = 0.002 ρ_h = 0.002	20 (+10)	30 (±10)	40 (±10)	50 (±10)	60 (±15)	70 (±15)
ρ_v = 0.003 ρ_h = 0.003	25 (±10)	40 (±10)	55 (±10)	70 (±10)	80 (±10)	90 (±10)
ρ_v > 0.003 ρ_h > 0.003	30 (±10)	50 (±10)	70 (±10)	85 (±10)	~ Ultimate	~ Ultimate

Notation:

w_{max} = maximum measured diagonal crack width (in.)

ρ_v = reinforcement ratio in vertical direction ($\rho_v = A_v / bs_v$)

ρ_h = reinforcement ratio in horizontal direction ($\rho_h = A_h / bs_h$)

A_v & A_h = total area of stirrups or horizontal bars in one spacing ($in.^2$)

s_v & s_h = spacing of stirrups or horizontal bars (in.)

b = width of web (in.)

Directions:

1). Determine ρ_v and ρ_h for bent cap

2). Measure maximum diagonal crack width, w_{max}, in inches

3). Use chart with w_{max}, ρ_v, and ρ_h to estimate % of capacity

Important Notes:

In this chart, the maximum width of the primary diagonal crack in a shear-critical member is linked to the load on the member, quantified as a percent of its ultimate capacity. The intent of this chart is to aide field engineers in evaluating residual capacity in diagonally-cracked, reinforced-concrete bent caps subjected to concentrated loads at a/d ratios between 1.0 and 2.0. This chart was developed from crack width data from 21 tests of simply-supported reinforced concrete beams with overall heights between 42" and 75". The testing was conducted at an a/d ratio of 1.85. Data has shown that diagonal crack widths may slightly decrease with decreasing a/d ratio. The same crack width at a smaller a/d ratio indicates that a higher percentage of capacity from the above chart has already been reached.

This chart should be used in conjunction with sound engineering judgement with consideration of the following limitations:

-variability in crack widths in general (± scatter)

-members loaded at a/d < 1.85 may be at slightly higher % of capacity

-differences between field and laboratory conditions

-implications of an unconservative estimate of capacity

This chart is not intended to be used for inverted-T bent caps.

Figure 5-8: Proposed chart to link diagonal crack width to percent of ultimate capacity for top-chord loaded specimens (Birrcher, et al. 2008)

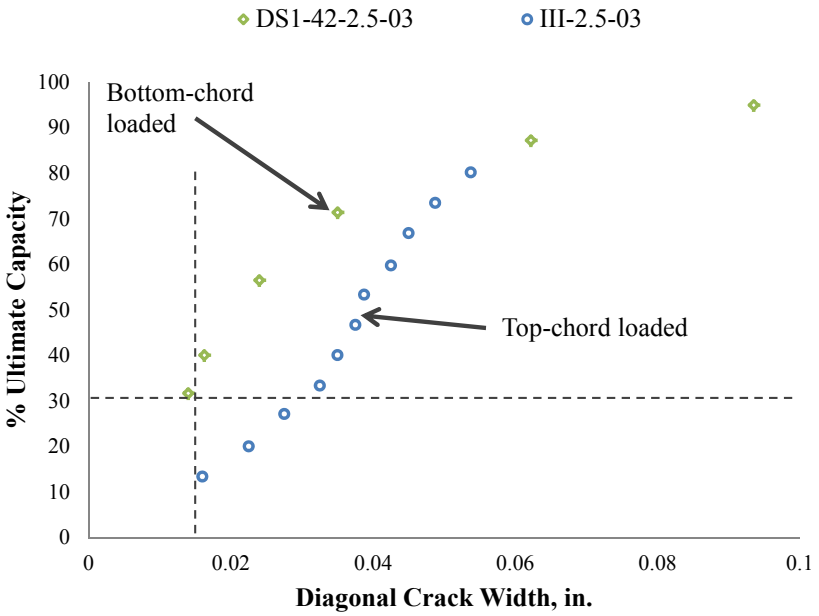

Figure 5-9: Diagonal crack widths versus percent ultimate capacity for bottom- and top- chord loaded specimens with a/d = 2.5 and reinforcement ratio of 0.003

DS1-42-2.5-03

V_{test} = 405 kips

$6.8\sqrt{f'_c}b_wd$

$0.09f'_cb_wd$

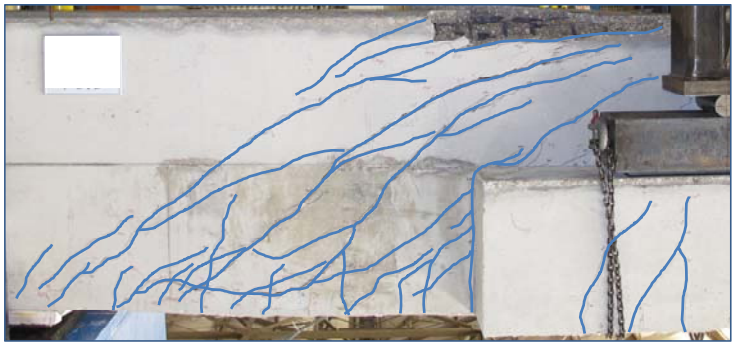

(a)

III-2.5-03

V_{test} = 516 kips

$9.0\sqrt{f'_c}b_wd$

$0.13f'_cb_wd$

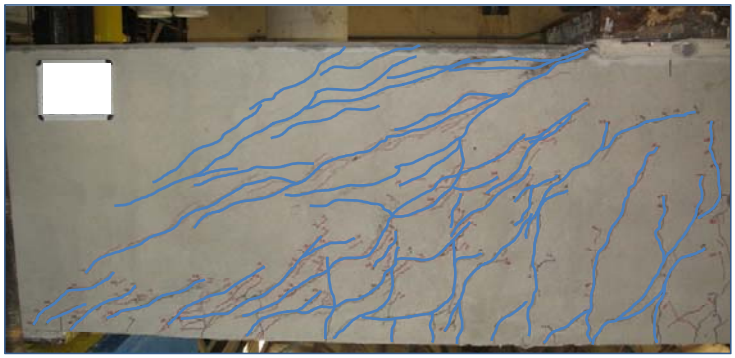

(b)

Figure 5-10 - Ultimate shear capacities and cracking at ultimate load for (a) bottom-chord and (b) top-chord loaded specimens with an a/d = 2.5 and 0.3% web reinforcement

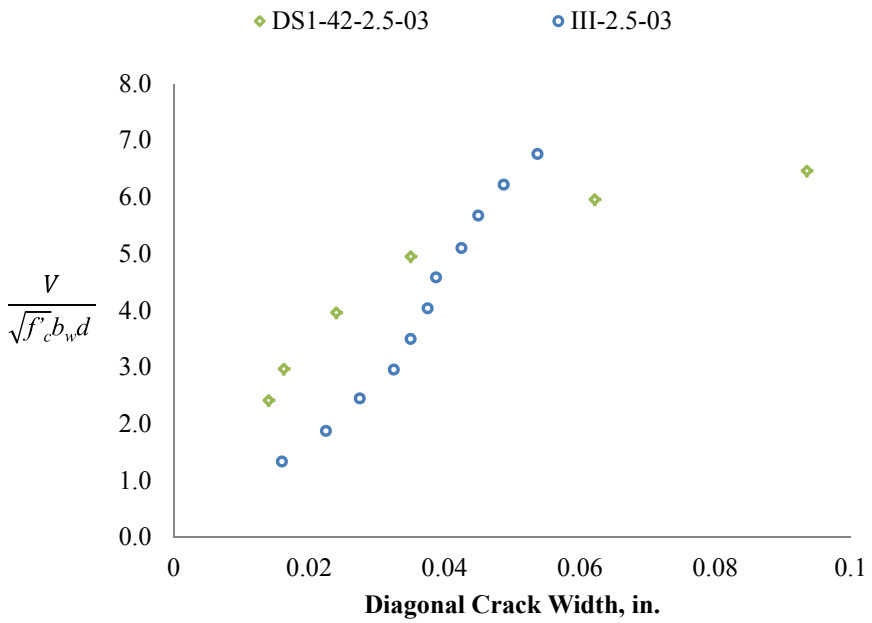

Figure 5-11 - Diagonal crack widths versus shear force for bottom- and top- chord loaded specimens with a/d = 2.5 and reinforcement ratio of 0.003

5.2.2 Applicability of TxDOT Project 0-5253 Provisions

Interpretation of the preliminary results is mixed due to a lack of data, but it appears that the strength and serviceability of deep beam and sectional shear spans are not adversely affected by bottom-chord loading (in relation to beams subject to top-chord loading). Please note that this statement requires further validation through more extensive testing. It is therefore expected that the provisions of TxDOT Project 0-5253, based upon the results of top-chord tests, will provide conservative estimates for the strength of inverted-T beams subject to bottom-chord loading. The overstrengths of the companion top- and bottom-chord tests described above are examined herein to evaluate the former statement. The overstrength, or rather conservatism, of the Project 0-5253 provisions will be calculated as the ratio of the measured failure shear to the calculated failure shear. At the completion of testing and issuance of a final report, the final strut-

and-tie modeling provisions will be deemed satisfactory for bottom-chord loading if they maintain the same level of conservatism and accuracy established for top-chord loading.

Figure 5-12 (a/d = 1.85), Figure 5-13 (a/d = 2.5, one panel model), and Figure 5-14 (a/d=2.5, two panel model) provide a visual summary of the overstrength of each inverted-T specimen tested to date, as well as the overstrength of the companion specimens from TxDOT Project 0-5253. Please note that in this comparison section, one short-shallow (SS) ledge specimen was provided in the comparison. This specimen was excluded in previous comparisons due to the possible behavioral difference using three loading points versus one loading point, but is included here because the loading difference can be accounted for in the strut-and-tie model. Also note that a value over 1.0 indicates a conservative estimation of the shear strength and is most desired as such. Overall, the strut-and-tie modeling provisions of Project 0-5253 provided conservative estimations (i.e. actual-to-calculated capacity greater than or equal to 1.0) of the strength with respect to both deep beam and sectional shear spans subject to bottom-chord loading. The average ratio of the measured capacity to the calculated capacity in deep beam, one-panel sectional, and two-panel sectional shear spans was 1.33, 1.43 and 1.69, respectively. The lowest overstrength of 1.0 (SS3-42-1.85-03) still exceeded that of the TxDOT Project 0-5253 evaluation database; equal to 0.73. In fact, these results are comparable to the performance of the Project -5253 provisions within the complete evaluation database of 179 tests. The average ratio of measured-to-calculated capacity was 1.54 in that case.

With a shear span-to-depth ratio of 2.5, it is important that the correct strut-and-tie model is chosen. As previously discussed in Section 2.4.2, as the shear span-to-depth ratio is increased from 2.0 to 2.5, the behavior of the section gradually transitions from deep beam behavior, where strains vary nonlinearly; to sectional shear behavior, where strains vary linearly with section depth. In deep beam regions, a one-panel model is appropriate to use, shown by the conservative results shown in Figure 5-12. As the shear span-to-depth ratio approaches 2.5, a one-panel strut-and-tie model is less appropriate and will produce less conservative results, as shown in Figure 5-13. When the

appropriate two-panel model is used, the strut-and-tie model exhibited adequate conservatism, as shown in Figure 5-14.

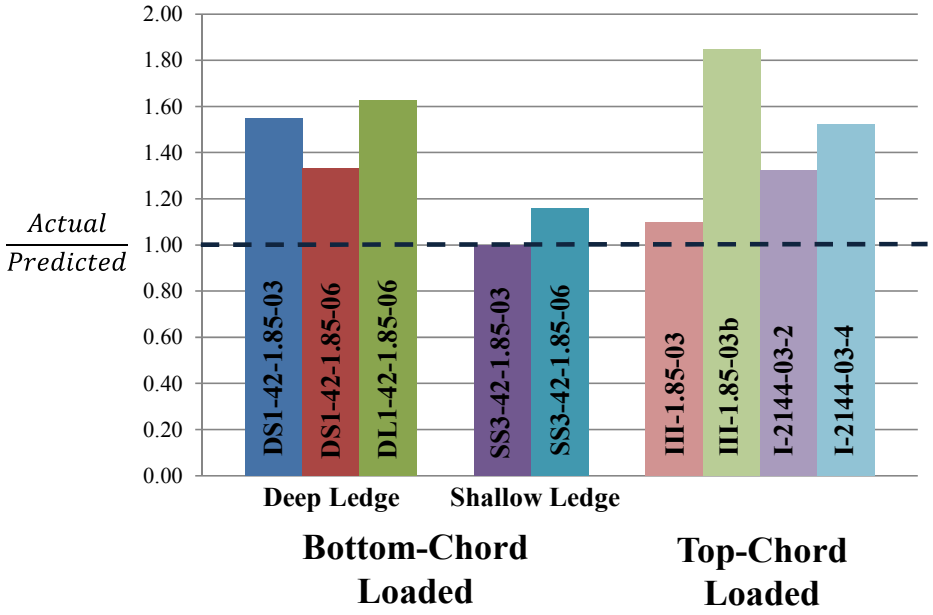

Figure 5-12: Actual capacity to predicted capacity ratio for specimens with a/d = 1.85

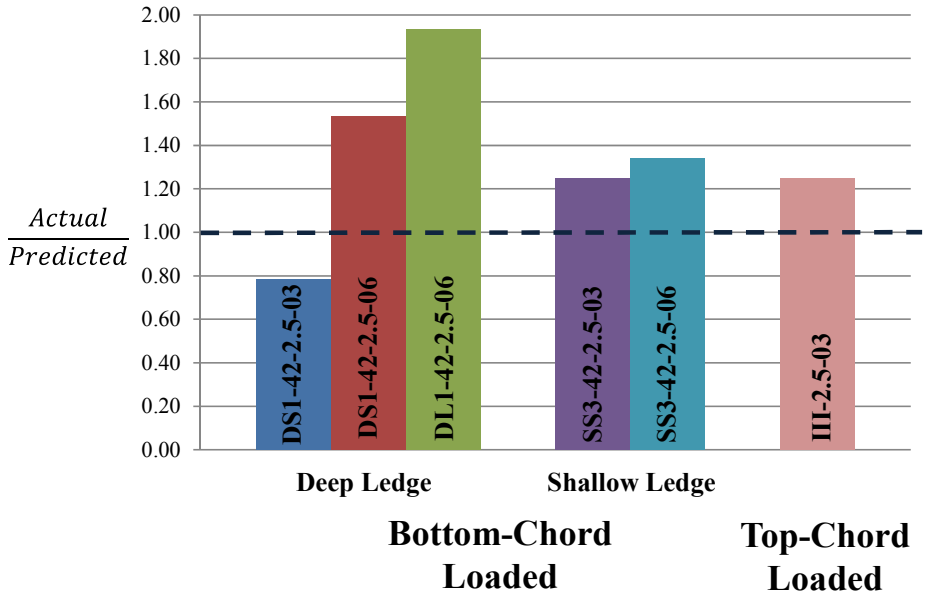

Figure 5-13: Actual capacity to predicted capacity ratio for specimens with a/d = 2.5 (using a one-panel model, grouped by ledge depth)

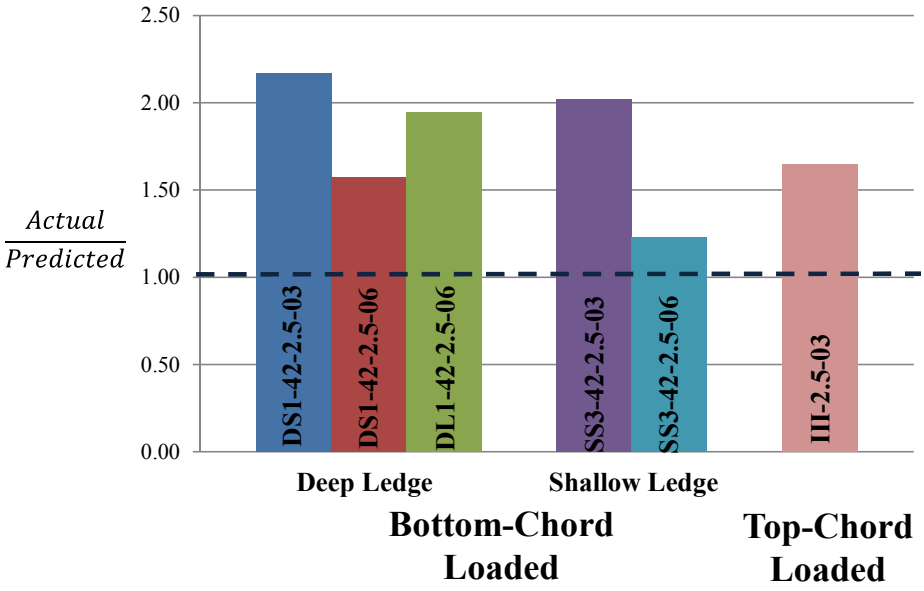

Figure 5-14: Actual capacity to predicted capacity ratio for specimens with a/d = 2.5 (using a two-panel model)

5.2.3 Summary

In general, the ultimate capacities, shear loads at first cracking, and crack widths of bottom-chord loaded specimens were similar to those of top-chord loaded specimens. A direct comparison could only be made between specimens with a web reinforcement ratio of 0.003 due to no top-chord loaded specimen with a reinforcement ratio of 0.006 being tested in the experimental program of Project 0-5253.

The design specifications suggested by Project 0-5253 were used for the design and analysis of all the specimens in the experimental program. The use of these design specifications for the bottom-chord loaded specimens provided similar conservativeness to top-chord loaded specimens for the majority of the tests. The importance of selecting the correct model when designing the specimen is evident by an unconservative result. For specimens with a shear span-to-depth ratio of 2.5, a two panel model is more appropriate. In general, the design specifications suggested by Project 0-5253 performed

similarly for both top- and bottom-chord loaded specimens. More information is needed to further confirm the design provisions use for bottom-chord loaded specimens.

5.3 LEDGE AND HANGER REINFORCEMENT FOR BOTTOM-CHORD LOADING

In order to fully adapt the TxDOT Project 0-5253 STM provisions to inverted-T beams, the final recommendations of the current project will likely include detailed guidance regarding the design of ledge and hanger reinforcement. Current design and detailing guidance for ledge and hanger reinforcement is based on successful past practices and very limited experimental data. Following a brief review of the rationale underlying the current provisions, the accuracy of those provisions is evaluated with experimental data from the current test program.

5.3.1 Background

The analysis and design of an inverted-T (bottom-chord loaded) member is far more complicated than an equivalent top-chord loaded member due to the necessary inclusion of a ledge. The ledge must successfully transfer the offset loads to the web of the beam, where it is picked up and transferred laterally to the support through a series of hangers, struts and ties. The primary load path with the cross-section of an inverted-T is illustrated in Figure 5-15 (a). A comparable strut-and-tie model for the cross-section is included in Figure 5-15 (b). In a standard rectangular beam, cross-sectional modeling is not necessary because the loads are generally applied through the top face and are closely aligned with the centroid of the section (i.e. no transverse flow of forces in the cross-section).

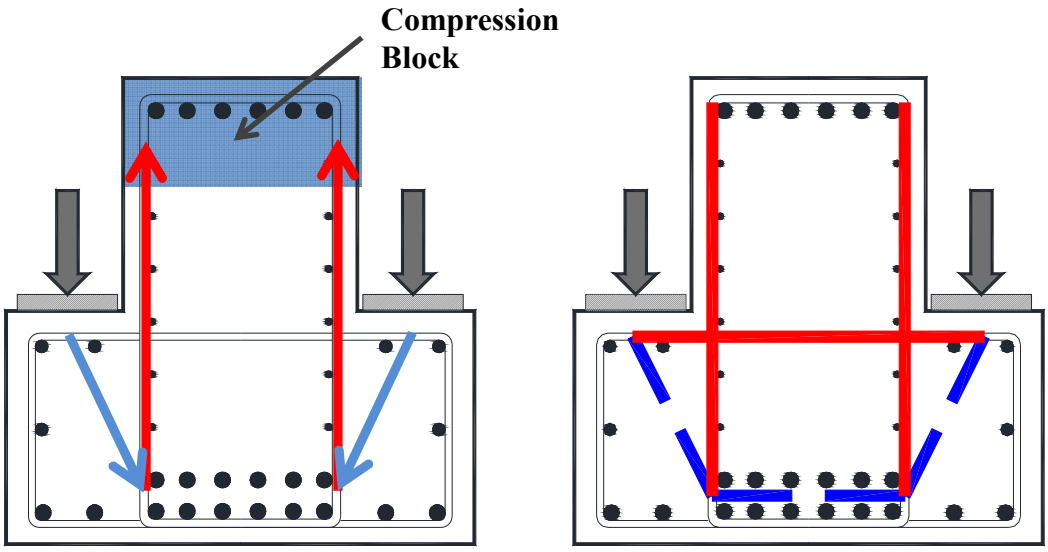

Figure 5-15: Cross-sectional (a) flow of forces and (b) STM

The cross-sectional strut-and-tie model contains two tension ties that must be properly reinforced, as shown in red within Figure 5-15 (b). The reinforcement used to satisfy these ties is referred to as "hanger reinforcement," as shown in Figure 5-16 (a), and "ledge reinforcement," as shown in Figure 5-16 (b).

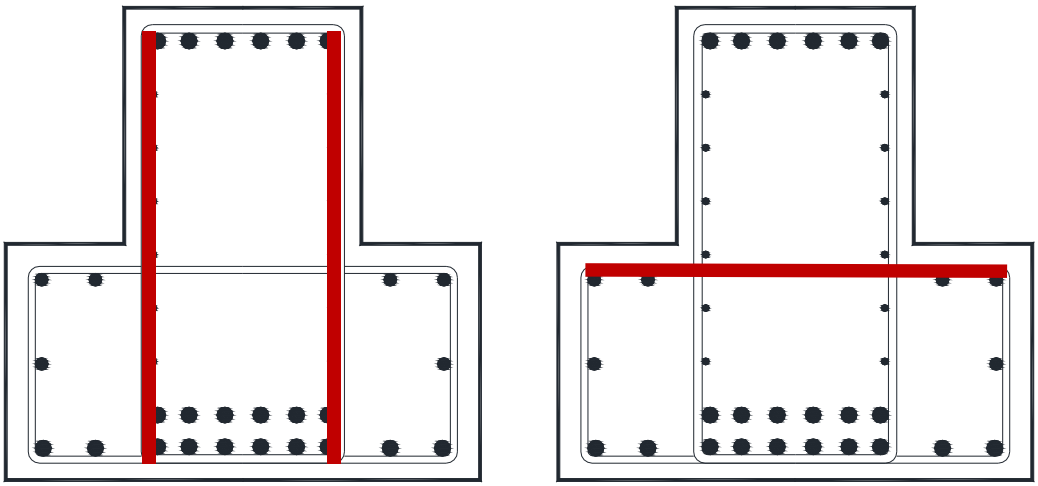

Figure 5-16: Cross-section showing (a) hanger and (b) ledge reinforcement

The cross-sectional location of both the hanger and ledge reinforcement was clearly defined from the strut-and-tie model and concrete cover requirements. However, the optimal placement (i.e. spacing along the beam length) of the hanger and ledge reinforcement to simultaneously satisfy the tie requirements and provide serviceable behavior was not as well defined. Current provisions regarding the design and detailing of ledge and hanger reinforcement for inverted-T members are not based upon the strut-and-tie models presented above. Methods currently presented within the AASHTO LRFD Bridge Design Specifications (2010) are empirical in nature. They are presented below to provide a point of comparison for the design assumptions made within the current project.

The current ledge and hanger reinforcement provisions (AASHTO 5.13.2.5) within the AASHTO LRFD include formulas (refer to Figure 5-17) for calculation of the effective width over which the ledge and hanger reinforcement should be distributed. The effective width to be used for distribution of the ledge reinforcement is based on the distance from the center of the outermost web stirrup to the center of the load point, denoted as a_f in Figure 5-17. This formulation purports that more of the ledge reinforcement is engaged in resisting ledge bending as the load is moved farther from the beam web.

In their study on strength criteria for inverted-T members, Mirza and Furlong (1983) suggested that the "effective distance" for the ledge reinforcement was a distance of $2a_f$ from the edge of each bearing pad. In a later study, Mirza, Furlong and Ma (1988) showed through experimental testing that the ledge steel up to $2.5a_f$ on each side of the load "appeared capable of developing as much force as did the steel directly beneath the point load." A similar width has since been adopted by the AASHTO LRFD Bridge Design Specifications (2010). The ledge tie width is then the lesser of: (1) two times the distance from the end of the ledge to the center of the outermost load point, and (2) the bearing width plus five times the a_f distance, as shown in Figure 5-17.

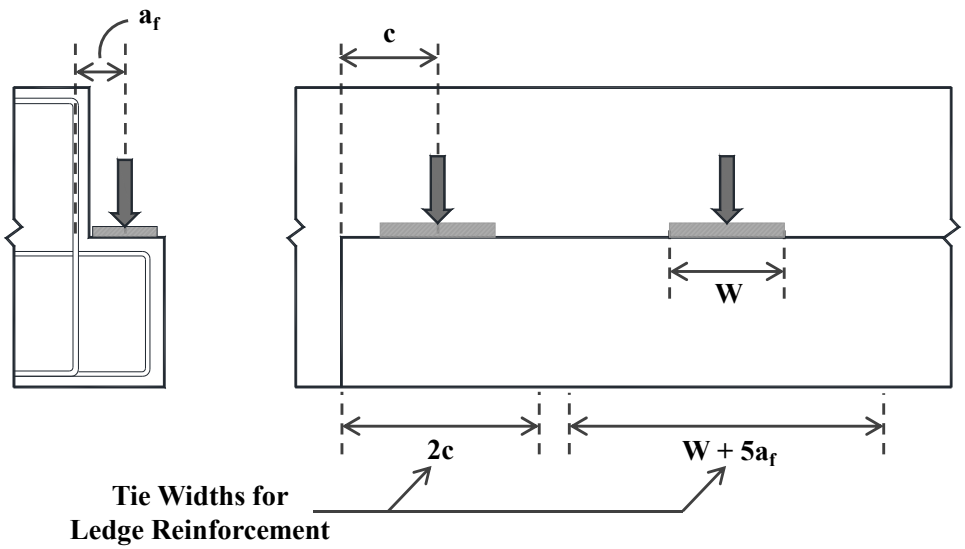

Figure 5-17: Suggested tie widths for ledge reinforcement, from Figure 5.13.2.5.3-1 (AASHTO 2009)

The AASHTO LRFD (2010) provision for the effective width of the hanger reinforcement is presented in Figure 5-18. It is based upon the design recommendations of Mirza and Furlong (1983). This tie width is determined from a 45-degree spread of the load between the outer edges of the bearing pad and the bottom of the stirrup, a distance d_f as shown in Figure 5-18.

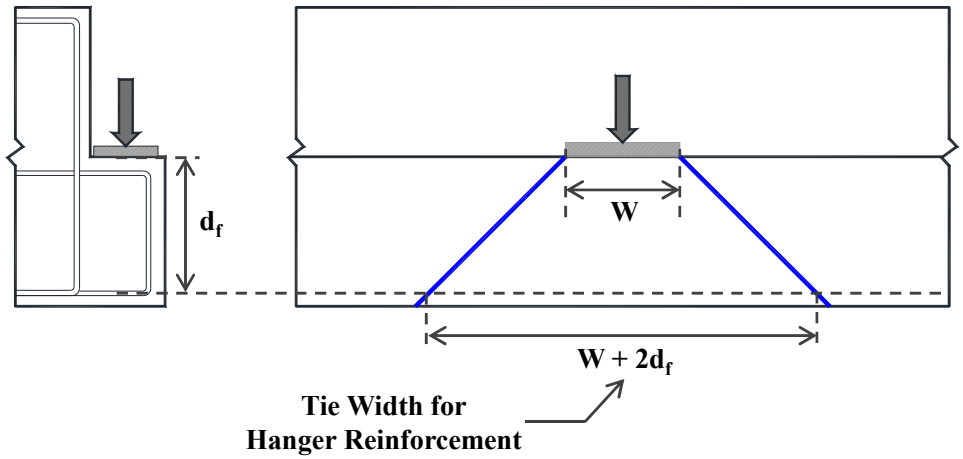

Figure 5-18: Suggested tie width for hanger reinforcement, from Figure 5.13.2.5.5-2 (AASHTO 2009)

5.3.2 Applicability of 45-Degree Load Spread

For design of the inverted-T specimens, assumptions had to be made regarding the width of the ledge and hanger ties. For the sake of determining the ledge and hanger tie widths, the load was assumed to spread at 45 degrees from the edges of the bearing pad, as shown in Figure 5-19. The width of the ledge tie was then taken at the mid-depth of the ledge as shown in Figure 5-19 (a). The width of the hanger tie was similarly determined in accordance with the current AASHTO LRFD provisions. The width of the hanger tie was defined by the intersection of the load spread and the bottom of the hanger reinforcement, as shown in Figure 5-19 (b).

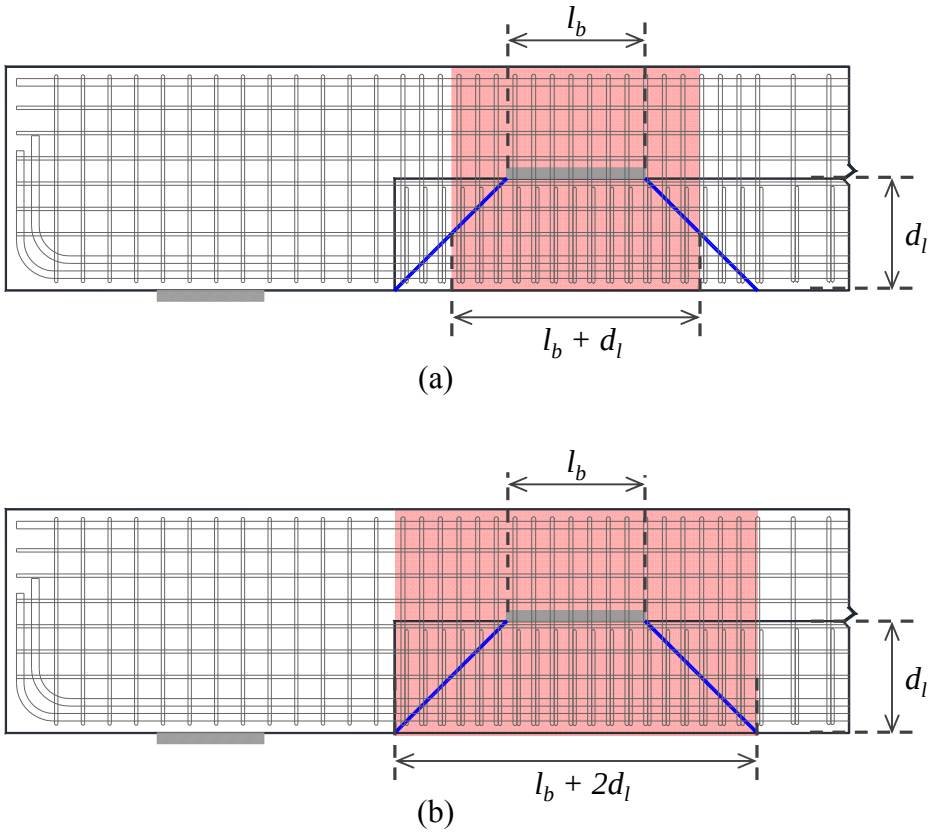

Figure 5-19: Width considered for determining the area of (a) ledge and (b) hanger reinforcement

In all of the specimens tested to date, every other piece of ledge and hanger reinforcement was instrumented with strain gages on both sides of the specimens, as

shown in Figure 5-20 and detailed in Chapter 3. The purpose of this instrumentation was to provide data for the evaluation of the 45-degree load spread assumption made during the design process.

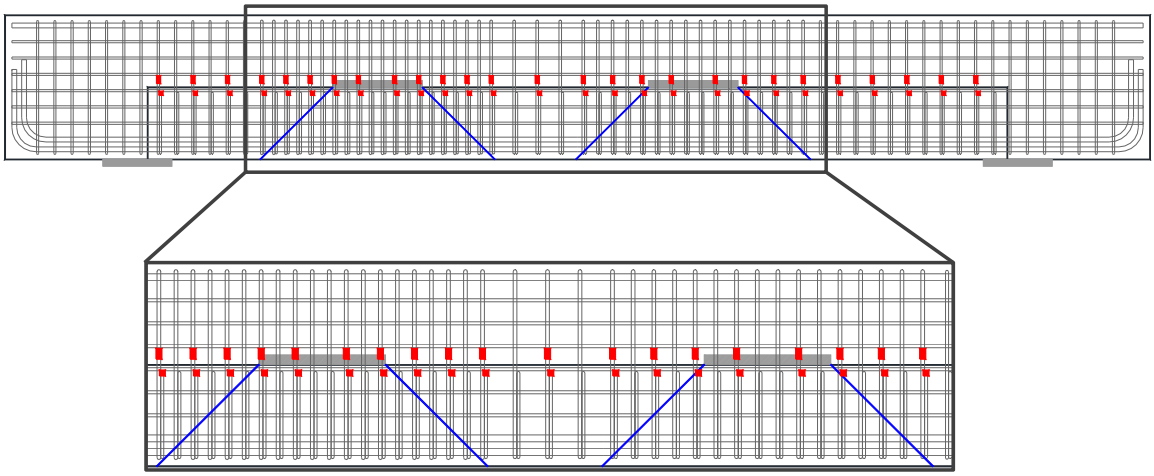

Figure 5-20: Location of internal strain gauges used for Figure 5-21 through Figure 5-24

Preliminary results of the effort to empirically establish the effective widths of both the ledge and hanger ties are presented in Sections 5.3.2.1 and 5.3.2.2, respectively. Only the ledge portion of the beam, as shown in Figure 5-20, is presented as a point of reference in the graphs within Figure 5-21 through Figure 5-24.

5.3.2.1 Ledge Reinforcement

The ledge reinforcement strains measured at the maximum applied shear of the deep ledge specimens with an a/d ratio of 1.85 are presented in Figure 5-21. Each colored line represents the ledge strain profile within one of the three deep ledge specimens. The maximum ledge reinforcement strains from the alternate three deep ledge specimens with an a/d ratio of 2.5 are similarly presented in Figure 5-22. The cross-section of the beam in both figures indicates the location of the internal strain gauges. These gauges were placed in the location where the maximum deformation of the ledge reinforcement was expected.

The preliminary results from these six tests indicate that a 45-degree load spread extending from the edge of the bearing pad to the mid-depth of the ledge was an accurate and conservative assumption for the specimens tested. The relative degree to which the reinforcement is engaged in transferring the load can be observed in Figure 5-21 and Figure 5-22. Strain measurements in excess of yield were considered indicative of significant participation in the transfer of forces. The most relevant data to the current task is located outside of the primary test region. The ledge gages between the load centerline and the closest support registered very high strains in all specimens, regardless of shear span-to-depth ratio. In both shear span configurations, data collected from the ledge reinforcement gages on the opposite side of the load centerline indicated that the reinforcement strains became increasingly insignificant beyond the assumed ledge tie width.

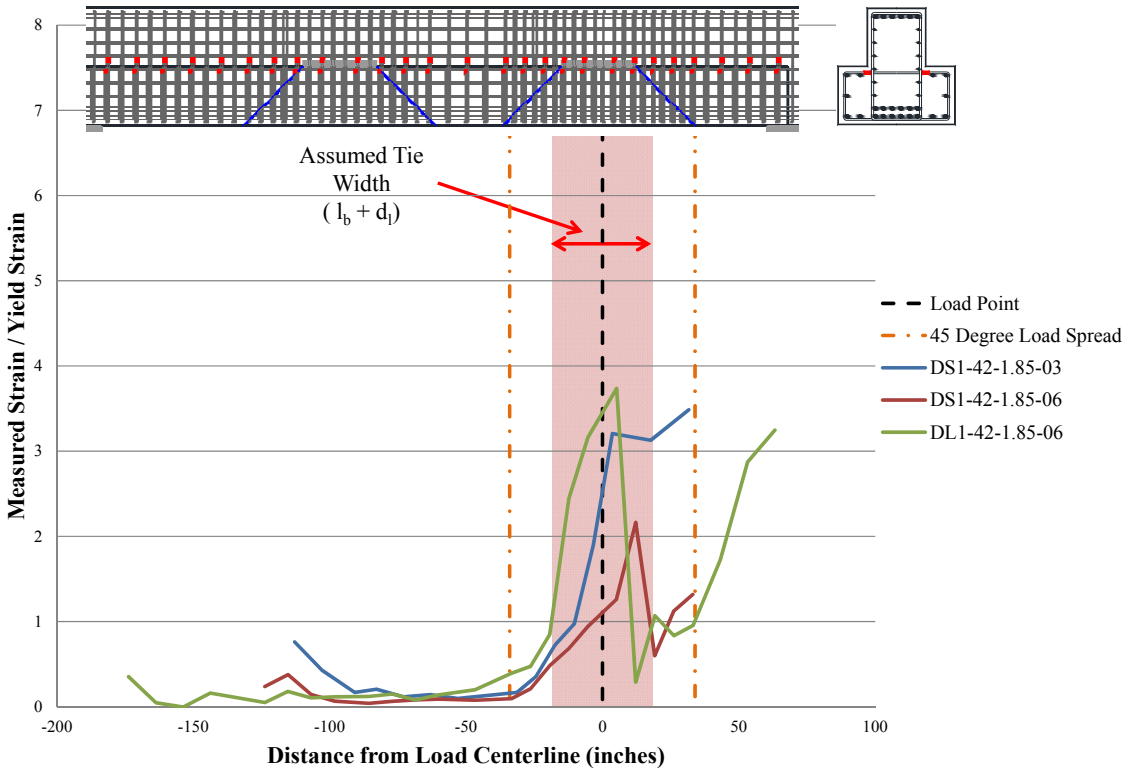

Figure 5-21: Normalized ledge strains for deep ledge specimens with a/d = 1.85

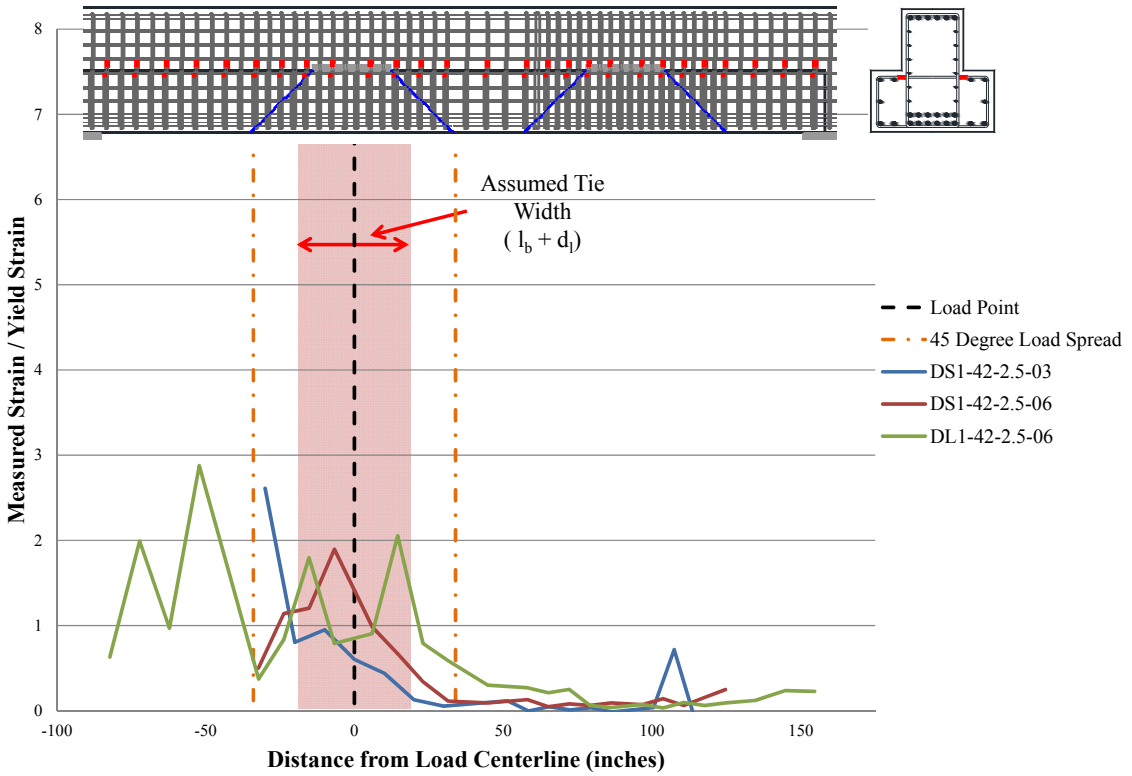

Figure 5-22: Normalized ledge strains for deep ledge specimens with a/d = 2.5

5.3.2.2 Hanger Reinforcement

The hanger reinforcement strains measured at the maximum applied shear of the deep ledge specimens with an a/d ratio of 1.85 are presented in Figure 5-23. Each colored line represents the ledge strain profile within one of the three deep ledge specimens. The maximum ledge reinforcement strains from the alternate three deep ledge specimens with an a/d ratio of 2.5 are similarly presented in Figure 5-24. The cross-section of the beam in both figures indicates the location of the internal strain gauges. These gauges were placed in the location where the maximum deformation of the ledge reinforcement was expected.

The preliminary results from the six tests indicate that the 45-degree load spread assumption was accurate for the hanger tie width. In general, the hanger strains peaked at the load centerline and progressively declined toward the farthest support. Hanger

reinforcement strains were considered to be insignificant at a distance of around one ledge depth from the edge of the bearing pad, as shown in Figure 5-23 and Figure 5-24. Again, hanger reinforcement strains measured within the primary shear span were relatively large throughout the duration of the test due to the high demand. These strains are in no way indicative of the demand and requisite distribution of the hanger reinforcement.

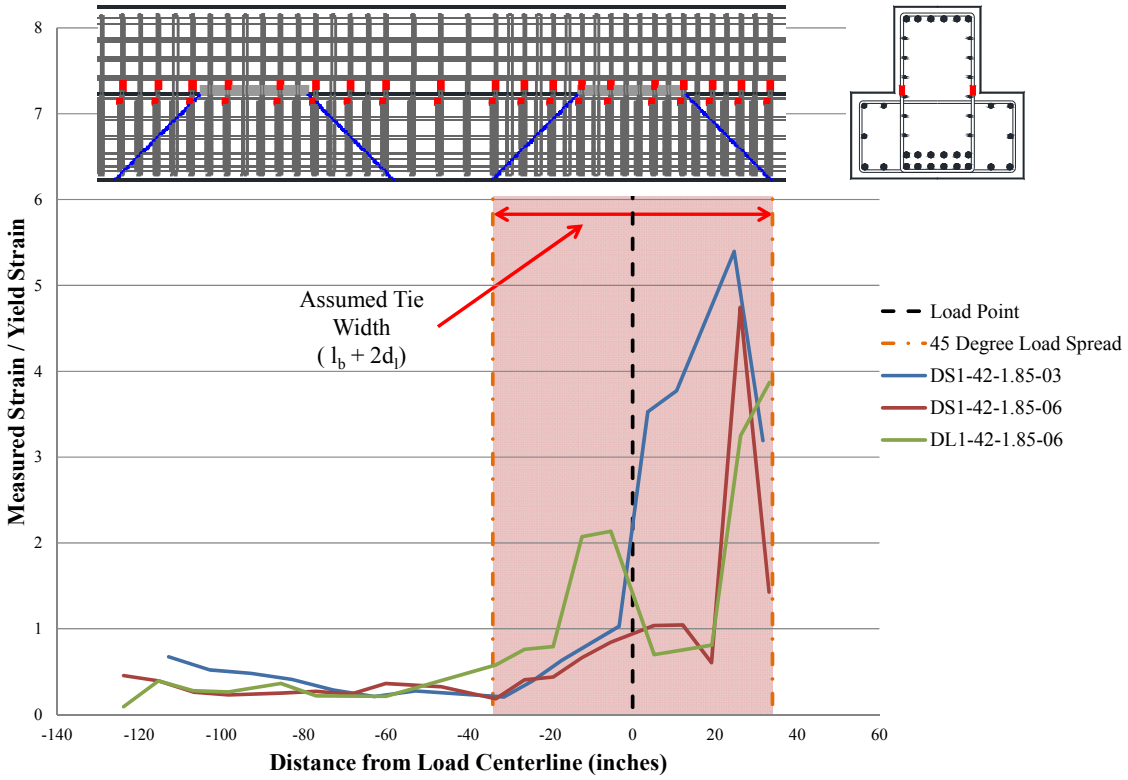

Figure 5-23: Normalized hanger strains for deep ledge specimens with a/d = 1.85

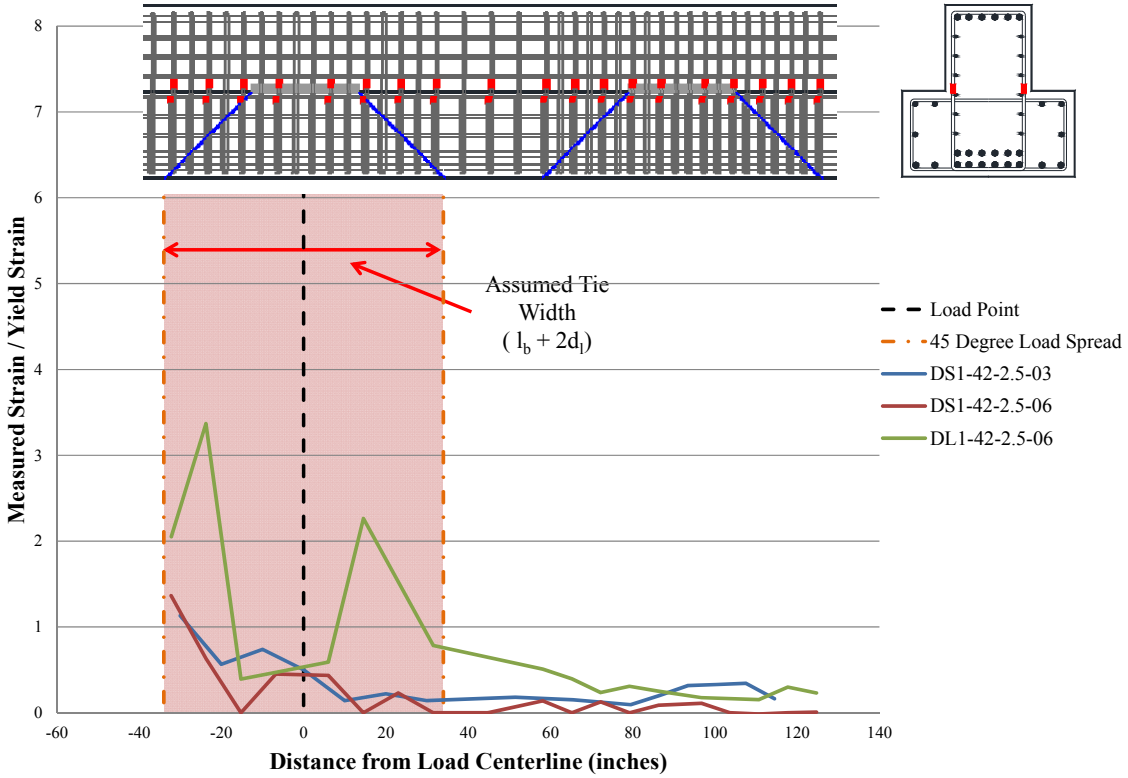

Figure 5-24: Normalized hanger strains for deep ledge specimens with a/d = 2.5

5.3.3 Summary

The experimental results suggest that for the width of the hanger reinforcement tie, the specified 45-degree spread from the edge of the bearing pad to the bottom of the hanger reinforcement is an accurate assumption. For the ledge reinforcement tie width the initial results show that the 45-degree load spread extending from the edge of the bearing pad to half of the ledge depth is a conservative assumption for this ledge configuration. In order to verify these ledge tie width results the effects of moving the load different distances from the web should be researched.

5.4 SUMMARY

This chapter discussed and analyzed experimental results that were not specifically covered previously in Chapter 4. The first topic discussed was a comparison

between experimental data collected in the current research program for bottom-chord loaded specimen to previously collected experimental data for top-chord loaded specimen. The ultimate capacities, shear loads at first cracking, and crack widths were all similar in both bottom- and top-chord loaded specimens for short shear spans, a/d ratio of 1.85. The ultimate capacity was about 33-percent less in the bottom-chord specimen for an a/d ratio of 2.5. A direct comparison could only be made between specimens with a web reinforcement ratio of 0.003 due to no top-chord loaded specimen with a reinforcement ratio of 0.006 being tested in the experimental program of Project 0-5253.

In order to determine the applicability of the design specifications presented by Project 0-5253, these design specifications were used for the design and analysis of all the specimens in the experimental program. Initial findings suggest that the design specification was generally an accurate and conservative method for design and analysis of bottom-chord loaded deep beams, i.e. inverted-T beams. More experimental research needs to be performed however to verify these results.

The initial experimental results suggest that for the width of the hanger reinforcement tie, the specified 45-degree spread from the edge of the bearing pad to the bottom of the hanger reinforcement is an accurate assumption. For the ledge reinforcement tie width the initial results show that the 45-degree load spread extending from the edge of the bearing pad to half of the ledge depth is a conservative assumption for this ledge configuration. In order to verify these ledge tie width results the effects of moving the load different distances from the web should be researched.

CHAPTER 6
Summary and Schedule

6.1 SUMMARY

Significant diagonal cracking in reinforced concrete inverted-T (IT) straddle bent caps has been reported throughout the State of Texas. Many of the distressed structures were recently constructed and have generally been in service for less than two decades. The unique nature of the problem prompted a closer look into the design and behavior of such structural components. A preliminary investigation highlighted outdated design requirements and a scarcity of experimental investigations pertaining to inverted-T bent caps. This research project aims to improve current understanding of the behavior of inverted-T caps, while delivering updated design provisions to Texas Department of Transportation (TxDOT) engineers.

The design specifications recommended by TxDOT Project 0-6416, *Shear Cracking in Inverted-T Straddle Bents,* will likely be based upon the strut-and-tie modeling provisions put forth by TxDOT Project 0-5253, *Strength and Serviceability Design of Reinforced Concrete Deep Beams.* Adaptation of the strut-and-tie modeling provisions will require comprehensive understanding of the differences between, and implications of, bottom- and top-chord loading configurations. The recommendations made by TxDOT Project 0-5253 were based upon a large database of specimens subject to top-chord loading only. Due to the unique load transfer mechanisms perceived in deep members loaded through the bottom chord, it is unclear whether the STM recommendations of TxDOT Project 0-5253 will be directly applicable to inverted-T straddle bents. Therefore, the primary objectives of TxDOT Project 0-6416, *Shear Cracking in Inverted-T Straddle Bents*, are to: (1) quantify the strength and serviceability effects of bottom-chord loading, and (2) identify any necessary modifications to the STM procedure outlined in TxDOT Project 0-5253.

In order to develop strength and serviceability guidelines for inverted-T, this thesis focused on the experimental results from a series of large-scale tests. These tests were designed to study the following parameters – shear span-to-depth (a/d) ratio, web reinforcement ratio, ledge height, ledge length, number of point loads, and member depth.

The experimental tests were subdivided into four series to isolate and investigate important variables:

- Series I: Web Reinforcement Effect
- Series II: Ledge Length Effect
- Series III: Ledge Depth Effect
- Series IV: Depth Effect

A thorough review of published literature has been conducted to date. Because of the small amount of relevant research conducted in the past, there is much more importance placed on the experimental program of this project. Specimens from the relevant literature are being assembled into an inverted-T database. Upon completion, this database will contain and organize most of the inverted-T specimens in literature.

Four inspections of inverted-T straddle bents in the field were completed and inspection reports were assembled summarizing the findings from the inspections. These inspection reports are presented in Appendix A.

The test specimens were designed to specifically address the effect of (1) web reinforcement; (2) ledge length; (3) ledge depth; and (4) beam depth on strength and serviceability performance. The number and relatively small size of experimental specimens found in literature led to the construction of specimens in the experimental program of comparable size to those found in the field. Twenty-seven tests were conducted or are planned with varying cross-sectional sizes and varying ledge depths and lengths.

A total of 22 load tests, focusing mainly on Series I and Series II objectives, have been performed to date. All specimens in in the experimental program were designed

and analyzed using strut-and-tie modeling provisions suggested by TxDOT Project 0-5253. These provisions were developed through testing of top-chord loaded specimens. Inverted-T beams are considered to be bottom-chord loaded specimens, which may change the behavior. When a deep beam is loaded in the bottom chord, as is the case in inverted-T deep beams, the forces in the vertical ties at the load points are increased, compared to a top chord loaded beam. This changes the behavior of the beam and also the STM.

Strut-and-tie modeling, summarized in Chapter 2, is used to simplify the flow of forces in D-regions, where strains vary nonlinearly across the depth of a section. An STM is comprised of compression elements (struts), tension elements (ties) and the intersection of such elements (nodes). When using STM for design, enough reinforcement must be provided to resist forces in all ties and stresses in the nodal faces must not cause crushing of the concrete.

Of the 22 load tests, only results from 10 of these tests have been examined and analyzed and are presented in this thesis. Results from these 10 tests were used to design the remainder of the tests and series. The results from these tests are presented in Chapter 4 and Chapter 5.

In both Series I and Series II, the applicability of the strut-and-tie modeling provisions recommended by TxDOT Project 0-5253 was evaluated through a comparison of the STM-generated strength estimates and the experimental capacities. Application of the TxDOT Project 0-5253 provisions generally yielded conservative strength estimates. However, more data is needed to comment on the overall accuracy of the method as applied to inverted-T (top-chord loaded) members.

In Chapter 5 the results were used to give initial comparisons between top and bottom-chord loaded specimens. The ultimate capacities, shear loads at first cracking, and crack widths were all similar in both bottom- and top-chord loaded specimens for short shear spans, a/d ratio of 1.85. The ultimate capacity was about 33-percent less in the bottom-chord specimen for an a/d ratio of 2.5. The crack width to ultimate shear relationship also seems to be similar in top- and bottom-chord loaded specimens.

It should be reinforced that all observations and conclusions drawn in this thesis are preliminary. Further results are needed before final conclusions regarding (1) the conservativeness of the TxDOT Project 0-5253 provisions for inverted-T beams, (2) the relationship between top- and bottom-chord loaded specimens, (3) the impact of web reinforcement and ledge length on the strength and serviceability performance on inverted-T members and (4) final design recommendations can be made.

6.2 CONCLUSION OF RESEARCH PROJECT

This thesis contains the preliminary results from a larger study of inverted-T straddle bents. In the upcoming months, the data from additional tests will be analyzed. The specimens in these tests focused on Series II (Ledge Length) and Series IV (Depth Effect). Results from the data from these tests will support findings discussed in this thesis.

Within the project, an inverted-T database will be assembled. The resulting database will be used to evaluate the applicability of the design provisions of Project 0-5253 to inverted-T deep beams. The *collection database* will contain all of the inverted-T beam test found in the literature review as well as the tests contained in the experimental program of this project. Following the assemblage of the collection database, a filtering process will eliminate the irrelevant specimens or tests lacking information required to perform a strut-and-tie modeling analysis, leaving a *filtered database*. Finally, relevant specimens from the filtered database will be used to evaluate the applicability of the design provisions of Project 0-5253 to inverted-T deep beams.

APPENDIX A
Field Inspections

A.1 INTRODUCTION

One of the tasks of the project was to perform thorough field inspections on multiple problematic inverted-t straddle bents in Texas. During a typical field inspection a bucket truck allowed for close inspection of the cracks, as shown in Figure A-1. Close correspondence with TxDOT employees allowed for proper traffic control and safety during the inspection.

Figure A-1 - Bucket truck allowed for close observation of the crack

While in the bucket truck, crack widths were measured using a standard crack gauge, as shown in Figure A-2. Measurements were recorded and photographs of the crack with the gauge were taken to ensure the proper crack width was measured during the inspection, as shown in Figure A-3. In general the inspection process took approximately one hour per corner of the bent inspected.

Figure A-2: Cracks were measured using crack gauge and recorded

Detailed reports from each inspection are included in this appendix. A typical report will include a brief description of the inverted-t straddle bent, including a table containing the web reinforcement ratios and shear span-to-depth ratios, as shown in Table A-1. Not all corners of the bent were always accessible; within the inspection report, the inspected corners are specified at the beginning, as shown in Figure A-4. Following are photographs of the cracking bent, with overall photographs showing the locations of the close ups of the cracks of interest.

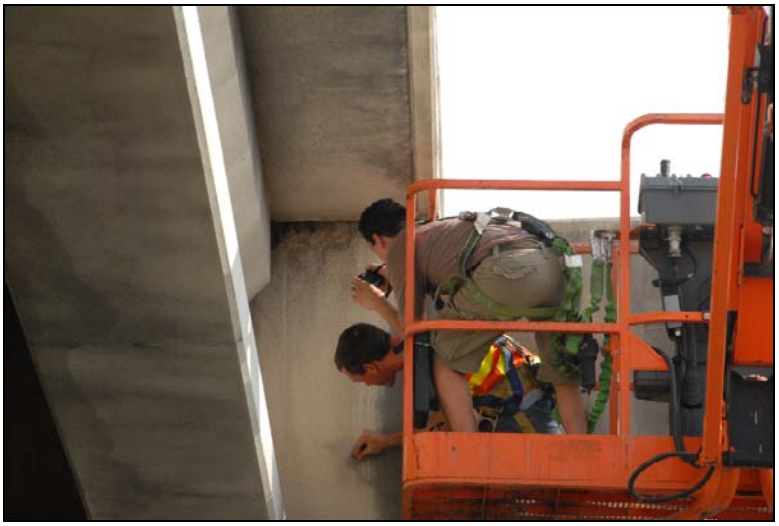

Figure A-3: Photographs were taken while measure the crack width

A.2 INSPECTION REPORTS

Inspection Date: December 10, 2009

Bridge Location: TX-290 W Connector to Frontage Road

Latitude: 30.322401, Longitude: -97.702838

Cap: Bent 3M

Table A-1 - Important Characteristics of Bent 3M

ρ_v^+	ρ_h^+	a/d* (North)	a/d* (South)
0.0043	0.0037	1.42	1.42

+: Calculated at the location of shear crack from the plan sheets

*:Taken from TxDOT's Straddle Cap Cracking Database

Observations:

Shear cracks were observed on both faces of the bent caps near both supports. Crack sizes were measured and photographs were taken of cracks on the southwest corner of the bent; these locations are shown in Figure A-4. These diagonal cracks measured up to 0.02 inches, which is a comparable crack size to measurements during an inspection in (early 2009). A shear crack, measuring 0.02 inches, ran from above the end of the ledge to the column, shown in Figure A-6. No cracking/very minor cracking was observed along the web-ledge interface, shown in Figure A-7. The southwest corner of the bent is shown in Figure A-5 through Figure A-8.

We were only able to access the southwest corner of the bent during our inspection. The northeast corner of the bent appeared to have much larger cracks but we were unable to access it to obtain measurements. Crack sizes of up to 0.03 inches were approximated from ground observation.

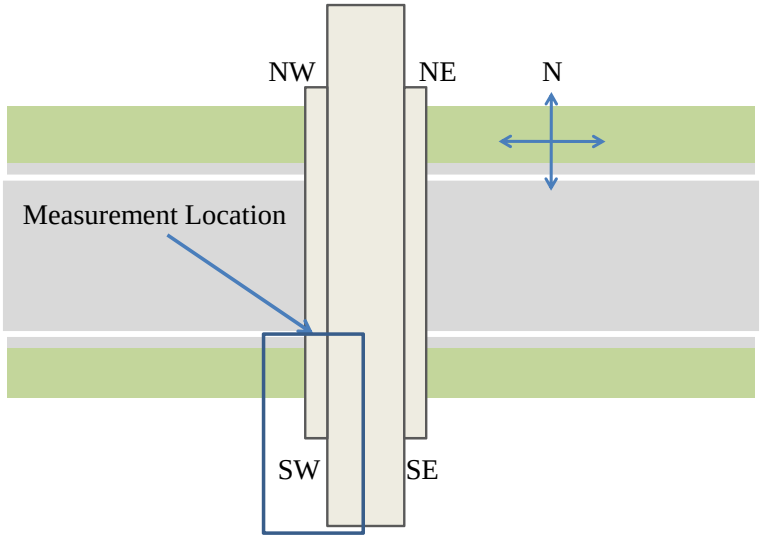

Figure A-4 - Cap orientation and measurement locations (Bent 3M)

Southwest Corner:

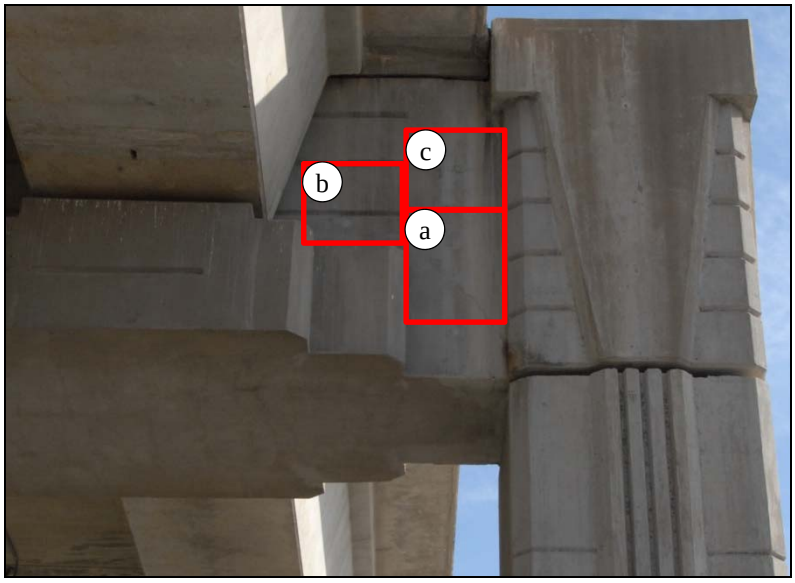

Figure A-5 - Overall view of SW corner of Bent 3M

Figure A-6 – Largest shear crack (0.02 inches) (a in Figure A-5)

Figure A-7 – Small crack above ledge (b in Figure A-5)

Figure A-8 – Horizontal cracking above shear crack (c in Figure A-5)

Inspection Date: December 10, 2009

Bridge Location: I-35 S to TX-290 E Connector

Latitude: 30.321920, Longitude: -97.703878

Cap: Bent 6K

Table A-2 – Important Characteristics of Bent 6K

ρ_v^+	ρ_h^+	a/d* (West)	a/d* (East)
0.0043	0.0037	1.71	1.71

+: Calculated at the location of shear crack from the plan sheets

*:Taken from TxDOT's Straddle Cap Cracking Database

Observations:

Shear cracks were observed on both faces of the bent caps near both supports shown in Figure A-9. Crack sizes were measured and photographs were taken of cracks on the southwest corner of the bent. These diagonal cracks measured up to 0.016 inches, which is the same crack size measured during an inspection in (early 2009). A shear crack, measuring 0.016 inches, ran from mid face of the U-beam to the end of the ledge shown in Figure A-13. Cracking was also observed along the top and side of the web-ledge interface; these cracks measuring 0.013 inches shown in Figure A-11 and Figure A-14. There was also cracking on the base of the beam extending diagonally from the web-ledge interface shown in Figure A-12. The southwest corner of the bent is shown in Figure A-10 through Figure A-15.

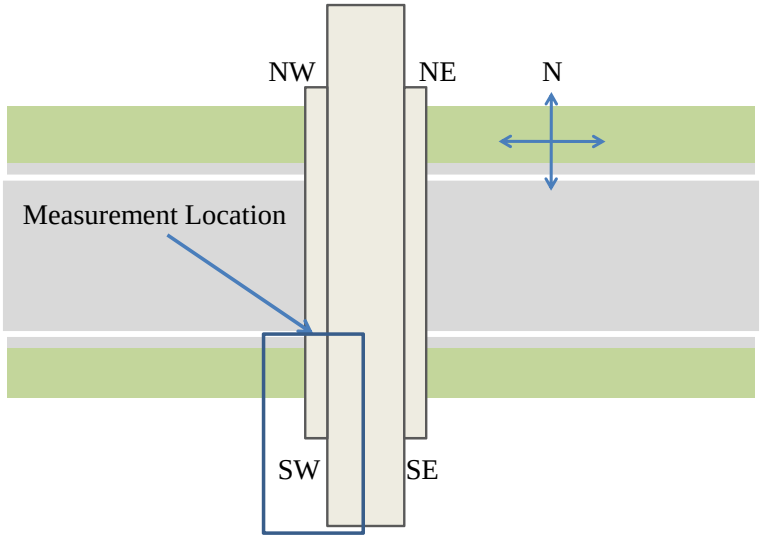

Figure A-9 - Cap orientation and measurement locations (Bent 6K)

Southwest Corner:

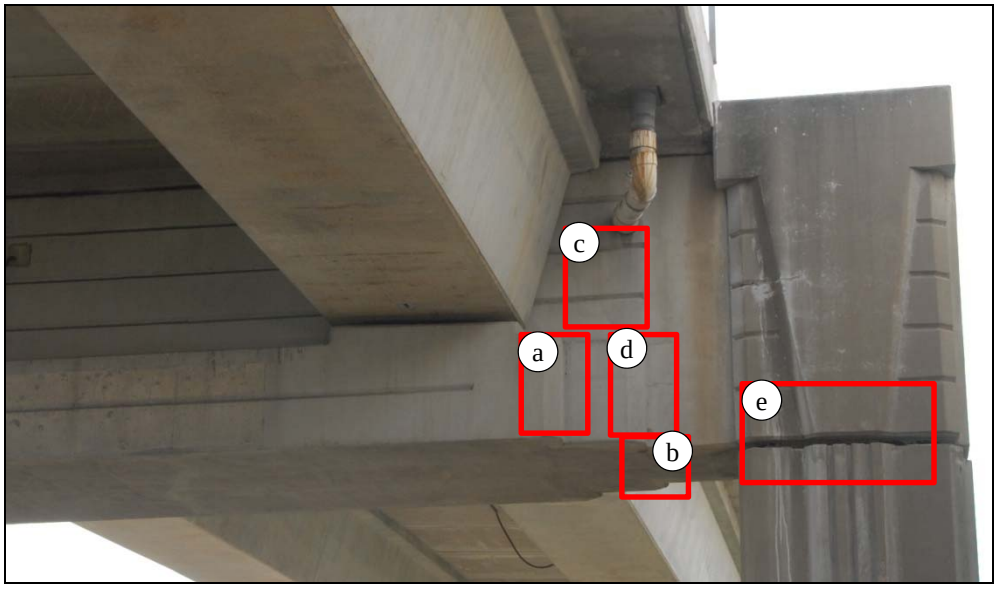

Figure A-10 - Overall view of SW corner of Bent 6K

Figure A-11 - Ledge cracking (a in Figure A-10)

Figure A-12 - Crack on base of cap (b in Figure A-10)

Figure A-13 - NW corner of cap (c in Figure A-10)

Figure A-14 - Web-ledge cracking (d in Figure A-10)

Figure A-15 - Cap on Bearing Pad (e in Figure A-10)

Inspection Date: December 10, 2009

Bridge Location: I-35 S to TX-290 E Connector

Latitude: 30.326788, Longitude: -97.706456

Cap: Bent 28K

Table A-3 – Important Characteristics of Bent 28K

ρ_v	ρ_h	a/d (North)	a/d (South)
0.0043	0.0037	1.42	1.42

Observations:

Shear cracks were observed on both faces of the bent caps near both supports. Crack sizes were measured and photographs were taken of cracks on the northwest and northeast corners of the bent; these locations are shown in Figure A-16. These diagonal cracks measured up to 0.03 inches (on the northwest) and 0.02 inches (on the northeast).

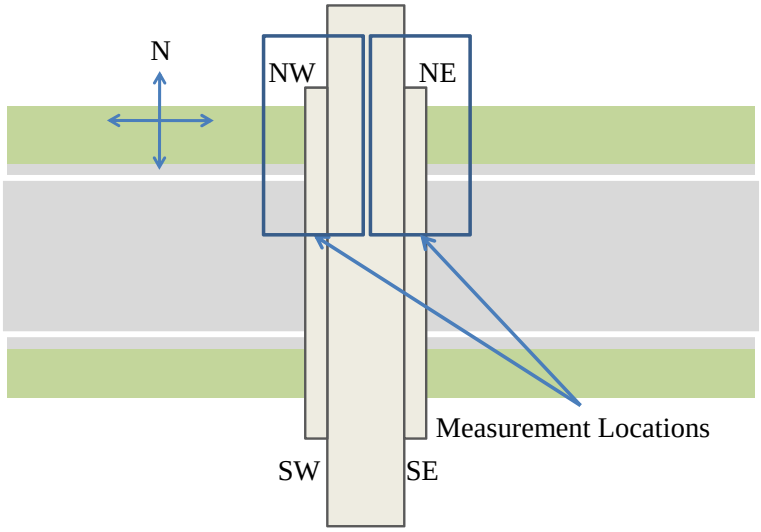

Figure A-16 - Cap orientation and measurement locations (Bent 28K)

Northwest Corner:

The northwest corner of the bent is shown in Figure A-17. Two shear cracks were observed in the web; one extended from mid face of the U-beam to the ledge (measuring 0.016), shown in Figure A-19, the other parallel to this crack extending from above the ledge to the column (measuring 0.03), shown in Figure A-18. The larger of these cracks was measured at 0.025 inches in the previous inspection. Cracking was also observed along the web-ledge interface and on the top side of the ledge with crack sizes up to 0.03 inches, shown in Figure A-20. This is considerably larger than the 0.016 inches that was measured in the previous inspection

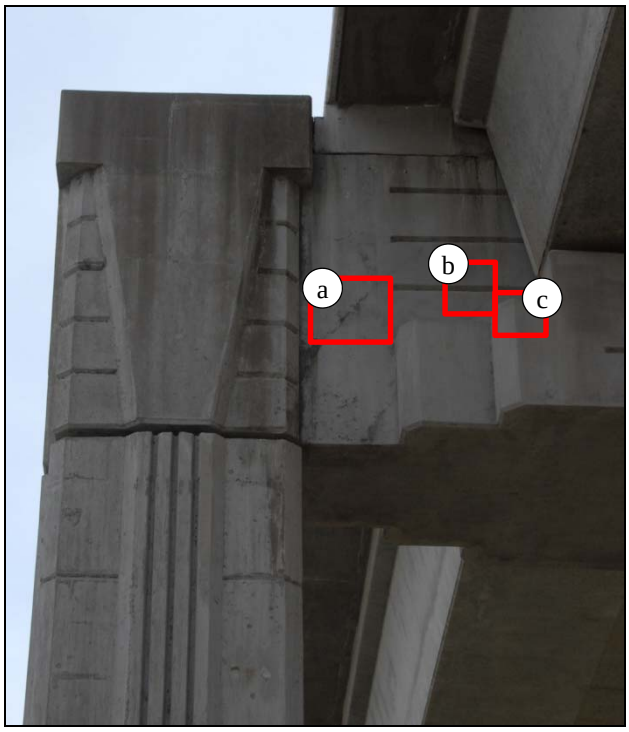

Figure A-17 – Overall view of NW corner of Bent 28K

Figure A-18 – Largest shear crack (0.03 inches) (a in Figure A-17)

Figure A-19 – Crack above ledge (0.016 inches) (b in Figure A-17)

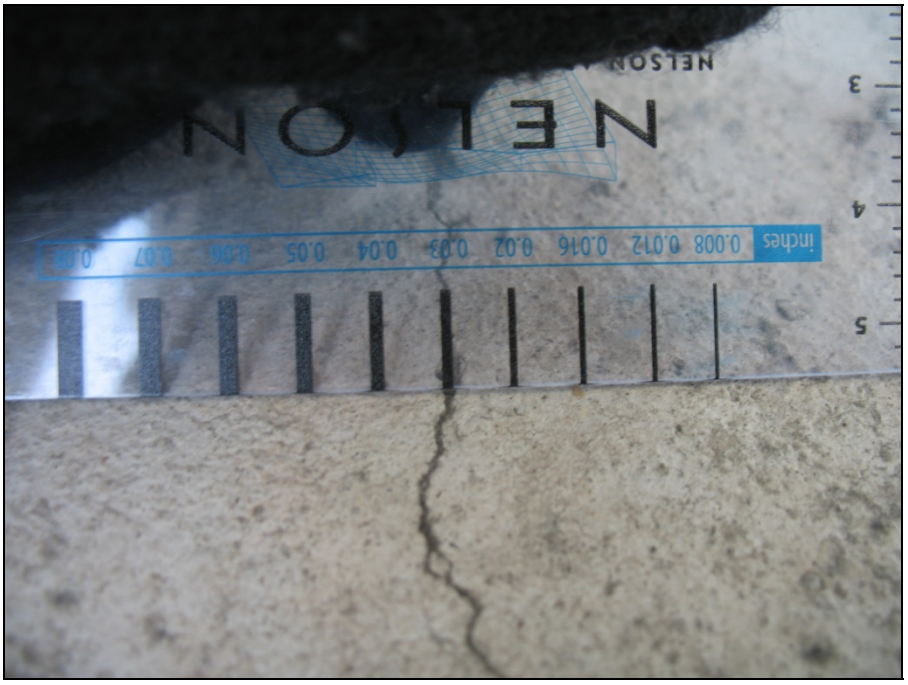

Figure A-20 – Top of ledge at interface (0.03 inches) (c in Figure A-17)

Northeast Corner:

The northeast corner of the bent is shown in Figure A-21. The same shear cracking pattern was observed as in the northwest corner, with cracks measuring 0.012 and 0.02 inches, shown in Figure A-26 and Figure A-24, respectively. Cracking was also observed along the web-ledge interfaces with cracks measuring up to 0.012 inches, shown in Figure A-22 and Figure A-25. These sizes were comparable to the previous inspection. The area around the bearing pad is shown in Figure A-23.

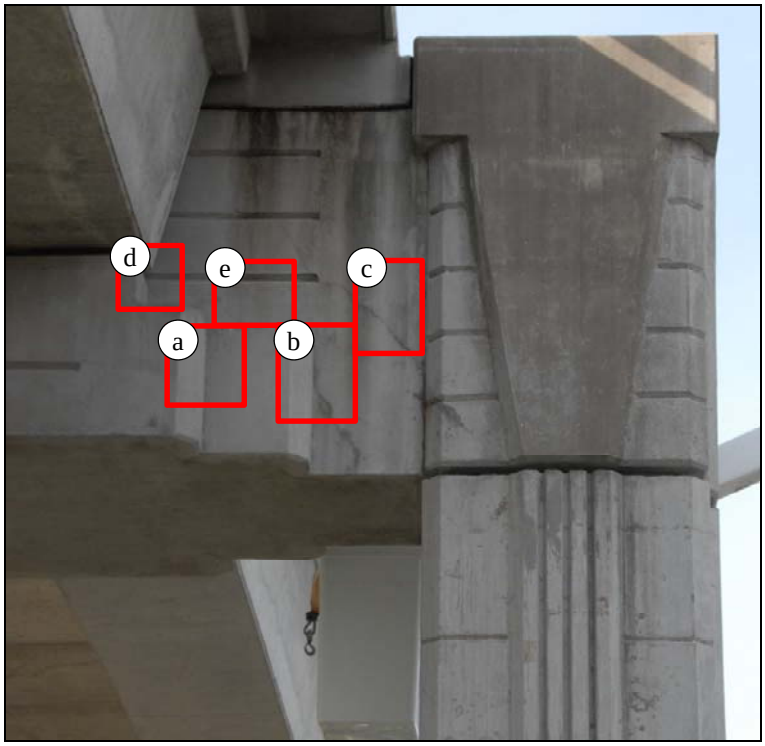

Figure A-21 - Overall view of NE corner of Bent 28K

Figure A-22 - Cracking along ledge-step interface (a in Figure A-21)

Figure A-23 – Bearing plate-ledge-web interface (b in Figure A-21)

Figure A-24 – Largest shear crack (0.02 inches) (c in Figure A-21)

Figure A-25 - Cracking at web-ledge interface (d in Figure A-21)

Figure A-26 – Crack above ledge (e in Figure A-21)

Inspection Date: July 26, 2010

Bridge Location: I-35 S Frontage Road to I-35 S, North of San Antonio
Latitude: 29.512478, Longitude: -98.397567

Table A-4 - Important Characteristics of San Antonio Bent Cap

ρ_v	ρ_h	a/d (West)	a/d (East)

*No bridge plans provided

Observations:

Shear cracks were observed on both faces of the bent caps near both supports. Crack sizes were measured and photographs were taken of cracks on the northwest, southwest and southeast corners of the bent; these locations are shown in Figure A-27. These diagonal cracks measured up to 0.015 inches.

The inverted-T bent cap ran over the off ramp from I-35 South to the access road. Framed into the bent are five TxDOT Type C I-girders. There are moment cracks in all the bent corners. Spalling near the beam-deck interface may suggest that the bent is both top and bottom chord loaded, loaded on both the ledge (from the I-girders) and on the top (from the deck).

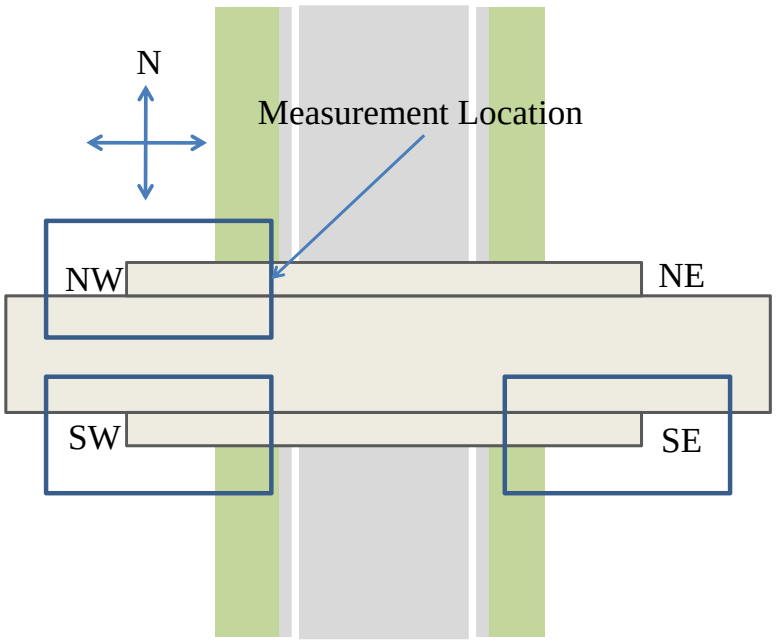

Figure A-27 - Cap Orientation

Northwest Corner:

The northwest corner of the bent cap had a one panel shear crack measuring 0.01 inches in width running from the top of the fascia I-girder to the corner of the web-ledge interface. The crack is shown in Figure A-28, with a close up of the crack shown in Figure A-29. A close up of the moment crack measurement is shown in Figure A-30. Spalling was observed at the end of the shear crack near the beam-deck interface.

Figure A-28 – Overall view of NW corner of bent

Figure A-29 - Shear crack (0.01 inches) (a in Figure A-28)

Figure A-30 - Moment crack (0.01 inches) (b in Figure A-28)

Northeast Corner:

Figure A-31 - Overall view of NE corner of bent

Southwest Corner:

The southwest corner of the bent cap had a one panel shear crack measuring 0.01 inches in width running from the top of the fascia I-girder to the corner of the web-ledge interface. The crack is shown in Figure A-32, with a close up of the crack shown in Figure A-33. A close up of the moment crack measurement is shown in Figure A-34.

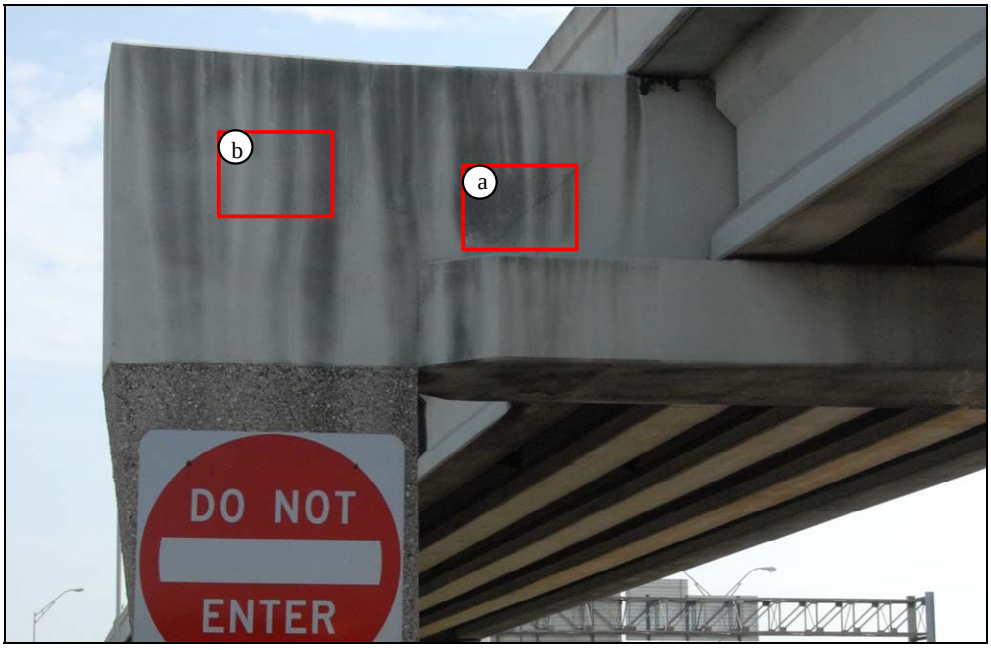

Figure A-32 - Overall view of SW corner of bent

Figure A-33 -Shear crack (0.01 inches) (a in Figure A-32)

Figure A-34 - Moment crack (0.01 inches) (b in Figure A-32)

Southeast Corner:

The southeast corner of the bent cap had cracking that would suggest two panel behavior, with shear cracks measuring up to 0.015 inches. These shear cracks are shown in Figure A-35, with close ups of the two shear cracks shown in Figure A-36 and Figure A-37.

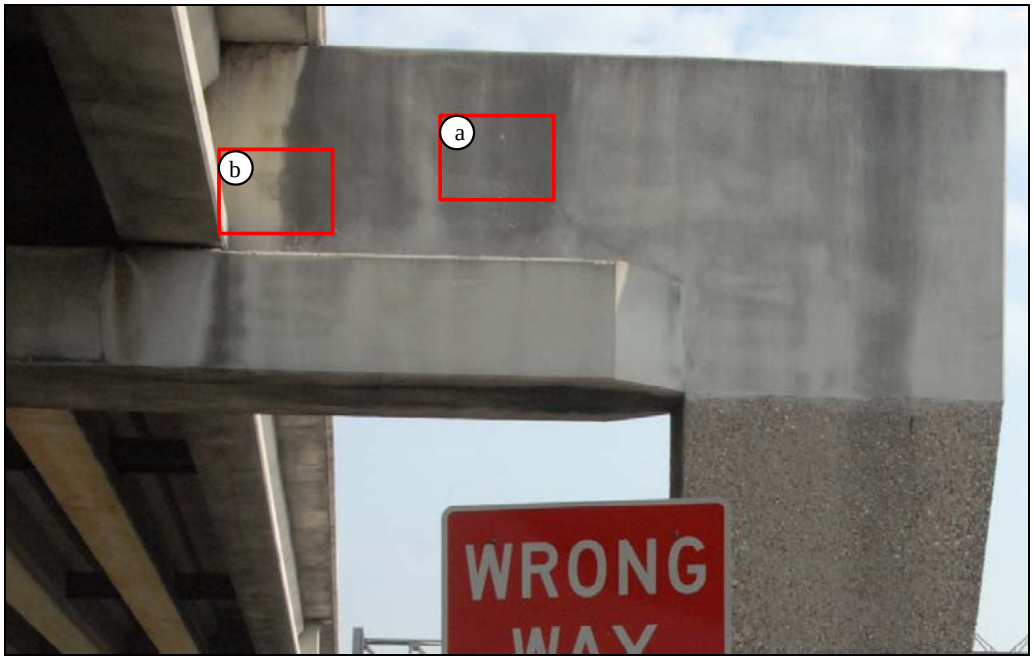

Figure A-35 - Overall view of SE corner of bent

Figure A-36 - Shear crack (0.015 inches) (a in Figure A-35)

Figure A-37 - Shear crack (0.015 inches) (b in Figure A-35)

Inspection Date: August 17, 2010

Bridge Location: I-10 East to Gateway Blvd East Connector (near Geronimo Drive), El Paso

Latitude: 31.78055, Longitude: -106.41599

Cap: Bent 4

Table A-5 - Important Characteristics of Bent 4

ρ_v^+	ρ_h^+	**a/d* (South)**
0.0057	0.0019	1.7

+: Calculated at the location of shear crack from the plan sheets
*:Taken from TxDOT's Straddle Cap Cracking Database

Observations:

Shear cracking was observed on both faces of the bent cap near the south support shown in Figure 4; access near the north support was not possible. Crack sizes were measured and photographs of the cracks were taken on the southwest and southeast corners of the bent. These diagonal shear cracks measured up to 0.040 inches on the west face and 0.030 inches on the east face. The prestressed concrete box beams framing into the west face of the cap are 82'-11$^3/_8$" long. The length of the beams framing into the east face is 61'-2". The difference in span lengths is likely a major contributing factor for the difference in crack widths measured on the east and west faces of the bent cap. The bent cap appeared to be painted. The shear span-to-depth ratio for the inspected shear span is 1.7 and the horizontal shear reinforcement ratio is 0.0019 and the vertical is 0.0057; all parameters were calculated by using the original design drawings.

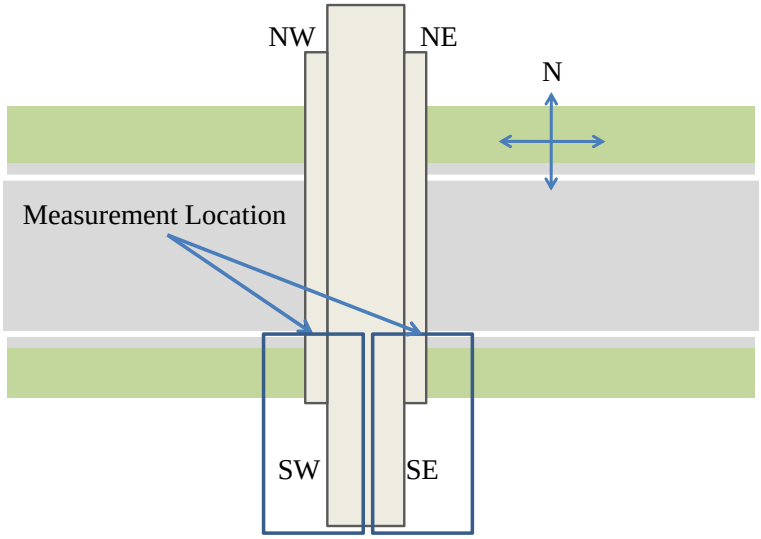

Figure A-38 - Cap orientation and measurement locations (Bent 4)

Southwest Corner:

The southwest corner of the bent cap had a one panel shear crack measuring 0.040 inches in size running from mid-height of the fascia girder to the lower corner of the cap-to-column connection, shown in Figure A-39. Spalling was observed at two points along the main shear crack, shown in Figure A-40 and Figure A-42. These spalls were labeled "11-8-95," likely implying that they were first inspected and documented on this date; data from this inspection has not yet been found. This face of the cap exhibited signs of water damage and cracking as shown in Figure A-41. A slight amount of map cracking was observed near the column, shown in Figure A-43. Moment cracks are shown in Figure A-44.

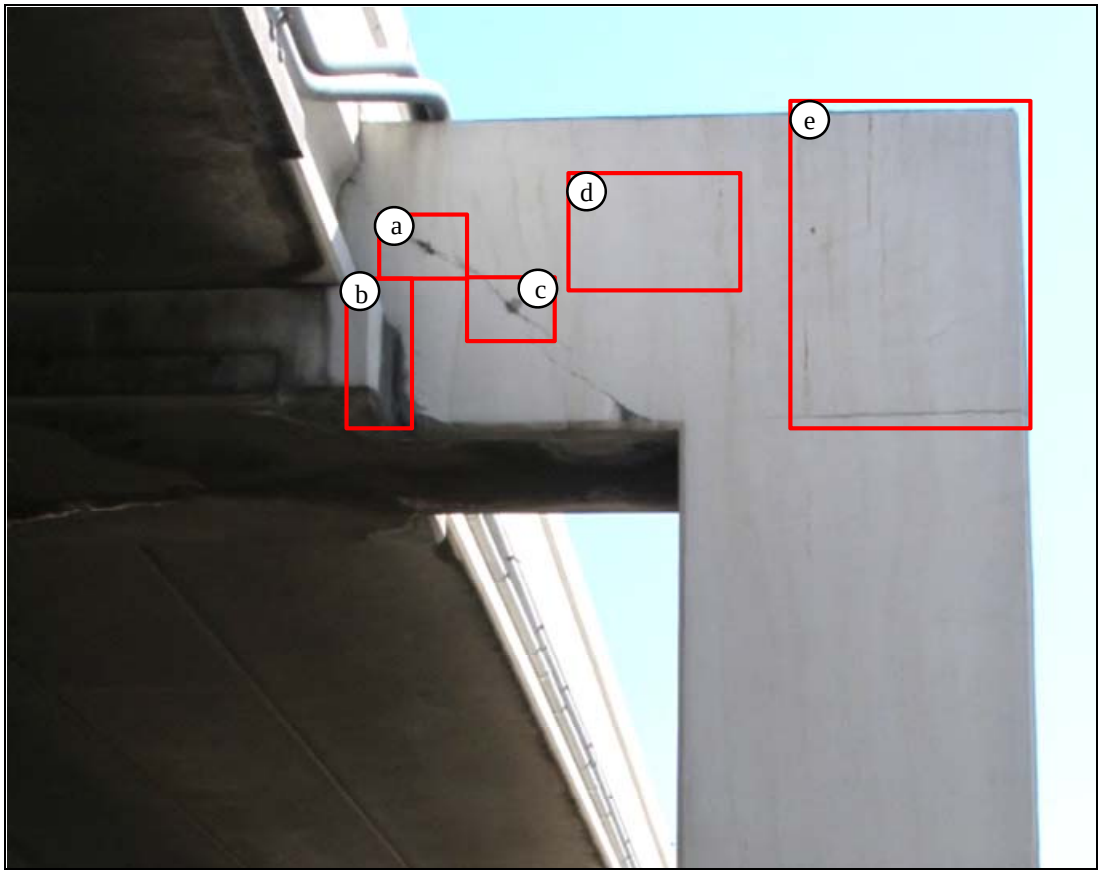

Figure A-39 - Overall view of SW corner of Bent 4

Figure A-40 - Largest shear crack (0.04 inches) and spalling (a in Figure A-39)

Figure A-41 –Water damage and cracking along web-ledge interface (b in Figure A-39)

Figure A-42 – Spalling located along main shear crack (c in Figure A-39)

Figure A-43 - Map cracking located in the middle of shear span (d in Figure A-39)

Figure A-44 - Moment cracking (e in Figure A-39)

Southeast Corner:

The southeast corner of the bent cap had a similar one panel shear crack to that of the southwest corner, but measured 0.030 inches in size; this shear crack is shown in

Figure A-45. As previously mentioned, this smaller crack size can likely be attributed to the difference in span length of the box beams supported by the inverted tee bent cap. Spalling occurred at two points along the main shear crack, shown in Figure A-47, Figure A-47, and Figure A-48. These spalls were not labeled as they were on the west face of the bent cap. A slight amount of map cracking was also observed on the eastern face. Moment cracks are shown in Figure A-46. Water damage and cracking along the web-ledge interface is shown in Figure A-49.

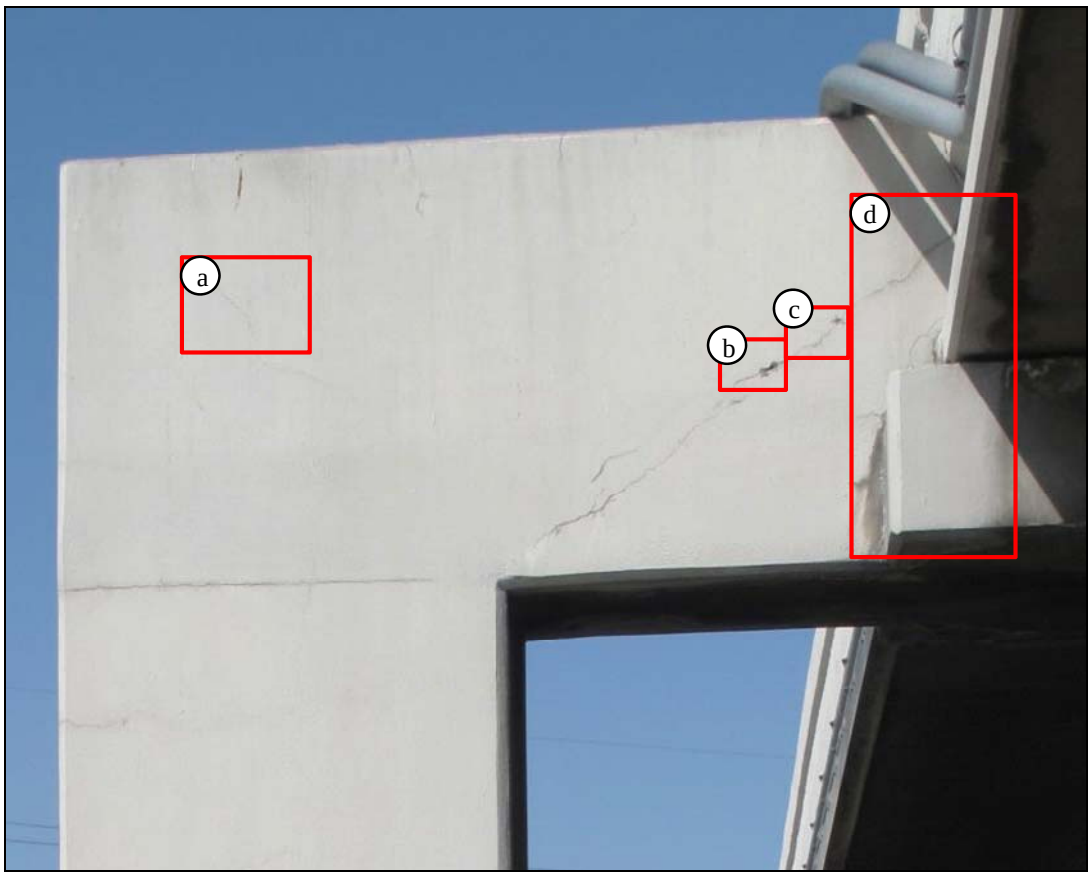

Figure A-45 – Overall view of SE corner of Bent 4

Figure A-46 - Moment crack (0.02 inches) (a in Figure A-45)

Figure A-47 - Spalling along main shear crack (b in Figure A-45)

Figure A-48 - Shear crack (0.03 inches) and spalling (c in Figure A-46)

Figure A-49 - Water damage and cracking along web-ledge interface (d in Figure A-45)

Inspection Date: August 17, 2010

Bridge Location: I-10 East to Gateway Blvd East Connector (near Geronimo Drive)

Cap: Bent 5

Table A-6 – Important Characteristics of Bent 5

ρ_v^+	ρ_h^+	**a/d* (South)**
0.0057	0.0019	3.6

+: Calculated at the location of shear crack from the plan sheets
*:Taken from TxDOT's Straddle Cap Cracking Database

Observations:

Shear cracking was observed on both faces of the bent cap near the north support; access near the south support was not possible. Crack sizes were measured and the photographs of the cracks were taken on the northwest and northeast corners of the bent; these locations are shown in Figure A-50. The shear cracking in the bent cap was typical of a cap exhibiting sectional shear behavior. The diagonal shear cracks measured 0.01 inches on the northeast corner and 0.02 inches on the northwest corner. The prestressed concrete box beams framing into both faces are 61'-2" long. The west face of the bent had an impact guard, shown in Figure A-51. The northwest corner of the bent is shown in Figure A-51 and Figure A-52. The northeast corner of the bent is shown in Figure A-53 and Figure A-54. This bent cap also appeared to be painted. The shear span-to-depth ratio for the inspected shear span is 3.6 and the horizontal shear reinforcement ratio is 0.0019 and the vertical is 0.0057; all the parameters were calculated by using the original design drawings.

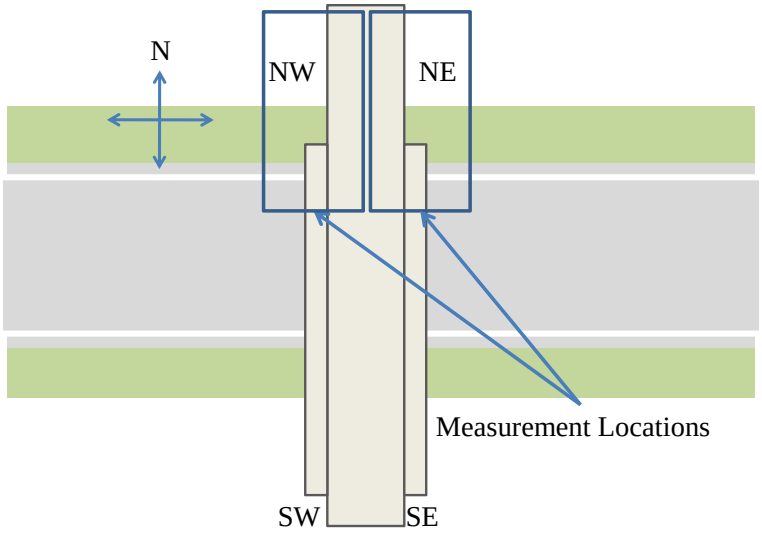

Figure A-50 - Cap orientation and measurement locations (Bent 5)

Northwest Corner:

Figure A-51 - Overall of NW corner of Bent 5

Figure A-52 - Shear crack and web ledge interface crack (a in Figure A-51)

Northeast Corner:

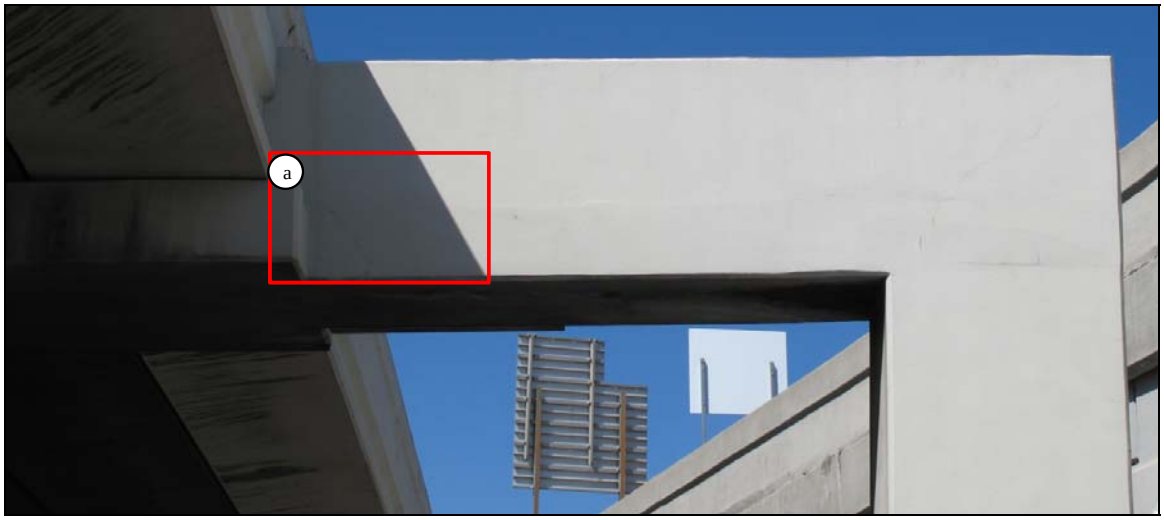

Figure A-53 - Overall of NE corner of Bent 5

Figure A-54 - Shear crack and web-ledge interface crack (a in Figure A-53)

Inspection Date: January 11, 2010

Bridge Location: TX-6 East to I-35 North Connector, Waco

Latitude: 31.496031, Longitude: -97.1486630

Cap: Bent 17

Table A-7 – Important Characteristics of Bent 17

ρ_v^+	ρ_h^+	a/d* (East)	a/d* (West)
0.0046	0.003	2.0	2.0

+: Calculated at the location of shear crack from the plan sheets
*:Taken from TxDOT's Straddle Cap Cracking Database

Observations:

Shear cracks were observed on both faces of the bent caps near both supports. Crack sizes were measured and photographs were taken of cracks on the west end of the bent; these locations are shown in Figure A-55. These diagonal cracks measure up to 0.010 inches. The cracks appeared to be larger than their actual size due to efflorescence leaking out. The efflorescence had to first be scraped off, shown in Figure A-56, before crack widths could be measured. The north side of the bent is shown in Figure A-58 through Figure A-61. The south side of the beam is shown in Figure A-62 through Figure A-66.

The inverted-T bent cap ran over an off ramp feeding onto the I-35 North access road. Framed into the bent are three TxDOT U-beams. No moment cracking was observed, but a large crack was observed at the beam-column interface suggesting the cap to be simply supported, confirmed by bridge plans.

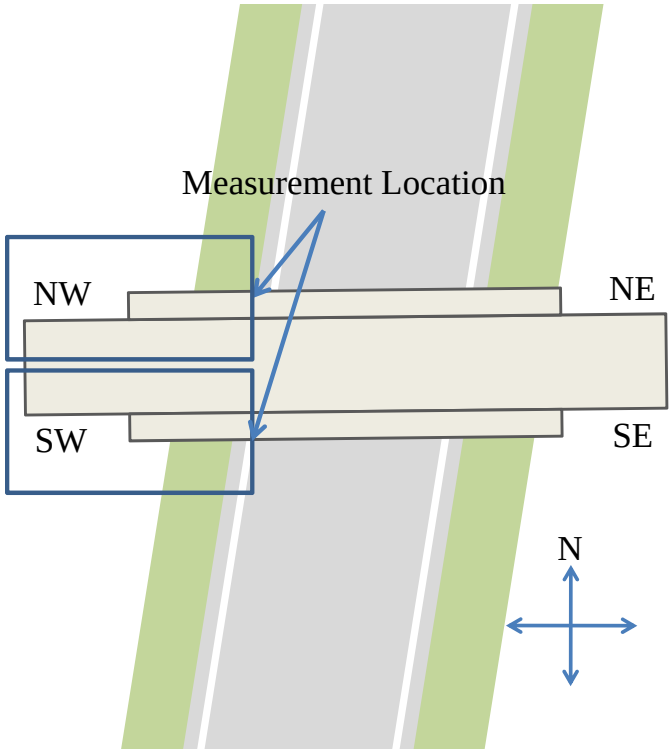

Figure A-55 – Cap orientation and measurement locations (Bent 17)

Figure A-56 – Efflorescence scraped off beam before crack widths were measured

Figure A-57 – Overall of north side of Bent 17

Northeast Corner

Figure A-58 - Overall of NE corner of Bent 17

Northwest Corner

Figure A-59 - Overall of NW corner of Bent 17

Figure A-60 – Shear crack (0.005 inches) (a in Figure A-59)

Figure A-61 - Shear crack (0.01 inches) (b in Figure A-59)

Figure A-62 – Overall view of south side of Bent 17

Southeast Corner

Figure A-63 – Overall view of SE corner of Bent 17

Southwest Corner

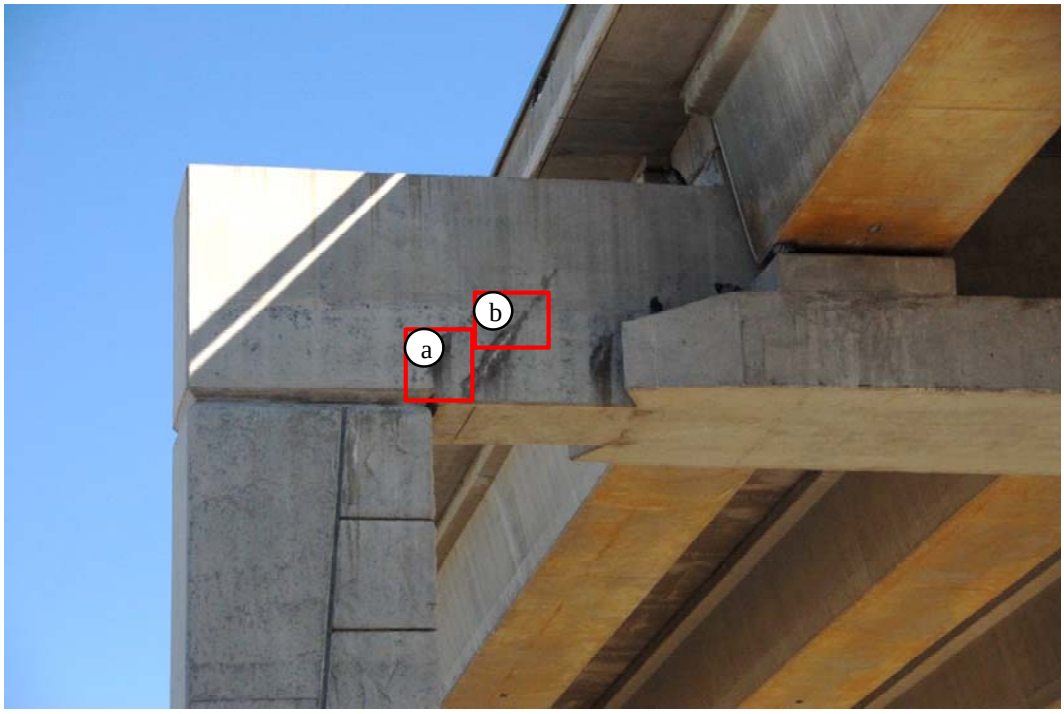

Figure A-64 – Overall view of SW corner of Bent 17

Figure A-65 - Shear crack (0.01 inches) extending from the edge of the column (a in Figure A-64)

Figure A-66 – Shear crack (0.01 inches) (b in Figure A-64)

Bridge Location: TX-6 East to I-35 North Connector, Waco

Latitude: 31.496031, Longitude: -97.1486630

Cap: Bent 19

Table A-8 – Important Characteristics of Bent 19

ρ_v^+	ρ_h^+	a/d* (East)	a/d* (West)
0.0046	0.003	2.0	2.0

+: Calculated at the location of shear crack from the plan sheets

*:Taken from TxDOT's Straddle Cap Cracking Database

Observations:

Shear cracks were observed on both faces of the bent caps near both supports. Crack sizes were measured and photographs were taken of cracks on the both ends of the bent; these locations are shown in Figure A-67. These diagonal cracks measure up to 0.015 inches. The north side of the bent is shown in Figure A-68 through Figure A-77. The south side of the bent is shown in Figure A-78 through Figure A-86.

The inverted-T bent cap was near to off ramp feeding onto the I-35 North access road. Framed into the bent are three TxDOT U-beams. No moment cracking was observed, but a large crack was observed at the beam-column interface suggesting the cap to be simply supported, confirmed by bridge plans.

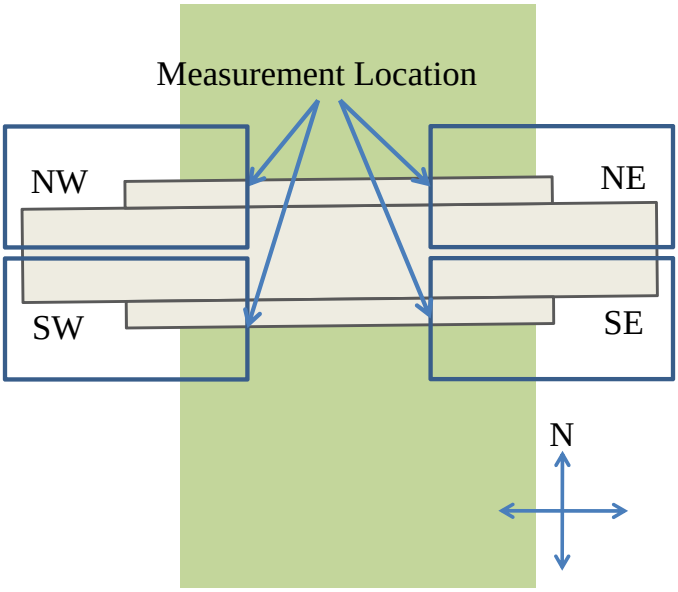

Figure A-67 - Cap orientation and measurement locations (Bent 19)

Figure A-68 – Overall view of north side of Bent 19

Northeast Corner

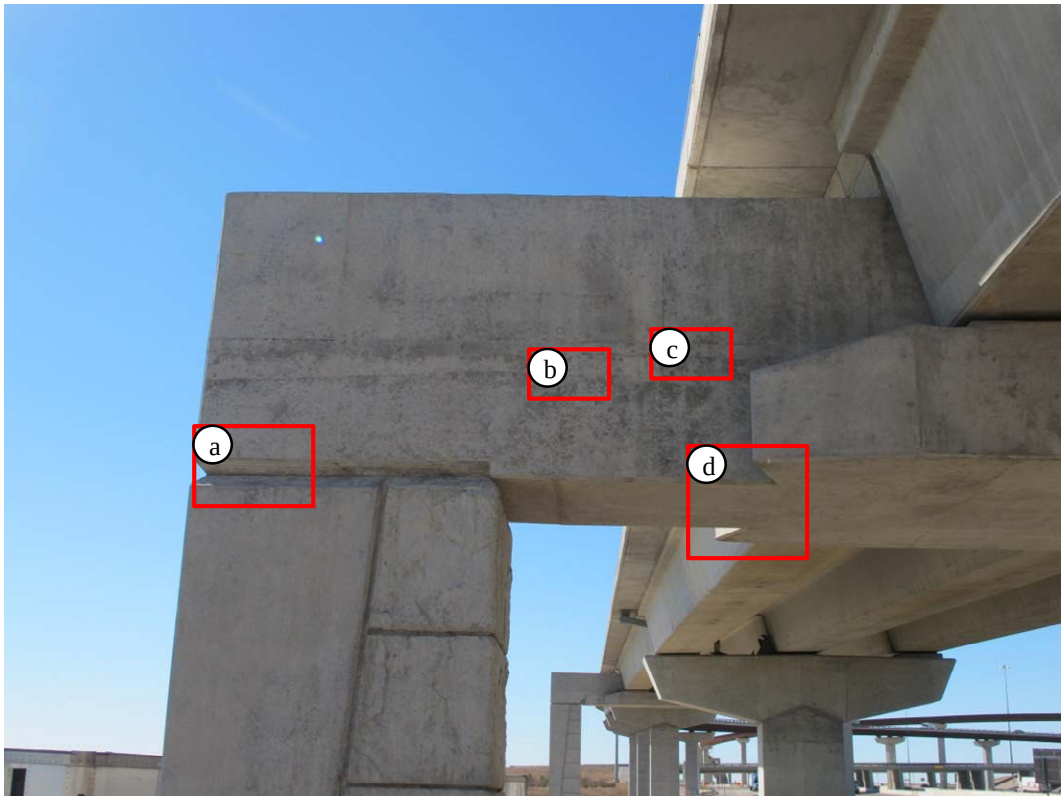

Figure A-69 - Overall view of NE corner of Bent 19

Figure A-70 – Cracking between the column and beam (0.375 inches) (a in Figure A-69)

Figure A-71 – Shear crack (0.005 inches) (b in Figure A-69)

Figure A-72 - Shear crack (0.005 inches) (c in Figure A-69)

Figure A-73 - Crack extending through the entire width of the beam (d in Figure A-69)

Northwest Corner

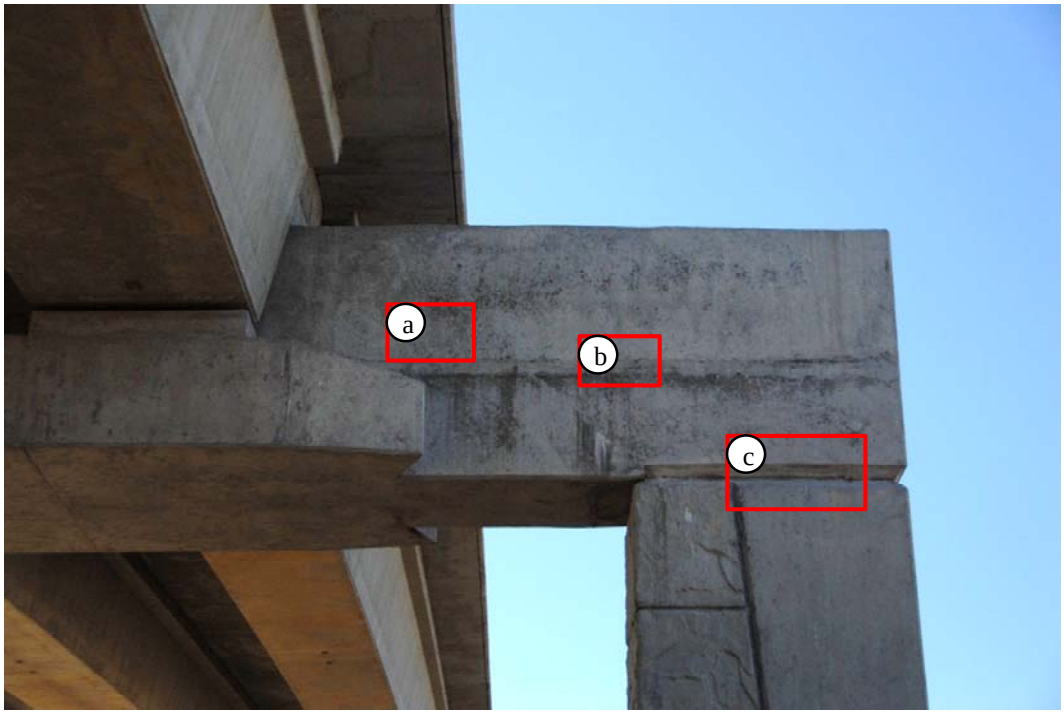

Figure A-74 - Overall view of NW corner of Bent 19

Figure A-75 – Shear crack (0.01 inches) (a in Figure A-74)

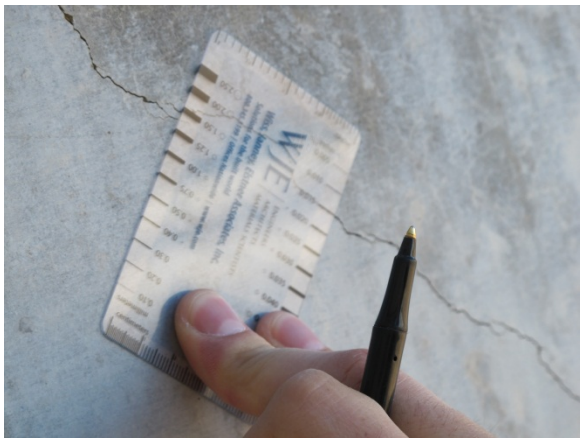

Figure A-76 – Largest shear crack (0.015 inches) (b in Figure A-74)

Figure A-77 – Cracking along column-beam interface (c in Figure A-74)

Figure A-78 – Overall view of south side of Bent 19

Southeast Corner

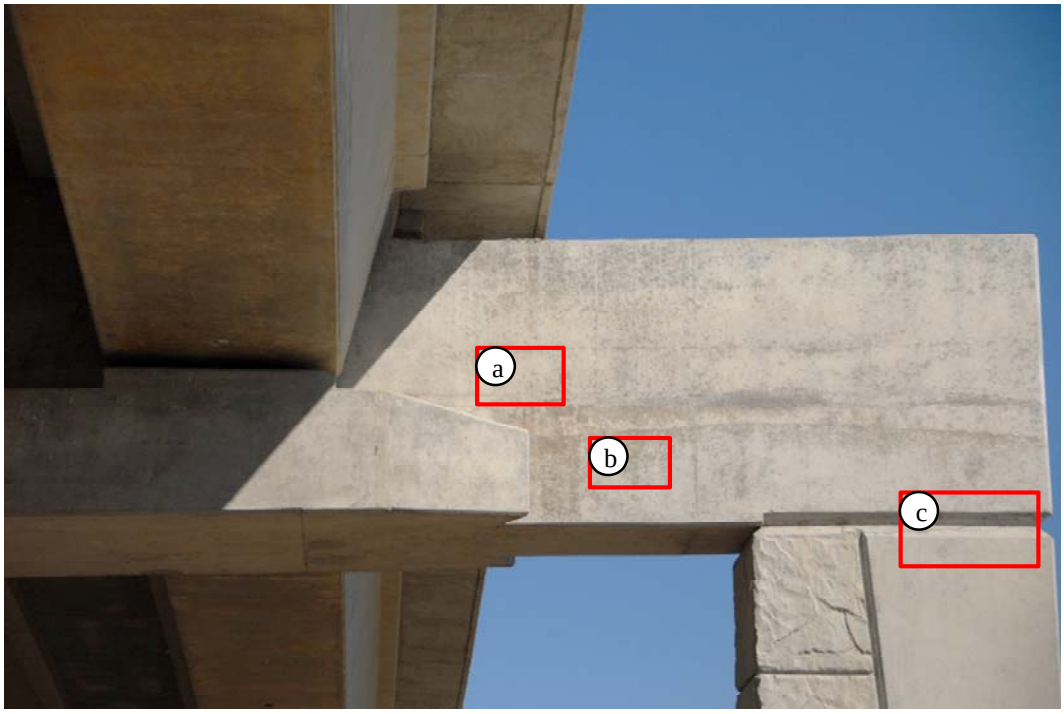

Figure A-79 – Overall view of SE corner of Bent 19

Figure A-80 – Shear crack (0.01 inches) (a in Figure A-79)

Figure A-81 – Shear crack (0.01 inches) (b in Figure A-79)

Figure A-82 – Cracking along column-beam interface (c in Figure A-79)

Southwest Corner

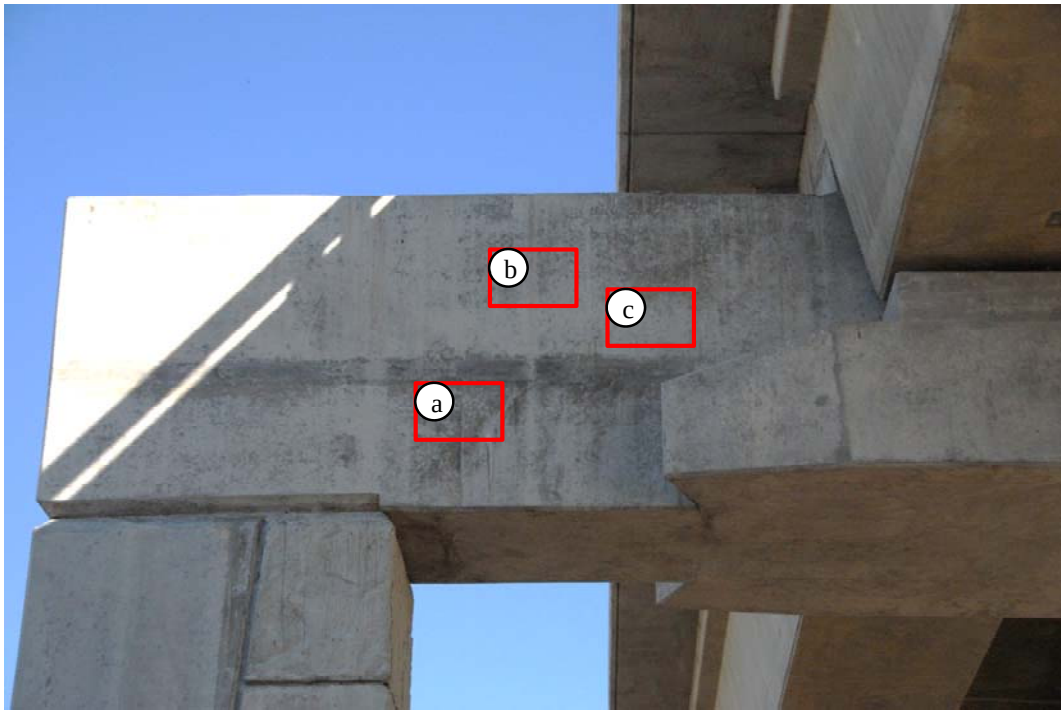

Figure A-83 – Overall view of SW corner of Bent 19

Figure A-84 - Shear crack (0.01 inches) (a in Figure A-83)

Figure A-85 - Shear crack (0.01 inches) (b in Figure A-83)

Figure A-86 - Shear crack (0.01 inches) (c in Figure A-83)

A.3 BRIDGE PLANS

TX-290 W Connector to Frontage Road, Cap 3M

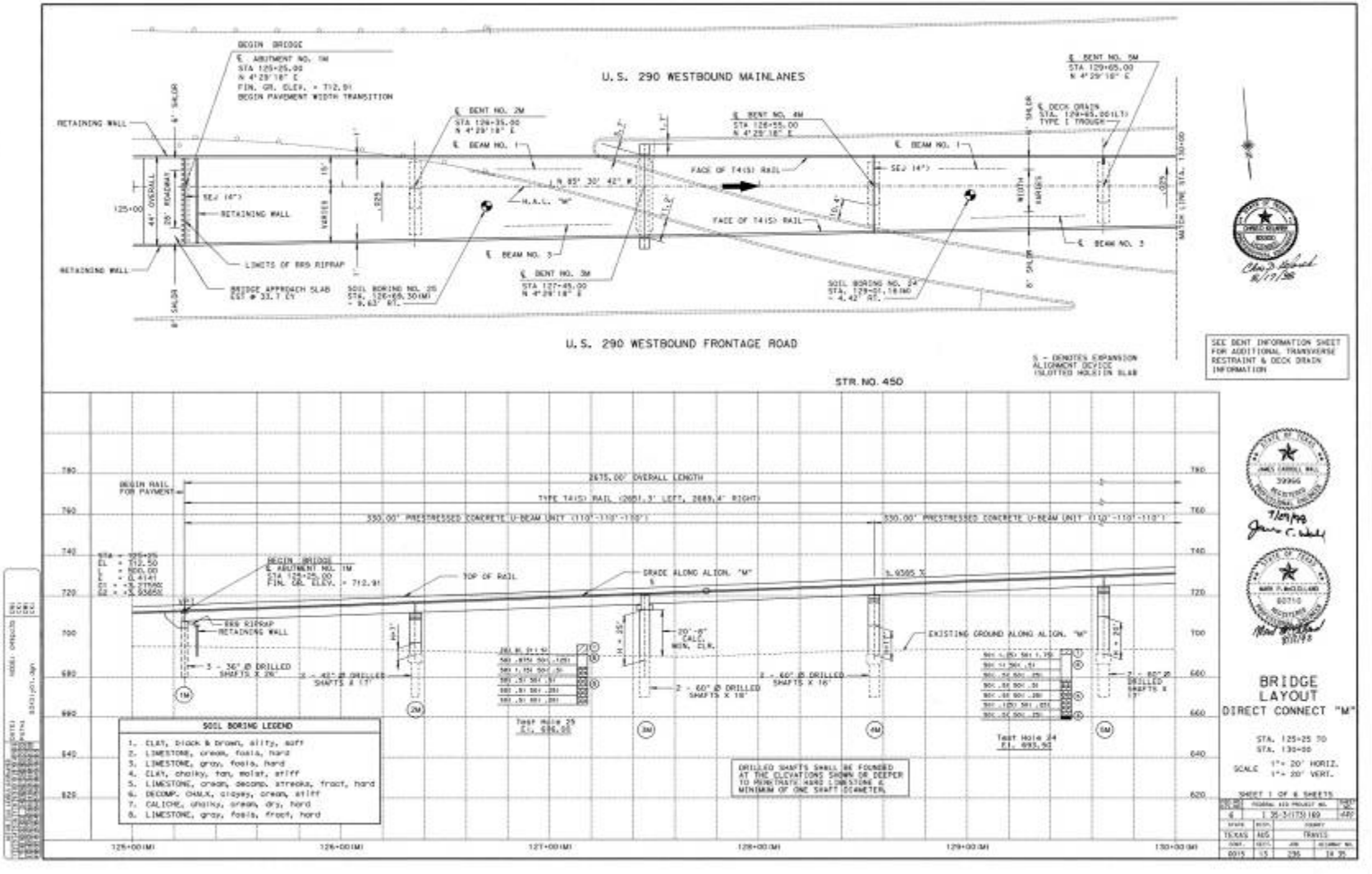

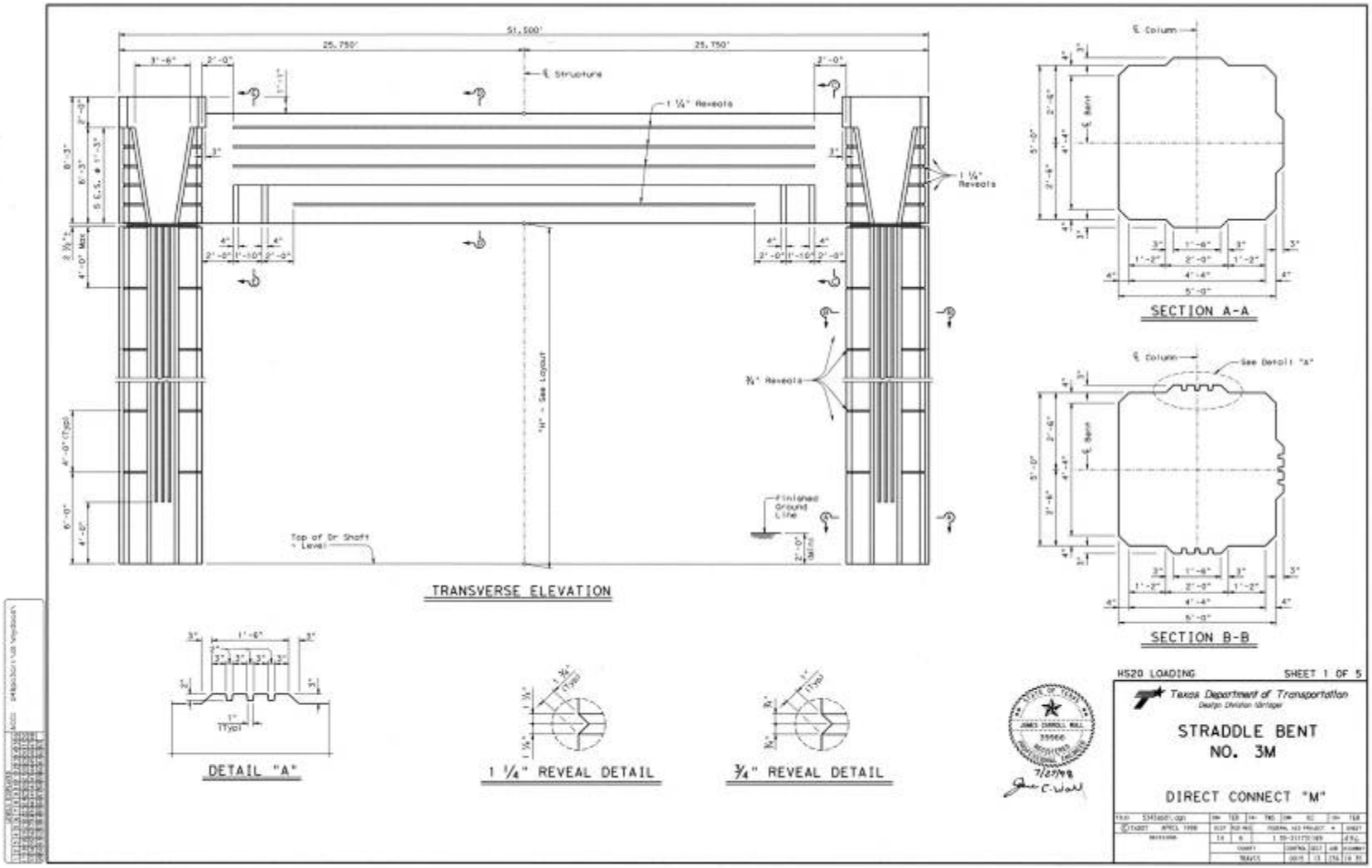
TRANSVERSE ELEVATION
SECTION A-A
SECTION B-B
DETAIL "A"
1 ¼" REVEAL DETAIL
¾" REVEAL DETAIL
HS20 LOADING
SHEET 1 OF 5
Texas Department of Transportation
STRADDLE BENT
NO. 3M
DIRECT CONNECT "M"

TX-290 W Connector to Frontage Road, Cap 3M

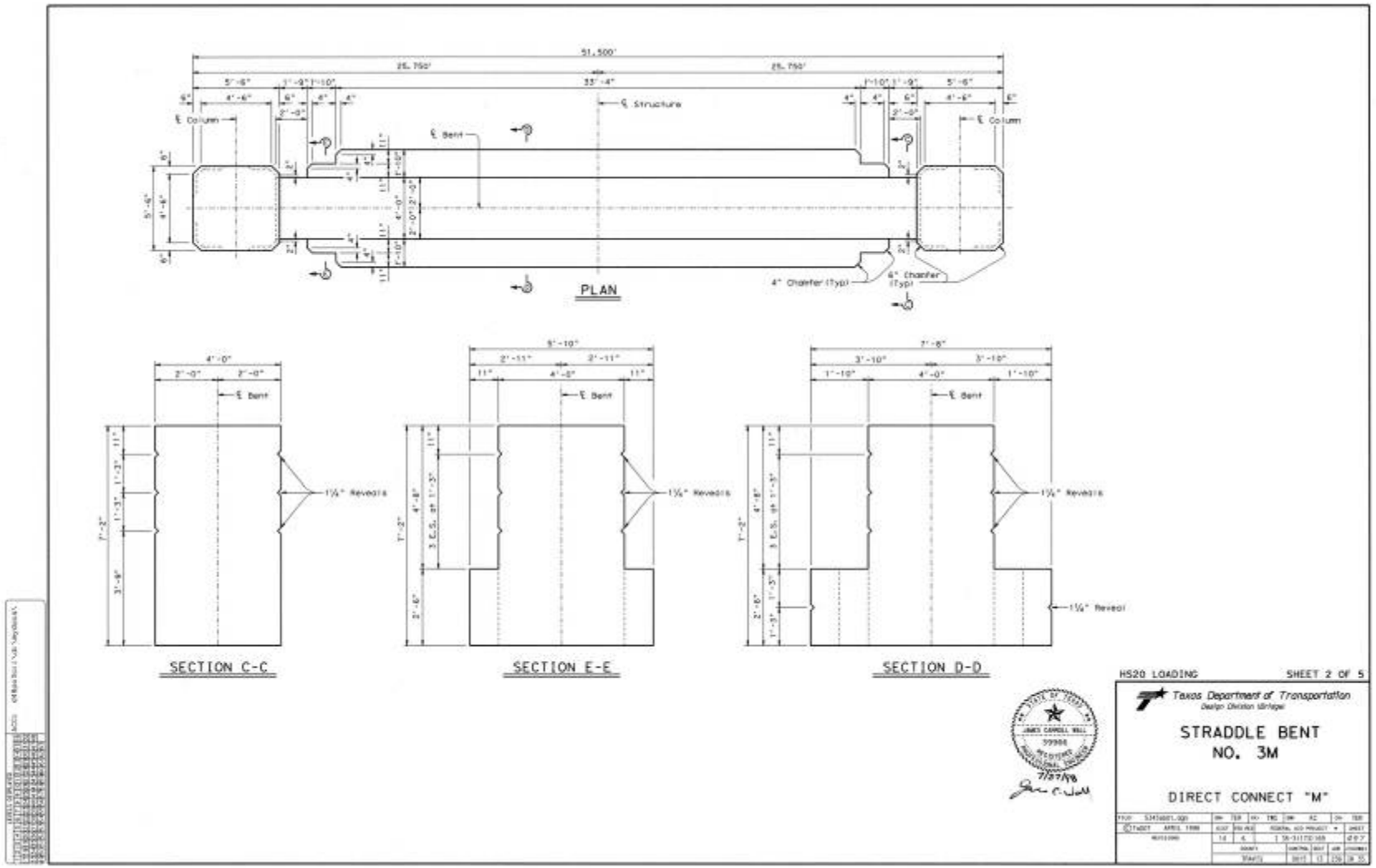

TX-290 W Connector to Frontage Road, Cap 3M

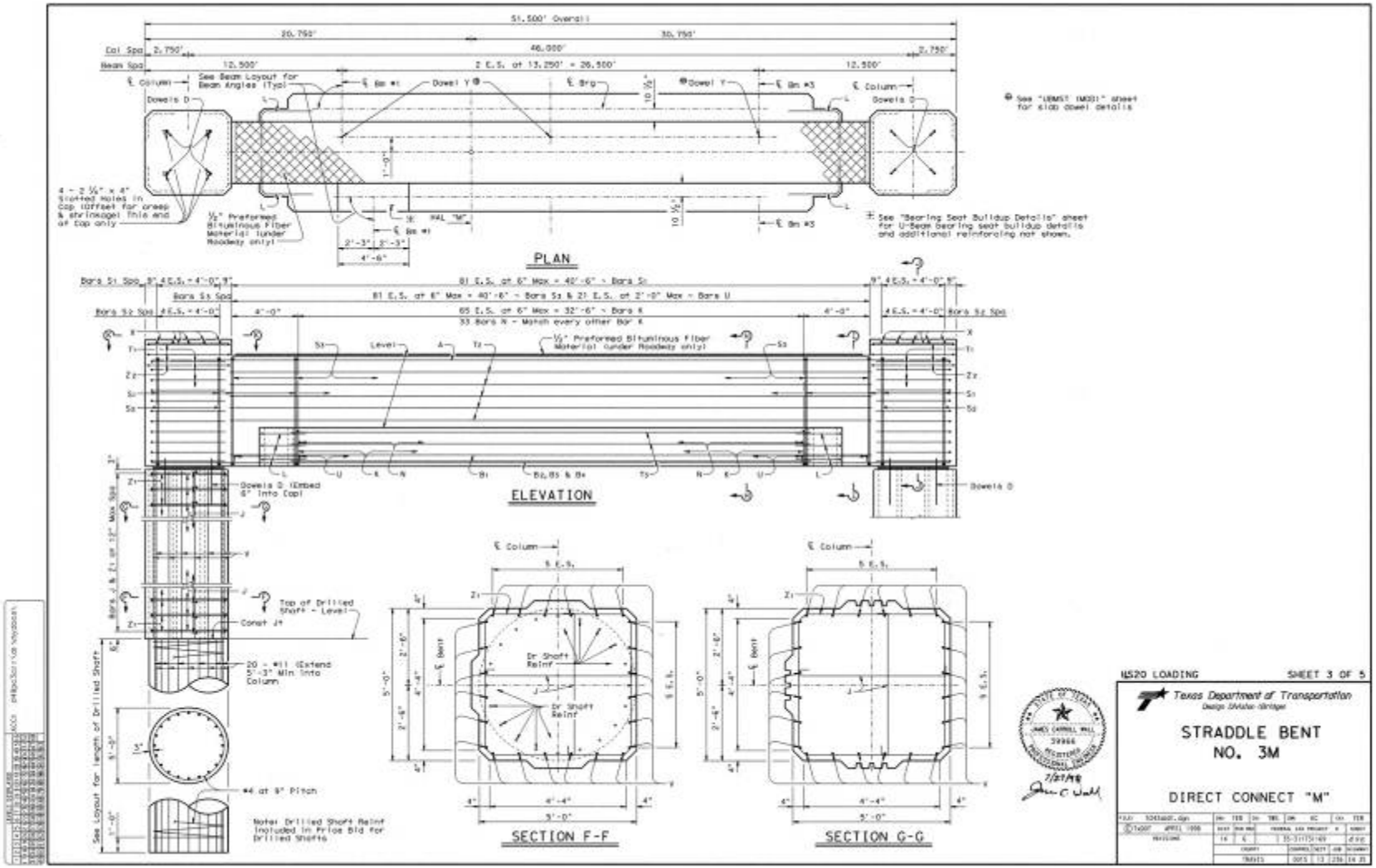

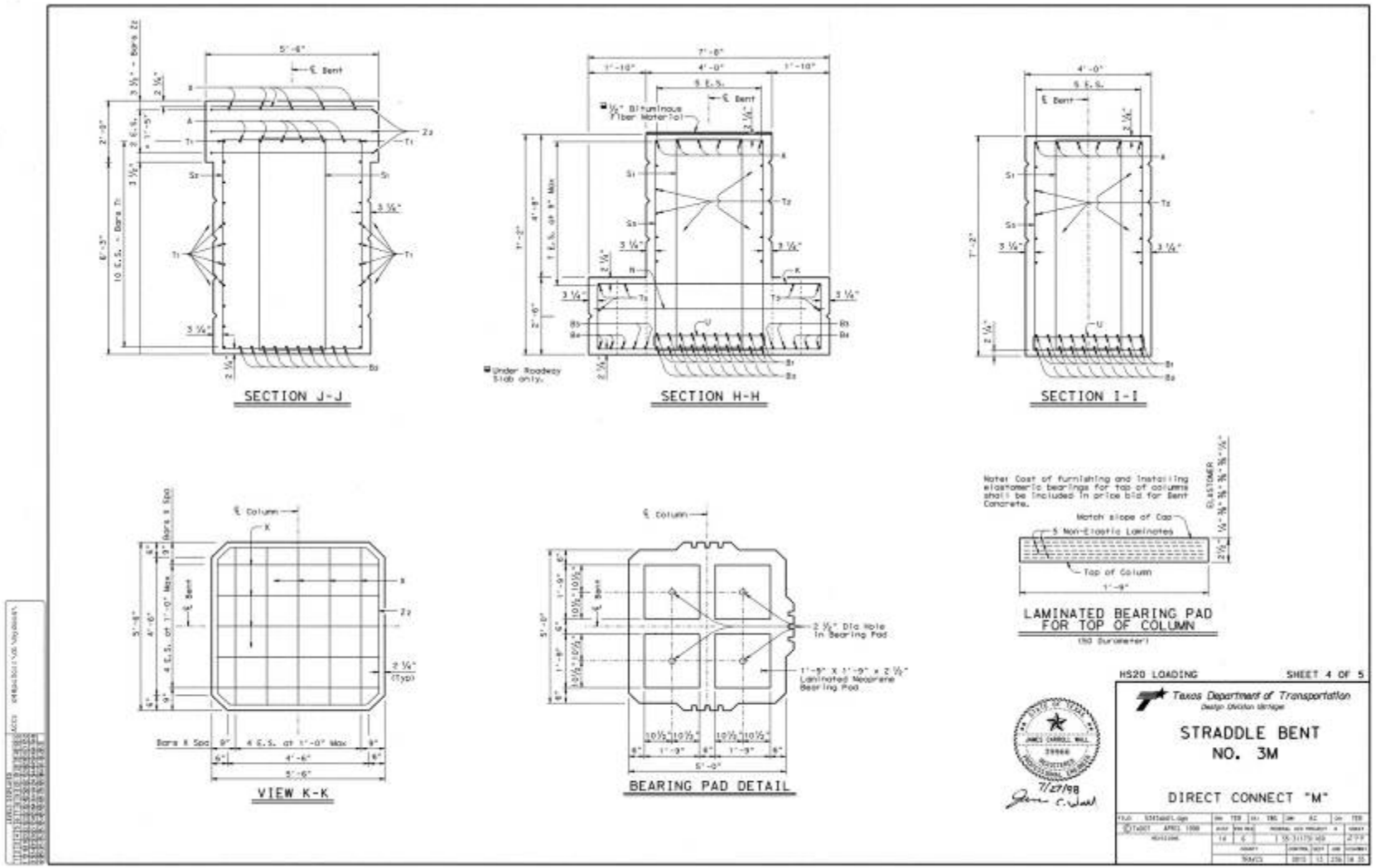
SECTION J-J
SECTION H-H
SECTION I-I
VIEW K-K
BEARING PAD DETAIL
LAMINATED BEARING PAD FOR TOP OF COLUMN
HS20 LOADING
SHEET 4 OF 5
Texas Department of Transportation
STRADDLE BENT
NO. 3M
DIRECT CONNECT "M"

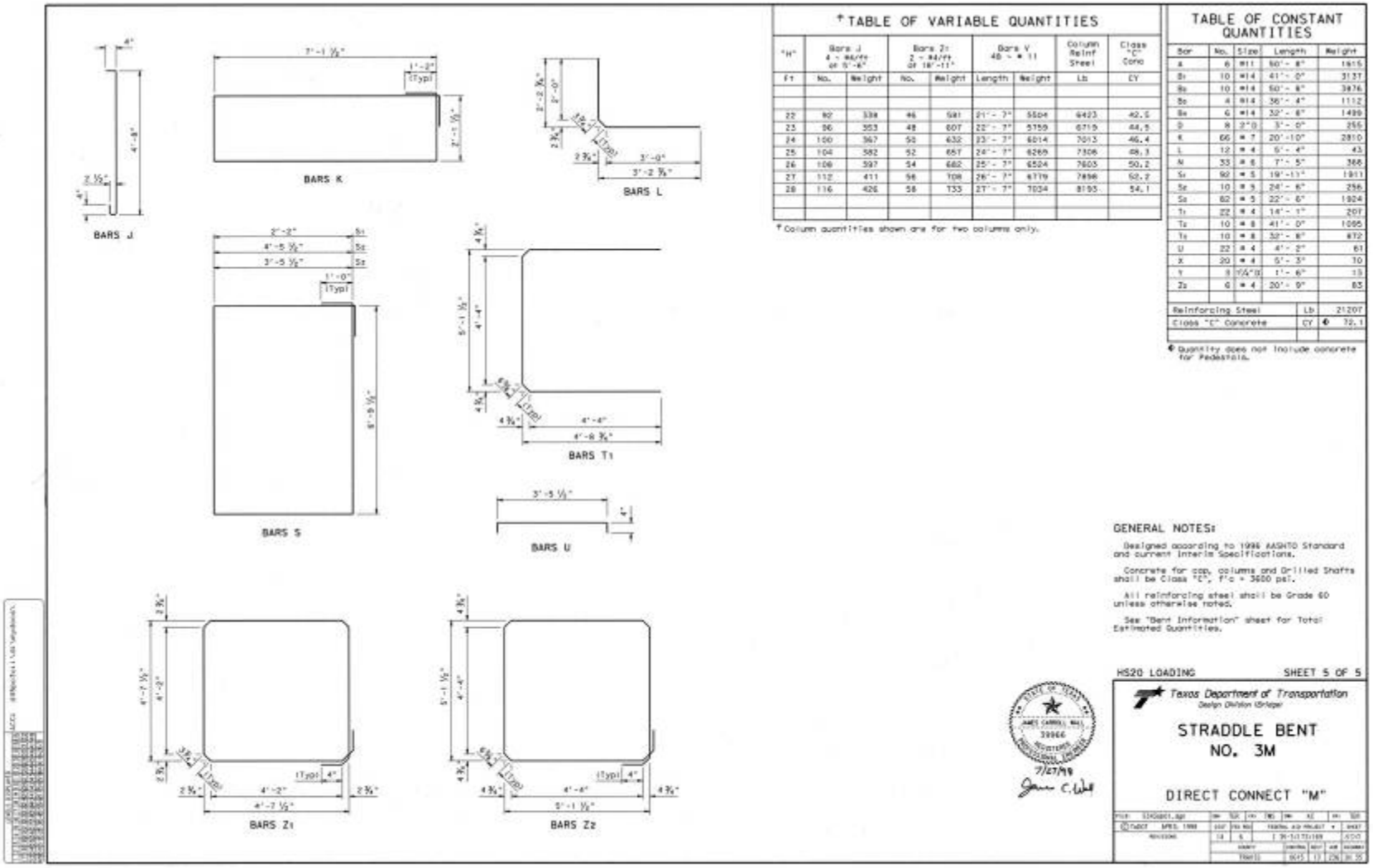

†TABLE OF VARIABLE QUANTITIES

"H"	Bars J #4 - 96/ft at 5'-6"		Bars Z1 Z - #4/ft at 18'-11"		Bars V #8 - # 11		Column Reinf Steel	Class "C" Conc
Ft	No.	Weight	No.	Weight	Length	Weight	Lb	CY
22	92	338	46	581	21'- 7"	5504	6423	42.6
23	96	353	48	607	22'- 7"	5759	6719	44.5
24	100	367	50	632	23'- 7"	6014	7013	46.4
25	104	382	52	657	24'- 7"	6269	7306	48.3
26	108	397	54	682	25'- 7"	6524	7603	50.2
27	112	411	56	708	26'- 7"	6779	7898	52.2
28	116	426	58	733	27'- 7"	7034	8193	54.1

†Column quantities shown are for two columns only.

TABLE OF CONSTANT QUANTITIES

Bar	No.	Size	Length	Weight
A	6	#11	50'- 8"	1815
B1	10	#14	41'- 0"	3137
B2	10	#14	50'- 8"	3876
B3	4	#14	36'- 4"	1112
B4	6	#14	32'- 6"	1489
D	8	2"Ø	3'- 0"	256
K	66	# 7	20'-10"	2810
L	12	# 4	5'- 4"	43
M	33	# 8	7'- 5"	388
S1	92	# 5	19'-11"	1911
S2	10	# 5	24'- 6"	256
S3	82	# 5	22'- 6"	1924
T1	22	# 4	14'- 1"	207
T2	10	# 8	41'- 0"	1095
T3	10	# 8	32'- 8"	872
U	22	# 4	4'- 2"	61
X	20	# 4	5'- 3"	70
Y	8	7/16"Ø	11'- 6"	13
Z3	6	# 4	20'- 9"	83
Reinforcing Steel			Lb	21207
Class "C" Concrete			CY	◐ 72.1

◐ Quantity does not include concrete for Pedestals.

GENERAL NOTES:

Designed according to 1996 AASHTO Standard and current Interim Specifications.

Concrete for cap, columns and Drilled Shafts shall be Class "C", f'c = 3600 psi.

All reinforcing steel shall be Grade 60 unless otherwise noted.

See "Bent Information" sheet for Total Estimated Quantities.

HS20 LOADING SHEET 5 OF 5

Texas Department of Transportation
Design Division (Bridge)

STRADDLE BENT
NO. 3M

DIRECT CONNECT "M"

I-35 S to TX-290 E Connector, Cap 6K

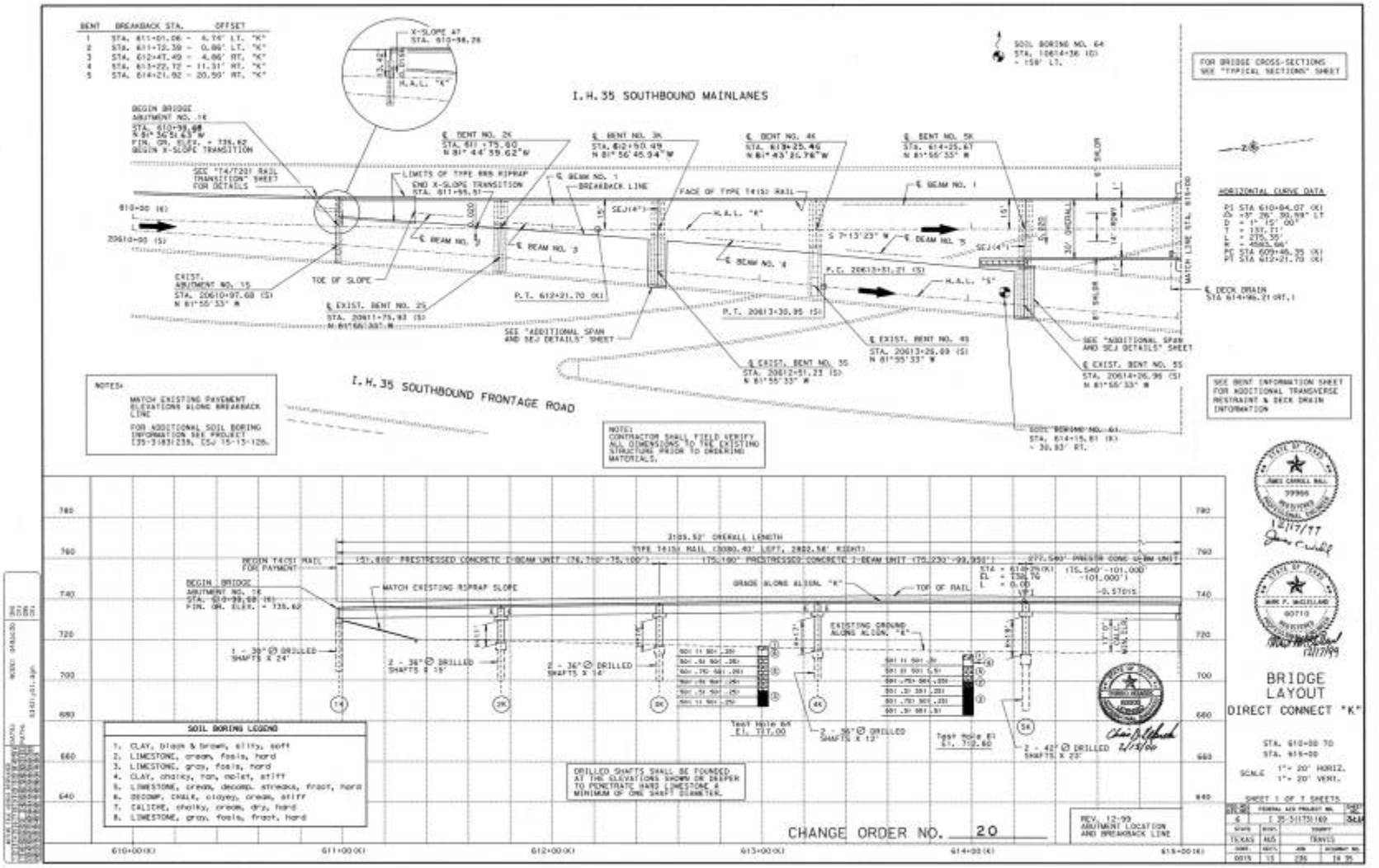

I-35 S to TX-290 E Connector, Cap 6K

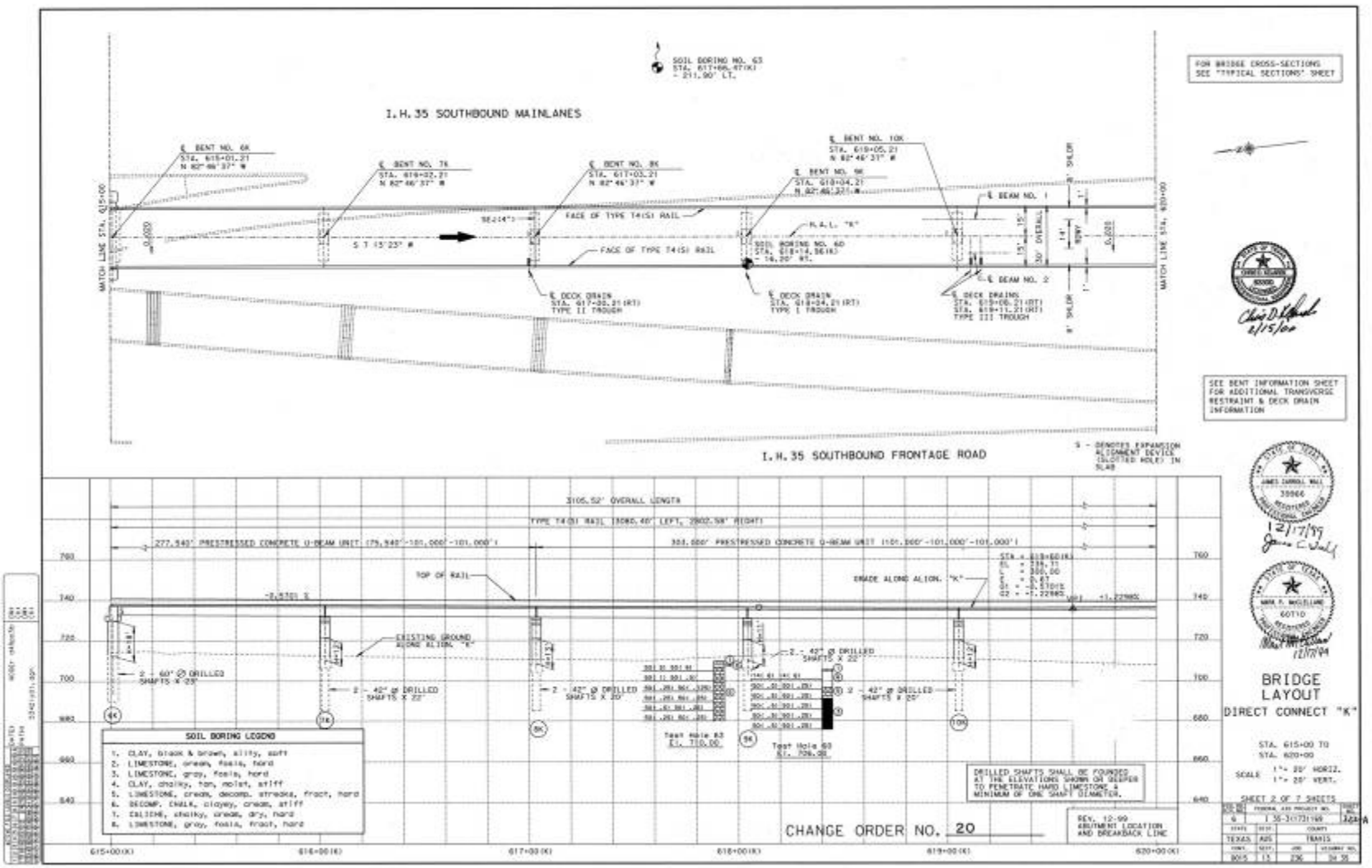

I-35 S to TX-290 E Connector, Cap 28K

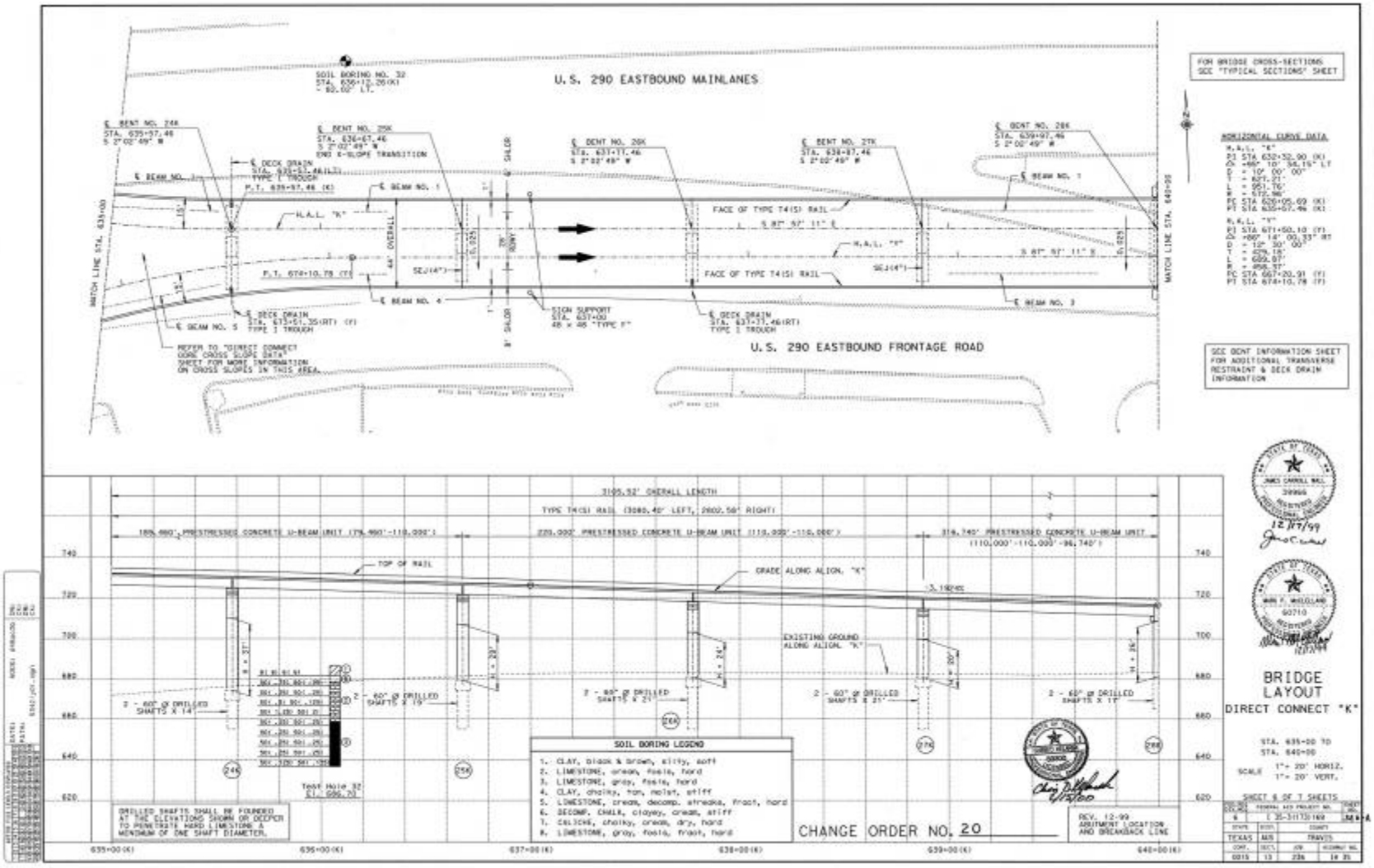

I-35 S to TX-290 E Connector, Cap 28K

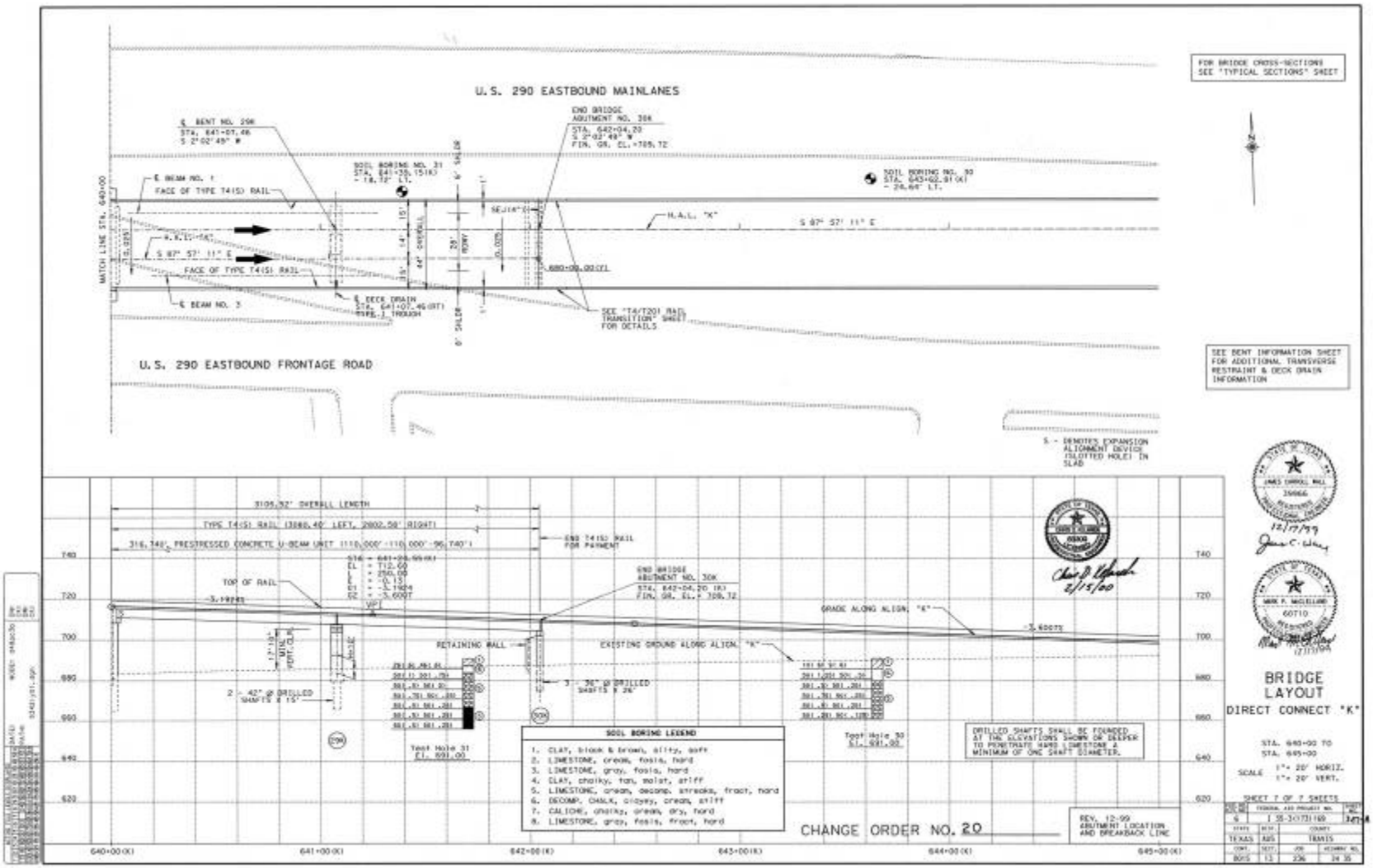

I-35 S to TX-290 E Connector, Cap 6K

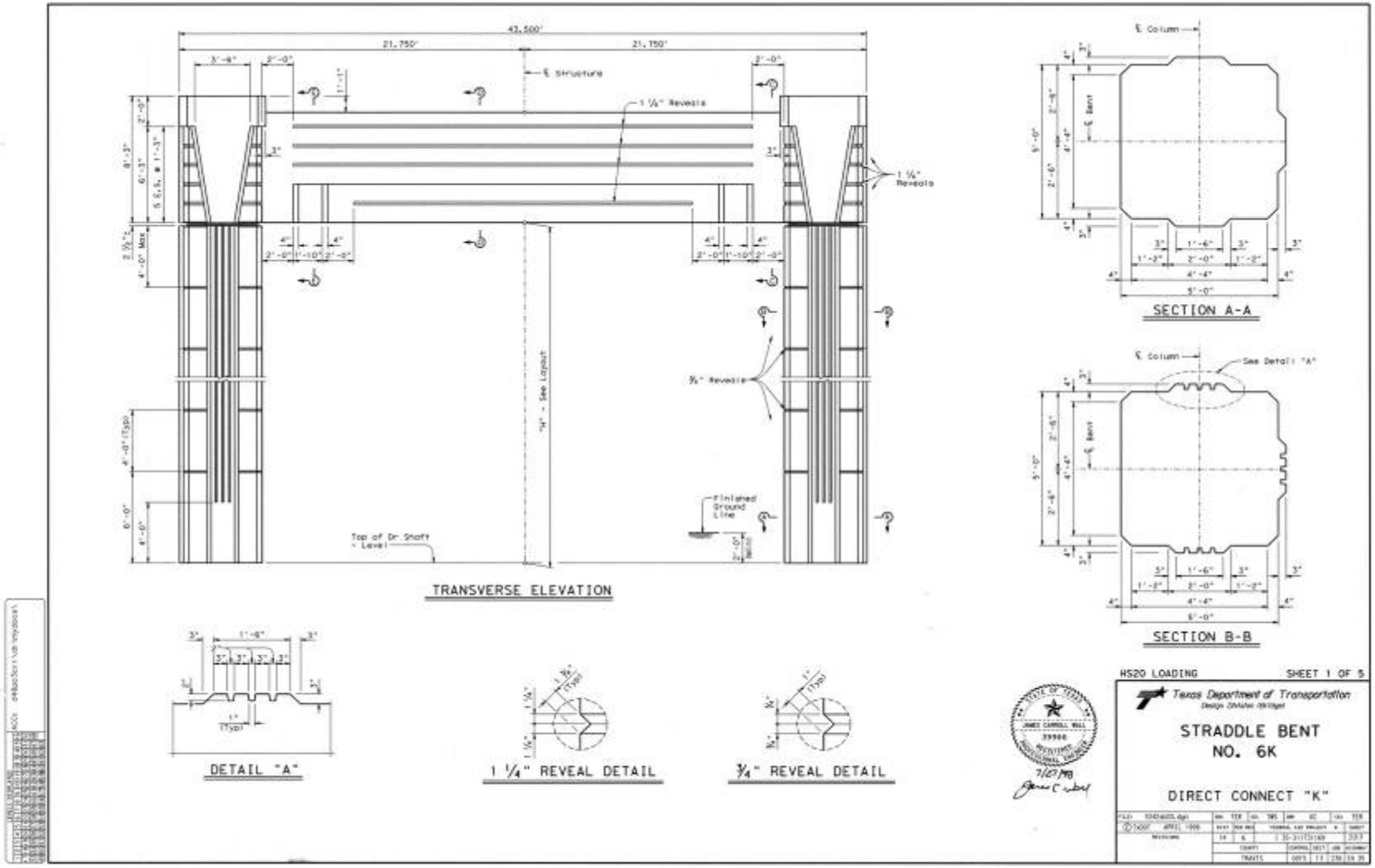

I-35 S to TX-290 E Connector, Cap 6K

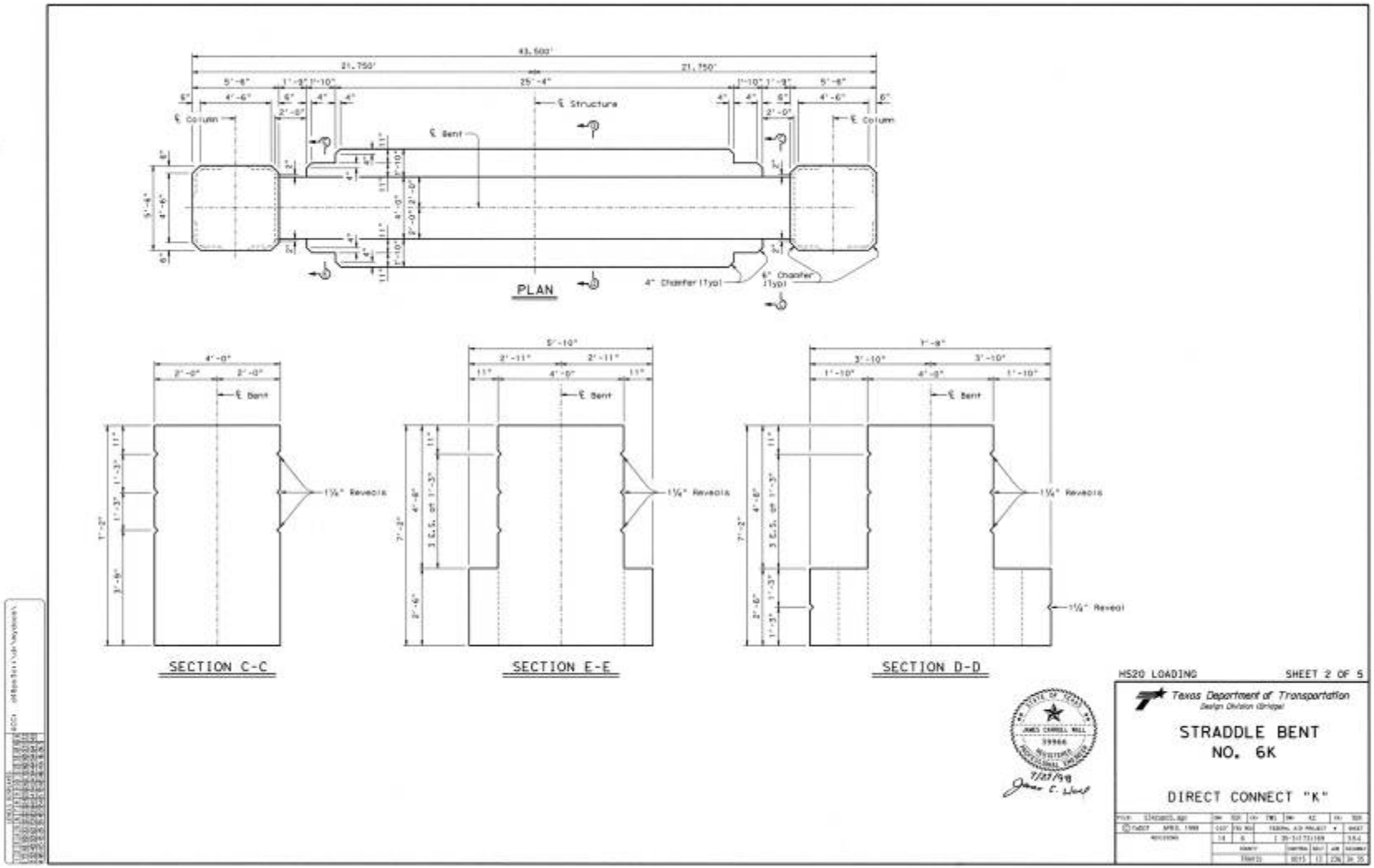

I-35 S to TX-290 E Connector, Cap 6K

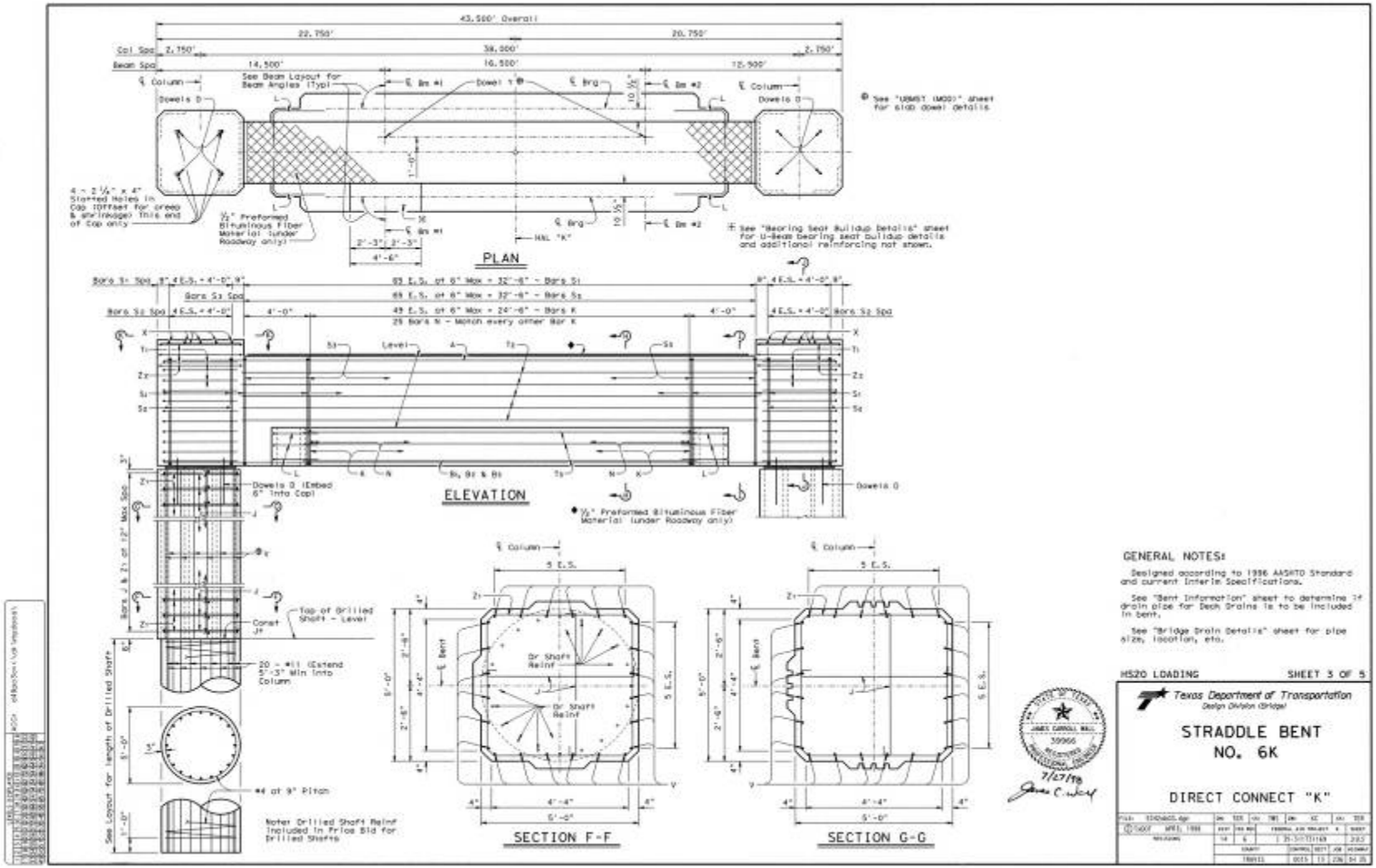

I-35 S to TX-290 E Connector, Cap 6K

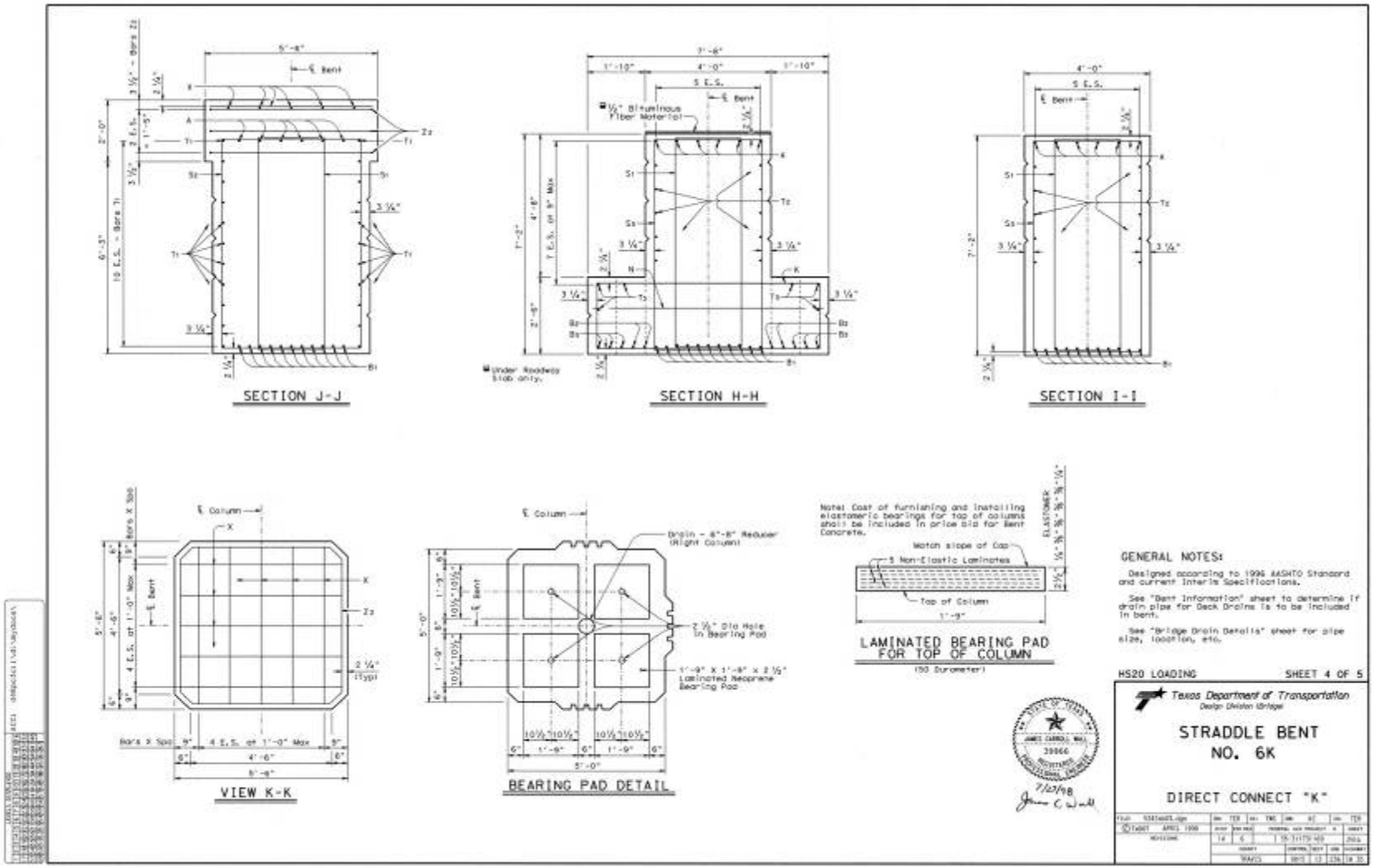

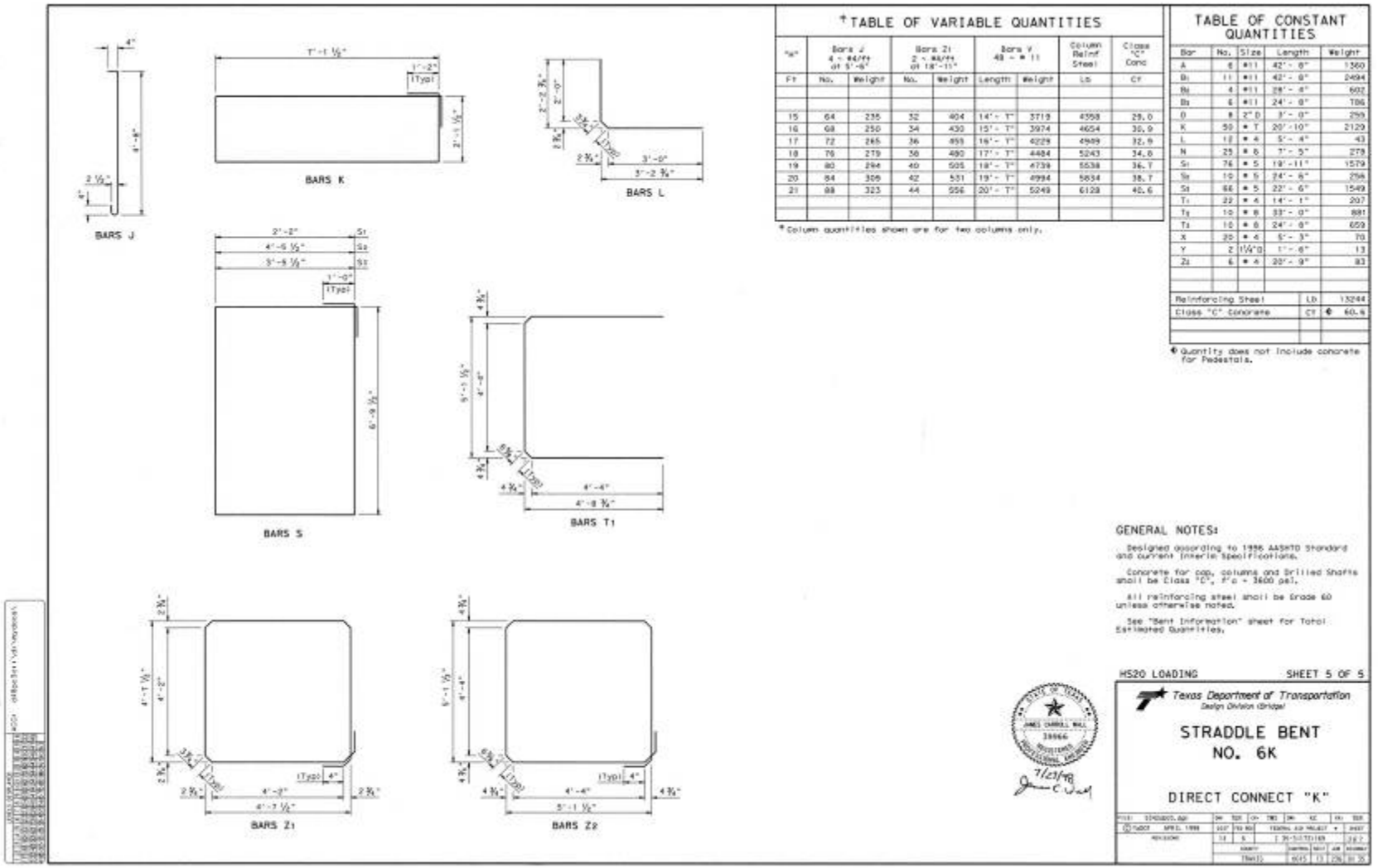

†TABLE OF VARIABLE QUANTITIES

"H"	Bars J 4 - #4/Ft at 5'-6"		Bars Z1 2 - #4/Ft at 18'-11"		Bars Y 48 - # 11		Column Reinf Steel	Class "C" Conc
Ft	No.	Weight	No.	Weight	Length	Weight	Lb	CY
15	64	235	32	404	14'- 1"	3713	4358	29.0
16	68	250	34	430	15'- 1"	3974	4654	30.9
17	72	265	36	455	16'- 1"	4229	4949	32.9
18	76	279	38	480	17'- 1"	4484	5243	34.8
19	80	294	40	505	18'- 1"	4739	5538	36.7
20	84	309	42	531	19'- 1"	4994	5834	38.7
21	88	323	44	556	20'- 1"	5249	6128	40.6

*Column quantities shown are for two columns only.

TABLE OF CONSTANT QUANTITIES

Bar	No.	Size	Length	Weight
A	6	#11	42'- 0"	1360
B1	11	#11	42'- 0"	2494
B2	4	#11	28'- 6"	602
B3	6	#11	24'- 0"	786
D	8	2" D	3'- 0"	299
K	50	# T	20'-10"	2129
L	12	# 4	5'- 4"	43
N	25	# 8	7'- 5"	278
S1	76	# 5	19'-11"	1579
S2	10	# 5	24'- 6"	256
S3	66	# 5	22'- 6"	1549
T1	22	# 4	14'- 1"	207
T2	10	# 8	33'- 0"	881
T3	10	# 8	24'- 0"	659
X	20	# 4	5'- 3"	70
Y	2	1¼"Ø	11'- 6"	13
Z1	6	# 4	20'- 9"	83
Reinforcing Steel			LB	13244
Class "C" Concrete			CY	◆ 60.6

◆ Quantity does not include concrete for Pedestals.

GENERAL NOTES:

Designed according to 1996 AASHTO Standard and current Interim Specifications.

Concrete for cap, columns and Drilled Shafts shall be Class "C", f'c = 3600 psi.

All reinforcing steel shall be Grade 60 unless otherwise noted.

See "Bent Information" sheet for Total Estimated Quantities.

HS20 LOADING SHEET 5 OF 5

Texas Department of Transportation
Design Division (Bridge)

STRADDLE BENT
NO. 6K

DIRECT CONNECT "K"

I-35 S to TX-290 E Connector, Cap 28K

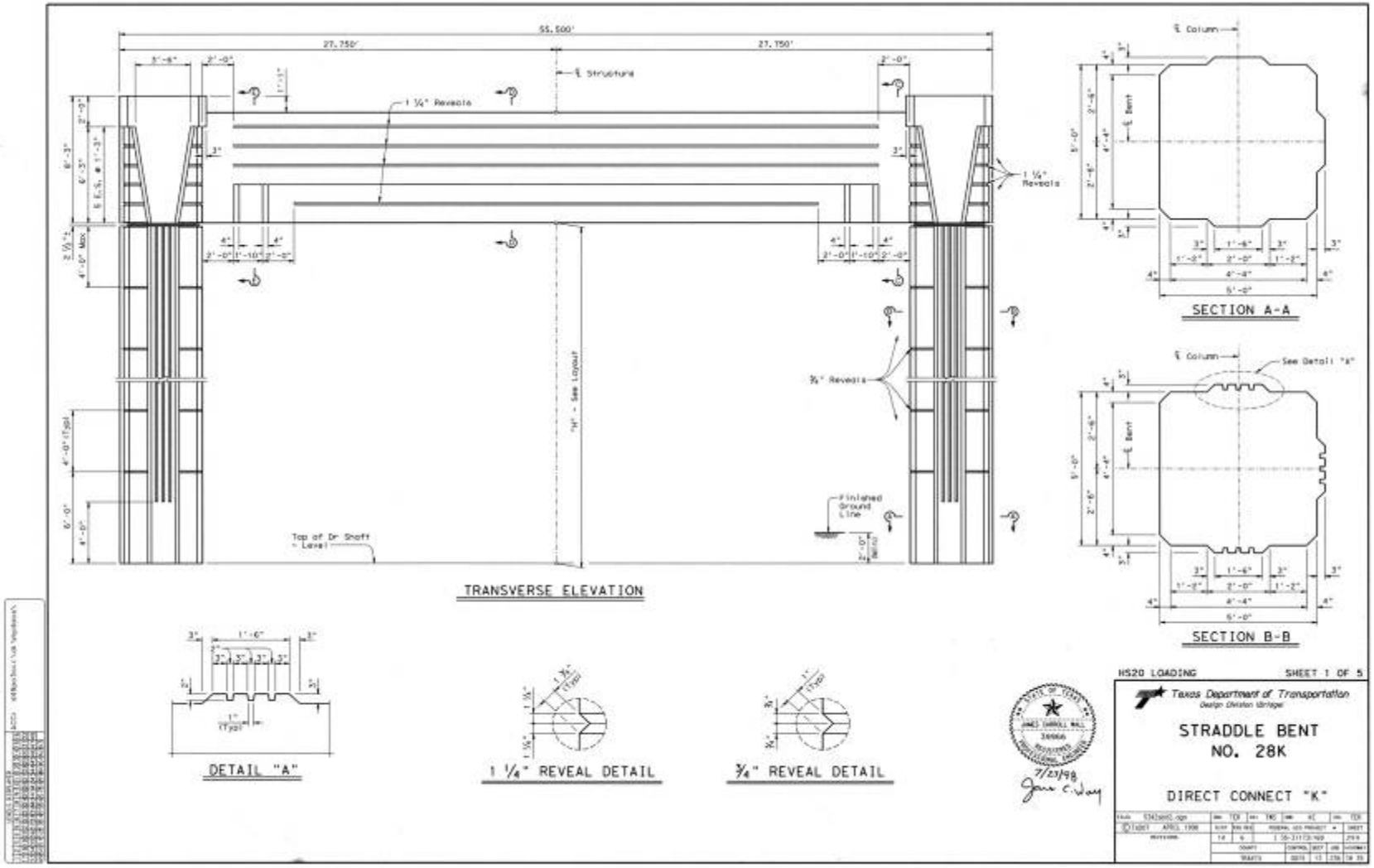

I-35 S to TX-290 E Connector, Cap 28K

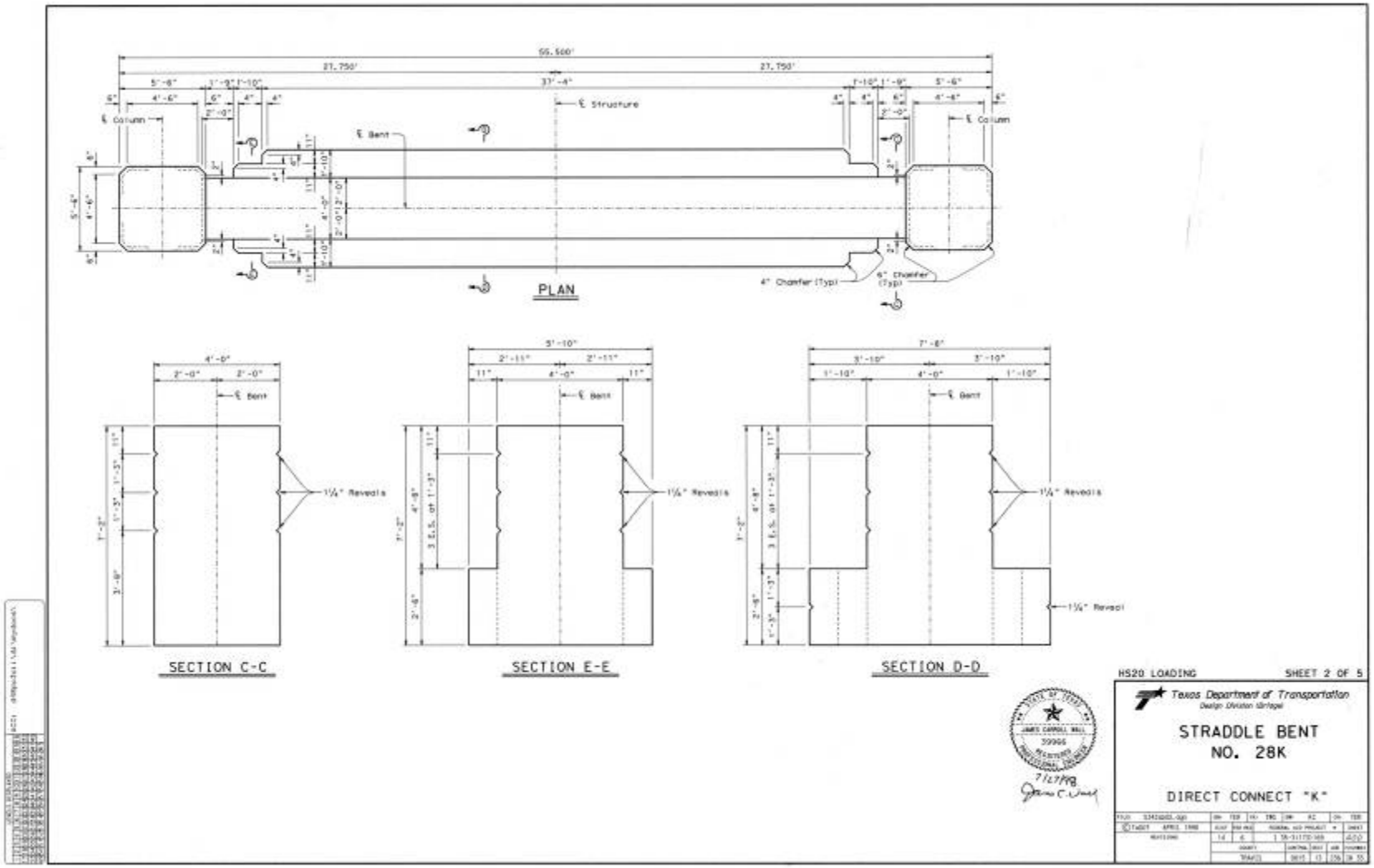

I-35 S to TX-290 E Connector, Cap 28K

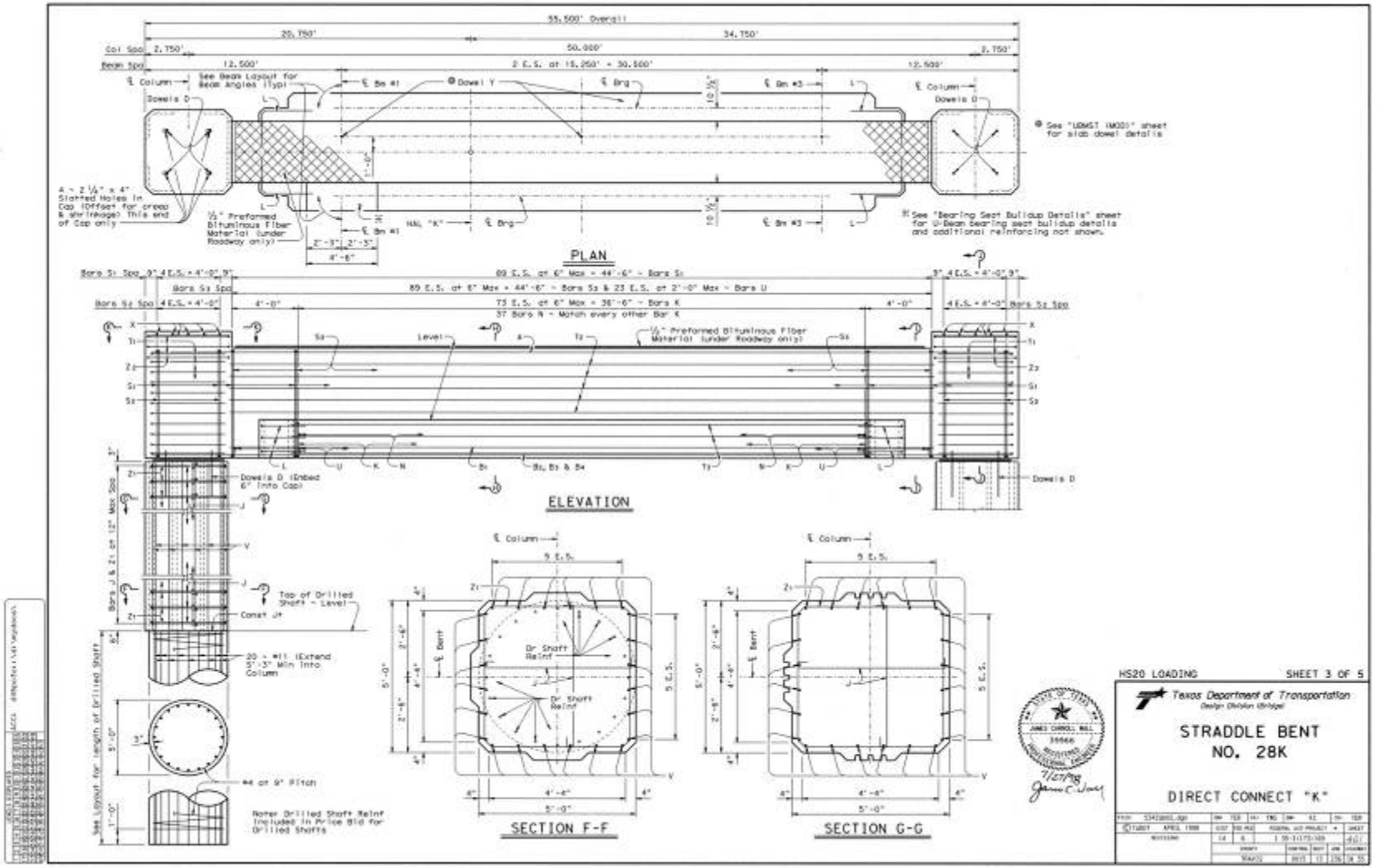

I-35 S to TX-290 E Connector, Cap 28K

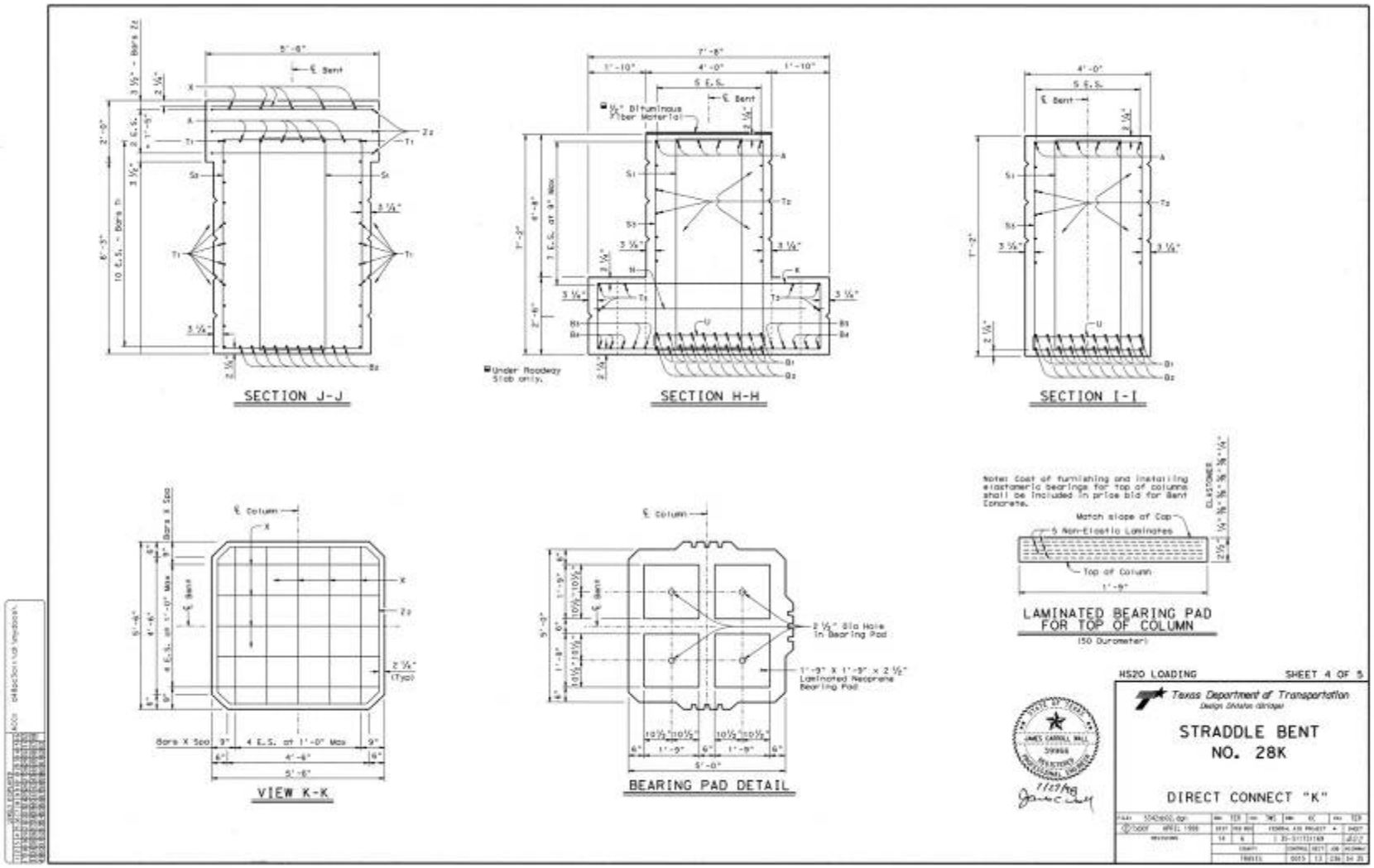

I-35 S to TX-290 E Connector, Cap 28K

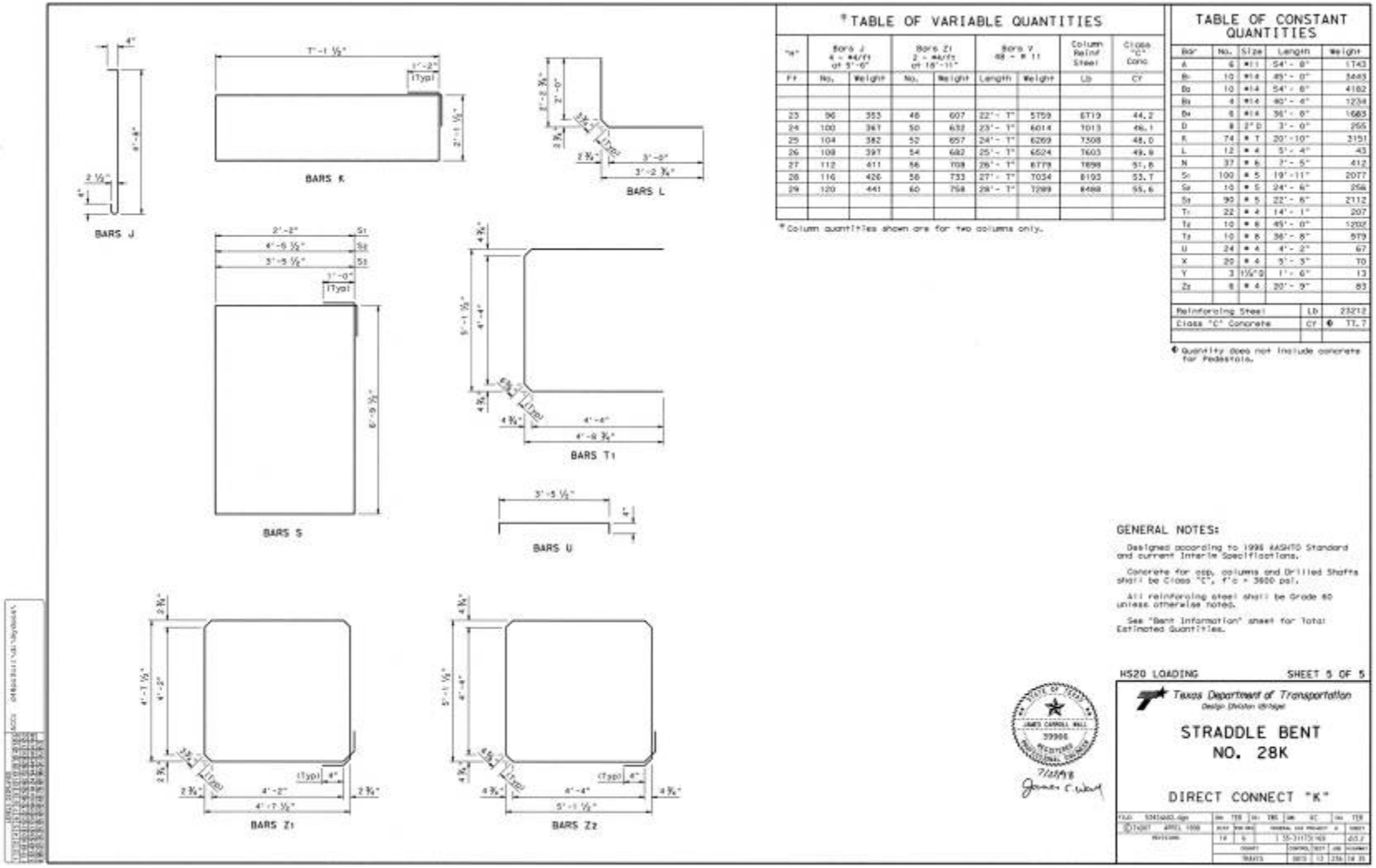

*TABLE OF VARIABLE QUANTITIES

"H"	Bars J #4 @ 1' 0"		Bars Z1 #4 @ 18"		Bars Y #8 - #11		Column Reinf Steel	Class "C" Conc
FT	No.	Weight	No.	Weight	Length	Weight	Lb	CY
23	96	353	48	607	22' - 1"	5759	6719	44.2
24	100	361	50	632	23' - 1"	6014	7013	46.1
25	104	382	52	657	24' - 1"	6269	7308	48.0
26	108	397	54	682	25' - 1"	6524	7603	49.9
27	112	411	56	708	26' - 1"	6779	7898	51.8
28	116	426	58	733	27' - 1"	7034	8193	53.7
29	120	441	60	758	28' - 1"	7289	8488	55.6

*Column quantities shown are for two columns only.

TABLE OF CONSTANT QUANTITIES

Bar	No.	Size	Length	Weight
A	6	#11	54' - 0"	1743
B1	10	#14	45' - 0"	3683
B2	10	#14	54' - 0"	4182
B3	4	#14	40' - 4"	1234
B4	6	#14	36' - 8"	1683
D	8	2" D	3' - 0"	255
E	74	# 7	20' - 10"	3151
L	12	# 4	5' - 4"	43
N	37	# 6	7' - 5"	412
S1	100	# 5	19' - 11"	2077
S2	10	# 5	24' - 6"	256
S3	90	# 5	22' - 6"	2112
T1	22	# 4	14' - 1"	207
T2	10	# 8	45' - 0"	1202
T3	10	# 8	36' - 8"	979
U	24	# 4	4' - 2"	67
X	20	# 4	5' - 3"	70
Y	3	11¼" D	1' - 6"	13
Z2	8	# 4	20' - 9"	83
Reinforcing Steel			Lb	23212
Class "C" Concrete			CY	◐ 77.7

◐ Quantity does not include concrete for Pedestals.

GENERAL NOTES:

Designed according to 1998 AASHTO Standard and current Interim Specifications.

Concrete for cap, columns and Drilled Shafts shall be Class "C", f'c = 3600 psi.

All reinforcing steel shall be Grade 60 unless otherwise noted.

See "Bent Information" sheet for Total Estimated Quantities.

HS20 LOADING SHEET 5 OF 5

Texas Department of Transportation

STRADDLE BENT NO. 28K

DIRECT CONNECT "K"

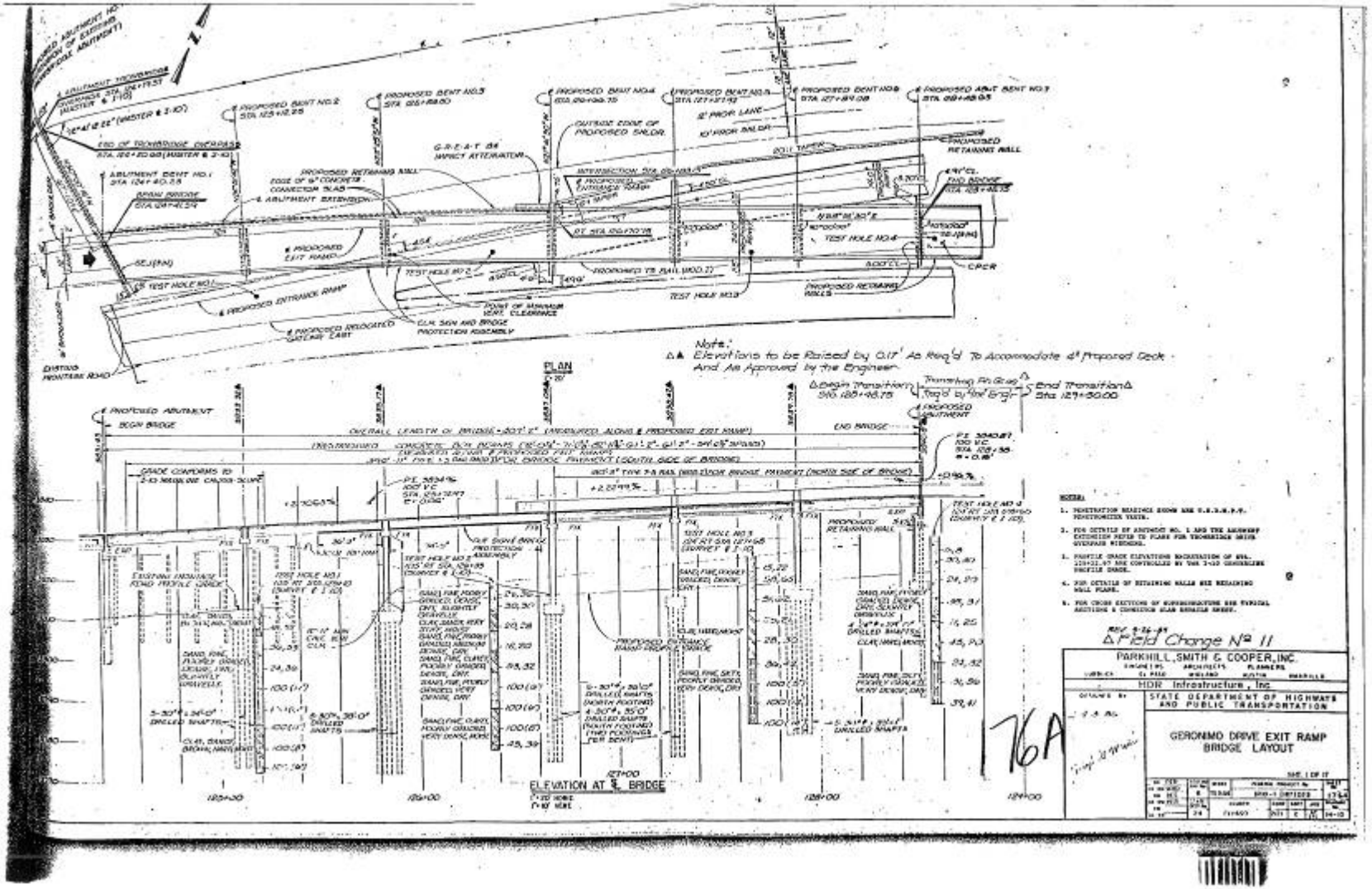
PLAN
ELEVATION AT ℄ BRIDGE
Note:
Elevations to be Raised by 0.17' As Req'd To Accomodate 4" Proposed Deck
And As Approved by the Engineer.
Δ Field Change № 11
PARKHILL, SMITH & COOPER, INC.
HDR Infrastructure, Inc.
STATE DEPARTMENT OF HIGHWAYS AND PUBLIC TRANSPORTATION
GERONIMO DRIVE EXIT RAMP
BRIDGE LAYOUT
SHT. 1 OF 17
176A

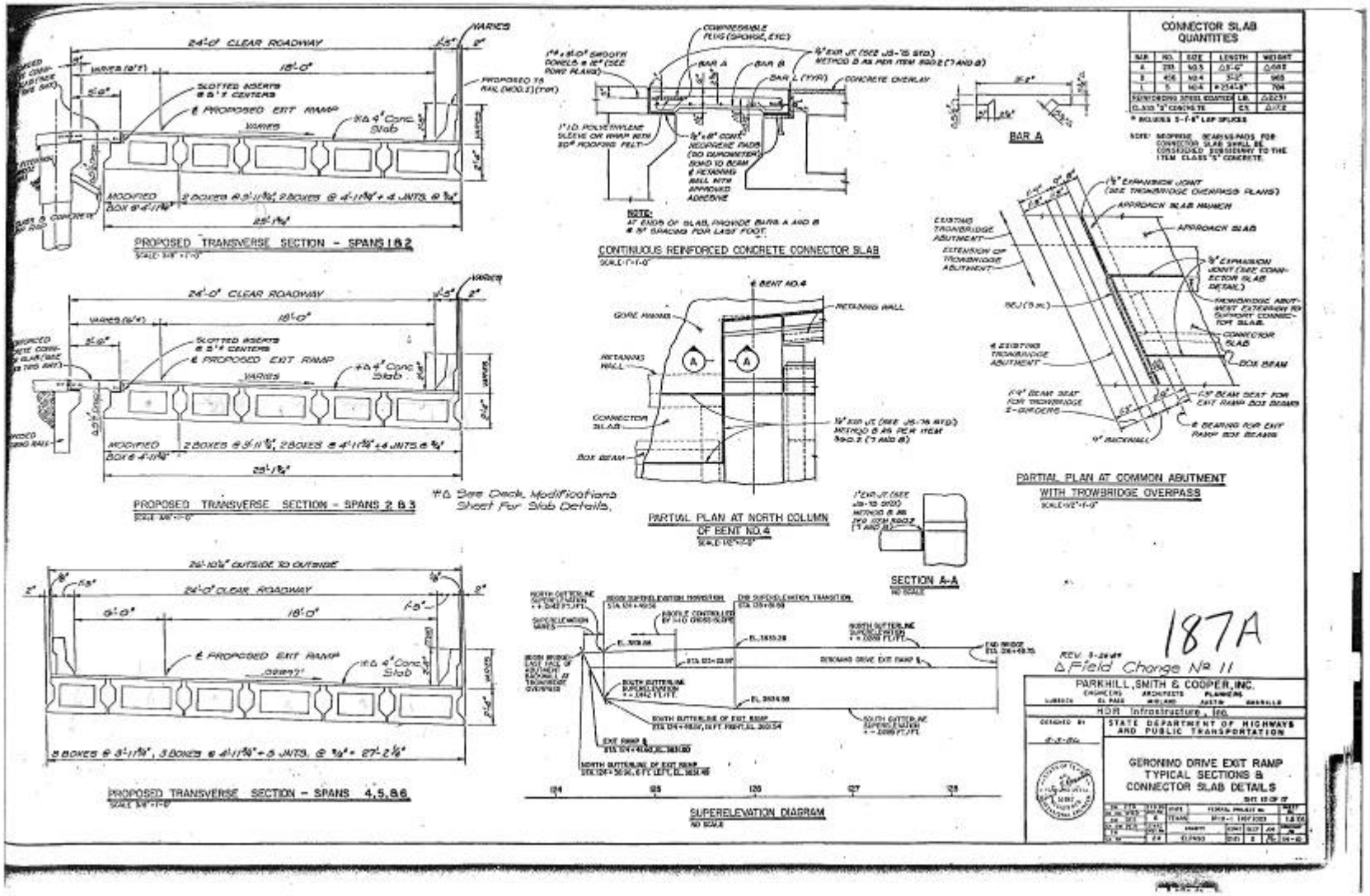
CONNECTOR SLAB QUANTITIES
PROPOSED TRANSVERSE SECTION - SPANS 1 & 2
CONTINUOUS REINFORCED CONCRETE CONNECTOR SLAB
BAR A
PARTIAL PLAN AT COMMON ABUTMENT WITH TROWBRIDGE OVERPASS
PROPOSED TRANSVERSE SECTION - SPANS 2 & 3
PARTIAL PLAN AT NORTH COLUMN OF BENT NO. 4
SECTION A-A
PROPOSED TRANSVERSE SECTION - SPANS 4, 5 & 6
SUPERELEVATION DIAGRAM
187A
Field Change No. 11
PARKHILL, SMITH & COOPER, INC.
HDR Infrastructure, Inc.
STATE DEPARTMENT OF HIGHWAYS AND PUBLIC TRANSPORTATION
GERONIMO DRIVE EXIT RAMP
TYPICAL SECTIONS & CONNECTOR SLAB DETAILS

I-10 East to Gateway Blvd East Connector (near Geronimo Drive), El Paso, Bent 4

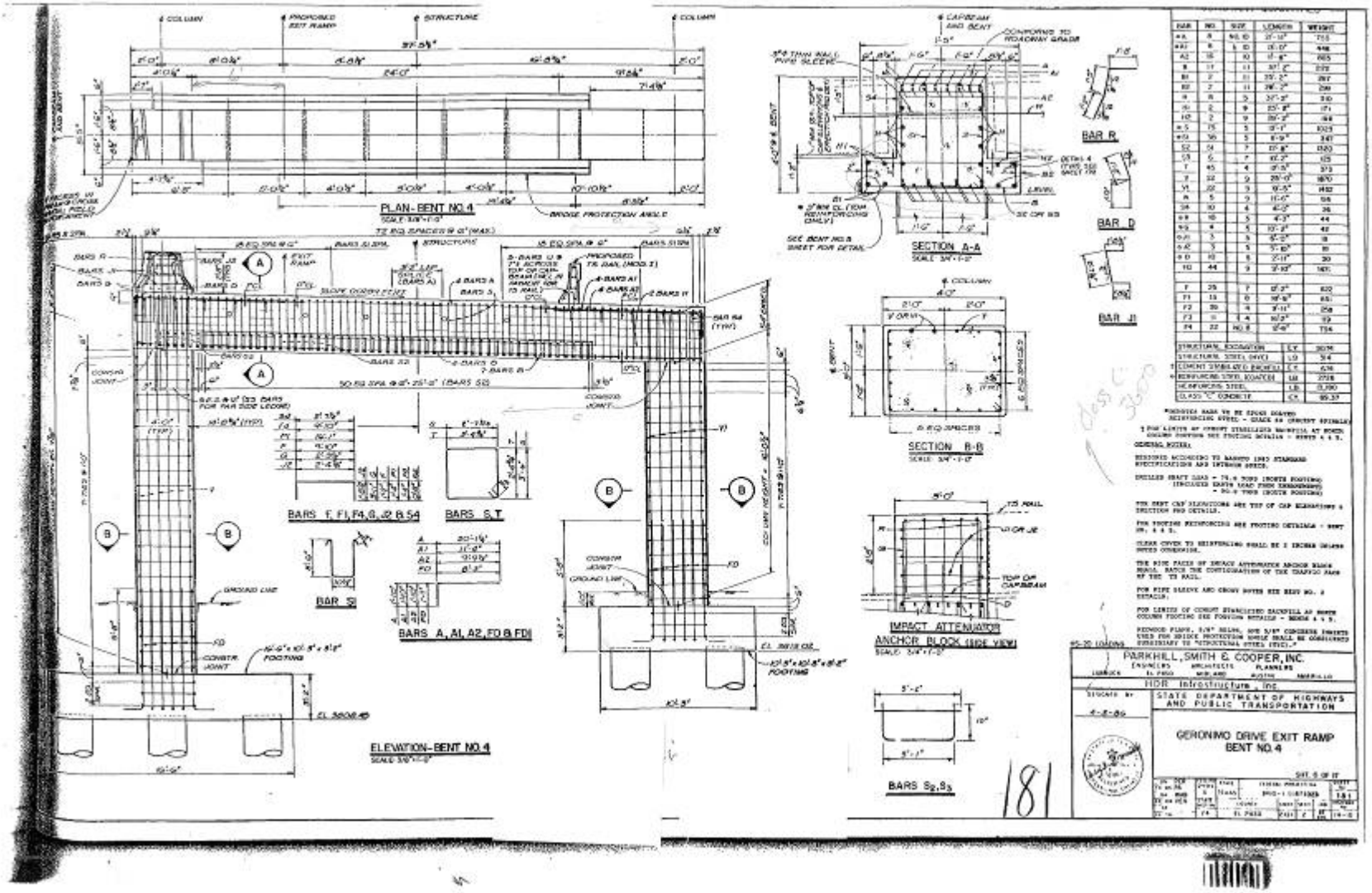

I-10 East to Gateway Blvd East Connector (near Geronimo Drive), El Paso, Bent 5

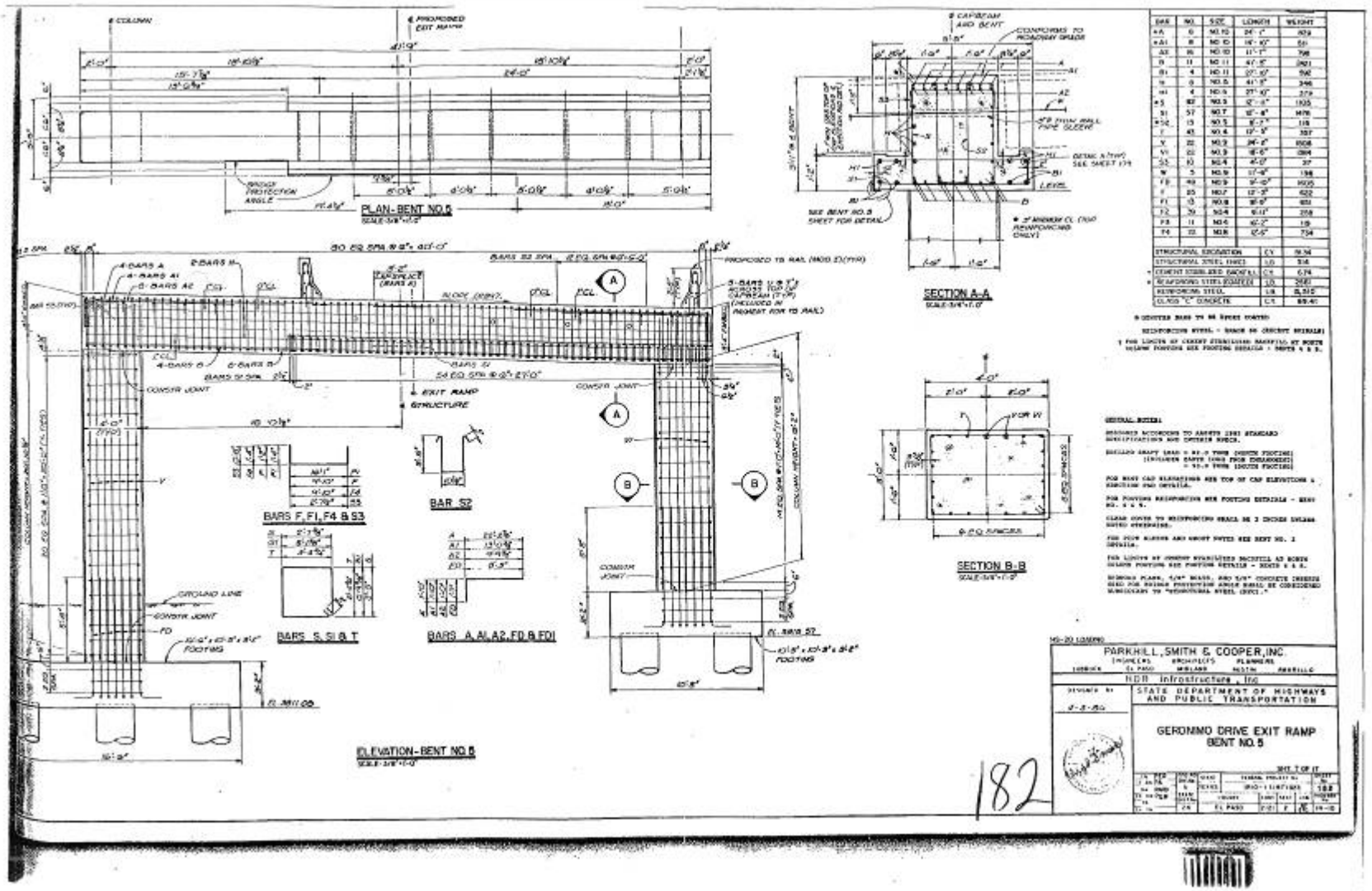

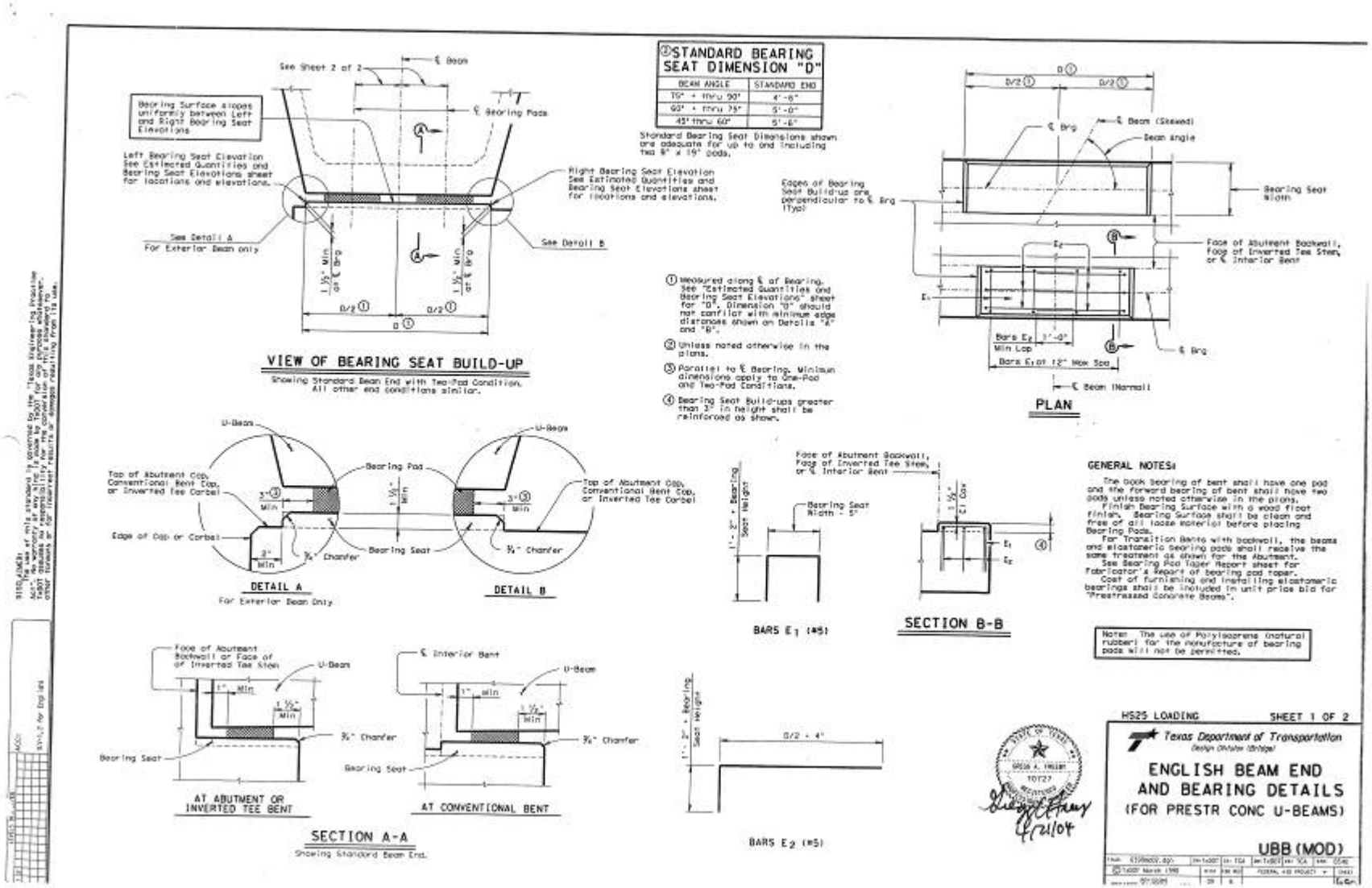
STANDARD BEARING SEAT DIMENSION "D"
BEAM ANGLE
STANDARD END
75° + thru 90°
4'-8"
63° + thru 75°
5'-0"
45° thru 60°
5'-6"
Standard Bearing Seat Dimensions shown are adequate for up to and including two 8" x 19" pads.
VIEW OF BEARING SEAT BUILD-UP
Showing Standard Beam End with Two-Pad Condition. All other end conditions similar.
PLAN
DETAIL A
For Exterior Beam Only
DETAIL B
SECTION B-B
BARS E1 (#5)
BARS E2 (#5)
SECTION A-A
Showing Standard Beam End.
AT ABUTMENT OR INVERTED TEE BENT
AT CONVENTIONAL BENT
GENERAL NOTES:
HS25 LOADING
SHEET 1 OF 2
Texas Department of Transportation
ENGLISH BEAM END AND BEARING DETAILS
(FOR PRESTR CONC U-BEAMS)
UBB (MOD)

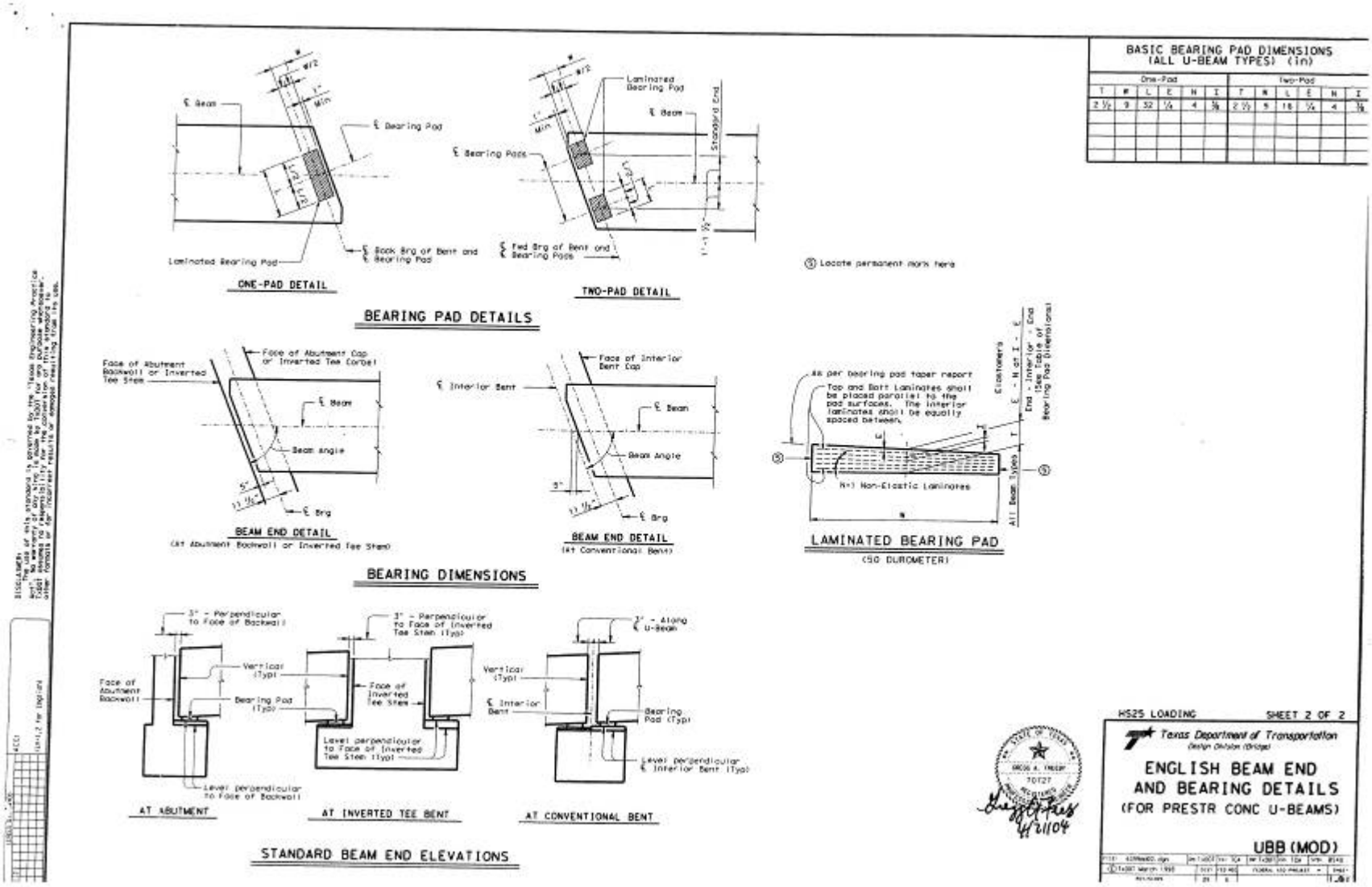
BASIC BEARING PAD DIMENSIONS
(ALL U-BEAM TYPES) (in)
ONE-PAD DETAIL
TWO-PAD DETAIL
BEARING PAD DETAILS
BEAM END DETAIL
BEAM END DETAIL
LAMINATED BEARING PAD
(50 DUROMETER)
BEARING DIMENSIONS
AT ABUTMENT
AT INVERTED TEE BENT
AT CONVENTIONAL BENT
STANDARD BEAM END ELEVATIONS
HS25 LOADING
SHEET 2 OF 2
Texas Department of Transportation
ENGLISH BEAM END
AND BEARING DETAILS
(FOR PRESTR CONC U-BEAMS)
UBB (MOD)

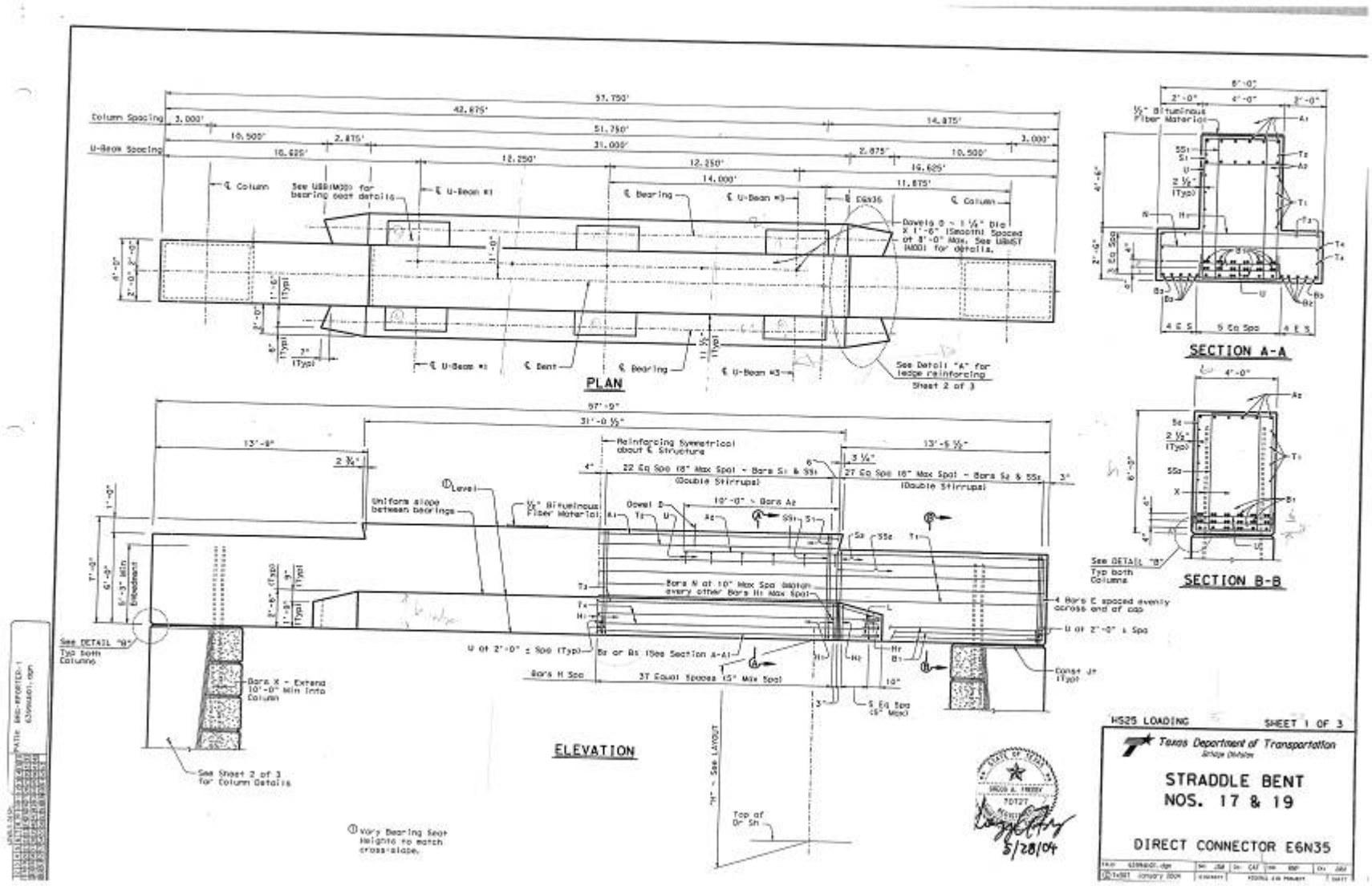
PLAN
ELEVATION
SECTION A-A
SECTION B-B
HS25 LOADING
SHEET 1 OF 3
Texas Department of Transportation
STRADDLE BENT
NOS. 17 & 19
DIRECT CONNECTOR E6N35
5/28/04

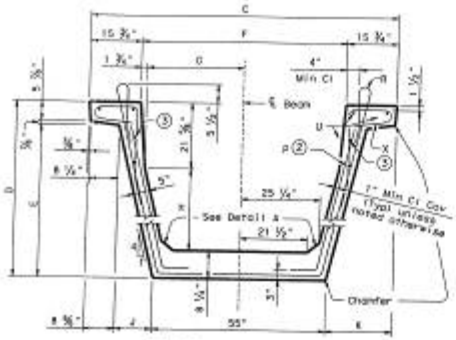

TYPICAL SECTION

(2) Required for exterior beams only.
(3) Optional Bar U for exterior beams only.

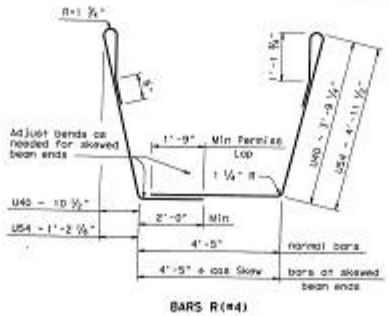

BARS R(#4)

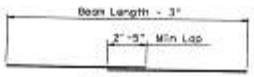

BARS U(#5)

Bars U may be placed with multiple segments, provided no segment is less than 10 Ft in length and 40 Ft min C-C splices.

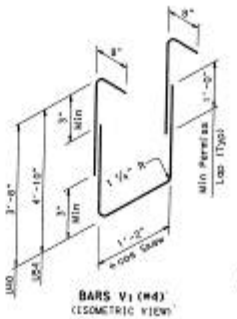

BARS V1(#4)
(ISOMETRIC VIEW)

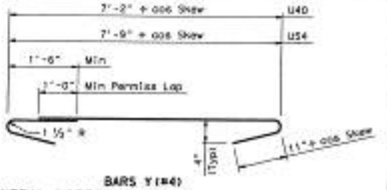

BARS Y(#4)

DETAIL A

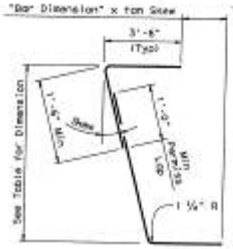

BARS DS1-5 (#4)

BAR DIMENSION		
Bar	Beam Type	
	U40	U54
DS1	4'-8"	4'-8"
DS2	4'-11"	5'-0"
DS3	5'-2"	5'-5"
DS4	5'-4 1/4"	5'-9 1/2"
DS5	5'-6 1/2"	6'-1 1/4"

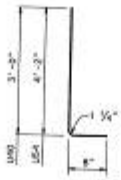

BARS F(#4)

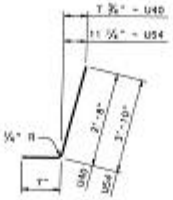

BARS P(#4)

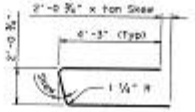

BARS W1(#4)

BAR DIMENSION		
Bar	Beam Type	
	U40	U54
D1	4'-9"	4'-9"
D2	4'-11 1/2"	5'-1"
D3	5'-2"	5'-5 1/2"
D4	5'-4"	5'-10"
D5	5'-6 1/2"	6'-1 1/4"

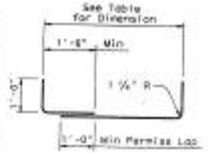

BARS D1-5 (#4)

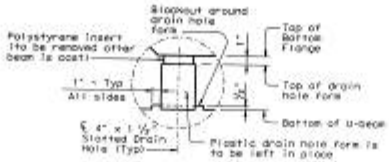

DRAIN HOLE DETAIL

Blockout to be used at all drain hole locations.

At all interior diaphragm locations, strands shall have 3/4" clear cover to edge of drain hole form.

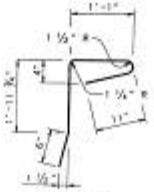

BARS X(#4)

BEAM DIMENSIONS AND SECTION PROPERTIES

Beam Type	C (in.)	D (in.)	E (in.)	F (in.)	G (in.)	H (in.)	J (in.)	K (in.)	Y_b (in.)	I_x (in.)	Area (in.²)	I (in.⁴)	Weight (plf)(1)
U40	89	40	33 1/4	57 1/2	27	10 1/8	8 3/8	17	23.66	16.30	975.5	183,108	1021
U54	98	54	47 1/8	64 1/2	30 1/2	24 1/8	11 3/8	20 1/2	31.58	22.36	1120.6	403,020	1167

(1) Weights shown assume a concrete density of 150 pcf and are for the typical section only. These weights do not include weight of diaphragms or endblocks.

BEAM TOLERANCES
(Deviation from planned dimensions)

Type	Tolerance	Maximum
Horizontal Alignment (upon release of stress)	± 1/8" per 10' of length	3/4"
Horizontal Skew at Ends	± 1/8" per 1" of width	1/2"
Vertical Bottom at Ends	± 1/8" per 1" of depth	1/2"

GENERAL NOTES :

All reinforcing steel shall be grade 60.
Reinforcing steel dimension and bend radii are shown to centerline of bars.
Reinforcing steel shall have 1" min clear cover unless noted otherwise.
All acute corners shall be chamfered for skews greater than 20 Degrees. Any corner of the beam noted with "chamfer" shall be chamfered 3/4" or rounded to a 1 3/4" radius. Optional chamfers, if used shall likewise conform.
Horizontal form joints (seams) will not be permitted.
The beam section dimensions in inches are approximate values converted from the metric beam section dimensions shown on the UBA(M) sheets. The beam section properties are exact conversions of the metric beam section properties shown on the UBA(M) sheets. New forms for U-Beams should be fabricated to the metric dimensions shown on the UBA(M) sheets.
An equal area of welded wire fabric may be substituted for Bars R, P, X and Y.
Shop drawings may be prepared with horizontal skews rounded to the nearest 1/4 degree and batter rounded to the nearest 1/8 inch. These design tolerances are in addition to the fabrication tolerances.
Fabrication tolerances shall be as required for Box Beams under the item, "Precast Concrete Structures (Fabrication)", except that the horizontal alignment, horizontal skew, and vertical batter shall be as shown above in table labeled "Beam Tolerances".
See Bridge Layout and Clearance Sign Bracket sheets for location of anchors in exterior beam for clearance sign bracket.

HS25 LOADING SHEET 1 OF 2

Texas Department of Transportation
Design Division (Bridge)

PRESTRESSED CONCRETE U-BEAM DETAILS

UBA (MOD)

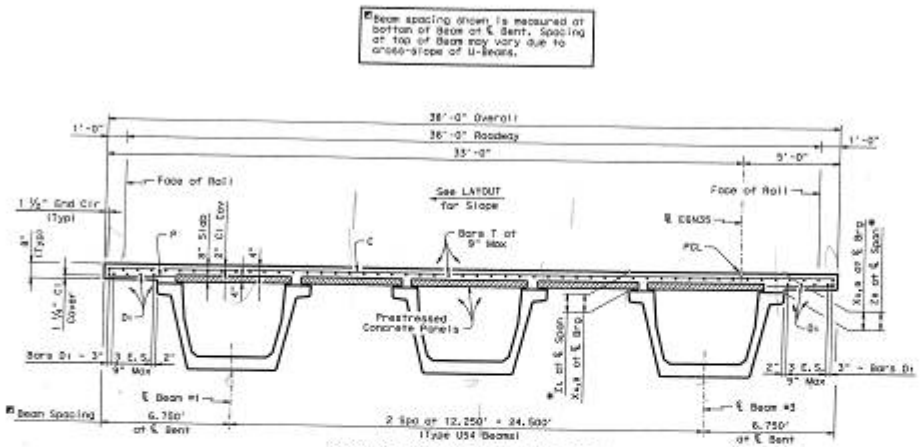

TYPICAL TRANSVERSE SECTION

TABLE OF ESTIMATED QUANTITIES

SPAN	REINF CONC SLAB	PRESTRESSED CONC U-BEAM (U54) ③	② CLASS "S" CONCRETE	① REINFORCING STEEL
NO.	SF	LF	CY	LB
18	3990	306.96	101.9	14763
19	3990	306.96	101.6	14763
20	3990	312.96	103.9	14763
TOTAL	11970	926.88	309.4	44289

① Reinforcing steel weight is calculated using an approximate factor of 3.7 Lbs per Sq Ft.

② Class "S" Concrete quantities include the volume of concrete required for Prestressed Concrete Panels.

③ Lengths shown are bottom beam flange lengths with adjustments made for beam slope. See BEAM LAYOUT for beam lengths.

BAR TABLE

BAR	SIZE
A	#5
C	#5
D	#5
E	#5
G	#5
H	#6
J	#5
K	#5
P	#4
T	#4

TABLE OF SECTION DEPTHS

Span No.	Beam No.	"X_A" at ℄ Brg	"X_B" at ℄ Brg	*"Z_A" at ℄ Span	*"Z_B" at ℄ Span
18 - 20	ALL	10 ½"	10 ½"	8 ¾"	8 ¾"

* Theoretical dimension

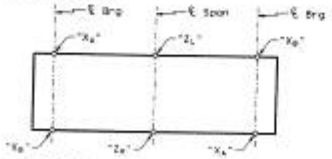

LOCATION OF SECTION DEPTHS
(SHOWING PLAN VIEW OF TOP OF BEAM)

Span No.	Beam No.	"A"	"B"
18 - 20	All	0.580"	0.139"

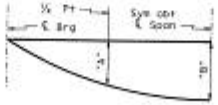

NOTE: Deflections shown are due to Slab concrete only. (Including Panels) (E_c= 5 x 10^6 psi)

DEAD LOAD DEFLECTION DIAGRAM

GENERAL NOTES:

Designed according to AASHTO 1996 Standard and current Interim Specifications.

Details shown are based on the use of Prestressed Concrete Panels. See PCP(II)(MOD) or PMOF(II) for details and quantity adjustments. See UBMS(MOD) for reinforcing details not shown.

All reinforcing shall be Grade 60.

Concrete strength f'_c = 3600 psi

Bar laps, where required, shall be as follows: #4 = 1'-5", #5 = 1'-9"

HS25 LOADING

SHEET 2 OF 2

Texas Department of Transportation
Bridge Division

315.00' PRESTRESSED CONCRETE U-BEAM UNIT

(SPANS 18 - 20)

DIRECT CONNECTOR E6N35

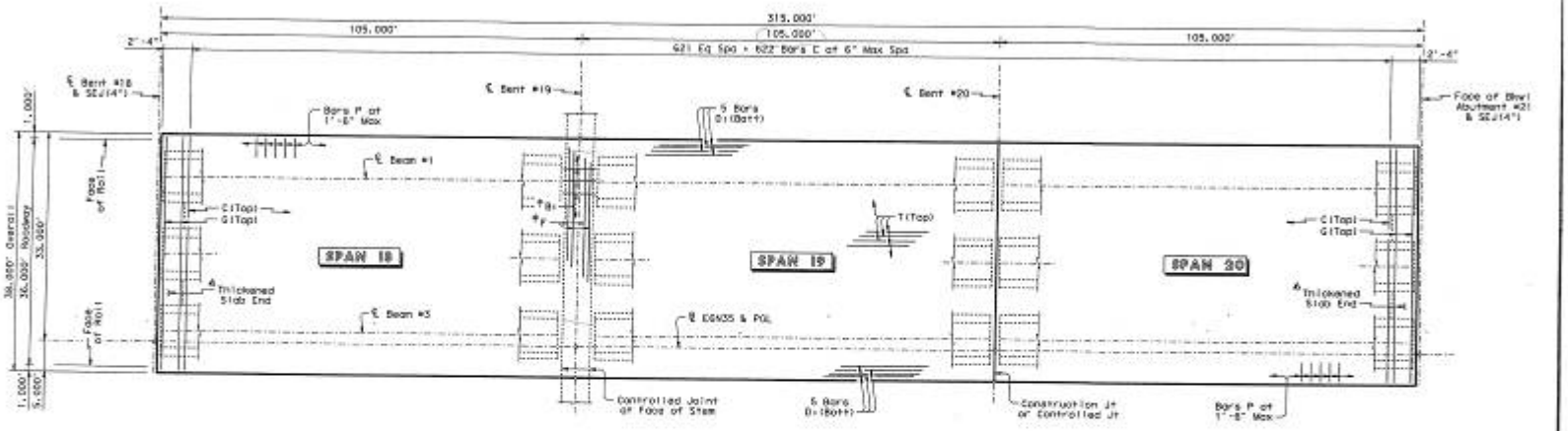

PLAN

Thickened Slab End Bars G, H & J - See U315(MOD) for details.

*See U315T(MOD) for location of Bars B & F.

HS25 LOADING SHEET 1 OF 2

Texas Department of Transportation
Bridge Division

315.00' PRESTRESSED CONCRETE U-BEAM UNIT

(SPANS 18 - 20)

DIRECT CONNECTOR E6N35

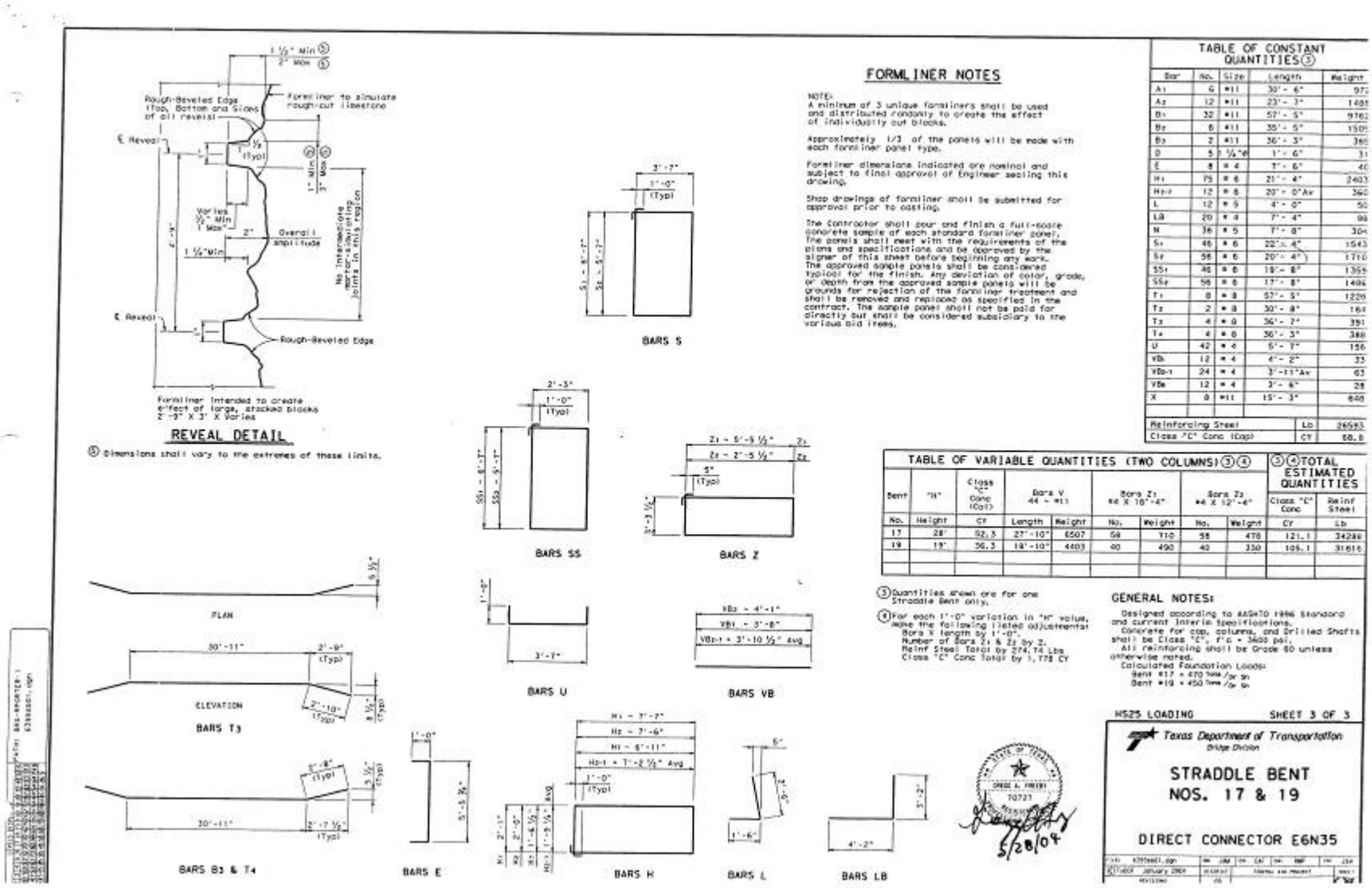
REVEAL DETAIL
⑤ Dimensions shall vary to the extremes of these limits.
FORMLINER NOTES
TABLE OF CONSTANT QUANTITIES ③
TABLE OF VARIABLE QUANTITIES (TWO COLUMNS) ③④
③④TOTAL ESTIMATED QUANTITIES
③Quantities shown are for one Straddle Bent only.
④For each 1'-0" variation in "H" value, make the following listed adjustments:
GENERAL NOTES:
HS25 LOADING
SHEET 3 OF 3
Texas Department of Transportation
Bridge Division
STRADDLE BENT NOS. 17 & 19
DIRECT CONNECTOR E6N35
BARS S
BARS SS
BARS Z
BARS U
BARS VB
BARS T3
BARS B3 & T4
BARS E
BARS H
BARS L
BARS LB

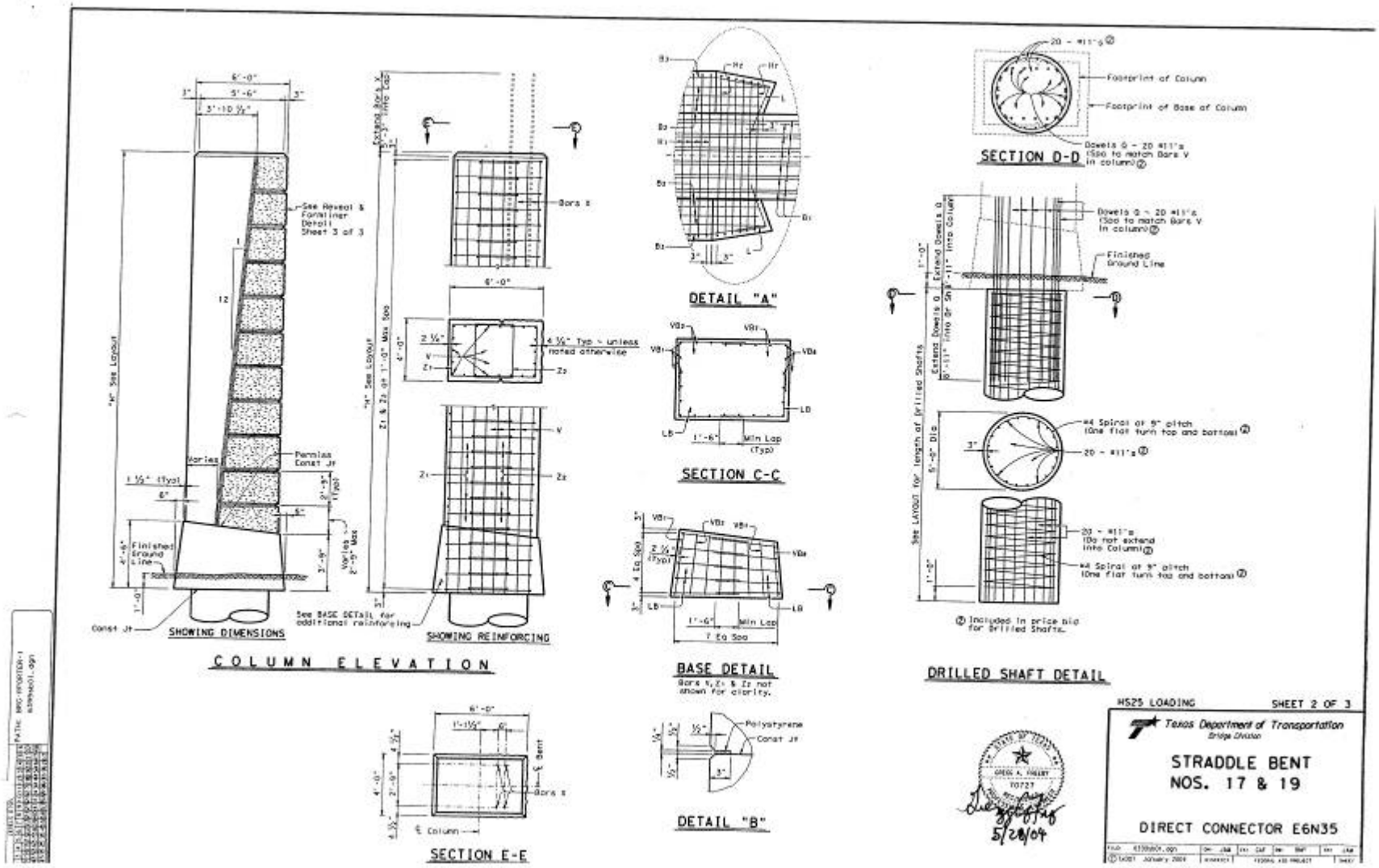
SHOWING DIMENSIONS
SHOWING REINFORCING
COLUMN ELEVATION
SECTION E-E
DETAIL "A"
SECTION C-C
BASE DETAIL
DETAIL "B"
SECTION D-D
DRILLED SHAFT DETAIL
HS25 LOADING
SHEET 2 OF 3
Texas Department of Transportation
Bridge Division
STRADDLE BENT
NOS. 17 & 19
DIRECT CONNECTOR E6N35
5/28/04

References

AASHTO LRFD. (2010). 2010 Interim Revisions, Bridge Design Specifications, 4th Edition. Washington, DC: American Association of State Highway and Transportation Officials.

ACI Committee 318-08. (2008). Building Code Requirements for Reinforced Concrete (ACI 318-08). Farmington Hills, MI: American Concrete Institute.

ACI Special Committee 208 (2008). Examples for the Design of Structural Concrete with Strut-and-Tie Models. Farmington Hills, MI: American Concrete Institute.

Bayrak, O. (2009). Straddle Cracking Database.

Birrcher, D., Tuchscherer, R., Huizinga, M., Bayrak, O., Wood, S., & Jirsa, J. (2008). Strength and Serviceability Design of Reinforced Concrete Deep Beams. University of Texas at Austin.

Grob, J., & Thurlimann, B. (September 1976). Ultimate Strength and Design of Reinforced Concrete Beams under Bending and Shear. IABSE Periodica, Zurich, 36, 105-120.

Kani, G. (1967). How Safe Are Our Large Reinforced Concrete Beams? ACI Journal, pp.128-141.

Kani, M. W., Huggins, M. W., & Wittkopp, R. R. (1979). Kani on Shear in Reinforced Concrete. (pp. 437-442).

Mirza, S. A., & Furlong, R. W. (August, 1983). Strength Criteria for Concrete Inverted T-Girders. Journal of Structural Engineering, Vol. 109, No. 8.

Mirza, S. A., Furlong, R. W., & Ma, J. S. (September-October 1988). Flexural Shear and Ledge Reinforcement in Reinforced Concrete Inverted T-Girders. ACI Structural Journal, 509-520.

Ramirez, J. A., & Breen, J. E. (1991). Evaluation of Modified Truss-Model Approach for Beams in Shear. Vol. 88(No. 2, pp. 562-571).

Schlaich, J., & Schafer, K. (1991). Design and detailing of structural concrete using strut-and-tie models. The Structural Engineer, Volume 69, No. 6, pp. 113-125.

Schlaich, J., Schafer, K., & Jennewein, M. (1987). Toward a Consistent Design of Structural Concrete. PCI Journal, Vol. 32, No. 3, pp. 74-150.

Tan, K. H., & Lu, H. Y. (1999). Shear behavior of Large Reinforced Concrete Deep Beams and Code Comparisons. ACI Structural Journal, V. 96, No. 5, pp. 836-845.

TxDOT. (May 2009). Bridge Design Manual - LRFD.

Walraven, J., & Lehwalter, N. (1994). Size Effects in Short Beams Loaded in Shear. ACI Journal, Vol. 91, No. 5, pp. 585-593.

Zhang, N., & Tan, K. H. (2007). Size effect in RC deep beams: Experimental investigation and STM verification. Engineering Structures, Vol. 29, pp. 3241-3254.

VITA

In 2005, David graduated from Donegal High School. He went on to study civil engineering at Johns Hopkins University from 2005 to 2009, graduating with a Bachelor of Science in May 2009. In August of 2009, he enrolled in the structural engineering graduate program at the University of Texas at Austin. During his time in Austin, he worked as a research assistant at the Phil M. Ferguson Structural Engineering Laboratory. David graduated with a Master of Science in Engineering in August 2011 and will continue to work towards a Doctor of Philosophy at the University of Texas at Austin.

Email Contact: dbgarber@utexas.edu

This thesis was typed by the author.